Dynamics of One-Dimensional Integrable Systems

PHD DISSERTATION

LEVENTE PRISTYÁK

Supervisor: Dr. Balázs Pozsgay
Senior Research Fellow
ELTE Institute of Physics and Astronomy
Department of Theoretical Physics

Budapest University of Technology and Economics

2024.

Acknowledgment

First and foremost, I would like to express my deepest gratitude to my PhD supervisor, Balázs Pozsgay, for his invaluable guidance and endless patience throughout my PhD studies. I am indebted to his deep knowledge and insightful introduction to the topic of quantum integrability which have been instrumental in shaping this thesis. I am also grateful for the many opportunities I had thanks to him and for his numerous useful comments regarding this manuscript.

I also like to thank all the individuals with whom I had the privilege to collaborate on the works that are presented in this thesis. Special thanks to Márton Borsi, Tamás Gombor and Arthur Hutsalyuk. I am especially thankful to Márton Kormos for his careful reading of the manuscript and for his valuable comments.

Finally, I extend my heartfelt appreciation to my friends and family and most importantly to my sister and my parents for their encouragement and support throughout the many years of my studies.

Contents

Chapter 1

Introduction

The scientific method of physics requires us to continuously test our theories against physical observations. Understanding a physical theory is not fully accomplished by simply writing down its fundamental, governing equations. In order to test its validity and to fully master and appreciate it, one needs to see it in action, applied to specific scenarios. This is also quite transparent in the way physics is taught: no physics course stops at writing down the basic equations, e.g. Newton's gravitational law or Schrödinger's equation. Instead, the courses turn to specific examples, such as Kepler's problem and the quantum harmonic oscillator in order to illustrate the workings of the respective theories and to show that their predictions are indeed in agreement with physical observations.

The aforementioned pedagogical problems have the appealing property that their solutions can be obtained in closed form analytically, which makes them perfect not just from a pedagogical standpoint, but also because they provide benchmarks that can be compared against experimental results without much ambiguity. Unfortunately, the situation is usually not that simple when one considers more complex scenarios, regardless of being in the classical or quantum realm. This is especially true when one looks at interacting many-body systems, where the possibly large number of degrees of freedom and the complexity introduced by the interactions make it generally impossible to derive any exact, closed form results. Instead, one usually needs to turn to some approximation technique such as perturbation or mean field theory, or resort to numerics, which also becomes more and more computationally demanding and less and less applicable as the degrees of freedom increase.

However, there are exceptions to this generic behavior, the most notable one being the class of integrable models. These are special many-body systems that allow for an analytic treatment. Since integrable models constitute the main topic of this dissertation, first let us define integrability in a somewhat rigorous way.

The notion of integrability is deeply connected to the existence of conserved quantities. In classical mechanics, integrability can be defined quite easily and unambiguously: a system with N degrees of freedom (accordingly with a $2N$ dimensional phase space), defined by some Hamiltonian function $\mathrm{H}(\{\mathrm{q}_i\}_N, \{\mathrm{p}_i\}_N)$ is said to be (Liouville) integrable, if it possesses N constants of motion (including the Hamiltonian itself), i.e. there are N independent functions F_i that have vanishing Poisson brackets with the Hamiltonian function

and with each other. In this case, the equations of motion governing the time evolution of the system can be solved by introducing action-angle variables. In the present thesis, we do not study classical models, therefore from now on we restrict our focus to quantum systems only.

The situation is a bit more complicated in the quantum case. The Hamiltonian function defined on the phase space is replaced by the Hamiltonian operator H, a Hermitian operator acting on a Hilbert space $\mathcal{H}$. The role of Poisson brackets is then played by the commutators of operators. Simply requiring the existence of a number of operators that commute with the Hamiltonian, however, does not yield a meaningful definition of integrability: for every Hermitian operator H, one can define the projectors $P_n = |n\rangle \langle n|$, where $|n\rangle$ are the eigenstates of the operator ($n = 1, \ldots, \dim(\mathcal{H})$). Obviously, $[H, P_n] = 0$ for every n. Therefore, it is essential to stipulate some other requirements about the conserved quantities. In the usual definition of integrability - and in the one that is used in this dissertation - this extra requirement is locality, meaning that the conserved quantities (also called charges) must be written as sums of charge density operators that act non-trivially only locally, at some finite part of the whole system. Mathematically this property is expressed by the following equation:

$$\hat{Q}_\alpha = \int dx \hat{q}_\alpha(x), \tag{1.1}$$

where $\hat{Q}_\alpha$ is the conserved charge, while $\hat{q}_\alpha(x)$ is its density that acts non-trivially only in a finite segment around the coordinate x. In (1.1), we assumed that the system lives in continuous space, but the definition of locality is straightforwardly extended to lattice models as well.

A quantum system is then called integrable, if it possesses extensively many local, conserved charges that are in involution, i.e. they commute with the Hamiltonian operator and with each other. In the case of lattice systems, the number of these charges usually scales polynomially with the volume.

Examples of integrable quantum systems include a wide variety of models from a range of different areas of physics: from condensed matter systems, such as the Heisenberg and Hubbard models, through non-relativistic quantum gases, like the Lieb-Liniger and Gaudin-Yang models to integrable quantum field theories, like the sine-Gordon model and to cellular automatons, for example the Rule 54 model, which attracted considerable research interest in recent years. Moreover, through different mathematical connections, quantum integrability also closely related to certain two-dimensional classical statistical systems, such as the six- and eight-vertex models and its formalism even comes up in string theory through the AdS/CFT correspondence.

As a consequence of the extra conservation laws, integrable systems are said to be exactly solvable. It is, however, not an easy task to objectively define what amounts as an exact solution. In this dissertation, we do not intend to dwell on this question, and will basically use the term „exactly solvable” as a synonym for models that are treatable by some form of the Bethe Ansatz techniques. These powerful analytic techniques enable one to reduce the eigenvalue problem of the time-independent Schrödinger equation, to solving a system of coupled, non-linear equations (Bethe equations), and to construct the eigenstates and eigenenergies of the system in terms of the solutions of these equations (Bethe roots). Moreover, it is also possible within these frameworks to treat the thermodynamics of integrable systems and even calculate correlation

functions in equilibrium. The different variants of Bethe Ansatz, used in this dissertation are introduced in Chapter 3.

Because of the exact solvability, integrable quantum systems provide a unique opportunity to gain insights into physical phenomena that otherwise might be inaccessible in generic systems. Furthermore, even though integrability usually requires a precise fine tuning, thanks to the experimental developments witnessed in recent times, integrable models can be experimentally realized and the analytic solutions can be tested. In light of all this, it might not be surprising that quantum integrability has been an active research area for almost a century now.

The study of integrable quantum systems dates back to the birth of quantum mechanics itself. The (isotropic) Heisenberg model, which is one of the most studied examples of an integrable quantum system was introduced by Heisenberg to explain the microscopic origins of magnetism in 1928 [1]. The model was later solved by Bethe [2] in 1931, who used his famous ansatz that nowadays bears his name. Bethe's result comprised the first exact solution of an interacting many-body quantum system, and later served as a guide to tackle other integrable models as well, such as the one-dimensional Bose gas with delta interaction, solved by Lieb and Liniger [3] and the XXZ Heisenberg model, solved by Yang and Yang [4]. Later, Yang and Yang were also able to extend the technique to infinite systems to describe the thermodynamics of integrable models [5].

At the same time, the understanding of integrable systems also greatly benefited from the study of certain two-dimensional classical statistical mechanical models, namely the six- and eight-vertex models. The former was solved by Lieb [6–8] and Sutherland [9] by using the transfer matrix technique introduced earlier by Onsager in his famous solution of the square lattice Ising model [10], while the latter was worked out by Baxter [11]. Through these solutions, it was observed that the transfer matrices of the six- and eight-vertex models commute with the Hamiltonians of the XXZ and XYZ Heisenberg models, respectively. This connection was finally understood within the unifying framework of the Quantum Inverse Scattering Method (QISM) that was developed in the 70's by the Leningrad group [12]. This framework made possible the systematic investigation of integrable models through the Yang-Baxter equation and the connection to quantum groups, while at the same time being able to recover previously obtained results through the introduction of the algebraic Bethe Ansatz. These tools proved to be extremely powerful to describe the equilibrium physics of integrable systems, even allowing to exactly calculate correlation functions and mean values of certain local operators.

In the last two decades, the interest in studying integrable models has renewed. This revived research activity was in big part propelled by the developments that took place in experimental techniques, such as cold atom experiments [13, 14]. These improvements made it possible to realize and investigate the out-of-equilibrium dynamics of (almost completely) closed quantum systems. Consequently, considerable effort was put into work from the theoretical side to explain the observed phenomena. During this work, it became evident that integrable models equilibrate fundamentally differently compared to generic systems. The research endeavor culminated in the establishment of the frameworks of Generalized Gibbs Ensembles

and Generalized Hydrodynamics, which are introduced in more detail in the next chapter.

The results discussed in the present dissertation fit into the line of research outlined above. On the one hand, they contribute to the general understanding of integrable quantum systems and to the broad topic of equilibrium correlation functions. They have, however, a more immediate connection to the out-of-equilibrium dynamics and relaxation properties of integrable models as well. Thus, it is necessary to discuss the topic of equilibration in more detail, in order to motivate our work and put it into context. This is done in the next chapter.

Chapter 2

Equilibration in many-body quantum systems

When dealing with physical systems that consist of macroscopically large numbers of degrees of freedom, describing the dynamics by the microscopic laws of physics (i.e. Newton's laws in the classical or Schrödinger's equation in the quantum case) becomes computationally intractable. The phenomenological laws of thermodynamics offer a way to deal with the macroscopic, measurable properties of such systems, however, without any considerations about the underlying microscopics. In the second half of the 19^{th} century, statistical physics was developed to fill this gap and to put thermodynamics on a firmer foundation. It was able to recover and explain the empirical formulae of thermodynamics starting from the motion of the constituent particles of the system by applying statistical methods. Most notably, statistical physics introduced the concept of statistical ensembles, which provide an effective means to explain and describe the equilibrium behaviour of systems by using the equivalence between time and ensemble averages. The theoretical justification of this equivalence, however, is far from trivial and has constituted for decades (and does so till this day) a prominent field of research.

In the case of generic classical systems, the emergence of the statistical description is quite well understood: due to the chaotic nature of the dynamics, the system explores all of its phase space (or at least the regions allowed by the possibly present, few conserved quantities) and this ergodicity allows one to calculate the long time averages of physical quantities by taking averages over the appropriate ensemble.

With the advent of quantum mechanics, statistical physical notions were successfully extended to quantum systems as well. However, giving a solid theoretical justification for the use of statistical ensembles posed a challenge in the quantum case: when considering an isolated quantum system, its time evolution is described by the time-dependent Schrödinger equation, which is completely unitary. As a result, a system initialized in a pure state, will remain in a pure state for all times. In contrast, thermal equilibrium in the statistical description is characterized by the Gibbs ensemble, whose density matrix is inherently mixed, leading to a seemingly insoluble contradiction.

In this chapter, we first present the main ideas behind how this problem was remedied for generic closed

quantum systems by the introduction of the Eigenstate Thermalization Hypothesis (ETH), before discussing some scenarios where ETH is violated and turning our attention to the main topic of this dissertation, integrable systems. Integrable models do not follow ETH and don't thermalize in the usual sense. Their equilibration and transport properties can be described instead by the Generalized Gibbs Ensembles (GGE) and Generalized Hydrodynamics (GHD), respectively, which are introduced here.

2.1 Thermalization in generic closed quantum systems

To better understand the key features of thermalization in closed quantum systems, one can consider a simple, but quite general scenario provided by the so-called quantum quench protocol. In (global) quantum quenches, the isolated system in question is prepared in some initial pure state $|\Psi_0\rangle$ (often chosen as the ground state of some pre-quench Hamiltonian H_0) and than time-evolved with the (post-quench) Hamiltonian of the system, denoted by H, of which $|\psi_0\rangle$ is not an eigenstate:

$$|\Psi(t)\rangle = e^{-itH}|\Psi_0\rangle\,. \tag{2.1}$$

This protocol has many advantageous properties: on the one hand, it introduces an extensive amount of energy (or finite energy density) into the system and takes it far out-of-equilibrium. On the other hand, it is also an experimentally realizable set up enabling one to compare theoretical calculations to actual measurements.

Since the Hamiltonian is a Hermitian operator, the time-evolution (2.1) is unitary, thus the state of the system remains pure at all times. On the other hand, a thermal state described by the Gibbs ensemble is characterized by a mixed state, given by the density operator

$$\hat{\rho}_{GE} = \frac{1}{Z}e^{-\beta H} = \frac{1}{Z}\sum_n e^{-\beta E_n}|n\rangle\langle n|\,, \tag{2.2}$$

with $Z = \sum_n \exp(-\beta E_n)$ being the partition function, β the inverse temperature and $|n\rangle$, E_n the eigenstates and eigenenergies of the system.

Subsequently, we cannot expect to witness the emergence of a thermal state described by a statistical mechanical ensemble, in terms of density matrices of the whole system. Instead, we can adopt an other point of view by focusing on local observables, rather than the system as a whole. By taking up this perspective, we can hope to observe thermalization in terms of the expectation values of these observables. This shift in perspective is justified by the fact that experimental setups that probe thermalization do not have access to the density matrix itself, but only to a set of observables.

Accordingly, we consider a local operator $\hat{\mathcal{O}}$ and study its expectation value during the time-evolution. If we expand the state (2.1) as $|\Psi(t)\rangle = \sum_n c_n e^{-itE_n}|n\rangle$, with $c_n = \langle n|\Psi_0\rangle$, the time-dependent expectation

value of $\hat{\mathcal{O}}$ reads as:

$$\left\langle \hat{\mathcal{O}}(t) \right\rangle = \langle \Psi(t)|\hat{\mathcal{O}}|\Psi(t)\rangle = \sum_{n,m} c_n \bar{c}_m e^{-it(E_n - E_m)} \langle m|\hat{\mathcal{O}}|n\rangle \,. \tag{2.3}$$

From the point of view of the local observable $\hat{\mathcal{O}}$, thermalization of the system would mean that the long-time average of $\left\langle \hat{\mathcal{O}}(t) \right\rangle$ coincides with the prediction of the Gibbs ensemble, and that the instantaneous values of $\left\langle \hat{\mathcal{O}}(t) \right\rangle$ remain close to this equilibrium value.

Assuming a generic Hamiltonian whose spectrum does not contain a vast number of degeneracies, long time-averaging in the thermodynamic limit leads to the cancellation of the off-diagonal terms and reduces (2.3) to the so-called diagonal ensemble:

$$\lim_{T\to\infty} \frac{1}{T} \int_0^T \left\langle \hat{\mathcal{O}}(t) \right\rangle dt = \sum_n |c_n|^2 \langle n|\hat{\mathcal{O}}|n\rangle \,. \tag{2.4}$$

To explain how thermalization occurs in closed quantum systems, one then needs to understand how the diagonal ensemble can produce the same expectation values as the thermal Gibbs ensemble. To this end, in the works [15, 16], the so-called Eigenstate Thermalization Hypothesis was introduced.

Crudely speaking, ETH encapsulates the following idea: every eingenstate of the Hamiltonian carries implicitly in itself a thermal state, but this thermal state is initially hidden by the coherence of the eigenstates. Due to the dephasing that takes place through the time evolution, the thermal state reveals itself. (This is a fundamentally different process compared to the classical case, where the initial state evolves ergodically through the phase space to become a thermal one. Here, the initial state usually does not resemble the thermal state at all.)

Mathematically more precisely, ETH assumes the following form for the matrix elements of local observables:

$$\mathcal{O}_{mn} = O(\overline{E})\delta_{nm} + e^{-S(\overline{E})} f_{\mathcal{O}}(\overline{E}, \omega) R_{nm}, \tag{2.5}$$

where $\overline{E} = (E_n + E_m)/2$, $\omega = E_n - E_m$, S is the entropy and the functions $O(\overline{E})$, $f_{\mathcal{O}}(\overline{E}, \omega)$ are smooth functions of their arguments, while R_{nm} are random variables with zero mean and unit variance. Moreover, the function $O(E)$ is such that its value coincides with the (micro)canonical (with energy E) expectation value of $\hat{\mathcal{O}}$. The ansatz (2.5) basically means that all eigenstates with energies close to each other have almost the same expectation values for local observables.

For operators for which the ETH (2.5) is satisfied, thermalization to the appropriate Gibbs ensemble value is then guaranteed, given that the initial state has a narrow energy distribution. To verify this, one only needs to substitute the ETH ansatz (2.5) into equation (2.4). Moreover, it can also be shown (see for example [17]) that the fluctuations around the equilibrium value remain exponentially small in the system size.

The ETH provides a mechanism to understand the thermalization processes of generic closed quantum systems and to recover the predictions of statistical mechanics in these systems. It has been verified numerically in various different settings, such as hard- and soft-core bosons on a lattice [18, 19], interacting spin

chains [20], interacting fermionic systems [21, 22] and the two-dimensional, transverse field Ising model [23] (also, for a more thorough review of the topic, see [17]).

2.1.1 ETH breaking

As it is clear from its name, ETH is a hypothesis and not a proven theorem with well-defined conditions for it to hold. Therefore, it is important to study the boundaries of its validity and ask the question: what are the possible scenarios to break ETH (and with it, thermalization) in closed quantum systems?

In the course of decades of research, numerous examples were found, where ETH is violated. The origin of ETH breaking in these examples can be mostly attributed to four different mechanisms:

- *Quantum integrability:* Probably the most studied and well-understood class of models that break the usual mechanism of thermalization outlined above, consists of the one-dimensional, integrable quantum systems [12, 24]. As we already pointed out in the Introduction, these are models with extra (extensively many) conservation laws. The existence of these additional conserved quantities lead to ergodicity breaking. Since integrable models are in the main focus of this dissertation, we discuss their equilibration in more detail in the next section.

- *Hilbert space fragmentation:* Another, more recently discovered form of thermalization breaking is the so-called Hilbert space fragmentation. The expression refers to the phenomenon when the Hilbert space of the system in question splits up to an exponentially large number of distinct sectors between which the Hamiltonian of the model has no transition matrix elements. Moreover, it is required that these sectors should be easily constructed by simple rules, without needing to solve the model. (Obviously, once the eigenvalue problem of the model is solved and the Hamiltonian is diagonalized, the Hilbert space is decomposed to $\dim(\mathcal{H})$ sectors, regardless of the properties of the system.)

  A mathematically more well-defined and rigorous definition of Hilbert space fragmentation was put forward in the work [25], where it was classified as the case when the dimension of the commutant algebra (the set of all operators that commute with each term of the Hamiltonian of the system) grows exponentially with the system size.

  The phenomenon was first observed in [26], where it arose as a result of simultaneous charge and dipole conservation. In later chapters, we introduce and investigate a spin chain model that exhibits Hilbert space fragmentation. We demonstrate the effects of Hilbert space fragmentation on equilibration in this model.

- *Quantum many-body scars:* Besides Hilbert space fragmentation, another recently heavily studied form of ETH breaking is QMBS, which describes a weak breaking of ETH. This means that in this case there are only finitely many (in the thermodynamic limit given by a zero-measure set) exceptional states in the spectrum that do not follow the predictions of ETH and have significantly different

properties, compered to thermal states with similar energy densities. The phenomenon was first discovered independently in experiments with Rydberg atoms [27] and theoretically by investigating the so-called AKLT spin-1 model [28]. In this dissertation, we will not study QMBS, for more details on the topic, see the reviews [29, 30] and the references therein.

- *Many-body localization:* MBL – the extension of Anderson localization [31] to interacting many-body systems – constitutes an other mechanism of ETH breaking, where the interplay between interaction and disorder hinders thermalization. The key characteristic of many-body localized systems is the presence of localized eigenstates, where particles become confined to specific regions rather than spreading throughout the entire system. As a result, the system retains memory of its initial conditions and does not exhibit the typical relaxation to thermal equilibrium. Again, MBL is not discussed further in this dissertation, for an extensive review on the subject, we refer to [32, 33].

2.2 Integrable systems

Thanks to the large number of conserved quantities possessed by integrable quantum models, their out-of-equilibrium dynamics fundamentally differs from those of generic systems. In recent years, to a great extent propelled by experimental developments, equilibration and transport in these integrable models were in the forefront of research. As a result, today we have well established frameworks to describe these phenomena in the form of the Generalized Gibbs Ensembles and the Generalized Hydrodynamics, respectively. Since most of our results discussed in the present dissertation are connected to the aforementioned concepts, here we briefly introduce them only to the extent that is necessary to put our work into context.

2.2.1 Generalized Gibbs Ensemble

Thermalization to a Gibbs ensemble through the mechanism encompassed by ETH falls short when it comes to describing the late time behaviour of integrable quantum systems. As it was first shown experimentally in the now famous *quantum Newton's cradle* experiment [34], integrable models do not thermalize in the usual sense, due to the restrictions imposed by the extra conservation laws.

To capture their equilibration process, one needs to extend the concept of Gibbs ensemble by considering entropy maximized states with the constraints of conserved quantities kept in mind. This construction leads to the introduction of the Generalized Gibbs Ensemble (GGE) [35, 36]. The density operator of a GGE state is given by

$$\hat{\rho}_{GGE} = \frac{1}{Z}\sum_{\alpha} e^{-\beta_\alpha \hat{Q}_\alpha}, \tag{2.6}$$

where $\hat{Q}_\alpha$ are the conserved charges of the model and β_α are the corresponding Lagrange multipliers/generalized inverse temperatures whose values are set by the initial values of the charges, $\langle\Psi_0|\hat{Q}_\alpha|\Psi_0\rangle$.

The inclusion of the conserved charges in the density operator and the appearance of the summation in (2.6) pose the question: what are the relevant charges that one needs to take into account in order to properly

describe the equilibrium state of an integrable model? This is a non-trivial question, since as it turns out simply including all the local conserved charges in (2.6) is not enough [37, 38]. To obtain a sufficient description, one needs to extend the summation to the so-called quasi-local charges [39, 40]. These are constants of motion with densities that, instead of a finite range, have infinite support, but with coefficients that decrease exponentially quickly with distance. Similarly to the local charges, there are extensively many quasi-local ones, with their number scaling polynomially with the system size. Their inclusion is necessary to build GGEs that correctly reproduce the equilibrium states of integrable systems [40, 41].

Just like the concept of the GGE is a generalization of the usual Gibbs ensemble to the case of extensively many conservation laws, ETH also can be extended to provide a mechanism that explains the equilibration to GGE states. This extension is the so-called generalized Eigenstate Thermalization Hypothesis (GETH) [42], which postulates a similar form for the matrix elements of physical observables as ETH does in (2.5). The fundamental difference is, however, that in the GETH the diagonal matrix elements are not only smooth functions of the energy, but rather all conserved charges. This modification guarantees that the expectation values of local observables equilibrate to the appropriate GGE values, in exactly the same way as ETH does for generic non-integrable systems.

It is worth mentioning that GGEs not only play an important role in the case of fine-tuned, exactly integrable systems, but also in the vicinity of integrability. Models close to being integrable exhibit pre-thermalization [43, 44]: during their equilibration process, they first approach a GGE state on an intermediate time-scale, before thermalizing to a Gibbs state.

2.2.2 Generalized Hydrodynamics

The equilibration of integrable systems following homogeneous quenches is well understood within the framework of generalized Gibbs Ensembles. However, the situation changes if one considers the out-of-equilibrium dynamics in a setup that breaks translational invariance. A paradigmatic example of such a scenario is the so-called Riemann problem of hydrodynamics or bipartitioning protocol, in which the physical system in question is split into two halves, which are initially prepared to be in two different equilibrium states. Then the two halves are connected together and let evolve under the time-evolution dictated by the Hamiltonian operator of the system. Due to the conservation laws and ballistic transport of charges, the imbalance built in the initial state will lead to the emergence of a non-equilibrium steady state (NESS) for long times. The characteristic trait of this NESS is the existence of constant currents that transport the conserved quantities ballistically, from one half of the system to the other.

To analyze an inhomogeneous setup like the one described above in a generic (non-integrable) model, hydrodynamics [45] presents an old and well-established framework. Hydrodynamics is a powerful emergent theory that can describe the dynamics of complex many-body systems by reducing the number of relevant degrees of freedom through coarse graining. It divides the system in question into mesoscopic fluid cells that are small compared to the macroscopic sizes of the whole system, but still large enough in comparison to the microscopic scale. By assuming local thermalization/entropy maximization in these fluid

cells and taking into account the few conserved quantities present in a generic model, one can derive hydrodynamic equations (Euler, Navier-Stokes) for the relevant degrees of freedom. Since its creation as a theory of fluid dynamics, hydrodynamics was successfully applied in several different fields, such as condensed matter and high energy physics.

However, conventional hydrodynamics (which only builds on the existence of the conservation of energy, momentum and particle number) cannot capture the transport properties of an integrable system. To overcome this problem, in the seminal works [46, 47] the so-called Generalized Hydrodynamics (GHD) was introduced. The main idea behind GHD is to combine the hydrodynamic separation of scales with the machinery of the (thermodynamic) Bethe Ansatz in order to give a quantitative description of the large scale transport properties of integrable systems. In summary, GHD extends the principles of hydrodynamics to the realm of integrable quantum systems, utilizing the concept of quasi-particle excitations and the Generalized Gibbs Ensemble to describe the macroscopic behavior of these unique quantum systems in inhomogeneous settings.

Since in the rest of the dissertation, we will mainly consider systems of finite volume, the usual (coordinate/algebraic) Bethe Ansatz technique is introduced in the next chapter. In order to give an introduction to GHD, however, we need to use the language of the thermodynamic Bethe Ansatz (TBA). Here we restrict ourselves to a minimal discussion of both the TBA and GHD, which is enough for us to motivate the work that is presented in the later chapters.

As we shall see in the next chapter, states of integrable quantum systems are characterized by long-lived quasi-particles. These particles have well-defined quasi-momenta which are described by the so-called Bethe roots, a set of complex parameters that satisfy a set of coupled, non-linear equations. When dealing with macroscopic systems, one can take the thermodynamic limit and can introduce the root density $\rho(\lambda)$[1], instead of the set of Bethe roots. In equilibrium, the mean values of the conserved charges of the system then can be computed using this root density according to

$$\langle \hat{Q}_\alpha \rangle = \int q_\alpha(\lambda)\rho(\lambda)d\lambda, \tag{2.7}$$

where $q_\alpha(\lambda)$ is the one-particle eigenvalue corresponding to the charge $\hat{Q}_\alpha$.

GHD exploits the hydrodynamic separation of spatial and temporal scales: it assumes that the system can be divided into mesoscopic fluid cells that are much smaller than the characteristic sizes of the macroscopic transport processes but still contain large numbers of particles and that each cell equilibrates to local entropy maximized states in a time-frame much shorter than the characteristic time-scales of the transport. Due to the integrability of the system, the local equilibrium states can be described by local GGEs, which are in turn uniquely characterized by the values of the (quasi) local charges, or equivalently by the root density $\rho(\lambda)$ [48, 49]. Accordingly, the function $\rho(\lambda)$ acquires space and time dependence, and the relation (2.7) becomes valid in each fluid cell individually.

[1] For simplicity, we assume that the system in question supports only one particle type. All of our considerations are trivially extended to models with multiple particle types present.

Due to the conservation of the charges, there exist current operators corresponding to each charge operator that together satisfy a continuity equation:

$$\partial_t \hat{q}_\alpha(x,t) + \partial_x \hat{J}_\alpha(x,t) = 0, \tag{2.8}$$

where $\hat{q}_\alpha$ and $\hat{J}_\alpha$ are the charge and current density operators, respectively.

The main goal of GHD is to derive hydrodynamic equations for the root density. To this end, one considers the expectation value of the continuity equation (2.8). A crucial step in the derivation is the calculation of the mean values of the current operators, for which a semi-classical expression was put forward in the works [46, 47]:

$$\langle \hat{J}_\alpha \rangle = \int q_\alpha(\lambda) v^{\text{eff}}(\lambda) \rho(\lambda) d\lambda, \tag{2.9}$$

where $v^{\text{eff}}(\lambda)$ is an effective velocity that describes the motion of quasi-particles in the sea of other quasi-particles by taking into account the interactions between them. The form (2.9) was proven in [46] for the case of integrable quantum field theories (iQFT), however, for lattice models a rigorous proof was missing for some time. One of the main results of the present thesis is the mathematically sound derivation of (2.9) in finite volume spin chain models. These results are presented in Chapters 4 and 5.

Based on the continuity equation (2.8) and the expressions for the charge (2.7) and current (2.9) mean values, a hydrodynamic equation for the root density $\rho(\lambda)$ can be derived, which in the first, ballistic order reads as

$$\partial_t \rho_{x,t}(\lambda) + \partial_x \left[\rho_{x,t}(\lambda) v^{\text{eff}}_{x,t}(\lambda) \right] = 0. \tag{2.10}$$

In the original papers [46, 47], the framework summarized above was used to treat the bi-partitioning protocol in the sinh-Gordon and XXZ Heisenberg models, respectively. Since then, GHD has been developed and applied to various different scenarios in a multitude of works, most notably its predictions were verified in experimental setups [50–52]. Instead of attempting to give a comprehensive picture of the framework, here we only sketched it in its simplest form in order to point out the motivations behind our work that is presented in the later chapters. Nevertheless, for (much) more details on GHD, we refer to the contributions of the special issue [53], while for a more pedagogical introduction, see [54].

The results discussed in this dissertation are connected to the aforementioned topics of out-of-equilibrium dynamics of integrable systems at several points: after presenting a review of the analytic tools, required to treat one-dimensional quantum integrable models in Chapter 3, in Chapters 4 and 5 the current operators of the XXZ and XYZ models are studied. An exact formula for the mean values of the current operators are derived in finite volume, which can be interpreted as the finite size version of the expression (2.9). As such, the current mean value formulae of Chapters 4 and 5 serve as a mathematically rigorous justification of equation (2.9), and as a theoretical foundation of one of the assumptions of GHD.

In the second half of the dissertation, in Chapters 6 and 8 two different one-dimensional, integrable spin models are introduced and investigated, their solutions by means of coordinate Bethe Ansatz are obtained.

The two models share the common property that their scattering phases are really simple functions of the quasi-momenta. As a result, the Bethe equations and the structure of the Bethe roots also massively simplify in these models. This simplification gives hope to calculate the exact out-of-equilibrium time evolution in certain situations, making these models good candidates to verify the predictions of GHD, starting from the microscopic equations of motion.

Moreover, the model of Chapter 6 (together with its non-integrable extension) exhibits Hilbert space fragmentation. As a consequence, thermalization in the usual sense breaks down in this model, and persistent oscillations can be observed following certain quench protocols. This phenomenon is investigated, using mostly numerical tools in Chapter 7.

Chapter 3

Elements of quantum integrability

One-dimensional integrable quantum models form a special class among many-body systems. Their defining property, the existence of a large number of conserved, extensive charges constrains their dynamics, and leads to the formation of stable quasi-particle excitations and to the factorization of scatterings between those particles. As a result, integrable models are exactly solvable. Here exact solvability means that the usual quantum mechanical eigenvalue problem can be reduced to solving a system of coupled, non-linear equations. Once the solutions of this system of equations, the so-called Bethe roots are known, the eigenenergies and eigenstates of the models can be constructed analytically.

In this chapter, we introduce the main tools that are necessary to construct these analytic solutions and are used in the rest of the dissertation to treat integrable systems. First, in Section 3.1, we define the most paradigmatic model among integrable lattice systems, the Heisenberg spin-1/2 chain. This model will both serve as an example to illustrate the use of the Bethe Ansatz techniques in this chapter, and will also be the main topic of Chapters 4 and 5. In Section 3.2 the coordinate Bethe Ansatz technique is summarized. In Section 3.3, we review the basic elements of the Quantum Inverse Scattering Method, the construction of the conserved charges and algebraic Bethe Ansatz. Here generic $U(1)$ symmetric integrable models without internal degrees of freedom are considered, but explicit formulae for the Heisenberg spin chains are also given. Finally, in Subsection 3.3.3 a generalization of the algebraic Bethe Ansatz is presented, which is used to solve the non $U(1)$ symmetric XYZ model.

3.1 Heisenberg model

One of the most fundamental and well-studied integrable systems is the spin-1/2 Heisenberg model. It describes nearest-neighbor interacting spin-1/2 particles along a one-dimensional chain (for a schematic depiction see Fig. 3.1). For a finite volume L, the Hamiltonian of the model acts on the 2^L dimensional

Hilbert space $\mathcal{H} = \otimes_{j=1}^{L} \mathbb{C}^2$, and (in the most general form) reads as:

$$H = \sum_{j=1}^{L} \left[J_x \sigma_j^x \sigma_{j+1}^x + J_y \sigma_j^y \sigma_{j+1}^y + J_z \sigma_j^z \sigma_{j+1}^z + h \sigma_j^z \right]. \tag{3.1}$$

Here σ_j^α is the α^{th} Pauli matrix, acting on site j:

$$\sigma_j^\alpha = \mathbb{1} \otimes \cdots \otimes \mathbb{1} \otimes \underbrace{\sigma^\alpha}_{j^{\text{th}} \text{ site}} \otimes \mathbb{1} \otimes \cdots \otimes \mathbb{1} \qquad (\alpha = x, y, z), \tag{3.2}$$

while $J_\alpha \in \mathbb{R}$, $(\alpha = x, y, z)$ are the anisotropy parameters of the model and h is a magnetic field. Throughout the dissertation (if otherwise not stated) we consider the model (and also other models that are treated later in this thesis) with periodic boundary condition:

$$\sigma_{L+1}^\alpha = \sigma_1^\alpha. \tag{3.3}$$

Moreover, we mainly restrict ourselves to the case of zero magnetic field, $h = 0$.

In the isotropic case ($J_x = J_y = J_z = -J$), the Hamiltonian (3.1) (without magnetic field) reduces to the form:

$$H = -J \sum_{j=1}^{L} \left[\sigma_j^x \sigma_{j+1}^x + \sigma_j^y \sigma_{j+1}^y + \sigma_j^z \sigma_{j+1}^z \right], \tag{3.4}$$

which is the so-called XXX model. The only role of the parameter J in the Hamiltonian (3.4) is to set the energy scale, however, its sign is relevant: $J > 0$ ($J < 0$) results in a ferromagnetic (antiferromagnetic) ground state. Nevertheless, for our purposes this distinction is not important, and in the following, we consider simply the Hamiltonian

$$H^{XXX} = \sum_{j=1}^{L} \left[\sigma_j^x \sigma_{j+1}^x + \sigma_j^y \sigma_{j+1}^y + \sigma_j^z \sigma_{j+1}^z - \mathbb{1} \right], \tag{3.5}$$

where the identity operator was introduced for later convenience. The XXX model has full $SU(2)$ symmetry, the Hamiltonian commutes with the full spin operator $\hat{\underline{S}}$:

$$[H^{XXX}, \hat{\underline{S}}] = 0, \qquad \text{with} \qquad \left(\hat{\underline{S}}\right)_\alpha = \sum_{j=1}^{L} \hat{S}_j^\alpha = \frac{1}{2} \sum_{j=1}^{L} \sigma_j^\alpha. \tag{3.6}$$

The XXX model was first introduced by Heisenberg [1] only a few years after the formulation of quantum mechanics, in order to describe the microscopic origins of ferromagnetism. The eigenenergies and eigenstates of the Hamiltonian were obtained later by Bethe in [2], by means of his famous technique, now known as (coordinate) Bethe Ansatz. This result constituted the first exact solution of an interacting quantum many-body system, and served as a starting point for the study of integrable models in the coming decades.

Introducing an anisotropy in the z-direction ($J_x = J_y = -J$ and $-J_z/J = \Delta$) leads to the so-called XXZ model

$$H = -J \sum_{j=1}^{L} \left[\sigma_j^x \sigma_{j+1}^x + \sigma_j^y \sigma_{j+1}^y + \Delta \sigma_j^z \sigma_{j+1}^z \right]. \tag{3.7}$$

Again, the parameter J sets the overall energy scale, and together with the anisotropy parameter Δ determines the ground state properties: while J aligns spins in the $x-y$ plane (ferromagneticly for $J > 0$, and antiferromagneticly for $J < 0$), as a competing term, Δ prefers order along the z-axis. However, because of symmetry reasons, the $J < 0$ case can be reached from the $J > 0$ case by rotating every other spins along the z-axis by π and changing the sign of Δ. Therefore, we can assume that $J > 0$. In this case, there are three phases of the model: for $\Delta > 1$ ($\Delta < -1$), the systems is a gapped (anti)ferromagnet, while for $|\Delta| < 1$, it is a gapless paramagnet. Still, most of our considerations apply all the same to all phases, and in the following we treat the Hamiltonian

$$H^{XXZ} = \sum_{j=1}^{L} \left[\sigma_j^x \sigma_{j+1}^x + \sigma_j^y \sigma_{j+1}^y + \Delta (\sigma_j^z \sigma_{j+1}^z - \mathbb{1}) \right]. \tag{3.8}$$

As a result of the anisotropy, the $SU(2)$ symmetry breaks down to $U(1)$ symmetry, and the Hamiltonian of the system commutes with the z-component of the total spin:

$$[H^{XXZ}, \hat{S}^z] = 0, \qquad \text{with} \qquad \hat{S}^z = \sum_{j=1}^{L} \hat{S}_j^z = \frac{1}{2} \sum_{j=1}^{L} \sigma_j^z. \tag{3.9}$$

This symmetry breaking, however, does not render Bethe's solution of the XXX model useless: it can be generalized, as it was shown by Yang and Yang in [4].

Finally, in the most general case ($J_x \neq J_y,\ J_x \neq J_z,\ J_y \neq J_z$), we arrive at the XYZ model:

$$H^{XYZ} = \sum_{j=1}^{L} \left[J_x \sigma_j^x \sigma_{j+1}^x + J_y \sigma_j^y \sigma_{j+1}^y + J_z \sigma_j^z \sigma_{j+1}^z \right]. \tag{3.10}$$

The phase diagram of the XYZ model is more complex, therefore we do not discuss it here, a detailed presentation on the topic can be found in [55, 56]. Due to the full anisotropy, the system no longer has $U(1)$ symmetry, which leads to the break-down of usual integrable techniques and makes it considerably harder to obtain eigenenergies and eigenstates. It is also important to note that while the XXX and XXZ models are integrable for arbitrary values of the magnetic field h, the XYZ model is only integrable at the point $h = 0$. The eigenvalue problem of the XYZ model was first solved by Baxter, using its connection to the eight-vertex model [11].

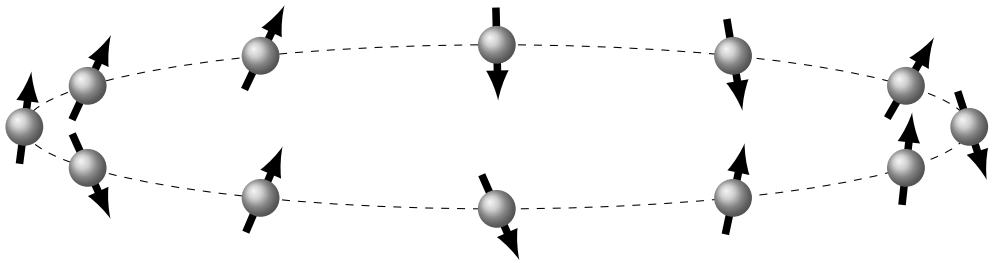

Figure 3.1: Schematic depiction of a finite-size spin chain with periodic boundary condition.

3.2 Coordinate Bethe Ansatz

Bethe constructed the eigenstates of the XXX model using his ingenious ansatz [2], assuming a particular functional form for the wave function. Nowadays, this method is called the coordinate Bethe Ansatz (CBA), in order to distinguish it from the so-called algebraic Bethe Ansatz (ABA), discussed in the next section. Here, we review the main steps of the CBA construction. The main ideas behind this construction are presented rather general, applicable to other $U(1)$ symmetric integrable systems as well, but explicit expressions for the XXX and XXZ models are also given. For more detailed, pedagogical discussions on the topic, see for example [57, 58].

As it was already pointed out, both the XXX and XXZ Hamiltonians commute with the z-component of the total spin. Therefore H and $\hat{S}^z$ share the same eigenstates, and it is enough to diagonalize the Hamiltonians in the invariant subspaces of $\hat{S}^z$, characterized by the magnetization quantum number S^z. Let's introduce the notation $|\uparrow\rangle\,/\,|\downarrow\rangle$ for the basis state with up/down spin at the local Hilbert space $\mathbb{C}^2$:

$$\sigma^z|\uparrow\rangle = |\uparrow\rangle\,, \quad \sigma^z|\downarrow\rangle = -|\downarrow\rangle\,, \quad \langle\uparrow|\uparrow\rangle = \langle\downarrow|\downarrow\rangle = 1, \quad \langle\uparrow|\downarrow\rangle = 0. \tag{3.11}$$

Then the states

$$|\sigma_1,\sigma_2,\ldots,\sigma_L\rangle = |\sigma_1\rangle\otimes|\sigma_2\rangle\otimes\cdots\otimes|\sigma_L\rangle\,, \qquad \text{with} \qquad \sigma_j = \uparrow\,/\,\downarrow, \quad j=1,2,\ldots,L \tag{3.12}$$

form an orthonormal basis in the tensor product Hilbert space $\mathcal{H} = \otimes_{j=1}^{L}\mathbb{C}^2$. Obviously, the subspace with $S^z = L/2$ is one-dimensional and contains only the state:

$$|0\rangle = |\uparrow\uparrow\uparrow\ldots\uparrow\rangle\,. \tag{3.13}$$

It is easy to check that the state $|0\rangle$ is an eigenstate both of the XXX and XXZ Hamiltonians (3.5) and (3.8), with eigenvalue zero. To construct the eigenstates in the other subspaces, $|0\rangle$ is used as a reference state/pseudo-vacuum. We denote the state with N down spins at sites $x_1,\ x_2,\ldots,\ x_N$ as

$$|x_1,x_2,\ldots,x_N\rangle = \prod_{j=1}^{N}\sigma_{x_j}^{-}|0\rangle\,. \tag{3.14}$$

Here we introduced the spin lowering operator $\sigma^- = (\sigma^x - i\sigma^y)/2$ (and similarly $\sigma^+ = (\sigma^x + i\sigma^y)/2$). Then the subspace with $S^z = L/2 - N$ is spanned by the $\binom{L}{N}$ states of the form (3.14) with N downspins. Since the number N is a conserved quantity, we can regard the downspins as particles. In the subspace with N particles, we can look for the eigenstates of the Hamiltonian as:

$$|\Psi\rangle = \sum_{1\le x_1<x_2<\cdots<x_N\le L} \chi(x_1,x_2,\ldots,x_N)\,|x_1,x_2,\ldots,x_N\rangle\,. \tag{3.15}$$

Following Bethe's inventive idea, we can assume a particular form for the coefficients $\chi(x_1,\ldots,x_N)$:

$$\chi(x_1,x_2,\ldots,x_N) = \sum_{\sigma\in S_N}\left[\exp\left(i\sum_{j=1}^{N} x_j p_{\sigma_j}\right)\prod_{\substack{j<k\\ \sigma_j>\sigma_k}} S(p_{\sigma_k},p_{\sigma_j})\right]. \tag{3.16}$$

Here $\sigma \in S_N$ runs over the $N!$ number of permutations of the integers $1,2,\ldots,N$, $\{p_j\}_{j=1}^N$ are the (yet undetermined) quasi-momenta and $S(p_j,p_k)$ is the two particle scattering amplitude, which is a pure phase. From a physical point of view, each term in the wave function (3.16) represents a superposition of plane waves with a particular particle ordering. The fact that the relative phases of these plane waves are given by the product of the two particle scattering amplitudes is a consequence of integrability: the extra conservation laws restrict the dynamics so severely that every multiparticle scattering event factorizes to subsequent two particle scatterings, and the order of these scatterings is not relevant.

The wave function (3.16) is rather general, model independent. The details of the specific models enter through the two-body scattering phase $S(p_j,p_k)$, which can be obtained by substituting the state (3.15) with (3.16) into the eigenvalue equation $H\,|\Psi\rangle = E\,|\Psi\rangle$. For the XXZ model this yields the result:

$$S(p_j,p_k) = e^{i\delta(p_j,p_k)} = -\frac{e^{i(p_j+p_k)} + 1 - 2\Delta e^{ip_k}}{e^{i(p_j+p_k)} + 1 - 2\Delta e^{ip_j}}. \tag{3.17}$$

The energy of the eigenstate is also obtained from the eigenvalue equation and can be written as a sum of one-particle contributions $E = \sum_{j=1}^N e(p_j)$. For the XXZ model, the one-particle energy takes the form

$$E = \sum_{j=1}^{N} e(p_j) = 4\sum_{j=1}^{N}(\cos p_j - \Delta), \tag{3.18}$$

while the total lattice momentum is simply given by the sum of the quasi-momenta:

$$P = \sum_{j=1}^{N} p_j \mod 2\pi. \tag{3.19}$$

The expressions corresponding to the XXX model are recovered from (3.17) and (3.18) by setting $\Delta = 1$. The scattering phase (3.17) does not depend on the difference of the quasi-momenta. However, a new

parametrization is possible by introducing the rapidity variables:

$$e^{ip(\lambda)} = \frac{\lambda - i/2}{\lambda + i/2} \qquad \text{(in the XXX model)}, \tag{3.20}$$

$$e^{ip(\lambda)} = \frac{\sin(\lambda - i\eta/2)}{\sin(\lambda + i\eta/2)} \qquad \text{(in the XXZ model)}, \tag{3.21}$$

where the newly introduced parameter η is related to the anisotropy Δ by $\cosh\eta = \Delta$. For simplicity, we assume that $\Delta > 1$ and $\eta \in \mathbb{R}$. We note that this is just a technical simplification and does not restrict the validity of our subsequent results. All other domains of the parameter space can be treated by either letting η become complex, or equivalently using different parametrizations for the different regions. For more details, we refer to the so-called Orbach parametrization, discussed for example in [58, 59]. Using the rapidity variables, the two-particle scattering phase simplifies and becomes of difference form, $S(p_j, p_k) = S(p(\lambda_j), p(\lambda_k)) = S(\lambda_j - \lambda_k)$, where

$$S(\lambda) = \frac{\lambda + i}{\lambda - i} \qquad \text{(in the XXX model)}, \tag{3.22}$$

$$S(\lambda) = \frac{\sin(\lambda + i\eta)}{\sin(\lambda - i\eta)} \qquad \text{(in the XXZ model)}. \tag{3.23}$$

With the rapidity variables, the eigenenergies can be written as $E = \sum_{j=1}^{N} e(p(\lambda_j)) = \sum_{j=1}^{N} e(\lambda)$, where the one-particle energy $e(\lambda)$ is given by

$$e(\lambda) = -\frac{2}{\lambda^2 + 1/4} \qquad \text{(in the XXX model)}, \tag{3.24}$$

$$e(\lambda) = \frac{4\sinh^2(\eta)}{\cos(2\lambda) - \cosh(\eta)} \qquad \text{(in the XXZ model)}. \tag{3.25}$$

So far we have seen that the states given by (3.15) and (3.16) together with (3.17) can be eigenstates of the Hamiltonian. However, the quasi-momenta $\{p_j\}_{j=1}^{N}$ are yet undetermined. To fix their values, we have to impose the periodic boundary condition. This leads to a set of consistency relations, known as the Bethe equations, which in a model independent way are written as:

$$e^{ip_j L} \prod_{k \neq j} S(p_j, p_k) = 1, \qquad j = 1, \ldots, L. \tag{3.26}$$

For the specific cases of the XXX and XXZ models, using the rapidity parametrization, the Bethe equations

take the explicit forms:

$$\left(\frac{\lambda_j - i/2}{\lambda_j + i/2}\right)^L \prod_{k\neq j} \frac{\lambda_j - \lambda_k + i}{\lambda_j - \lambda_k - i} = 1, \quad j = 1,\dots,L \quad \text{(in the XXX model)}, \tag{3.27}$$

$$\left(\frac{\sin(\lambda_j - i\eta/2)}{\sin(\lambda_j + i\eta/2)}\right)^L \prod_{k\neq j} \frac{\sin(\lambda_j - \lambda_k + i\eta)}{\sin(\lambda_j - \lambda_k - i\eta)} = 1, \quad j = 1,\dots,L \quad \text{(in the XXZ model)}. \tag{3.28}$$

This completes the CBA solution: the quantum mechanical eigenvalue problem is reduced to solving a set of coupled, non-linear equations, and the eigenstates and eigenenergies are constructed analytically. Even though in the calculations above our main focus was on the Heisenberg models, it may be evident even from this brief summary that the CBA technique is rather general and applicable to other integrable models as well. An important example for such a system is the Lieb-Liniger model [3, 60]. The main steps of the method are always the same: first, finding the two particle scattering amplitude. Then constructing the Bethe wave function and checking that it is indeed an eigenstate, and at the same time obtaining the eigenenergy. Finally, imposing the periodic boundary condition, which selects the admissible values of the quasi-momenta through the Bethe equations.

Before turning to the next section, we need to introduce one more quantity that will play a key role later in the dissertation. As a first step, let's take the logarithm of the Bethe equations (3.26), which leads to

$$p(\lambda_j)L + \sum_{k\neq j} \delta(\lambda_j - \lambda_k) = 2\pi I_j, \qquad j = 1,\dots,L, \tag{3.29}$$

where the $I_j \in \mathbb{Z}$ quantum numbers can be used to parametrize the states. Taking the derivative of this equation with respect to the rapidities defines the so-called Gaudin matrix:

$$G_{jk} = \frac{\partial}{\partial \lambda_k}(2\pi I_j) = \delta_{jk}\left[p'(\lambda_j)L + \sum_{l=1}^{N} \varphi(\lambda_j - \lambda_l)\right] - \varphi(\lambda_j - \lambda_k), \qquad j,k = 1,\dots,N, \tag{3.30}$$

where $\varphi(\lambda) = -i\frac{\partial}{\partial\lambda}\log(S(\lambda)) = \frac{\partial}{\partial\lambda}\delta(\lambda)$. The Gaudin matrix has two physical meanings: on the one hand, its determinant describes the state density in rapidity space. This can be seen from the first equality in (3.30): states are evenly distributed in the space of the quantum numbers and the determinant of the Gaudin matrix is the Jacobian of the variable change $\lambda_j \leftrightarrow I_j$. On the other hand, $\det G$ also gives the norm of the Bethe wave function [61, 62]. (This is true in other integrable models as well, not just in the Heisenberg spin chain. For the case of the Lieb-Liniger model, see [63].) For the precise mathematical relation, see Eq. (3.65) in the next section.

As we shall see in Chapters 4 and 5, the Gaudin matrix is also an important ingredient in the calculation of current mean values in integrable models.

3.3 Quantum Inverse Scattering Method

In the previous section, it was shown how the coordinate Bethe Ansatz enables one to solve the eigenvalue problem of integrable quantum systems. Even though the CBA is a useful tool to obtain eigenenergies and eigenstates, it does not reveal too much about why these models are solvable in the first place. The factorization of scatterings is argued based on the existence of extra conserved charges, however CBA does not provide a method to construct such charges. Moreover, the representation of the eigenstates (3.15) involves a huge sum over permutations. This complexity makes it hard to use this representation to obtain more involved quantities, such as correlation functions.

A better understanding of quantum integrability is provided by the so-called Quantum Inverse Scattering Method (QISM), which was developed by the Leningrad School in the 1970's and 80's (their work is contained in [12]). The QISM was introduced as a quantization of the classical inverse scattering method, which in turn was established as a powerful framework to solve classical integrable non-linear differential equations. (In this dissertation, we do not discuss classical integrability; a very deep treatment of the classical inverse scattering method can be found in [64], while a more general introduction to classical integrability in [65].) Building on notions coming from its classical counterpart, QISM provides a systematic way of constructing and solving integrable quantum systems. It also sheds light on the connection between one-dimensional quantum systems and two-dimensional classical statistical physics models. Here we do not explain this connection, only refer to [11].

In this section, we briefly summarize the main elements of the QISM. For a deeper understanding of the method, we refer to [12, 66].

3.3.1 Transfer matrix

Before turning to the examples of the spin-1/2 Heisenberg models, first let's discuss the main ideas of the QISM framework in a more general setting: we consider integrable spin systems on a lattice of size L, with periodic boundary condition and with some local Hilbert space $\mathcal{H}_j = \mathbb{C}^d$ at each site j, where d is an integer (for spin-1/2 systems, $d = 2$). The Hilbert space of the whole system is then the tensor product space $\mathcal{H} = \otimes_{j=1}^{L} \mathcal{H}_j$. Furthermore, we introduce an auxiliary space V_a, which in general can differ from $\mathcal{H}_j$. The main objective of the QISM framework is to construct a family of commuting operators, so-called transfer matrices acting on $\mathcal{H}$ that can generate the conserved charges of the system, and to diagonalize these operators. The main roles in this construction are played by the so-called Lax-operator $\mathcal{L}_{aj}(u)$ that acts on $\mathcal{H}_j \otimes V_a$ and the R-matrix $R_{ab}(u,v)$, acting on two different copies of the auxiliary space $V_a \otimes V_b$. These operators are the functions of the spectral parameters $u, v \in \mathbb{C}$. The Lax-operator is used to build up the monodromy matrix

$$T_a(u) = \mathcal{L}_{aL}(u)\mathcal{L}_{aL-1}(u)\dots\mathcal{L}_{a1}(u), \tag{3.31}$$

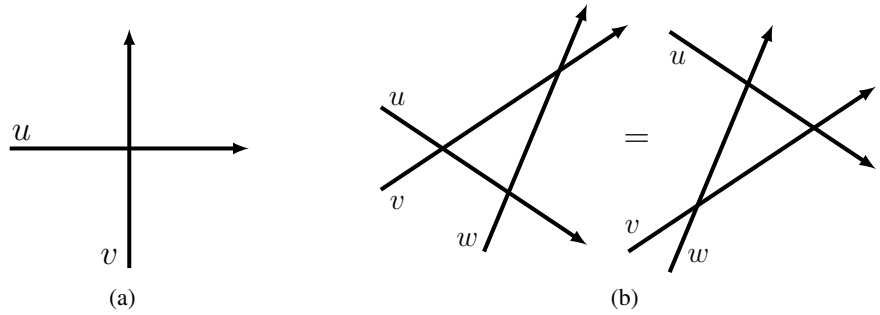

Figure 3.2: (a) Graphical representation of $R(u,v)$: the arrows represent the spaces on which the R-matrix acts, u and v are the spectral parameters. (b) Graphical representation of the Yang-Baxter equation: the order of the R-matrices in the products is determined by their positions along the horizontal direction.

which is an operator that acts on the space $\mathcal{H} \otimes V_a$. The transfer matrix $t(u)$ is then defined as the trace of the monodromy matrix over the auxiliary space:

$$t(u) = \mathrm{Tr}_a T_a(u). \tag{3.32}$$

In order to use the transfer matrix as a generator of the conserved, local charges of an integrable system, we require that transfer matrices evaluated at different spectral parameters commute with each other:

$$[t(u), t(v)] = 0. \tag{3.33}$$

Obviously, this constraint isn't satisfied in general, but only for special choices of $\mathcal{L}(u)$ and $R(u,v)$. In order for (3.33) to hold, the Lax-operators have to satisfy the exchange relation

$$R_{ab}(u,v)\mathcal{L}_{aj}(u)\mathcal{L}_{bj}(v) = \mathcal{L}_{bj}(v)\mathcal{L}_{aj}(u)R_{ab}(u,v), \tag{3.34}$$

while the R-matrix has to satisfy a similar relation, the so-called Yang-Baxter equation:

$$R_{ab}(u,v)R_{ac}(u,w)R_{bc}(v,w) = R_{bc}(v,w)R_{ac}(u,w)R_{ab}(u,v). \tag{3.35}$$

The R-matrix and the Yang-Baxter equation have a useful graphical representation shown in Fig. 3.2 that can be used to simplify calculations with these quantities.

It is not hard to show that when (3.34) and (3.35) hold, the monodromy matrix also satisfies an exchange relation

$$R_{ab}(u,v)T_a(u)T_b(v) = T_b(v)T_a(u)R_{ab}(u,v). \tag{3.36}$$

This relation is trivially verified by using the graphical notation, see Fig. 3.3. The commutation of the transfer matrices then can be derived rather easily from (3.36). Once this commutation is established, the

transfer matrix can generate the conserved, local charges:

$$\hat{Q}_\alpha \propto \frac{d^{\alpha-1}}{du^{\alpha-1}} \log t(u)\Big|_{u=u^*}, \tag{3.37}$$

where the special point u^* around which the expansion is made has to be specified for a given model in order for (3.37) to yield local and Hermitian charges (as we will see, in the models that we consider, $u^* = 0$ can be chosen). The operators $\hat{Q}_\alpha$ mutually commute with each other $[\hat{Q}_\alpha, \hat{Q}_\beta] = 0$, which is guaranteed by (3.33), and the Hamiltonian of the model in question is a member of this family. The locality of the charges means that they can be written as a sum of local charge density operators

$$\hat{Q}_\alpha = \sum_{j=1}^{L} \hat{q}_\alpha(j), \tag{3.38}$$

where $\hat{q}_\alpha(j)$ is an operator with a support of α sites: it acts non-trivially only on α sites, around site j. Since the relation (3.37) only specifies the total charges, the charge densities are not uniquely defined: for any local operator $\hat{G}(j)$, the modified charge density $\hat{q}'_\alpha(j) = \hat{q}_\alpha + \hat{G}(j+1) - \hat{G}(j)$ produces the same integrated charge as the original density. This transformation can be thought of as a gauge freedom and is explained in more detail in [67]. Nevertheless, our main focus will be on the mean values of the charges, which are not effected by this gauge choice, therefore we do not discuss it further here. Also, explicit expressions for some of the charge densities of the Heisenberg models can be found in Appendix B.

Finding the integrable structure behind a model given by its Hamiltonian is not necessary trivial. However, the construction works in the other way around as well and can be used to systematically find integrable systems. From this point of view, the Yang-Baxter equation (3.35) is the central element: after fixing the dimension of the auxiliary space, one can look for solutions of (3.35). Once a solutions is found, the corresponding Lax-operators have to be obtained from (3.34). With the known $R(u,v)$ and $\mathcal{L}(u)$, the transfer matrix, and the charges are easily calculated.

So far, we kept our description rather general. Now, we make some specifications that will be pertinent to the models treated in this dissertation. First, we consider the case when the auxiliary space V_a is isomorphic to the local physical space $\mathcal{H}_j$. In this case, the Lax-operators can be chosen to be identical to the R-matrix, since from the Yang-Baxter equation (3.35), it follows that this choice satisfies (3.34). Consequently, the monodromy matrix is built from the R-matrices. In general, one can include arbitrary inhomogeneity parameters $\xi_j \in \mathbb{C}$ for each site, leading to

$$T_a(u) = R_{aL}(u, \xi_L) R_{aL-1}(u, \xi_{L-1}) \dots R_{a1}(u, \xi_1), \tag{3.39}$$

however we will stick to the homogeneous case, when $\xi_j = 0$ for all $j = 1, \dots, L$.

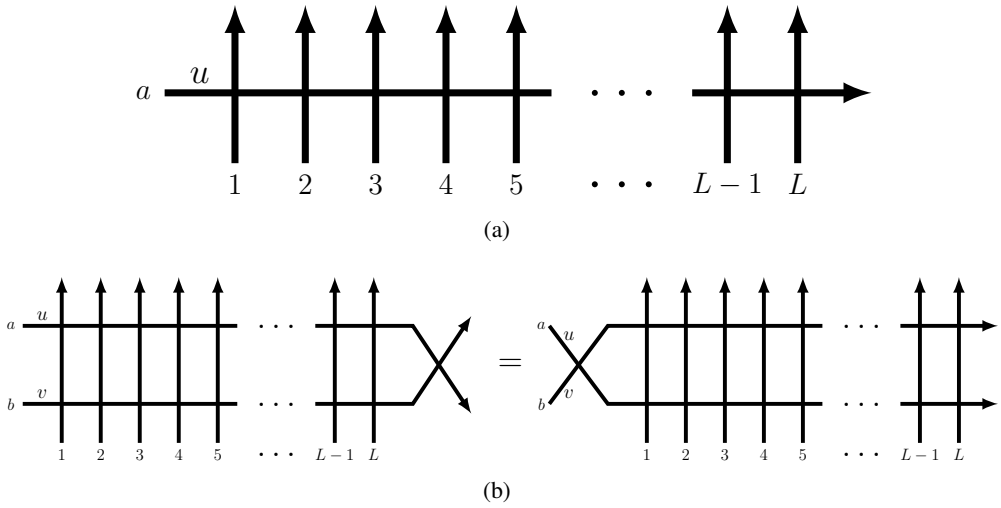

Figure 3.3: (a) Graphical representation of the monodromy matrix: the horizontal arrow corresponds to the auxiliary space with rapidity u, while the vertical arrows represent the physical spaces. Here we illustrate the case when the Lax-operators are chosen to be identical to the R-matrix without inhomogeneities. (b) Graphical representation of the RTT-relation: by consecutively using the graphical Yang-Baxter equation, the crossing of the horizontal lines can be moved from one end of the chain to the other, verifying the equality.

Second, we will assume that the R-matrix satisfies the so-called regularity and unitarity conditions

$$\begin{aligned} R(u,u) &= \mathcal{P}, \\ R_{ab}(u,v)R_{ba}(v,u) &= \mathbb{1}, \end{aligned} \tag{3.40}$$

where $\mathcal{P}$ is the permutation operator that acts as $\mathcal{P}R_{ab}(u,v)\mathcal{P} = R_{ba}(u,v)$.

Finally, we will be interested in R-matrices that are of difference form:

$$R(u,v) = R(u-v). \tag{3.41}$$

It is worth mentioning that there are examples of integrable systems, whose R-matrix is not of this form, the most notable one being the one-dimensional Hubbard model [68].

As an explicit example, we present here the specific expressions for the R-matrices of the Heisenberg models. In the case of the $U(1)$ symmetric XXX and XXZ models, the R-matrix takes the form

$$R^{XXX/XXZ}(u) = \begin{pmatrix} 1 & 0 & 0 & 0 \\ 0 & b(u) & c(u) & 0 \\ 0 & c(u) & b(u) & 0 \\ 0 & 0 & 0 & 1 \end{pmatrix}, \tag{3.42}$$

with the functions $b(u)$ and $c(u)$ defined as

$$b(u) = \frac{u}{u+i}, \qquad c(u) = \frac{i}{u+i} \qquad \text{(in the XXX model)}, \tag{3.43}$$

$$b(u) = \frac{\sin(u)}{\sin(u+i\eta)}, \qquad c(u) = \frac{\sin(i\eta)}{\sin(u+i\eta)} \qquad \text{(in the XXZ model)}. \tag{3.44}$$

In the case of the XYZ model, the breaking of the $U(1)$ symmetry changes the form of the R-matrix as well:

$$R^{XYZ}(u) = \frac{1}{h(u+\eta)} \begin{pmatrix} a(u) & 0 & 0 & d(u) \\ 0 & b(u) & c(u) & 0 \\ 0 & c(u) & b(u) & 0 \\ d(u) & 0 & 0 & a(u) \end{pmatrix}, \tag{3.45}$$

Here the inclusion of the normalization factor $1/h(u+\eta)$ is for later convenience and the significant difference compared to the XXZ R-matrix is the appearance of the non-zero $d(u)$ function in the bottom left and upper right elements of the matrix. The newly introduced functions in (3.45) are given by

$$\begin{aligned} a(u) &= \vartheta_4(\eta|\tau)\vartheta_1(u+\eta|\tau)\vartheta_4(u|\tau), \\ b(u) &= \vartheta_4(\eta|\tau)\vartheta_4(u+\eta|\tau)\vartheta_1(u|\tau), \\ c(u) &= \vartheta_1(\eta|\tau)\vartheta_4(u+\eta|\tau)\vartheta_4(u|\tau), \\ d(u) &= \vartheta_1(\eta|\tau)\vartheta_1(u+\eta|\tau)\vartheta_1(u|\tau), \\ h(u) &= \vartheta_4(0|\tau)\vartheta_4(u|\tau)\vartheta_1(u|\tau), \end{aligned} \tag{3.46}$$

where $\eta \in \mathbb{C}$ is a parameter of the model, while $\vartheta_i(u|\tau)$ ($i \in \{1,2,3,4\}$) denote the elliptic theta functions with parameter τ and argument u. The definition of these functions and a list of their useful properties are presented in Appendix D. For brevity, from now on we omit the dependence on the parameter τ, and simply write $\vartheta_i(u) = \vartheta_i(u|\tau)$.

It is easy to check that both (3.42) and (3.45) possess the regularity and unitarity properties (3.40). Moreover, $R^{XYZ}(u)$ also satisfies the so-called crossing relation:

$$R_{12}^{XYZ}(u)\sigma_1^y[R_{12}^{XYZ}(u-\eta)]^{t_1}\sigma_1^y = \frac{h(u-\eta)}{h(u)}\mathbb{1}, \tag{3.47}$$

where $[\ldots]^{t_1}$ denotes partial transpose with respect to the first space. This property will be used in Chapter 5.

For the XXX/XXZ models the conserved charges are obtained from their corresponding transfer matrices as

$$\hat{Q}_\alpha = i\,\frac{d^{\alpha-1}}{du^{\alpha-1}}\big(\log t^{XXX/XXZ}(u)\big)\Big|_{u=0}, \tag{3.48}$$

where the factor of i was included to ensure the hermiticity of the operators. The appropriate Hamiltonians

(3.5) and (3.8) are given by $H = \kappa \hat{Q}_2$, with κ being $\kappa = 2$ and $\kappa = 2\sinh\eta$ for the XXX and XXZ models, respectively, and with $\Delta = \cosh\eta$.

In the case of the XYZ model, our conventions for the R-matrix (3.45) lead to a slightly different relation between the transfer matrix and the conserved charges. Namely, the Hamiltonian (3.10) can be derived as

$$\frac{d}{du}\big(\log t^{XYZ}(u)\big)\Big|_{u=0} = H^{XYZ} - \frac{1}{2}LJ_0, \tag{3.49}$$

with the coefficients in the Hamiltonian defined as

$$\begin{aligned} J_x &= \frac{\vartheta_1'(0)}{\vartheta_4(0)}\left(\frac{\vartheta_4(\eta)}{\vartheta_1(\eta)} + \frac{\vartheta_1(\eta)}{\vartheta_4(\eta)}\right), \qquad J_z = \frac{\vartheta_1'(\eta)}{\vartheta_1(\eta)} - \frac{\vartheta_4'(\eta)}{\vartheta_4(\eta)}, \\ J_y &= \frac{\vartheta_1'(0)}{\vartheta_4(0)}\left(\frac{\vartheta_4(\eta)}{\vartheta_1(\eta)} - \frac{\vartheta_1(\eta)}{\vartheta_4(\eta)}\right), \qquad J_0 = \frac{\vartheta_1'(\eta)}{\vartheta_1(\eta)} + \frac{\vartheta_4'(\eta)}{\vartheta_4(\eta)}. \end{aligned} \tag{3.50}$$

The higher charges of the XYZ model are obtained as

$$\hat{Q}_\alpha = (i)^{\alpha-2}\frac{d^{\alpha-1}}{du^{\alpha-1}}\left(\log t^{XYZ}(u)\right)\big|_{u=0}. \tag{3.51}$$

3.3.2 Algebraic Bethe Ansatz

In the framework of QISM, the diagonalization of the transfer matrix (and the Hamiltonian) is achieved by the algebraic Bethe Ansatz (ABA) method. The ABA can be considered as a second quantization of the coordinate Bethe Ansatz: the eigenstates of the system are constructed by applying certain operators (which from this point of view are quasi-particle creation operators) to a reference state. It is important to note that the usual ABA technique is only applicable to $U(1)$ symmetric models. A generalization of the method to non $U(1)$ symmetric systems is considered in the next subsection.

To obtain the eigenstates of a general $U(1)$ symmetric integrable model with an R-matrix of the form (3.42), first let's consider the monodromy matrix (3.31) as a 2×2 matrix in the auxiliary space:

$$T_a(u) = \begin{pmatrix} A(u) & B(u) \\ C(u) & D(u) \end{pmatrix}, \tag{3.52}$$

where now the elements $A(u)$, $B(u)$, $C(u)$ and $D(u)$ are operators acting on the physical Hilbert space $\mathcal{H}$. These operators satisfy certain commutation relations that are encoded in the RTT-relation (3.36). Here we only list those of these commutation relations that are used in the ABA construction, the rest can be found in Appendix A:

$$\begin{aligned} &[A(u),A(v)] = [B(u),B(v)] = [C(u),C(v)] = [D(u),D(v)] = 0, \\ &A(u)B(v) = f(v,u)B(v)A(u) + g(u,v)B(u)A(v), \\ &D(u)B(v) = f(u,v)B(v)D(u) + g(v,u)B(u)D(v), \end{aligned} \tag{3.53}$$

where

$$f(u,v) = \frac{1}{b(u-v)}, \qquad g(u,v) = \frac{c(u-v)}{b(u-v)}. \tag{3.54}$$

To construct the eigenstates of the transfer matrix $t(u) = A(u) + D(u)$, we can choose (just like in CBA) the state $|0\rangle$ with all spins up as a reference-state/pseudo vacuum. The action of the operators $A(u)$, $D(u)$ and $C(u)$ on $|0\rangle$ easily follow from the form of the R- and monodromy matrix:

$$A(u)\,|0\rangle = a(u)\,|0\rangle\,, \qquad D(u)\,|0\rangle = d(u)\,|0\rangle\,, \qquad C(u)\,|0\rangle = 0, \tag{3.55}$$

with $a(u) = 1$ and $d(u) = \big(b(u)\big)^L$. (Here we introduced the function $a(u)$ just to keep the computation general. With other normalizations of the R-matrix, $a(u)$ can differ from 1.) Using $|0\rangle$ as a reference state, we can construct the eigenstates of $t(u)$ by repeatedly applying the operator $B(u)$ on $|0\rangle$:

$$|\lambda_1 \ldots, \lambda_N\rangle = B(\lambda_1 - \xi) \ldots B(\lambda_N - \xi)\,|0\rangle\,, \tag{3.56}$$

where the constant ξ was introduced to keep the conventions consistent with the ones introduced in the previous section, and the values of the rapidities $\{\lambda_j\}_{j=1}^N$ are yet undetermined. (Similarly, the dual eigenstates can be constructed by applying the $C(\lambda)$ operators on the dual vacuum $\langle 0|$.) Using the commutation relations (3.53) and the properties of the reference state (3.55), direct computation gives that the operators $A(u)$ and $D(u)$ act on the states (3.56) as follows:

$$\begin{aligned}
A(u)\,|\lambda_1, \ldots, \lambda_N\rangle &= \Lambda^A\big(u|\{\lambda_j\}\big)\,|\lambda_1, \ldots, \lambda_N\rangle + \sum_{j=1}^N \Lambda_j^A\big(u|\{\lambda_j\}\big)\,\big|\lambda_1, \ldots, \lambda_{j-1}, u, \lambda_{j+1}, \ldots, \lambda_N\big\rangle\,, \\
D(u)\,|\lambda_1, \ldots, \lambda_N\rangle &= \Lambda^D\big(u|\{\lambda_j\}\big)\,|\lambda_1, \ldots, \lambda_N\rangle + \sum_{j=1}^N \Lambda_j^D\big(u|\{\lambda_j\}\big)\,\big|\lambda_1, \ldots, \lambda_{j-1}, u, \lambda_{j+1}, \ldots, \lambda_N\big\rangle\,,
\end{aligned} \tag{3.57}$$

with

$$\begin{aligned}
\Lambda^A\big(u|\{\lambda_j\}\big) &= a(u)\prod_{j=1}^N f(\lambda_j - \xi, u), \\
\Lambda_j^A\big(u|\{\lambda_j\}\big) &= a(\lambda_j - \xi)g(u, \lambda_j - \xi)\prod_{k\neq j} f(\lambda_k - \xi, \lambda_j - \xi), \\
\Lambda^D\big(u|\{\lambda_j\}\big) &= d(u)\prod_{j=1}^N f(u, \lambda_j - \xi), \\
\Lambda_j^D\big(u|\{\lambda_j\}\big) &= d(\lambda_j - \xi)g(\lambda_j - \xi, u)\prod_{k\neq j} f(\lambda_j - \xi, \lambda_k - \xi).
\end{aligned} \tag{3.58}$$

From (3.57) and (3.58) it trivially follows that the state (3.56) is an eigenstate of the transfer matrix, given

that the rapidities $\{\lambda_j\}_{j=1}^N$ satisfy a set of constraints, the Bethe equations:

$$\frac{a(\lambda_j-\xi)}{d(\lambda_j-\xi)}\prod_{k\neq j}\frac{f(\lambda_k-\xi,\lambda_j-\xi)}{f(\lambda_j-\xi,\lambda_k-\xi)}=1, \qquad j=1,\ldots,N. \tag{3.59}$$

If the set of rapidities satisfy the Bethe equations (3.59), the state (3.56) is called an on-shell Bethe state, while if they do not, an off-shell Bethe state. The transfer matrix eigenvalue for an on-shell state is then given by

$$\Lambda\big(u|\{\lambda_j\}\big)=\Lambda^A\big(u|\{\lambda_j\}\big)+\Lambda^D\big(u|\{\lambda_j\}\big)=a(u)\prod_{j=1}^N f(\lambda_j-\xi,u)+d(u)\prod_{j=1}^N f(u,\lambda_j-\xi). \tag{3.60}$$

This completes the diagonalization of the transfer matrix. Since the Hamiltonian and the higher charges are related to the transfer matrix according to (3.48), the energy and charge eigenvalues can be obtained from (3.60) by taking the appropriate derivatives:

$$H\,|\lambda_1,\ldots,\lambda_N\rangle=\left(\sum_{j=1}^N e(\lambda_j)\right)|\lambda_1,\ldots,\lambda_N\rangle\,, \qquad \text{with} \quad e(\lambda)=\kappa q_2(\lambda), \tag{3.61}$$

$$\hat{Q}_\alpha\,|\lambda_1,\ldots,\lambda_N\rangle=\left(\sum_{j=1}^N q_\alpha(\lambda_j)\right)|\lambda_1,\ldots,\lambda_N\rangle\,, \quad \text{with} \quad q_\alpha(\lambda)=\frac{\partial^{\alpha-2}}{\partial x^{\alpha-2}}q_2(\lambda-x)\bigg|_{x=0}. \tag{3.62}$$

To recover the explicit expressions for the cases of the XXX and XXZ models that were obtained from CBA in the previous section, one only needs to substitute the functions (3.43) or (3.44) into (3.54) and then to the appropriate equations. The constant shift ξ is equal to $\xi=i/2$ and $\xi=i\eta/2$, while $\kappa=2$ and $\kappa=2\sinh\eta$ for the XXX and XXZ models, respectively. The charge eigenvalue function $q_2(\lambda)$ is given by

$$q_2(\lambda)=\frac{-1}{\lambda^2+1/4} \qquad \text{(in the XXX model)}, \tag{3.63}$$

$$q_2(\lambda)=\frac{-\sinh\eta}{\sin(\lambda-i\eta/2)\sin(\lambda+i\eta/2)} \qquad \text{(in the XXZ model)}. \tag{3.64}$$

It can be easily checked that (3.63) and (3.64) are equivalent to the previous results (3.24) and (3.25).

As it was already mentioned in the previous section, the norms of the on-shell Bethe states (3.56) are given by the Gaudin determinant [62]:

$$\langle 0|\prod_{j=1}^N C(\lambda_j)\prod_{j=1}^N B(\lambda_j)|0\rangle=\tilde{\kappa}^N\left(\prod_{j\neq k}f(\lambda_j,\lambda_k)\right)\det G_\lambda, \tag{3.65}$$

where $\tilde{\kappa}=1$ and $\tilde{\kappa}=\sinh(\eta)$ for the XXX and XXZ models, respectively. To clarify our notation, from now on the expression $|\lambda_1,\ldots,\lambda_N\rangle$ will refer to Bethe states that are normalized to 1, while when we use the states (3.56), we will write out the expression $\prod_j B(\lambda_j)\,|0\rangle$.

3.3.3 Generalized Algebraic Bethe Ansatz

The coordinate and algebraic Bethe Ansatz methods discussed in previous sections are robust analytical approaches for addressing the eigenvalue problems in integrable quantum systems. However, each approach has certain limitations. For CBA, the model's $U(1)$ symmetry and particle number conservation are essential: eigenstates are built from a reference state $|0\rangle$, with the Hamiltonian diagonalized within subspaces invariant under the symmetry operator (e.g., $\hat{S}^z$ in the XXX/XXZ models). Similarly, ABA also utilizes the $U(1)$ symmetry, though this may not be immediately obvious. Here, the reference state $|0\rangle$ is required to be annihilated by the lower left element of the monodromy matrix across all rapidity values, a feature ensured by the $U(1)$ symmetry.

Some integrable models, however, lack $U(1)$ symmetry. Unlike the XXX and XXZ spin chains, the XYZ model does not include $\hat{S}^z$ among its commuting conserved quantities, thus lacking $U(1)$ symmetry. Consequently, the standard coordinate/algebraic Bethe Ansatz methods fail for this model. Nonetheless, the XYZ model remains exactly solvable, with its eigenvalues and eigenstates first derived by Baxter using his $T-Q$ relations [11]. Later work [69] successfully extended the ABA to apply to the XYZ model, and other diagonalization approaches have since been developed as well. For instance, the Separation of Variables (SoV) method was employed in [70], while the so-called off-diagonal Bethe Ansatz was utilized in [71, 72]. Here, we focus on the construction of [69] as it aligns best with our aims. (Our description below closely follows that of [73].)

As it was already mentioned, the challenge with ABA arises because, for the XYZ model, no global reference state $|0\rangle$ exists that is annihilated by $C(u)$ for all values of u. To address this, a gauge transformation was introduced in [69] on the R-matrix, which enables the construction of a family of reference states. (For brevity, in this subsection we omit the XYZ superscript when referring to the R-matrix of the XYZ model.)

To illustrate this transformation, we first examine the local R-matrix (3.45) as a 2×2 matrix in the auxiliary space, with elements that act on the local physical space $\mathbb{C}^2$:

$$R_{aj}(u)=\begin{pmatrix}\alpha_j(u) & \beta_j(u)\\ \gamma_j(u) & \delta_j(u)\end{pmatrix}, \tag{3.66}$$

where $\alpha_j(u),\beta_j(u),\gamma_j(u),\delta_j(u)\in \mathrm{End}(\mathbb{C}^2_j)$. Now let's introduce a local gauge transformation in the following way:

$$R^l_{aj}(u)=M^{-1}_{j+l}(u)R_{aj}(u)M_{j+l-1}(u)=\begin{pmatrix}\alpha^l_j(u) & \beta^l_j(u)\\ \gamma^l_j(u) & \delta^l_j(u)\end{pmatrix}, \tag{3.67}$$

where M_k is a 2×2 invertible, numerical matrix and l is an integer. Obviously, this transformation affects the monodromy matrix only by a simple linear transformation:

$$T^l_a(u)=R^l_{aL}(u)\dots R^l_{a1}(u)=M^{-1}_{L+l}(u)T_a(u)M_l(u)=\begin{pmatrix}A_l(u) & B_l(u)\\ C_l(u) & D_l(u)\end{pmatrix}. \tag{3.68}$$

Now $M_k(u)$ can be chosen in such a way that ensures the existence of a local reference state at each site, annihilated by the bottom left element of the corresponding local matrix $R^l_{aj}(u)$, for all u. To this end, we define $M_k(u)$ as:

$$M_k(u;s,t) = \begin{pmatrix} \vartheta_1(s+k\eta-u) & \frac{1}{g(\tau_k)}\vartheta_1(t+k\eta+u) \\ \vartheta_4(s+k\eta-u) & \frac{1}{g(\tau_k)}\vartheta_4(t+k\eta+u) \end{pmatrix}, \tag{3.69}$$

where $g(x) = \vartheta_1(x)\vartheta_4(x)$, $\tau_k = \frac{s+t}{2} + k\eta - \pi/2$ and s and t are two arbitrary, but fixed complex parameters, which we will not denote in the following. By using the theta function addition theorems listed in Appendix D, it is easily verified that the local state $\left|\omega^l_j\right\rangle \in \mathbb{C}^2_j$, defined as

$$\left|\omega^l_j\right\rangle = \vartheta_1(s+(j+l)\eta)\left|\uparrow_j\right\rangle + \vartheta_4(s+(j+l)\eta)\left|\downarrow_j\right\rangle, \tag{3.70}$$

is annihilated by $\gamma^l_j(u)$ for all u:

$$\gamma^l_j(u)\left|\omega^l_j\right\rangle = 0. \tag{3.71}$$

Here, $\left|\uparrow_j / \downarrow_j\right\rangle$ denote the standard basis elements at site j. We can also compute the actions of $\alpha^l_j(u)$ and $\delta^l_j(u)$ on $\left|\omega^l_j\right\rangle$:

$$\begin{aligned} \alpha^l_j(u)\left|\omega^l_j\right\rangle &= \left|\omega^{l-1}_j\right\rangle, \\ \delta^l_j(u)\left|\omega^l_j\right\rangle &= \frac{h(u)}{h(u+\eta)}\left|\omega^{l+1}_j\right\rangle. \end{aligned} \tag{3.72}$$

Using the local relations (3.71) and (3.72), we can see that the monodromy matrix elements act on the global state $|\Omega_l\rangle \in \mathcal{H}$, defined as

$$|\Omega_l\rangle = \left|\omega^l_1\right\rangle \otimes \left|\omega^l_2\right\rangle \otimes \cdots \otimes \left|\omega^l_L\right\rangle, \tag{3.73}$$

in the following way:

$$\begin{aligned} A_l(u)|\Omega_l\rangle &= |\Omega_{l-1}\rangle, \\ D_l(u)|\Omega_l\rangle &= \left(\frac{h(u)}{h(u+\eta)}\right)^L |\Omega_{l+1}\rangle, \\ C_l(u)|\Omega_l\rangle &= 0. \end{aligned} \tag{3.74}$$

Therefore, the vectors $\{|\Omega_l\rangle\}_{l\in\mathbb{Z}}$ form a family of reference states, on which the actions of the transformed monodromy matrix elements are known.

To construct the model's eigenstates, we consider the more general transformations of the monodromy matrix, without restrictions on the integer indices k and l:

$$T^{k,l}_a(u) = M^{-1}_k(u)T_a(u)M_l(u) = \begin{pmatrix} A_{k,l}(u) & B_{k,l}(u) \\ C_{k,l}(u) & D_{k,l}(u) \end{pmatrix}. \tag{3.75}$$

As it turns out, the commutation relations between $A_{k,l}(u)$, $B_{k,l}(u)$, $C_{k,l}(u)$ and $D_{k,l}(u)$ take a simple form. They can be derived from the RTT-relation (3.36), with the help of the known form of the transformation matrix (3.69) and the properties of the elliptic functions. The actual computation is rather long and technical, therefore we only present here the formulae that are used in the remaining steps of the calculation. For more details on how to actually obtain these relations, we refer to [69]. The commutation relations necessary for us are given by:

$$\begin{aligned}
&B_{k,l+1}(u)B_{k+1,l}(v) = B_{k,l+1}(v)B_{k+1,l}(u),\\
&A_{k,l}(u)B_{k+1,l-1}(v) = \alpha(u,v)B_{k,l-2}(v)A_{k+1,l-1}(u) - \beta_{l-1}(u,v)B_{k,l-2}(u)A_{k+1,l-1}(v),\\
&D_{k,l}(u)B_{k+1,l-1}(v) = \alpha(v,u)B_{k+2,l}(v)D_{k+1,l-1}(u) + \beta_{k+1}(u,v)B_{k+2,l}(u)D_{k+1,l-1}(v),
\end{aligned} \tag{3.76}$$

where the functions $\alpha(u,v)$ and $\beta(u,v)$ are defined as:

$$\alpha(u,v) = \frac{h(u-v-\eta)}{h(u-v)}, \qquad \beta_k(u,v) = \frac{h(\eta)h(\tau_k+v-u)}{h(v-u)h(\tau_k)}. \tag{3.77}$$

From here, the calculation closely parallels the conventional ABA, enabling the construction of the transfer matrix eigenstates by considering the vector

$$|\Psi_l(\lambda_1,\ldots,\lambda_n)\rangle = B_{l+1,l-1}(\lambda_1)\ldots B_{l+n,l-n}(\lambda_n)\,|\Omega_{l-n}\rangle\,, \tag{3.78}$$

where the rapidities $\{\lambda_k\}_{k=1}^n$ are not yet specified, and $n = L/2$. From (3.75) it is obvious that $t(u) = A(u)+D(u) = A_{l,l}(u)+D_{l,l}(u)$ for any l. By using the commutation relations (3.76), the actions of $A_{l,l}(u)$ and $D_{l,l}(u)$ on the state (3.78) are easily obtained:

$$\begin{aligned}
A_{l,l}(u)\,|\Psi_l(\lambda_1,\ldots,\lambda_n)\rangle &= \Lambda(u|\lambda_1,\ldots,\lambda_n)\,|\Psi_{l-1}(\lambda_1,\ldots,\lambda_n)\rangle +\\
&\quad + \sum_{j=1}^{n} \Lambda_j^l(u|\lambda_1,\ldots,\lambda_n)\,\big|\Psi_{l-1}(\lambda_1,\ldots,\lambda_{j-1},u,\lambda_{j+1},\ldots,\lambda_n)\big\rangle\,,\\
D_{l,l}(u)\,|\Psi_l(\lambda_1,\ldots,\lambda_n)\rangle &= \tilde{\Lambda}(u|\lambda_1,\ldots,\lambda_n)\,|\Psi_{l+1}(\lambda_1,\ldots,\lambda_n)\rangle +\\
&\quad + \sum_{j=1}^{n} \tilde{\Lambda}_j^l(u|\lambda_1,\ldots,\lambda_n)\,\big|\Psi_{l+1}(\lambda_1,\ldots,\lambda_{j-1},u,\lambda_{j+1},\ldots,\lambda_n)\big\rangle\,,
\end{aligned} \tag{3.79}$$

with

$$\begin{aligned}
\Lambda(u|\lambda_1,\ldots,\lambda_n) &= \prod_{k=1}^{n}\alpha(u,\lambda_k),\\
\Lambda_j^l(u|\lambda_1,\ldots,\lambda_n) &= -\beta_{l-1}(u,\lambda_j)\prod_{k\neq j}\alpha(\lambda_j,\lambda_k),\\
\tilde{\Lambda}(u|\lambda_1,\ldots,\lambda_n) &= \left(\frac{h(u)}{h(u+\eta)}\right)^L\prod_{k=1}^{n}\alpha(\lambda_k,\lambda),\\
\tilde{\Lambda}_j^l(u|\lambda_1,\ldots,\lambda_n) &= \beta_{l+1}(u,\lambda_j)\left(\frac{h(\lambda_j)}{h(\lambda_j+\eta)}\right)^L\prod_{k\neq j}\alpha(\lambda_k,\lambda_j).
\end{aligned} \tag{3.80}$$

The condition $n = L/2$ is necessary, because after $A_{l,l}(u)$ is commuted through all the $B(\lambda_k)$ operators in (3.78), finally the expression $A_{l+n,l-n}(u)\,|\Omega_{l-n}\rangle$ has to be evaluated. This is only possible by using (3.74), if $n = L/2$. The restriction on n also means that the method presented here only works for chains of even length.

As a last step, we multiply (3.78) with the factor $\exp(2\pi i l\theta)$ $(0 \leq \theta \leq 1)$ and sum it over all the integers:

$$|\Psi_\theta(\lambda_1,\ldots,\lambda_n)\rangle = \sum_{l=-\infty}^{\infty} e^{2\pi i l\theta}\,|\Psi_l(\lambda_1,\ldots,\lambda_n)\rangle\,. \tag{3.81}$$

Eq. (3.79) implies that the state (3.81) is an eigenstate of the transfer matrix, with eigenvalue

$$\Lambda_f(u) = e^{2\pi i\theta}\Lambda(u|\lambda_1,\ldots,\lambda_n) + e^{-2\pi i\theta}\tilde{\Lambda}(u|\lambda_1,\ldots,\lambda_n), \tag{3.82}$$

given that the rapidities satisfy the Bethe equations:

$$\left(\frac{h(\lambda_j)}{h(\lambda_j+\eta)}\right)^L = e^{4\pi i\theta}\prod_{\substack{k=1\\k\neq j}}^{n}\frac{\alpha(\lambda_j,\lambda_k)}{\alpha(\lambda_k,\lambda_j)}. \tag{3.83}$$

Since the Hamiltonian of the XYZ model is related to the transfer matrix through (3.49), it is obvious that the states (3.81) are also eigenstates of the Hamiltonian (3.10). The energy eigenvalues are given by

$$E = \frac{d}{du}\big(\log t(u)\big)\bigg|_{u=0} + \frac{LJ_0}{2}. \tag{3.84}$$

Equivalently, we can write the energies (3.84) as sums over the Bethe roots:

$$E = \sum_{j=1}^{n} e(\lambda_j) + \frac{LJ_0}{2} \quad \text{with} \quad e(\lambda) = \frac{h'(\lambda)}{h(\lambda)} - \frac{h'(\lambda+\eta)}{h(\lambda+\eta)}. \tag{3.85}$$

Furthermore, from (3.51) it follows that the eigenvalues of the higher charges can also be written as sums

over the rapidities:

$$\hat{Q}_\alpha |\lambda_1,\ldots,\lambda_n\rangle = \left(\sum_{j=1}^{n} q_\alpha(\lambda_j)\right) |\lambda_1,\ldots,\lambda_n\rangle \quad \text{with} \quad q_\alpha(\lambda) = (-i)^{\alpha-2}\frac{d^{\alpha-2}}{d\lambda^{\alpha-2}}e(\lambda). \tag{3.86}$$

The convergence of the sum in (3.81) requires a careful analysis. The results of [11] and [69] show that (3.81) sums to zero for all θ expect finitely many values of θ_j, and that 0 is among these θ_j. The situation simplifies by imposing the following restriction on η:

$$K\eta = m_1 2\pi + m_2 \pi\tau, \tag{3.87}$$

with K, m_1 and m_2 being integers. The quasi-periodicity of the elliptic theta functions makes $M_k(u)$, $T_a^{k,l}(u)$ and $|\Psi_l(\lambda_1,\ldots,\lambda_n)\rangle$ quasi-periodic functions of k and l in this case. With an appropriately chosen common normalizing factor, it can be achieved that they become periodic in k and l with period K. Consequently, the sum in (3.81) becomes finite, with $\theta = k/K$ for $k = 0,1,\ldots,K-1$. For further details on this special choice of η see [69]. However, in Chapter 5, when treating the problem of the current mean values in the XYZ model, we consider the general case, with no restriction on η.

Chapter 4

Current mean values in the XXZ model

As it was pointed out in Chapter 2, the current operators of integrable models play a crucial role in the formulation of the theory of Generalized Hydrodynamics. In the derivation of the equations of motion (2.10), GHD builds on the assumption that the current mean values can be expressed in a simple form, given by (2.9). However, in the seminal papers [46, 47] the expression (2.9) was only rigorously proven for the case of integrable quantum field theories. Separately, in [74] the spin current of the XXZ model was considered and (2.9) was verified. Nevertheless, the treatment of general current operators of interacting lattice models and quantum gases was missing, leaving a hole in the theoretical foundation of GHD.

Moreover, the question of current mean values is also interesting independently from GHD, from a more theoretical point of view. The equilibrium correlation functions of integrable models attracted significant research interest for decades (far from being a comprehensive list, see for example [12, 75–79]), with emphasis on the asymptotic behavior of two-point functions [80] and the expectation values of short range local operators in equilibrium [81]. The current operators fit in this line of work since they are special short-range operators, and (as we shall see in the following two chapters) their finite volume mean values take a remarkably simple form.

In this chapter, we present a simple formula for the finite volume mean values of current operators in integrable models, based on our work [82]. Our expression is the finite size version of (2.9). The formula is rather general and applicable to a range of Bethe Ansatz solvable models, however at some points of our calculations we restrict ourselves to the XXZ model. After stating the main result in Section 4.1, the formula is proven in the subsequent Sections 4.2, 4.3 and 4.4, by using methods introduced in the previous chapter.

4.1 Current mean value formula

As it was discussed in the previous chapters, integrable systems possess extra local conserved charges that can be obtained from the QISM framework. The locality of these charges means that they can be written as sums of charge density operators with some finite span. When summed over the whole of the chain, the charges commute with the Hamiltonian, therefore their time-derivatives are zero (as it should be for

conserved quantities). However, when the charge densities are summed over a finite segment of the system, they no longer commute with H, their dynamics is non-trivial and is described by the lattice version of the continuity equation:

$$\frac{d}{dt}\sum_{j=j_1}^{j_2}\hat{q}_\alpha(j) = i\left[H, \sum_{j=j_1}^{j_2}\hat{q}_\alpha(j)\right] = \hat{J}_\alpha(j_1) - \hat{J}_\alpha(j_2+1), \tag{4.1}$$

where we introduced the current operator density $\hat{J}_\alpha(j)$, corresponding to the conserved charge $\hat{Q}_\alpha$. From the locality of the Hamiltonian and the charges, it follows that the current operators are also local objects. Since the charge densities are not uniquely defined, as it was pointed out in Subsection 3.3.1, the equation (4.1) does not define the currents unambiguously either. The resulting gauge freedom however does not effect the mean values of the currents, therefore for our purposes is irrelevant. The continuity equation also allows for an additive normalization, which we choose so that in the reference state the current mean values are zero:

$$\langle 0|\hat{J}_\alpha(j)|0\rangle = 0. \tag{4.2}$$

Explicit real space forms of current operators in the Heisenberg model are presented in Appendix B.

Other than the physical currents, it is also useful to consider so-called generalized currents. These operators describe the dynamics of the charge densities under the time-evolution generated by a conserved charge other than the Hamiltonian:

$$i\left[\hat{Q}_\beta, \sum_{j=j_1}^{j_2}\hat{q}_\alpha(j)\right] = \hat{J}_\alpha^\beta(j_1) - \hat{J}_\alpha^\beta(j_2+1). \tag{4.3}$$

Explicit expressions for some generalized current operators can also be found in Appendix B.

Our main goal is to determine the expectation values of the currents in the eigenstates of integrable models. As it was shown in the previous chapter, in Bethe Ansatz solvable models the exact eigenstates can be characterized by a set of rapidities $\{\lambda_1,\dots,\lambda_N\}$, satisfying the Bethe equations. Our main result, obtained originally in [82], for the (physical) current mean values is the following formula:

$$\langle\lambda_1,\dots,\lambda_N|\hat{J}_\alpha(j)|\lambda_1,\dots,\lambda_N\rangle = \mathbf{e}'\cdot G^{-1}\cdot\mathbf{q}_\alpha. \tag{4.4}$$

For the generalized currents an analogous expression holds:

$$\langle\lambda_1,\dots,\lambda_N|\hat{J}_\alpha^\beta(j)|\lambda_1,\dots,\lambda_N\rangle = \mathbf{q}'_\beta\cdot G^{-1}\cdot\mathbf{q}_\alpha. \tag{4.5}$$

Here $\mathbf{e}'$, $\mathbf{q}_\alpha$ and $\mathbf{q}'_\beta$ are N-component vectors with elements

$$(\mathbf{e}')_j = \frac{de(\lambda_j)}{d\lambda}, \qquad (\mathbf{q}_\alpha)_j = q_\alpha(\lambda_j), \qquad (\mathbf{q}'_\beta)_j = \frac{dq_\beta(\lambda_j)}{d\lambda}, \tag{4.6}$$

where $e(\lambda)$ and $q_\alpha(\lambda)$ are the energy and charge eigenvalue functions defined in (3.61) and (3.62), while

G^{-1} is the inverse of the Gaudin matrix.

4.1.1 Semiclassical picture

The current mean value formula (4.4) is the finite size version of (2.9), which can be mathematically rigorously shown, by considering the string solutions of the Bethe equations and taking the thermodynamic limit of (4.4). For the case of the XXX model, this was done in [83]. Here however, instead of reproducing this rather long and technical calculation, we only present a simple semi-classical picture that illustrates the connection between (4.4) and (2.9).

In this semi-classical picture (also depicted on Fig. 4.1), the spin chain with periodic boundary condition can be thought of as a continuous ring. Particles far from each other, represented by individual wave packets, are assumed to have well-defined trajectories: they travel along the ring with constant velocities given by their group velocities

$$v(\lambda) = \frac{de}{dp} = \frac{e'(\lambda)}{p'(\lambda)}. \tag{4.7}$$

Since these group velocities generally differ for different rapidities, the particles meet and scatter on each other along the ring. The scattering events are taken into account by using the solution of the full quantum mechanical two-body problem: from the Bethe wave function (3.16), it is clear that the scattering of particle j on particle k results in the multiplication of the wave function by the phase $S(\lambda_j - \lambda_k)$. For the individual wavepackets, this phase gives rise to a (momentum dependent) time delay, or equivalently spatial displacement [84–86]. As the particles continue to collide, the time delays suffered from the individual scatterings accumulate and eventually lead to the emergence of an effective velocity $v^{\text{eff}}(\lambda)$, different from the group velocity $v(\lambda)$. During this process, integrability guarantees that the values of the rapidities do not change. In the semi-classical picture, the current mean values are simply given by the sum of the one-particle contributions:

$$J_\alpha^{cl} = \frac{1}{L}\sum_{j=1}^{N} q_\alpha(\lambda_j) v^{\text{eff}}(\lambda_j). \tag{4.8}$$

The effective velocities, however, can be computed building on the semi-classical picture. This was done in [82] by Márton Borsi. Here we present this simple self-consistent calculation.

The spatial displacement suffered by particle j as a result of scattering on particle k is given by

$$\Delta s_{jk} = \sigma_{jk}\frac{\partial\delta(p_j,p_k)}{\partial p_j} = \sigma_{jk}\frac{\varphi(\lambda_j-\lambda_k)}{p'(\lambda_j)}, \qquad \text{with} \qquad \sigma_{jk} = \begin{cases} +1 & \text{if } v^{\text{eff}}(\lambda_j) > v^{\text{eff}}(\lambda_k) \\ -1 & \text{if } v^{\text{eff}}(\lambda_j) < v^{\text{eff}}(\lambda_k) \end{cases} \tag{4.9}$$

where the sign σ_{jk} takes care of the ordering of the particles and the quantities $\delta(p_j,p_k)$ and $\varphi(\lambda)$ are defined in (3.17) and (3.30), respectively. The period with which these two particles collide is trivially calculated as

$$T_{jk} = \frac{L}{|v^{\text{eff}}(\lambda_j) - v^{\text{eff}}(\lambda_k)|}. \tag{4.10}$$

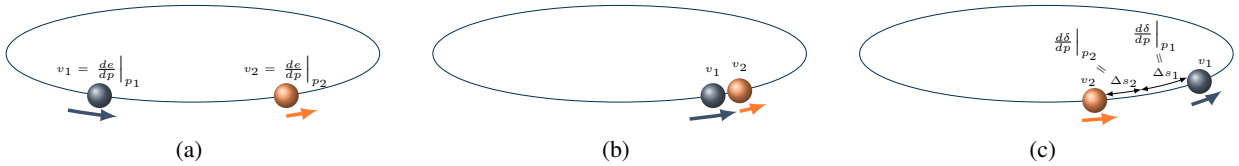

(a) (b) (c)

Figure 4.1: Semi-classical picture: (a) Particles far from each other travel with their constant group velocities. (b) Due to the difference in their velocities, the particles meet and scatter on each other. (c) As a result of the scattering, the particles suffer a spatial displacement given by the derivative of the scattering phase. The accumulating displacements change the average velocities of the particles.

After an asymptotically long time t, the space shifts suffered by particle j add up, leading to the total displacement

$$\Delta s_j(t) = \sum_{k\neq j} \Delta s_{jk} \frac{t}{T_{jk}}. \tag{4.11}$$

Obviously, this same displacement is the result of the difference between the bare and effective velocities of particle j:

$$\Delta s_j(t) = \big(v(\lambda_j) - v^{\text{eff}}(\lambda_j)\big)t. \tag{4.12}$$

Equating (4.11) and (4.12) leads to a self-consistent equation for the velocities. Rearranging this equation, taking into account the definition of the bare group velocity (4.7), the sign σ_{jk}, and multiplying both sides by $p'(\lambda_j)L$, finally yields the following expression

$$e'(p_j)L = Lp'(\lambda_j)v^{\text{eff}}(\lambda_j) + \sum_{k\neq j} \varphi(\lambda_j - \lambda_k)\big(v^{\text{eff}}(\lambda_j) - v^{\text{eff}}(\lambda_k)\big). \tag{4.13}$$

On the r.h.s. we can recognize the action of the Gaudin matrix (3.30), therefore (4.13) is equivalent to the matrix equation

$$L\mathbf{e}' = G\cdot\mathbf{v}^{\text{eff}}. \tag{4.14}$$

From (4.8), it then follows that the current mean values in the semi-classical picture are written as

$$J^{cl}_\alpha = \mathbf{e}'\cdot G^{-1}\cdot\mathbf{q}_\alpha, \tag{4.15}$$

which is the same as our main result. The fact that the formulae (4.4) and (4.5) are exact on the level of the full, interacting quantum theory signals a complete classical/quantum correspondence, which is ultimately the result of integrability.

4.1.2 Outline of the proof

In the rest of this chapter, we prove the formulae (4.4) and (4.5), following a number of steps:

1. First, in Section 4.2 we introduce the notion of form factors, and prove an expansion theorem that

connects the symmetric form factors and the mean values of operators.

2. Then, in Section 4.3 we calculate the form factors of the conserved charge operators, using their known mean values and the expansion theorem mentioned above. With the help of the continuity equations (4.1) and (4.3), the form factors of the current operators are also obtained.

3. By utilizing the form factor expansion again, in Section 4.4 we calculate the mean values of the current operators, hence completing the proof of the formulae (4.4) and (4.5).

The ideas behind this proof are quite general and pertinent to a wide range of Bethe Ansatz solvable models. Most of our derivations are therefore model independent, however in Section 4.2, we give a proof of the expansion theorem specifically to the XXZ model.

4.2 Form factor expansion

The crucial element of our proof of the mean value formula is an expansion theorem that relates the mean values of local operators to quantities called form factors. The form factor $F^{\mathcal{O}}(\{\lambda\}_N|\{\mu\}_M)$ of an arbitrary operator $\mathcal{O}$ is a meromorphic function that describes the generic off-diagonal matrix elements of $\mathcal{O}$ between unnormalized Bethe states:

$$\langle\{\lambda\}_N|\mathcal{O}|\{\mu\}_M\rangle = \frac{F^{\mathcal{O}}(\{\lambda\}_N|\{\mu\}_M)}{\sqrt{\det G_\lambda \det G_\mu}}, \tag{4.16}$$

where $\{\lambda\}_N$ and $\{\mu\}_M$ are two normalized eigenstates of the system in question, while the Gaudin determinants are responsible for the proper normalization. It is important to note that while (4.16) is valid when both $\{\lambda\}_N$ and $\{\mu\}_M$ are on-shell Bethe states, the form factors are generally well defined functions. A crucial property of the form factors that will be utilized later on, is that they are volume independent: the only L dependence in the on-shell case comes through the Bethe roots. The behavior of form factors were heavily investigated in the literature: equation (4.16) was introduced for QFTs in [87], while for lattice systems in [12]. The analytic properties of form factors were also studied both in QFTs [88], in lattice systems, using ABA [12] and in the Lieb-Liniger model, using CBA [89].

Even though the off-diagonal matrix elements of operators are easily expressed with the help of their form factors, this is not the case for the mean values. This is caused by the appearance of the so-called disconnected terms: mathematically, they are the results of the dynamical poles of the form factors, while on a more physical level they describe those scenarios when a subset of quasi particles do not interact with the operator in question. To establish a connection between mean values and form factors, let's introduce the so-called symmetric diagonal evaluation of $F^{\mathcal{O}}$:

$$F_S^{\mathcal{O}}(\{\lambda\}_N) = \lim_{\varepsilon\to 0} F^{\mathcal{O}}(\lambda_1+\varepsilon,\dots,\lambda_N+\varepsilon|\lambda_1,\dots,\lambda_N). \tag{4.17}$$

It is worth mentioning that other diagonal evaluations of the form factors are possible, however for our purposes the symmetric one is the most suited, therefore we do not consider any other case. (For details on

the so-called connected form factors see [90].)

Before turning to the expansion theorem, first we set up a connection between the form factors of the conserved charge and corresponding current operators, by taking the off-diagonal matrix element of the continuity equation (4.3). Although, the final goal is to calculate mean values, taking the diagonal matrix elements of (4.3) would result in zeros on both sides of the equation. Nevertheless, among the off-diagonal matrix elements we can restrict our attention to those that are taken between states with the same particle number N:

$$i\left(Q_\beta(\{\mu\}_N)-Q_\beta(\{\lambda\}_N)\right)\,\langle\{\lambda\}_N|\hat{q}_\alpha(j)|\{\mu\}_N\rangle=\left(e^{iP(\{\mu\}_N)}e^{-iP(\{\lambda\}_N)}-1\right)\,\langle\{\lambda\}_N|\hat{j}^\beta_\alpha(j)|\{\mu\}_N\rangle\,. \quad (4.18)$$

Here we used that translations on the chain are generated by the operator $\exp(-iP)$, where P is the total quasi-momentum. Taking the symmetric diagonal limit in (4.18) immediately yields a relation between the form factors of charges and currents. In order to keep the notation more readable, we introduce the symbols $\mathcal{Q}_\alpha$ and $\mathcal{J}^\beta_\alpha$ for the symmetric form factors of the charge and current operators, respectively:

$$\mathcal{Q}_\alpha(\{\lambda\}_N)=F_S^{\hat{q}_\alpha}(\{\lambda\}_N),\qquad \mathcal{J}^\beta_\alpha(\{\lambda\}_N)=F_S^{\hat{j}^\beta_\alpha}(\{\lambda\}_N). \quad (4.19)$$

With this notation, the relation between the form factors of the charges and currents reads as

$$\mathcal{J}^\beta_\alpha(\{\lambda\}_N)=\frac{\sum_{k=1}^N q'_\beta(\lambda_k)}{\sum_{k=1}^N p'(\lambda_k)}\mathcal{Q}_\alpha(\{\lambda\}_N). \quad (4.20)$$

As a last step before presenting the expansion theorem, it is useful to introduce the function $\rho(\lambda_1,\dots,\lambda_N)$ as the Gaudin determinant evaluated at the rapidities $\{\lambda_1,\dots,\lambda_N\}$:

$$\rho(\{\lambda_1,\dots,\lambda_N\})=\det G_\lambda\,. \quad (4.21)$$

Notice that while $\det G_\lambda$ has a physical meaning describing the norm of on-shell Bethe states, $\rho(\{\lambda\}_N)$ is generally defined for arbitrary values of the rapidities.

At this point, we are ready to state the expansion theorem connecting the mean values of local operators to their form factors.

Theorem 1. *In a finite volume L, the mean values of any local operator $\mathcal{O}$ in the normalized eigenstates of the model, can be computed as*

$$\langle\{\lambda\}_N|\mathcal{O}|\{\lambda\}_N\rangle=\frac{1}{\rho(\{\lambda\}_N)}\sum_{\{\lambda^+\}\cup\{\lambda^-\}}F_S^{\mathcal{O}}(\{\lambda^+\})\rho(\{\lambda^-\}), \quad (4.22)$$

where the sum runs over all bipartitions $\{\lambda^+\}\cup\{\lambda^-\}=\{\lambda\}_N$ of the set of rapidities, including the cases when either subset is the empty set (and in these cases $\rho(\emptyset)=1$ and $F_S^{\mathcal{O}}(\emptyset)=\langle\mathcal{O}\rangle$ is the vacuum expectation value).

In the rest of this section, we present the proof of Theorem 1 for the specific case of the XXZ model. We note that similar expressions are known in other integrable models: for integrable QFTs an equivalent theorem was introduced in [90], which holds up to exponentially small corrections in system size. (This is because in iQFTs the Bethe states are only approximate and not exact eigenstates.) Also, in [91] it was shown that the expansion (4.22) can be considered as the finite size version of the well-known LeClair-Mussardo series [92], which is an integral series for mean values, valid in the thermodynamic limit. Moreover, a similar expansion theorem was also proven for certain operators of the Lieb-Liniger model in [93]. However, for the case of the XXZ model Theorem 1 was first proven in [82].

Our proof is carried out by investigating the analytic properties of the form factors, a technique that can be originated from Korepin, who used the same ideas to calculate the norms of Bethe states [62]. The proof presented here follows very similar steps to that of [91].

Our ultimate goal is to derive a form factor expansion for mean values, however as a first step, let's just consider the scalar product of two arbitrary off-shell Bethe states

$$\langle 0|\prod_{k=1}^{N} C(\lambda_k^C)\prod_{k=1}^{N} B(\lambda_k^B)|0\rangle\,, \tag{4.23}$$

where $\{\lambda^B\}_N$ and $\{\lambda^C\}_N$ are two sets of arbitrary rapidities. To evaluate this expression, one should commute the C operators through the B operators, and use the fact that $C(\lambda)$ and $B(\lambda)$ annihilates the state $|0\rangle$ and $\langle 0|$, respectively. Using the commutation relations between the elements of the monodromy matrix (A.1), it can be shown [12] that the scalar product (4.23) possesses a pole, whenever two elements of the sets $\{\lambda^B\}_N$ and $\{\lambda^C\}_N$ approach each other. (This pole comes from the function $g(\lambda^C,\lambda^B)$ that appears from the commutator $[C(\lambda^C),B(\lambda^B)]$.) Since both the B and C operators commute among each other, we can consider the $\lambda_N^C\to\lambda_N^B$ case without loss of generality:

$$\langle 0|\prod_{k=1}^{N} C(\lambda_k^C)\prod_{k=1}^{N} B(\lambda_k^B)|0\rangle \xrightarrow{\lambda_N^C\to\lambda_N^B} \\ \to \frac{\sin(i\eta)}{\lambda_N^C-\lambda_N^B}\left(a_N^B d_N^C - a_N^C d_N^B\right)\langle 0|\prod_{k=1}^{N-1} C(\lambda_k^C)\prod_{k=1}^{N-1} B(\lambda_k^B)|0\rangle^{mod}\,, \tag{4.24}$$

where to shorten the expressions we introduced the notation $a_N^{B/C}=a(\lambda_N^{B/C})$ and $d_N^{B/C}=d(\lambda_N^{B/C})$ (also note that for simplicity, here we omitted the constant shift $\xi=i\eta/2$ that was introduced in Chapter 3). The scalar product on the r.h.s. has to be evaluated with the modified reference state eigenvalues that are defined as $a^{mod}(\lambda)=a(\lambda)f(\lambda_N,\lambda)$ and $d^{mod}(\lambda)=d(\lambda)f(\lambda,\lambda_N)$. To somewhat simplify the calculations, it is useful to introduce the normalized operators $\mathbb{B}(u)=B(u)/d(u)$ and $\mathbb{C}(u)=C(u)/d(u)$. Note that due to the Bethe equations (3.59), the on-shell states created by these operators have the same norm as in (3.65). States

created by the normalized operator satisfy a similar recursive property:

$$\langle 0|\prod_{k=1}^{N}\mathbb{C}(\lambda_k^C)\prod_{k=1}^{N}\mathbb{B}(\lambda_k^B)|0\rangle \xrightarrow{\lambda_N^C\to\lambda_N^B} \\ \to \frac{\sin(i\eta)}{\lambda_N^C-\lambda_N^B}\left(l_N^B-l_N^C\right)\left(\prod_{k=1}^{N-1}f_{kN}^C f_{kN}^B\right)\langle 0|\prod_{k=1}^{N-1}\mathbb{C}(\lambda_k^C)\prod_{k=1}^{N-1}\mathbb{B}(\lambda_k^B)|0\rangle^{mod}, \quad (4.25)$$

where again, we introduced the notation $f_{NK}^{B/C}=f^{B/C}(\lambda_N,\lambda_k)$ and $l_N^{B/C}=l^{B/C}(\lambda_N)$ with $l(\lambda)=a(\lambda)/d(\lambda)$ for brevity, and on the r.h.s. the the scalar product is evaluated with the modified function $l_{mod}(\lambda)=l(\lambda)\frac{f(\lambda_N,\lambda)}{f(\lambda,\lambda_N)}$. In the rest of the calculations in this section, we will use the states created by the normalized operators $\mathbb{B}$ and $\mathbb{C}$, because they are more convenient to study mean values. The key feature of our derivation is that we treat the functions $a(\lambda)$ and $d(\lambda)$ (or equivalently $l(\lambda)$) as freely varying parameters, and not fixed functions. Therefore the scalar product on the l.h.s. of (4.25) depends on $4N$ independent variables, $\{\lambda^B\}_N$, $\{\lambda^C\}_N$, $\{l^B\}_N$ and $\{l^C\}_N$. Of course, in the physical case, when both $a(\lambda)$ and $d(\lambda)$ are well-defined continuous functions, these variables stop being independent, and the pole in (4.25) disappears:

$$\frac{\sin(i\eta)}{\lambda_N^C-\lambda_N^B}\left(l_N^B-l_N^C\right) \;\to\; -\sinh(\eta)l_N z_N, \quad (4.26)$$

where $z(\lambda)=i\partial_\lambda\log l(\lambda)$. The first step toward the proof of Theorem 1 is to show that the matrix elements of an arbitrary operator $\mathcal{O}$ satisfy the same recursive relation as the scalar product in (4.25). Introducing the notation

$$M_N^{\mathcal{O}}(\{\lambda^C\}_N,\{\lambda^B\}_N,\{l^C\}_N,\{l^B\}_N)=\langle 0|\prod_{k=1}^{N}\mathbb{C}(\lambda_k^C)\mathcal{O}\prod_{k=1}^{N}\mathbb{B}(\lambda_k^B)|0\rangle, \quad (4.27)$$

we want to show that

$$M_N^{\mathcal{O}}(\{\lambda^C\}_N,\{\lambda^B\}_N,\{l^C\}_N,\{l^B\}_N) \xrightarrow{\lambda_N^C\to\lambda_N^B} \\ \to \frac{\sin(i\eta)}{\lambda_N^C-\lambda_N^B}\left(l_N^B-l_N^C\right)\left(\prod_{k=1}^{N-1}f_{kN}^C f_{kN}^B\right)M_{N-1}^{\mathcal{O}}(\{\lambda^C\}_{N-1},\{\lambda^B\}_{N-1},\{l_{mod}^C\}_{N-1},\{l_{mod}^B\}_{N-1}). \quad (4.28)$$

Again, we stress that the matrix element (4.27) is a function of $4N$ independent variables. Instead of considering an arbitrary operator $\mathcal{O}$, it is enough to treat the case when $\mathcal{O}$ is of the form

$$\mathcal{O}=\prod_{j=1}^{L}E_{a_j,b_j}(j), \quad (4.29)$$

where $E_{a,b}(j)$ $(a,b=1,2)$ is the elementary matrix with elements $\left(E_{a,b}\right)_{kl}=\delta_{ak}\delta_{bl}$ that acts on site j. It is clear that any operator on the finite chain can be written as a linear combination of operators of the form (4.29). Because of the linearity of the scalar product, it is then enough to consider just one such product of

elementary operators. However, the matrix elements of these elementary building blocks can be evaluated by using the solution of the quantum inverse problem. This method expresses the local operators $E_{a,b}(j)$ by the entries of the monodromy matrix, embedding them therefore into the Yang-Baxter algebra. The solution of the quantum inverse problem was worked out in [94–96].

Using the elements of the monodromy matrix, the product of elementary operators (4.29) can be written as

$$\prod_{j=L}^{1} E_{a_j,b_j}(j) = \prod_{j=L}^{1} T_{a_j,b_j}(0). \tag{4.30}$$

Therefore our approach is to show that the singularity property (4.28) holds for operators of the form $\mathcal{O} = X(\mu_M)\dots X(\mu_1)$, where X may stand for any entry of the monodromy matrix, and then evaluate the limit $\mu_k \to 0$. (We note that here we use the un-normalized monodromy matrix elements to express local operators.) We can simplify the calculation even further by noticing that in any product of the form $X(\mu_M)\dots X(\mu_1)$, the operators can be ordered in the following way:

$$X(\mu_1)X(\mu_2)\dots X(\mu_M) = \sum G(\mu_1,\dots,\mu_M) CC\dots CDD\dots DAA\dots ABB\dots B, \tag{4.31}$$

where $G(\mu_1,\dots,\mu_M)$ is some numerical coefficient. To reach the ordering in (4.31), one can use the commutation relations (A.1) through the following steps:

1. First, take every B operator (starting with the first from the right) to the right hand side of the product. Looking at the commutation relations, we can see that as a result of this step, we end up with a sum of products, in which each term contains B operators solely on the right.

2. Similarly, we can take every C operator to the left hand side. Now, we are left with a sum of products, where in every product the C operators are on the left, while the B operators are on the right end of the product.

3. Finally, we can order the remaining A and D operators. To do this, we need to use the commutation relation $[A,D]$, which yields the operators C and B in the desired order CB. Then these operators can be taken again to the appropriate side of the product, and in order to achieve this, we only need to commute them through other A and D operators. However, this step does not produce any new A and D operators. Therefore the algorithm outlined here finishes after a finite number of steps. The numerical coefficient $G(\mu_1,\dots,\mu_M)$ is composed of the functions f and g, appearing from the commutation relations.

After all these reasoning and simplification, our task is to prove the singularity property (4.28) for a single product of the monodromy matrix elements, ordered like in (4.31). First, let's just consider one A operator. Its action on an off-shell Bethe state, created by the un-normalized B operators is given by (3.57) and (3.58). From these expressions, it simply follows that its matrix element between states created by the normalized

operators is written as

$$\begin{aligned}\langle 0|\prod_{k=1}^{N}\mathbb{C}(\lambda_k^C)A(\mu)\prod_{k=1}^{N}\mathbb{B}(\lambda_k^B)|0\rangle = a(\mu)\prod_{k=1}^{N}f(\lambda_k^B,\mu)\,\langle 0|\prod_{k=1}^{N}\mathbb{C}(\lambda_k^C)\prod_{k=1}^{N}\mathbb{B}(\lambda_k^B)|0\rangle + \\ +\sum_{n=1}^{N}a(\lambda_n^B)g(\mu,\lambda_n^B)\frac{d(\mu)}{d(\lambda_n^B)}\prod_{\substack{k=1\\k\neq n}}^{N}f_{kn}^B\,\langle 0|\prod_{k=1}^{N}\mathbb{C}(\lambda_k^C)\mathbb{B}(\mu)\prod_{\substack{k=1\\k\neq n}}^{N}\mathbb{B}(\lambda_k^B)|0\rangle\,.\end{aligned} \tag{4.32}$$

Using (4.25), by taking the limit $\lambda_N^C\to\lambda_N^B$ we arrive at

$$\begin{aligned}&\langle 0|\prod_{k=1}^{N}\mathbb{C}(\lambda_k^C)A(\mu)\prod_{k=1}^{N}\mathbb{B}(\lambda_k^B)|0\rangle \quad\xrightarrow{\lambda_N^C\to\lambda_N^B}\quad \frac{\sin(i\eta)}{\lambda_N^C-\lambda_N^B}\left(l_N^B-l_N^C\right)\left(\prod_{k=1}^{N-1}f_{kN}^Cf_{kN}^B\right)\times\\ &\times\Bigg[\underbrace{a(\mu)f(\lambda_N^B,\mu)}_{a^{mod}(\mu)}\prod_{k=1}^{N-1}f(\lambda_k^B,\mu)\,\langle 0|\prod_{k=1}^{N-1}\mathbb{C}(\lambda_k^C)\prod_{k=1}^{N-1}\mathbb{B}(\lambda_k^B)|0\rangle^{mod}+\\ &\sum_{n=1}^{N-1}g(\mu,\lambda_n^B)\underbrace{a(\lambda_n^B)f(\lambda_N^B,\lambda_n^B)}_{a^{mod}(\lambda_n^B)}\prod_{\substack{k=1\\k\neq n}}^{N-1}f_{kn}^B\underbrace{\frac{d(\mu)f(\mu,\lambda_N^B)}{d(\lambda_n^B)f(\lambda_n^B,\lambda_N^B)}}_{\frac{d^{mod}(\mu)}{d^{mod}(\lambda_n^B)}}\langle 0|\prod_{k=1}^{N-1}\mathbb{C}(\lambda_k^C)\mathbb{B}(\mu)\prod_{\substack{k=1\\k\neq n}}^{N-1}\mathbb{B}(\lambda_k^B)|0\rangle^{mod}\Bigg]\,.\end{aligned} \tag{4.33}$$

The expression on the r.h.s. in the square brackets is however nothing else, but the matrix element calculated between states with $N-1$ particles and with the modified reference state eigenvalues. Exactly in the same way, for the matrix element of a single D operator we get:

$$\begin{aligned}&\langle 0|\prod_{k=1}^{N}\mathbb{C}(\lambda_k^C)D(\mu)\prod_{k=1}^{N}\mathbb{B}(\lambda_k^B)|0\rangle \xrightarrow{\lambda_N^C\to\lambda_N^B}\\ &\qquad\to\frac{\sin(i\eta)}{\lambda_N^C-\lambda_N^B}\left(l_N^B-l_N^C\right)\left(\prod_{k=1}^{N-1}f_{kN}^Cf_{kN}^B\right)\langle 0|\prod_{k=1}^{N-1}\mathbb{C}(\lambda_k^C)D(\mu)\prod_{k=1}^{N-1}\mathbb{B}(\lambda_k^B)|0\rangle^{mod}\,.\end{aligned} \tag{4.34}$$

For a single A or D operator this proves the singularity property. We can now move onto the case of products of A and D operators. In order to calculate their matrix elements, we need to evaluate their action on the off-shell Bethe states. First, let's look at products of A operators (here for brevity, we omit the superscript B for the rapidities of the state):

$$\prod_{l=1}^{M}A(\mu_l)\prod_{k=1}^{N}\mathbb{B}(\lambda_k)\,|0\rangle\,. \tag{4.35}$$

To evaluate this expression, the A operators have to be commuted through the $\mathbb{B}$ operators. It is obvious that the result will be a linear combination of states with N particles. The rapidities of these N particles are chosen from the set $\{\lambda\}_N\cup\{\mu\}_M$. We can break up this linear combination according to how many of these

rapidites are chosen from the set $\{\mu\}_M$. Denoting the number of rapidities coming from $\{\mu\}_M$ by K, we can write

$$\prod_{l=1}^{M} A(\mu_l) \prod_{k=1}^{N} \mathbb{B}(\lambda_k)\,|0\rangle = \sum_{K=0}^{\max(N,M)} \sum_{K} G^{n_1,n_2,\ldots,n_K}_{l_1,l_2,\ldots,l_K}(\{\lambda\}_N|\{\mu\}_M) \prod_{q=1}^{K} \mathbb{B}(\mu_{l_q}) \prod_{\substack{k=1 \\ k\neq n_1,\ldots,n_K}}^{N} \mathbb{B}(\lambda_k)\,|0\rangle\,, \tag{4.36}$$

where G is a numerical coefficient and $\sum_K$ runs over all those subsets of the set $\{\lambda\}_N \cup \{\mu\}_M$ that have N elements, with K of those elements chosen from $\{\mu\}_M$. Explicitly, if $\mu_{l_1},\ldots,\mu_{l_K}$ denotes those K elements that are chosen from $\{\mu\}_M$ for the subset and $\lambda_{n_1},\ldots,\lambda_{n_K}$ those K elements that are not chosen from $\{\lambda\}_N$, $\sum_K$ is written as

$$\sum_{K} = \sum_{l_1=1}^{M} \sum_{\substack{l_2=1 \\ l_2\neq l_1}}^{M} \cdots \sum_{\substack{l_K=1 \\ l_K\neq l_1,\ldots,l_{K-1}}}^{M} \sum_{n_1=1}^{N} \sum_{\substack{n_2=1 \\ n_2\neq n_1}}^{N} \cdots \sum_{\substack{n_K=1 \\ n_K\neq n_1,\ldots,n_{K-1}}}^{N} . \tag{4.37}$$

The coefficient G can be calculated using the commutation relation of the A and $\mathbb{B}$ operators. Since $\mathbb{B}$ is defined as $B(\lambda)/d(\lambda)$, its commutation relation with A simply follows from (3.53):

$$A(\mu)\mathbb{B}(\lambda) = f(\lambda,\mu)\mathbb{B}(\lambda)A(\mu) + g(\mu,\lambda)\frac{d(\mu)}{d(\lambda)}\mathbb{B}(\mu)A(\lambda). \tag{4.38}$$

The important feature of this expression is that the r.h.s contains two terms: one where the arguments of the operators are unchanged, and one where they are switched.

Using (4.38), the coefficients in (4.36) can be computed. For example, in the case of $K = 0$ all the rapidities of the resulting state is chosen from $\{\lambda\}_N$, which means that during the commutation of the A's through the $\mathbb{B}$'s, we always keep the term from the commutation relation that preserves the arguments of the operators. The coefficient $G^{\emptyset}_{\emptyset}\big(\{\lambda\}_N|\{\mu\}_M\big)$ is therefore given by

$$G^{\emptyset}_{\emptyset}(\{\lambda\}_N|\{\mu\}_M) = \prod_{l=1}^{M}\left(a(\mu_l)\prod_{k=1}^{N} f(\lambda_k,\mu_l)\right). \tag{4.39}$$

Similarly, for $K = 1$, we only substitute one element from the set $\{\mu\}_M$ (let's say μ_{l_1}) into the rapidities to replace one element from the set $\{\lambda\}_N$ (let's say λ_{n_1}). Therefore when commuting $A(\mu_{l_1})$ through $\mathbb{B}(\lambda_{n_1})$ we need to take the term from the commutation relation that switches the arguments, while in all other cases we take the term that keeps the arguments. Looking at the commutation relation (4.38), it is not hard to see that the resulting coefficient reads as

$$G^{n_1}_{l_1}(\{\lambda\}_N|\{\mu\}_M) = a(\lambda_{n_1})g(\mu_{l_1},\lambda_{n_1})\left(\prod_{\substack{k=1 \\ k\neq n_1}}^{N} f(\lambda_k,\lambda_{n_1})\right)\prod_{\substack{j=1 \\ j\neq l_1}}^{M}\left(a(\mu_j)\Big(\prod_{\substack{k=1 \\ k\neq n_1}}^{N} f(\lambda_k,\mu_j)\Big)f(\mu_{l_1},\mu_j)\right). \tag{4.40}$$

Now, let's look at a generic term of the sum (4.36), in which K number of rapidities are chosen from $\{\mu\}_M$,

and let's denote these rapidities by $\mu_{l_1},\dots,\mu_{l_K}$, while the ones that are substituted for by $\lambda_{n_1},\dots,\lambda_{n_K}$. The necessary commutations can be evaluated by keeping in mind that whenever the arguments of the operators are exchanged a factor of $g(\mu,\lambda)d(\mu)/d(\lambda)$, while when the arguments are left untouched, a factor of $f(\lambda,\mu)$ appears.

Let μ_{l_1} be the first substituted rapidity and λ_{n_1} the one which is replaced. In this case there will be a $g(\mu_{l_1},\lambda_{n_1})d(\mu_{l_1})/d(\lambda_{n_1})$ factor coming from the commutation relation of $A(\mu_{l_1})$ and $\mathbb{B}(\lambda_{n_1})$, describing the replacement. From the commutation of $A(\lambda_{n_1})$ and the other $\mathbb{B}$ operators will appear the factor $\prod_{\substack{k=1\\k\neq n_1}} f(\lambda_k,\lambda_{n_1})$. Finally, the effect of $A(\lambda_{n_1})$ on the pseudo vacuum will result in the factor $a(\lambda_{n_1})$. In the case of the next substituted rapidity (μ_{l_2} replacing λ_{n_2}) the same factors will appear, except that now it has to be taken into consideration that one of the commutations will be with $\mathbb{B}(\mu_{l_1})$ and not with $\mathbb{B}(\lambda_{n_1})$. The rest of the substitutions go the same way. The remaining A operators with the non-substituted rapidities commute through the $\mathbb{B}$ operators without exchanging the arguments. To take into consideration all of the possible cases, we have to sum over every n and l. But since both the A and $\mathbb{B}$ operators commute with each other, it is invariant which λ is replaced by which μ. Therefore, to obtain the right result we have to divide by $K!$. This leads to the following result for a generic coefficient:

$$G^{n_1,n_2,\dots,n_K}_{l_1,l_2,\dots,l_K}(\{\lambda\}_N|\{\mu\}_M)=\frac{1}{K!}a(\lambda_{n_1})g(\mu_{l_1},\lambda_{n_1})\frac{d(\mu_{l_1})}{d(\lambda_{n_1})}\left(\prod_{\substack{k=1\\k\neq n_1}}^{N}f(\lambda_k,\lambda_{n_1})\right)\times$$
$$\times a(\lambda_{n_2})g(\mu_{l_2},\lambda_{n_2})\frac{d(\mu_{l_2})}{d(\lambda_{n_2})}\left(\prod_{\substack{k=1\\k\neq n_1,n_2}}^{N}f(\lambda_k,\lambda_{n_2})\right)f(\mu_{l_1},\lambda_{n_2})\ \dots a(\lambda_{n_K})g(\mu_{l_K},\lambda_{n_K})\frac{d(\mu_{l_K})}{d(\lambda_{n_K})}\times$$
$$\times\left(\prod_{\substack{k=1\\k\neq n_1,\dots,n_{K-1}}}^{N}f(\lambda_k,\lambda_{n_K})\right)\left(\prod_{p}^{K-1}f(\mu_{l_p},\lambda_{n_K})\right)\prod_{\substack{r=1\\r\neq l_1,\dots,l_K}}^{M}\left(a(\mu_r)\prod_{\substack{k=1\\k\neq n_1,\dots,n_K}}^{N}f(\lambda_k,\mu_r)\prod_{q\in\{l_1,\dots,l_K\}}f(\mu_q,\mu_r)\right). \quad (4.41)$$

Multiplying (4.36) from the left with $\langle 0|\prod_{k=1}^{N}\mathbb{C}(\lambda_k^C)$ and taking the $\lambda_N^C\to\lambda_N^B$ limit, in the r.h.s. only those terms will give a contribution to the pole, in which λ_N^B is still among the arguments of the $\mathbb{B}$ operators. All these terms will get multiplied by $\frac{\sin(i\eta)}{\lambda_N^C-\lambda_N^B}\left(l_N^C-l_N^B\right)\prod_{k=1}^{N-1}f_{Nk}^C f_{Nk}^B$ according to (4.25), and the modified scalar products will appear with $N-1$ particles. Since in every such $G(\{\lambda\}_N|\{\mu\}_M)$ coefficient where $N\notin\{n_1,\dots,n_K\}$ there is a $f(\lambda_N^B,\xi)$ factor next to every vacuum expectation value $a(\xi)$, it is true that:

$$G^{n_1,n_2,\dots,n_K}_{l_1,l_2,\dots,l_K}(\{\lambda\}_N|\{\mu\}_M)=G^{n_1,n_2,\dots,n_K}_{l_1,l_2,\dots,l_K}(\{\lambda\}_{N-1}|\{\mu\}_M)^{mod}\qquad(N\notin\{n_1,\dots,n_K\}),\quad(4.42)$$

which means that (4.28) holds for $\mathcal{O}=\prod_{k=1}^{M}A(\mu_k)$. This computation goes the same way for the product of D operators (only the order of the arguments of the g and f functions are reversed). But because of the linearity of the scalar product this also prove that (4.28) is true for an operator of the form $\mathcal{O}=D(\mu_1)D(\mu_2)\dots D(\mu_m)A(\mu_{m+1})\dots A(\mu_M)$: the effect of the products of the A operators on an arbi-

trary state is a linear combination of states computed above. The effect of the product of the D operators on each term in this linear combination is another linear combination, with coefficients that can be similarly calculated. However, if the original term (the one obtained after acting with the A operators) doesn't contain λ_N^B among the arguments of the $\mathbb{B}$ operators then it won't appear there after acting with the D operators. If it is still an argument of a $\mathbb{B}$ operator in the original term, than the appropriate f factor is present next to the reference state eigenvalue, and it will appear also after acting with the D operators. This means that in every term that contains $\mathbb{B}(\lambda_N^B)$ the appropriate $f(\lambda_N,\xi)$ or $f(\xi,\lambda_N)$ factor will appear next to the reference state eigenvalue $a(\xi)$ or $d(\xi)$. Therefore (4.28) holds for operators of the form $\mathcal{O}=D(\mu_1)D(\mu_2)\dots D(\mu_m)A(\mu_{m+1})\dots A(\mu_M)$.

Finally, we need to treat the case when there are C and B operators present in $\mathcal{O}$, like in (4.31). However, since these additional C and B operators are sorted to the left and right ends of the product, respectively, they can be considered as extra creation operators for the off-shell Bethe states. Therefore their presence does not effect the singularity property at all. To show this, we can consider the simplest case, when $\mathcal{O}=C(\mu^C)B(\mu^B)$.

$$\langle 0|\prod_{k=1}^{N}\mathbb{C}(\lambda_k^C)C(\mu^C)B(\mu^B)\prod_{k=1}^{N}\mathbb{B}(\lambda_k^B)|0\rangle \xrightarrow{\lambda_N^C\to\lambda_N^B}$$
$$\to \frac{\sin(i\eta)}{\lambda_N^C-\lambda_N^B}\left(l_N^B-l_N^C\right)\left(\prod_{k=1}^{N-1}f_{kN}^C f_{kN}^B\right)\langle 0|\prod_{k=1}^{N-1}\mathbb{C}(\lambda_k^C)C(\mu^C)B(\mu^B)\prod_{k=1}^{N-1}\mathbb{B}(\lambda_k^B)|0\rangle^{mod}. \quad (4.43)$$

Similar reasoning verifies that the singularity property holds, even with more C and B operators present, together with A and D operators. This concludes the proof of (4.28).

In order to calculate mean values, first we need to take the diagonal limit in the matrix elements (4.27):

$$M_{N,d}^{\mathcal{O}}(\{\lambda\}_N,\{l\}_N,\{z\}_N)=\lim_{\lambda_k^C\to\lambda_k^B}M_N^{\mathcal{O}}(\{\lambda^C\}_N,\{\lambda^B\}_N,\{l^C\}_N,\{l^B\}_N),\qquad k=1,\dots,N. \quad (4.44)$$

It is important to note that here the rapidities $\{\lambda\}_N$ are still assumed to be arbitrary, and not the solutions of the Bethe equations. From (4.26) and (4.28) it follows that the diagonal limit (4.44) is a function of $3N$ independent variables: $\{\lambda\}_N$, $\{l\}_N$, and $\{z\}_N$. Moreover, the dependence on z is linear, with the proportionality factor given by

$$\frac{\partial}{\partial z_N}M_{N,d}^{\mathcal{O}}(\{\lambda\}_N,\{l\}_N,\{z\}_N)=$$
$$=-\sinh(\eta)l(\lambda_N)\left(\prod_{k=1}^{N-1}f_{kN}^C f_{kN}^B\right)M_{N-1,d}^{\mathcal{O}}(\{\lambda\}_{N-1},\{l_{mod}\}_{N-1},\{z_{mod}\}_{N-1}), \quad (4.45)$$

where the modification rule for z simply follows from its definition:

$$z_{mod}(\lambda) = i\frac{\partial}{\partial\lambda}\log\big(l_{mod}(\lambda)\big) = z(\lambda) + \underbrace{i\frac{\partial}{\partial\lambda}\log\left(\frac{f(\lambda_N,\lambda)}{f(\lambda,\lambda_N)}\right)}_{\varphi(\lambda-\lambda_N)} = z(\lambda)+\varphi(\lambda-\lambda_N). \tag{4.46}$$

Here we used the fact that the ratio of the f functions gives the scattering phase S. Similarly, from the definitions it follows that the z variables appear in the Gaudin matrix:

$$G_{jk} = \delta_{jk}\big[z(\lambda_j)+\sum_{l=1}^{N}\varphi(\lambda_j-\lambda_l)\big]-\varphi(\lambda_j-\lambda_k). \tag{4.47}$$

In order to compute the expectation values in the eigenstates of the system, the rapidities have to be taken to the solutions of the Bethe equations. The quantities obtained this way do not depend on the variables $\{l\}_N$ anymore, because they can be expressed by the Bethe roots, using the Bethe equations. Therefore these expectation values are the functions of $2N$ variables:

$$\langle\mathcal{O}\rangle_N(\{\lambda\}_N,\{z\}_N) = M^{\mathcal{O}}_{N,d}(\{\lambda\}_N,\{l\}_N,\{z\}_N)|_{\{\lambda\}\text{ solves the BEs}}, \tag{4.48}$$

since

$$l(\lambda_n) = \prod_{\substack{k=1\\k\neq n}}^{N}\frac{f(\lambda_n,\lambda_k)}{f(\lambda_k,\lambda_n)}. \tag{4.49}$$

Note that the expectation values in (4.48) are non-normalized. The dependence on the z variables is still linear, with the proportionality factor given by

$$\frac{\partial}{\partial z_N}\langle\mathcal{O}\rangle_N(\{\lambda\}_N,\{z\}_N) = -\sinh(\eta)\left(\prod_{k=1}^{N-1}f_{kN}f_{Nk}\right)\langle\mathcal{O}\rangle_{N-1}(\{\lambda\}_{N-1},\{z_{mod}\}_{N-1}). \tag{4.50}$$

To continue the calculations, it is useful to introduce the form factor $\mathbb{F}^{\mathcal{O}}_N$ in the following way:

$$\mathbb{F}^{\mathcal{O}}_N(\{\lambda^C\}_N,\{\lambda^B\}_N) = M^{\mathcal{O}}_N(\{\lambda^C\}_N,\{\lambda^B\}_N,\{l^C\}_N,\{l^B\}_N)|_{\{\lambda^C\}_N,\{\lambda^B\}_N\text{ are different solutions of BEs}}. \tag{4.51}$$

We note that the form factors defined in (4.51) only differ from the ones introduced in (4.16) by their normalization. It is however more convenient to use (4.51) to finish the proof of the expansion theorem, and only restore the proper normalization at the end, to recover (4.22). The singularity property for the form factors are obtained from (4.28) by using the observation that if a set of rapidities $\{\lambda\}_N$ satisfy the Bethe equations together with the set of $\{l\}_N$, then the set $\{\lambda\}_{N-1}=\{\lambda\}_N\backslash\{\lambda_N\}$ will satisfy the Bethe equations

with the set $\{l_{mod}\}_{N-1}$:

$$l(\lambda_n)\prod_{\substack{k=1\\k\neq n}}^{N}\frac{f(\lambda_k,\lambda_n)}{f(\lambda_n,\lambda_k)} = \underbrace{l(\lambda_n)\frac{f(\lambda_N,\lambda_n)}{f(\lambda_n,\lambda_N}}_{l_{mod}(\lambda_n)})\prod_{\substack{k=1\\k\neq n}}^{N-1}\frac{f(\lambda_k,\lambda_n)}{f(\lambda_n,\lambda_k)} = 1. \tag{4.52}$$

This means that when in (4.28) the rapidities are taken to be solutions of the Bethe equations, the modified matrix element appearing on the r.h.s. will be the appropriate form factor with $N-1$ particles:

$$\mathbb{F}_N^{\mathcal{O}}(\{\lambda^C\}_N,\{\lambda^B\}_N) \xrightarrow{\lambda_N^C\to\lambda_N^B} \frac{\sinh(\eta)}{\lambda_N^C-\lambda_N^B}\left(\prod_{k=1}^{N-1}f_{kN}^C f_{Nk}^B - \prod_{k=1}^{N-1}f_{Nk}^C f_{kN}^B\right)\mathbb{F}_{N-1}^{\mathcal{O}}(\{\lambda^C\}_{N-1},\{\lambda^B\}_{N-1}). \tag{4.53}$$

The symmetric form factor is defined as the symmetric diagonal limit of (4.51):

$$\mathbb{F}_{N,S}^{\mathcal{O}}(\{\lambda\}_N) = \lim_{\varepsilon\to 0}\mathbb{F}_N^{\mathcal{O}}(\{\lambda+\varepsilon\}_N,\{\lambda\}_N). \tag{4.54}$$

This quantity is connected to the expectation values by the following theorem:

Theorem 2. *The symmetric form factor as defined in* (4.54) *is equal to the non-normalized expectation value* $\langle\mathcal{O}\rangle_N(\{\lambda\}_N,\{z\}_N)$ *when* $z_j=0,\ j=1,\ldots,N$*:*

$$\mathbb{F}_{N,S}^{\mathcal{O}}(\{\lambda\}_N) = \langle\mathcal{O}\rangle_N(\{\lambda\}_N,\{0\}_N). \tag{4.55}$$

Proof. From (4.28), it is clear that the z dependence of the expectation value originates from $l(\lambda)$ being a function of the rapidities. Thus the z independent irreducible part of $\langle\mathcal{O}\rangle_N$ can be obtained by setting $l(\lambda_j^B)=l(\lambda_j^C)$, where $\{l^B\}_N$ is a solution of the Bethe equations:

$$\langle\mathcal{O}\rangle_N(\{\lambda\}_N,\{0\}_N) = \lim_{\varepsilon\to 0}M_N^{\mathcal{O}}(\{\lambda^B+\varepsilon\}_N,\{\lambda^B\}_N,\{l^B\}_N,\{l^B\}_N). \tag{4.56}$$

On the other hand, the symmetric form factors are – by definition – given by

$$\mathbb{F}_{N,S}^{\mathcal{O}}(\{\lambda\}_N) = \lim_{\varepsilon\to 0}M_N^{\mathcal{O}}(\{\lambda^B+\varepsilon\}_N,\{\lambda^B\}_N,\{\tilde{l}^B\}_N,\{l^B\}_N), \tag{4.57}$$

where both $\{l^B\}_N$ and $\{\tilde{l}^B\}_N$ are solutions of the Bethe equations. This means that the elements of both sets can be written as the products of the appropriate scattering phases S, therefore:

$$\{l^B\}_N = \{\tilde{l}^B\}_N. \tag{4.58}$$

This concludes the proof. □

To continue with the calculations, we introduce the function S for every bipartitions of the set of rapidities $\{\lambda\} = \{\lambda^+\} \cup \{\lambda^-\}$ in the following way:

$$S_N(\{\lambda^+\}_n, \{\lambda^-\}_{N-n}, \{z^-\}_{N-n}) = \big(-\sinh(\eta)\big)^{N-n} \times \\ \times \left(\prod_{\lambda_j \in \{\lambda^+\}} \prod_{\lambda_k \in \{\lambda^-\}} f_{jk}^{+-} f_{kj}^{-+} \right) \left(\prod_{1 \le j < k \le n} f_{jk}^{--} f_{kj}^{--} \right) \rho(\{\lambda^-\}_{N-n}, \{z^-\}_{N-n}), \quad (4.59)$$

where $f_{jk}^{+-} = f(\lambda_j^+, \lambda_k^-)$. This quantity depends on the z variables only through the Gaudin determinant, so it's derivative with respect to z_N is simply reads as

$$\frac{1}{\big(-\sinh(\eta)\big)^{N-n}} \frac{\partial}{\partial z_N} S_N(\{\lambda^+\}_n, \{\lambda^-\}_{N-n}, \{z\}_{N-n}) = \\ = \begin{cases} \left(\prod_{\lambda_j \in \{\lambda^+\}} \prod_{\lambda_k \in \{\lambda^-\}} f_{jk}^{+-} f_{kj}^{-+} \right) \left(\prod_{1 \le j < k \le n} f_{jk}^{--} f_{kj}^{--} \right) \frac{\partial}{\partial z_N} \rho(\{\lambda^-\}_{N-n}, \{z^-\}_{N-n}), & \text{if} \quad \lambda_N \in \{\lambda^-\}, \\ 0, & \text{if} \quad \lambda_N \in \{\lambda^+\}. \end{cases} \quad (4.60)$$

The derivative of the Gaudin determinant with respect to z_N is easily calculated if the determinant is expanded according to its N^{th} row or column. Trivially, the dependence is linear and the proportionality coefficient is given by the sub-determinant:

$$\frac{\partial}{\partial z_N} \rho(\{\lambda\}_N, \{z\}_N) = \begin{vmatrix} z_1 + \sum_{l=2}^{N} \varphi_{1l} & -\varphi_{12} & \dots & -\varphi_{1N-1} \\ -\varphi_{12} & \ddots & & \\ \vdots & & \ddots & \\ -\varphi_{1N-1} & & & z_{N-1} + \sum_{\substack{l=1 \\ l \neq N-1}}^{N} \varphi_{lN-1} \end{vmatrix} = \rho(\{\lambda\}_{N-1}, \{z_{mod}\}_{N-1}), \quad (4.61)$$

where on the r.h.s. the determinant is calculated with the modified z values. Hence the derivative of S becomes

$$\frac{1}{\big(-\sinh(\eta)\big)} \frac{\partial}{\partial z_N} S_N(\{\lambda^+\}_n, \{\lambda^-\}_{N-n}, \{z\}_N) = \\ = \begin{cases} \left(\prod_{k=1}^{N-1} f_{kN} f_{Nk} \right) S_{N-1}(\{\lambda^+\}_n, \{\lambda^-\}_{N-n-1}, \{z_{mod}^-\}_{N-n-1}), & \text{if} \quad \lambda_N \in \{\lambda^-\}, \\ 0, & \text{if} \quad \lambda_N \in \{\lambda^+\}. \end{cases} \quad (4.62)$$

It is important to note that when all the z^- variables in the argument of S are set to zero, S itself becomes

zero:

$$S(\{\lambda^+\}_n,\{\lambda^-\}_{N-n},\{0\}_{N-n})=0. \tag{4.63}$$

This is because in this case the Gaudin determinant is zero. (This can easily be seen from Theorem 4 that is presented and used in the next section.) With the help of all the expressions that we derived so far, we are now in the position to prove Theorem 1. In order to do this, we first reformulate it a little bit:

Theorem 3. *For an arbitrary local operator $\mathcal{O}$, the non-normalized expectation values of the operator in the eigenstates of the system can be written as*

$$\langle\{\lambda\}_N|\mathcal{O}|\{\lambda\}_N\rangle=\sum_{\{\lambda^+\}\cup\{\lambda^-\}}\mathbb{F}^{\mathcal{O}}_{n,S}(\{\lambda^+\}_n)S_N(\{\lambda^+\}_n,\{\lambda^-\}_{N-n},\{z^-\}_{N-n}), \tag{4.64}$$

where the summation runs over all bipartitions of the set of rapidities $\{\lambda\}_N=\{\lambda^+\}_n\cup\{\lambda^-\}_{N-n}$.

Proof. We use induction in the particle number N. Let us consider both sides as the multi-linear function of the z_j variables. Our goal is to show that both sides depend the same way on every z_j and that their z independent parts are also equal. We look at the first N for which the matrix element defined by (4.27) is not zero, and we denote this number by N_{min}. In the case when $N<N_{min}$, both sides of (4.64) are zero, therefore the equation is satisfied. If $N=N_{min}$, there is only one non-zero term in the summation in the r.h.s., namely when $\{\lambda^+\}=\{\lambda\}_N$. This means that on the r.h.s. there is only $\mathbb{F}^{\mathcal{O}}_{N,s}(\{\lambda\}_N)$ (since $S(\{\lambda^+\},\emptyset,\emptyset)=1$), therefore it is z independent. The l.h.s. is also independent of z, which follows from (4.50) and the fact that $\langle\mathcal{O}\rangle_{N_{min}-1}=0$. But the z independent parts are equal according to Theorem 2. Thus (4.64) is satisfied in this case. Now let us suppose that (4.64) is satisfied for every $N<M$, and examine the $N=M$ case. In the r.h.s. only those terms depend on z_j, where $z_j\in\{\lambda^-\}$. By taking the partial derivative of it with respect to z_j, the initial summation is getting modified to a new one, going over all the bi-partitions of the set $\{\lambda\}_{N-1}=\{\lambda\}_N\backslash\{\lambda_j\}$ (this follows from (4.62)). This new summation, however, gives exactly $\langle\mathcal{O}\rangle(\{\lambda\}_{N-1},\{z_{mod}\}_{N-1})$ (multiplied by the factor $-\sinh(\eta)\prod_{k\neq j}f_{kj}f_{jk}$):

$$\begin{aligned}\frac{\partial}{\partial z_j}\left(\sum_{\{\lambda^+\}\cup\{\lambda^-\}}\mathbb{F}^{\mathcal{O}}_{n,S}(\{\lambda^+\}_n)S_N(\{\lambda^+\}_n,\{\lambda^-\}_{N-n},\{z^-\}_{N-n})\right)=\\ =\big(-\sinh(\eta)\big)\left(\prod_{\substack{k=1\\k\neq j}}^{N}f_{kN}f_{Nk}\right)\underbrace{\sum_{\{\lambda^+\}^*\cup\{\lambda^-\}^*}\mathbb{F}^{\mathcal{O}}_{n,S}(\{\lambda^+\}_n)S_{N-1}(\{\lambda^+\}_n,\{\lambda^-\}_{N-n-1},\{z^-_{mod}\}_{N-n-1})}_{\langle\mathcal{O}\rangle(\{\lambda\}_{N-1},\{z_{mod}\}_{N-1})}=\\ =\frac{\partial}{\partial z_j}\Big(\langle\mathcal{O}\rangle_N(\{\lambda\}_N,\{z\}_N)\Big).\end{aligned} \tag{4.65}$$

Here we used the induction assumption, equation (4.50) and that $\{\lambda^+\}^*\cup\{\lambda^-\}^*=\{\lambda\}_N\backslash\{\lambda_j\}=\{\lambda\}_{N-1}$. This demonstrates that the z dependence of the two sides are equal. To investigate the part independent of

the z variables, we have to take all of them to zero. In this case on the r.h.s. only $\mathbb{F}^{\mathcal{O}}_{N,s}(\{\lambda\}_N)$ remains. Since $\langle\mathcal{O}\rangle_N(\{\lambda\}_N,\{0\}_N)=\mathbb{F}^{\mathcal{O}}_{N,s}(\{\lambda\}_N)$, the two sides are equal. This completes the proof. □

Theorem 1 and Theorem 3 are equivalent: the former is recovered from the latter by dividing (4.64) by the normalization factor (3.65):

$$\frac{1}{\langle 0|\prod_{k=1}^{N}C(\lambda_k)\prod_{k=1}^{N}B(\lambda_k)|0\rangle}\sum_{\{\lambda^+\}\cup\{\lambda^-\}}\mathbb{F}^{\mathcal{O}}_{n,S}(\{\lambda^+\}_n)S_N(\{\lambda^+\}_n,\{\lambda^-\}_{N-n},\{z^-\}_{N-n})=$$
$$=\frac{1}{\rho(\{\lambda\}_N)}\sum_{\{\lambda^+\}\cup\{\lambda^-\}}\underbrace{\mathbb{F}^{\mathcal{O}}_{n,S}(\{\lambda^+\}_n)\left(\big(-\sinh(\eta)\big)^n\prod_{j<k}f(\lambda_k^+,\lambda_j^+)f(\lambda_j^+,\lambda_k^+)\right)^{-1}}_{F^{\mathcal{O}}_{n,S}(\{\lambda^+\})}\rho(\{\lambda^-\}_{N-n}). \quad (4.66)$$

With this, the proof of Theorem 1 is complete. In the remaining sections of this chapter, we use this theorem to prove the current mean formulae (4.4) and (4.5).

4.3 Calculation of the form factors

The expectation values of the conserved charges are known from the Bethe Ansatz solution, therefore the symmetric form factors corresponding to these operators can be calculated directly, using the expansion (4.22):

$$\frac{1}{\rho(\{\lambda\}_N)}\sum_{\{\lambda^+\}\cup\{\lambda^-\}}\mathcal{Q}_\alpha(\{\lambda^+\})\rho(\{\lambda^-\})=\frac{1}{L}\sum_{k=1}^{N}q_\alpha(\lambda_k). \quad (4.67)$$

This is an algebraic relation valid for any finite volume L and particle number N that can be used to recursively obtain the form factors of the charge operators. Before turning to the general case with arbitrary N, it is useful to examine the form factors with few-particle states to gain insight.

4.3.1 Few particle cases

Starting from $N=1$, one can recursively find the form factors of the charge operators:

- $\mathbf{N=1}$:
  Substituting $\rho(\emptyset)=1$ and $\mathcal{Q}_\alpha(\emptyset)=0$ to (4.67) leads to

$$\mathcal{Q}_\alpha(\lambda)=\frac{\rho(\lambda)}{L}q_\alpha(\lambda). \quad (4.68)$$

  Using that $\rho(\lambda)=p'(\lambda)L$, yields the result

$$\mathcal{Q}_\alpha(\lambda)=q_\alpha(\lambda)p'(\lambda). \quad (4.69)$$

- $\mathbf{N=2}$:

  Writing out (4.67) in the two particle case gives

$$\frac{1}{L}(q_\alpha(\lambda_1)+q_\alpha(\lambda_2))=\frac{1}{\rho(\lambda_1,\lambda_2)}\big(\mathcal{Q}_\alpha(\lambda_1,\lambda_2)+\mathcal{Q}_\alpha(\lambda_1)\rho(\lambda_2)+\mathcal{Q}_\alpha(\lambda_2)\rho(\lambda_1)\big). \tag{4.70}$$

  Rearranging for the two particle form factor, using the expression obtained for the one particle case above and the determinant of the 2×2 Gaudin matrix

$$\rho(\lambda_1,\lambda_2)=\begin{vmatrix} p'(\lambda_1)L+\varphi_{12} & -\varphi_{12} \\ -\varphi_{12} & p'(\lambda_2)L+\varphi_{12} \end{vmatrix}=L^2p'(\lambda_1)p'(\lambda_2)+L\varphi_{12}\big(p'(\lambda_1)+p'(\lambda_2)\big), \tag{4.71}$$

  result in:

$$\begin{aligned}\mathcal{Q}_\alpha(\lambda_1,\lambda_2)&=\frac{\rho(\lambda_1,\lambda_2)-\rho(\lambda_1)\rho(\lambda_2)}{L}(q_\alpha(\lambda_1)+q_\alpha(\lambda_2))=\\&=(q_\alpha(\lambda_1)+q_\alpha(\lambda_2))(p'(\lambda_1)+p'(\lambda_2))\varphi_{12}.\end{aligned} \tag{4.72}$$

- $\mathbf{N=3}$:

  In the three particle case, after using the expressions for the one and two particle form factors, the expansion (4.67) leads to:

$$\begin{aligned}&\mathcal{Q}_\alpha(\lambda_1,\lambda_2,\lambda_3)=\frac{q_\alpha(\lambda_1)+q_\alpha(\lambda_2)+q_\alpha(\lambda_3)}{L}\times\\&\times\big[\rho(\lambda_1,\lambda_2,\lambda_3)-\rho(\lambda_1)\rho(\lambda_2,\lambda_3)-\rho(\lambda_2)\rho(\lambda_1,\lambda_3)-\rho(\lambda_3)\rho(\lambda_1,\lambda_2)+2\rho(\lambda_1)\rho(\lambda_2)\rho(\lambda_3)\big].\end{aligned} \tag{4.73}$$

  Substituting the value of the 3×3 Gaudin determinant

$$\begin{aligned}\rho(\lambda_1,\lambda_2,\lambda_3)=&\begin{vmatrix} p'(\lambda_1)L+\varphi_{12}+\varphi_{13} & -\varphi_{12} & -\varphi_{13} \\ -\varphi_{12} & p'(\lambda_2)L+\varphi_{12}+\varphi_{23} & -\varphi_{23} \\ -\varphi_{13} & -\varphi_{23} & p'(\lambda_3)L+\varphi_{13}+\varphi_{23} \end{vmatrix}=\\&=L^3p'(\lambda_1)p'(\lambda_2)p'(\lambda_3)+L^2\big[\big(\varphi_{13}+\varphi_{23}\big)p'(\lambda_1)p'(\lambda_2)+\big(\varphi_{12}+\varphi_{23}\big)p'(\lambda_1)p'(\lambda_3)+\\&+\big(\varphi_{12}+\varphi_{13}\big)p'(\lambda_2)p'(\lambda_3)\big]+L\big[\big(p'(\lambda_1)+p'(\lambda_2)+p'(\lambda_3)\big)\big(\varphi_{12}\varphi_{13}+\varphi_{12}\varphi_{23}+\varphi_{13}\varphi_{23}\big)\big],\end{aligned} \tag{4.74}$$

  back to (4.73) produces the result for the three particle form factor:

$$\begin{aligned}&\mathcal{Q}_\alpha(\lambda_1,\lambda_2,\lambda_3)=\\&=\big(q_\alpha(\lambda_1)+q_\alpha(\lambda_2)+q_\alpha(\lambda_3)\big)\big(p'(\lambda_1)+p'(\lambda_2)+p'(\lambda_3)\big)\big(\varphi_{12}\varphi_{13}+\varphi_{12}\varphi_{23}+\varphi_{13}\varphi_{23}\big).\end{aligned} \tag{4.75}$$

The expressions (4.69), (4.72) and (4.75) give the symmetric form factors of the conserved charges in the one, two and three particle cases, respectively. Using (4.20), one can easily obtain the corresponding form

factors of the (generalized) current operators as well:

$$\begin{aligned}
&\mathcal{J}^{\beta}_{\alpha}(\lambda) = q_{\alpha}(\lambda)q_{\beta+1}(\lambda),\\
&\mathcal{J}^{\beta}_{\alpha}(\lambda_1,\lambda_2) = (q_{\alpha}(\lambda_1)+q_{\alpha}(\lambda_2))(q_{\beta+1}(\lambda_1)+q_{\beta+1}(\lambda_2))\varphi_{12},\\
&\mathcal{J}^{\beta}_{\alpha}(\lambda_1,\lambda_2,\lambda_3) =\\
&= \big(q_{\alpha}(\lambda_1)+q_{\alpha}(\lambda_2)+q_{\alpha}(\lambda_3)\big)\big(q_{\beta+1}(\lambda_1)+q_{\beta+1}(\lambda_2)+q_{\beta+1}(\lambda_3)\big)\big(\varphi_{12}\varphi_{13}+\varphi_{12}\varphi_{23}+\varphi_{13}\varphi_{23}\big).
\end{aligned} \tag{4.76}$$

In principle, this recursive method can yield all higher symmetric form factors of the charge and current operators. However, for $N > 3$, the procedure becomes more and more tedious. For the general value of N, an alternative treatment is more convenient.

4.3.2 General case

To obtain the form factors in the general case, we have to recall that they are do not depend explicitly on the volume L (this is transparent from the already calculated form factors above). Their only volume dependence comes through the solutions of the Bethe equations, the Bethe roots and the normalization of the eigenstates. Therefore, an expression for the Gaudin determinants is needed that allows for examining their dependence on L and can be substituted into the expansion (4.67). There exists such an expression, the so-called matrix-tree expansion that represents the determinants of matrices with special properties, using graph theoretical notions:

Theorem 4. *Let G_{jk} be an $m \times m$ matrix that can be written as the difference of a diagonal matrix D and a matrix K with elements summing up to zero in all of its rows:*

$$\begin{aligned}
&G_{jk} = D_k\delta_{jk} - K_{jk},\\
&\sum_{k=1}^{m} K_{jk} = 0, \qquad\qquad j = 1,\dots,m.
\end{aligned} \tag{4.77}$$

Then the determinant of G_{jk} is given as a sum over the directed spanning forests of the totally connected graph with m vertices. A graph $\mathcal{F}$ is said to be the directed spanning forest of the graph Γ, if $\mathcal{F}$ is a directed subgraph of Γ and satisfies the following properties:

1. *$\mathcal{F}$ contains all vertices of Γ,*
2. *$\mathcal{F}$ does not contain any circle,*
3. *each vertex of $\mathcal{F}$ has at most one incoming edge.*

Vertices without incoming edges are called roots. Every spanning forest is made up of connected subgraphs, called trees. Every tree contains exactly one root. With the help of these notions, the determinant of G_{jk} is

given by:

$$\det G = \sum_{\mathcal{F}} \left(\prod_{j \in R(\mathcal{F})} D_j \prod_{l_{uv} \in \mathcal{F}} K_{uv} \right), \tag{4.78}$$

where $\mathcal{F}$ goes over all spanning forests of the totally connected graph, while j and l_{uv} run through the roots and the edges of $\mathcal{F}$, respectively.

For a proof, see [97]. It is obvious that the Gaudin matrix satisfies the conditions in Theorem 4, therefore (4.78) can be used to express the Gaudin determinants:

$$\rho(\lambda_1, \ldots, \lambda_N) = \sum_{\mathcal{F}} \left(\prod_{j \in R(\mathcal{F})} p'(\lambda_j) L \prod_{l_{uv} \in \mathcal{F}} \varphi_{uv} \right). \tag{4.79}$$

For better understanding, the graphs present in the right hand side of (4.79), and the factors corresponding to them are presented in Fig. 4.2 for the cases of $N = 1, 2, 3$. Since every spanning forest contains at least one root, therefore the Gaudin determinant $\rho(\lambda_1, \ldots, \lambda_N)$ is a polynomial of degree N without a 0^{th} order term with respect to L. This means that in the $L \to 0$ limit ρ also goes to zero. We can use this property to obtain the form factors of the charge operators, by rearranging (4.67) and taking formally the $L \to 0$ limit:

$$\mathcal{Q}_\alpha(\{\lambda\}_N) = \left(\sum_{k=1}^{N} q_\alpha(\lambda_k) \right) \lim_{L \to 0} \left(\frac{\rho(\lambda_1, \ldots, \lambda_N)}{L} \right), \tag{4.80}$$

where we used the fact that neither the form factors, nor the charge eigenvalues depend explicitly on the volume. From the expansion (4.79), it is easy to see that the terms linear in L in the Gaudin determinant are given by those spanning forests that contain exactly one root, that is the spanning trees. To add up all the contributions coming from these spanning trees, one can use the fact that the function $\varphi(\lambda_j - \lambda_k)$ is even, therefore $\varphi_{jk} = \varphi_{kj}$ and the direction of edges in the directed spanning graphs is irrelevant. As a result, it is enough to consider every possible tree-like spanning graph of the totally connected graph with N vertices, without directions of the edges. To consider every possibility, in every such non-directed spanning tree each vertex has to be chosen once as root. But since the factors coming from the edge-structure is the same for a fixed spanning-tree, the factors $p'(\lambda)L$ corresponding to the roots can be pulled out. Finally this leads to the result

$$\lim_{L \to 0} \left(\frac{\rho(\lambda_1, \ldots, \lambda_N)}{L} \right) = \left(\sum_{k=1}^{N} p'(\lambda_k) \right) \left(\sum_{\mathcal{F}_1} \prod_{l_{uv}} \varphi_{uv} \right), \tag{4.81}$$

where now $\mathcal{F}_1$ runs through all rootless spanning trees. From (4.80) then it follows that the symmetric form factors of the conserved charge operators are given by

$$\mathcal{Q}_\alpha(\{\lambda\}_N) = \left(\sum_{k=1}^{N} q_\alpha(\lambda_k) \right) \left(\sum_{k=1}^{N} p'(\lambda_k) \right) \left(\sum_{\mathcal{F}_1} \prod_{l_{uv}} \varphi_{uv} \right). \tag{4.82}$$

N = 1 :

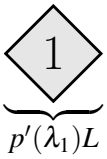

N = 2 :

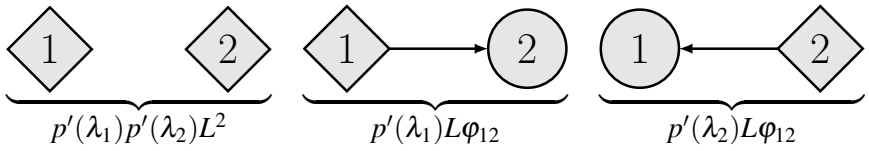

N = 3 :

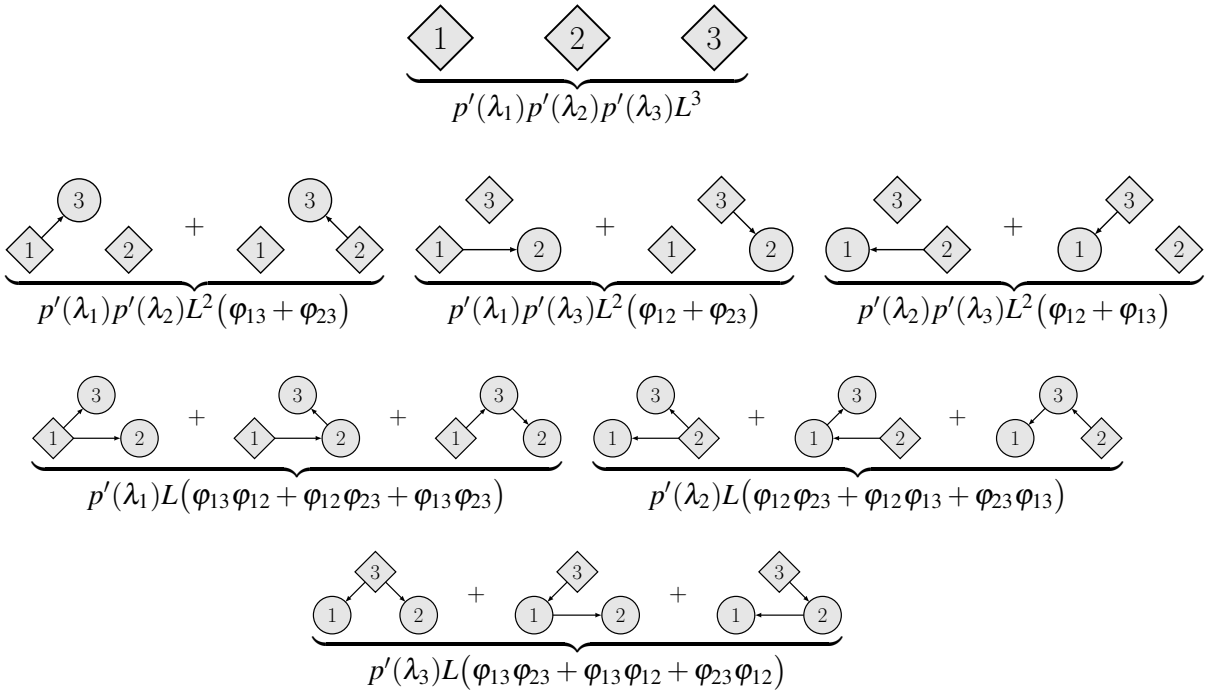

Figure 4.2: The graphs and the corresponding factors present in (4.79) *for the cases $N = 1,2,3$. The numbers label the Bethe roots, the squares denote the roots, while the circles the other vertices. The edges are directed, however $\varphi_{jk} = \varphi_{kj}$, therefore the directions are not relevant. The expansion* (4.79) *indeed reproduces the appropriate Gaudin determinants.*

Using the fact that $\frac{\partial q_\beta}{\partial \lambda} = q_{\beta+1}(\lambda)$ and the connection between the charge and current form factors (4.20),

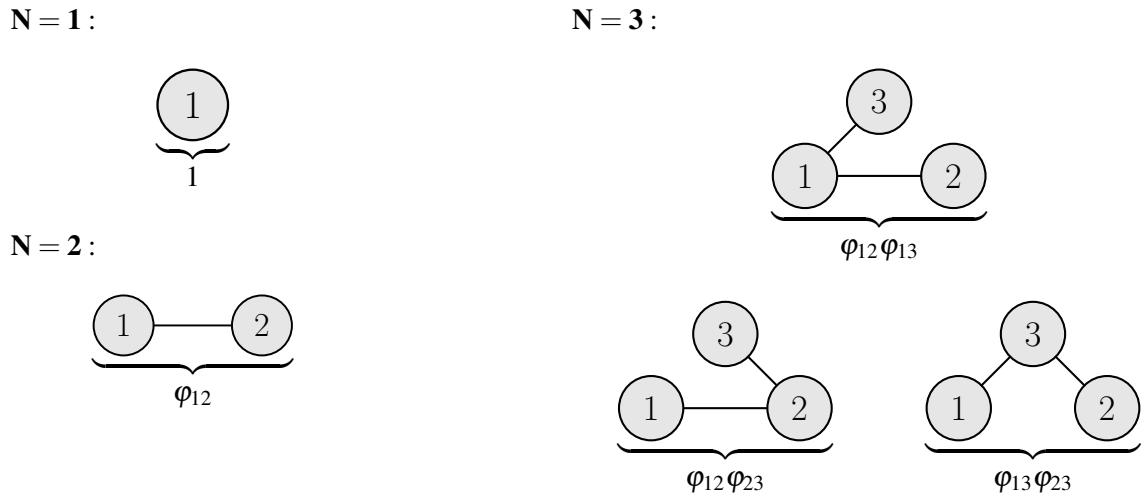

Figure 4.3: The graphs and the factors corresponding to them summed up in the expression (4.83)*. Comparison to* (4.76) *shows that* (4.83) *indeed correctly reproduces the symmetric form factors of the current operators.*

we get for the latter that

$$\mathcal{J}^{\beta}_{\alpha}(\{\lambda\}_N) = \left(\sum_{k=1}^{N} q_{\alpha}(\lambda_k)\right)\left(\sum_{k=1}^{N} q_{\beta+1}(\lambda_k)\right)\left(\sum_{\mathcal{F}_1}\prod_{l_{uv}}\varphi_{uv}\right). \tag{4.83}$$

Again for better understanding, the graphs summed over in (4.82) and (4.83), together with their contributions to the form factors are depicted in Fig. 4.3 for the cases $N = 1,2,3$, showing that (4.83) indeed recovers the already obtained form factors (4.76).

4.4 Summation of the form factor series

With the knowledge of the symmetric form factors of the current operators, their mean values are obtained by summing up the expansion

$$\langle\{\lambda\}_N|\hat{J}^{\beta}_{\alpha}(j)|\{\lambda\}_N\rangle = \frac{1}{\rho(\{\lambda\}_N)}\sum_{\{\lambda^+\}\cup\{\lambda^-\}}\mathcal{J}^{\beta}_{\alpha}(\{\lambda^+\})\rho(\{\lambda^-\}). \tag{4.84}$$

Similarly to the calculation of the form factors, it is useful to first consider the few particle cases explicitly to verify the mean value formulae (4.4) and (4.5), before treating the general situation with N particles.

4.4.1 Few particle cases

Using the symmetric form factors (4.76) obtained in the previous subsection and the form of the Gaudin matrix, it is easy to calculate the current mean values for the one and two particle cases.

- $\mathbf{N = 1}$:

In the one particle case, the form factor expansion (4.84) gives

$$\langle\lambda|J_\alpha^\beta|\lambda\rangle = \frac{\mathcal{J}_\alpha^\beta(\lambda)}{\rho(\lambda)} = \frac{q_\alpha(\lambda)q_{\beta+1}(\lambda)}{p'(\lambda)L}. \tag{4.85}$$

This is indeed agrees with the value obtained from the mean value formula (4.5):

$$\mathbf{q}_{\beta+1}\cdot G^{-1}\cdot\mathbf{q}_\alpha = \frac{q_\alpha(\lambda)q_{\beta+1}(\lambda)}{p'(\lambda)L}, \tag{4.86}$$

where we used that in the one particle case the Gaudin matrix is just a scalar $G = p'(\lambda)L$.

- $\mathbf{N=2}$:
  The form factor expansion now reads as

$$\begin{aligned}\langle\lambda_1,\lambda_2|J_\alpha^\beta|\lambda_1,\lambda_2\rangle = \frac{\rho(\lambda_1)\mathcal{J}_\alpha^\beta(\lambda_2)+\rho(\lambda_2)\mathcal{J}_\alpha^\beta(\lambda_1)+\mathcal{J}_\alpha^\beta(\lambda_1,\lambda_2)}{\rho(\lambda_1,\lambda_2)} = \frac{1}{\rho(\lambda_1,\lambda_2)}\times\\ \times\Big[p'(\lambda_1)Lq_\alpha(\lambda_2)q_{\beta+1}(\lambda_2)+p'(\lambda_2)Lq_\alpha(\lambda_1)q_{\beta+1}(\lambda_1)+\\ +\varphi_{12}\big(q_\alpha(\lambda_1)+q_\alpha(\lambda_2)\big)\big(q_{\beta+1}(\lambda_1)+q_{\beta+1}(\lambda_2)\big)\Big].\end{aligned} \tag{4.87}$$

  The inverse of the 2×2 Gaudin matrix is given by

$$G^{-1}(\lambda_1,\lambda_2) = \frac{1}{\rho(\lambda_1,\lambda_2)}\begin{pmatrix} p'(\lambda_2)L+\varphi_{12} & \varphi_{12}\\ \varphi_{12} & p'(\lambda_1)L+\varphi_{12}\end{pmatrix}, \tag{4.88}$$

  and the mean value formula reproduces (4.87):

$$\begin{aligned}\mathbf{q}_{\beta+1}\cdot G^{-1}\cdot\mathbf{q}_\alpha = \frac{1}{\rho(\lambda_1,\lambda_2)}\Big[p'(\lambda_1)Lq_\alpha(\lambda_2)q_{\beta+1}(\lambda_2)+p'(\lambda_2)Lq_\alpha(\lambda_1)q_{\beta+1}(\lambda_1)+\\ +\varphi_{12}\big(q_\alpha(\lambda_1)+q_\alpha(\lambda_2)\big)\big(q_{\beta+1}(\lambda_1)+q_{\beta+1}(\lambda_2)\big)\Big].\end{aligned} \tag{4.89}$$

4.4.2 General case

The Gaudin determinants do not contain the charge eigenvalues, therefore it is clear that on the right hand side of (4.84) they can enter only through the form factors. It is also obvious that every possible product of the form $q_\alpha(\lambda_j)q_{\beta+1}(\lambda_k)$ will appear with some coefficient. These coefficients are built up of many contributions, stemming from the Gaudin determinants and the part of the form factors given by the summation over spanning trees in (4.83). Nevertheless, it is trivial that the r.h.s. of (4.84) can be written in the form

$$\sum_{\{\lambda^+\}\cup\{\lambda^-\}}\mathcal{J}_\alpha(\{\lambda^+\})\rho(\lambda^-) = \mathbf{q}_{\beta+1}\cdot A\cdot\mathbf{q}_\alpha, \tag{4.90}$$

where A is an $N\times N$ matrix containing all the coefficients of the terms $q_\alpha(\lambda_j)q_{\beta+1}(\lambda_k)$, and is given by

$$A_{jk}=\sum_{\substack{\{\lambda^+\}\cup\{\lambda^-\}\\ \lambda_{j,k}\in\{\lambda^+\}}}\left(\sum_{\mathcal{T}}\prod_{l_{pq}\in\mathcal{T}}\varphi_{pq}\right)\rho(\lambda^-). \tag{4.91}$$

Here the summation inside runs over $\mathcal{T}$, the non-directed spanning trees of $\{\lambda^+\}$. Using this notation, proving the mean value formulae (4.4) and (4.5) is reduced to showing that A is the adjugate matrix of the Gaudin matrix G, or equivalently that $A\cdot G=\det G\cdot\mathbb{1}_N$, where $\mathbb{1}_N$ is the $N\times N$ identity matrix.

Thus in the rest of the section, we show that $\sum_{l=1}^N G_{jl}A_{lk}=\delta_{jk}\cdot\det G$. This matrix product can be written out explicitly using the matrix-tree theorem for the Gaudin determinant:

$$\sum_{l=1}^N\left(\left[\delta_{jl}\left[p'_jL+\sum_{s=1}^N\varphi_{js}\right]-\varphi_{jl}\right]\times\sum_{\substack{\{\lambda^+\}\cup\{\lambda^-\}\\ \lambda_{k,l}\in\{\lambda^+\}}}\left(\sum_{\mathcal{T}}\prod_{l_{pq}\in\mathcal{T}}\varphi_{pq}\right)\left(\sum_{\mathcal{F}}\prod_{n\in R(\mathcal{F})}p'_nL\prod_{l_{uv}\in\mathcal{F}}\varphi_{uv}\right)\right), \tag{4.92}$$

where $\mathcal{F}$ denotes the directed spanning forests of $\{\lambda^-\}$. First, we show that the diagonal elements of this matrix product give $\det G$. To do this, we consider the $j=k$ case in (4.92) and we split the outer summation over l into two parts: to the $l=j$ and $l\neq j$ cases.

In the case of $l=j$, the sum of the φ terms from the Gaudin matrix appears, multiplying the appropriate terms in A. These can be written in the following way:

$$\begin{aligned}&\left(\sum_{\substack{s=1\\ s\neq j}}^N\varphi_{js}\right)\sum_{\substack{\{\lambda^+\}\cup\{\lambda^-\}\\ \lambda_j\in\{\lambda^+\}}}\left(\sum_{\mathcal{T}}\prod_{l_{pq}\in\mathcal{T}}\varphi_{pq}\right)\left(\sum_{\mathcal{F}}\prod_{n\in R(\mathcal{F})}p'_nL\prod_{l_{uv}\in\mathcal{F}}\varphi_{uv}\right)=\\ &=\sum_{\substack{s=1\\ s\neq j}}\left[\varphi_{js}\sum_{\substack{\{\lambda^+\}\cup\{\lambda^-\}\\ \lambda_{j,s}\in\{\lambda^+\}}}\Big(\dots\Big)\Big(\dots\Big)+\varphi_{js}\sum_{\substack{\{\lambda^+\}\cup\{\lambda^-\}\\ \lambda_j\in\{\lambda^+\}\\ \lambda_s\in\{\lambda^-\}}}\Big(\dots\Big)\Big(\dots\Big)\right].\end{aligned} \tag{4.93}$$

Here in the second line, we denoted the terms inside the summation with $(\dots)$ for brevity. Using this equation and renaming the summation variable l to s in (4.92), we can finally arrive at the following expression

for the diagonal elements of the matrix product (4.92):

$$p'_j L \sum_{\substack{\{\lambda^+\}\cup\{\lambda^-\} \\ \lambda_j\in\{\lambda^+\}}} \left(\sum_{\mathcal{T}} \prod_{l_{pq}\in\mathcal{T}} \varphi_{pq}\right)\left(\sum_{\mathcal{F}} \prod_{n\in R(\mathcal{F})} p'_n L \prod_{l_{uv}\in\mathcal{F}} \varphi_{uv}\right) + \sum_{\substack{s=1 \\ s\neq j}}^{N} \left(\varphi_{js} \sum_{\substack{\{\lambda^+\}\cup\{\lambda^-\} \\ \lambda_j\in\{\lambda^+\} \\ \lambda_s\in\{\lambda^-\}}} \left(\sum_{\mathcal{T}} \prod_{l_{pq}\in\mathcal{T}} \varphi_{pq}\right)\left(\sum_{\mathcal{F}} \prod_{n\in R(\mathcal{F})} p'_n L \prod_{l_{uv}\in\mathcal{F}} \varphi_{uv}\right) \right). \tag{4.94}$$

Looking at this expression from the graph theoretical point of view, and using the matrix-tree theorem, it can be shown that this is indeed $\det G$: in the first term for every bi-partition the summation over $\mathcal{T}$ (together with the $p'_j L$ factor) gives the contribution of every such directed spanning tree of $\{\lambda^+\}$ in which λ_j is the root. Together with the summation over $\mathcal{F}$, which is just the contribution from every directed spanning forest of $\{\lambda^-\}$, the first term contains all such directed spanning forests of $\{\lambda\}$ in which λ_j is one of the roots. On the other hand in the second term the summation over $\mathcal{T}$ gives the contributions from the free (rootless) spanning trees of $\{\lambda^+\}$. These are „connected" to one of the spanning trees in the spanning forests of $\{\lambda^-\}$ by the factor φ_{js}. Since $\{\lambda^+\}$ and $\{\lambda^-\}$ are disjoint sets, this connection cannot create circles, so the result is still a spanning tree. Furthermore, since we sum over s, this connection is realized in every possible way, which means that the second term gives the contribution of every spanning forest of $\{\lambda\}$ in which λ_j is not among the roots. Altogether the two terms contain the contribution from all of the directed spanning forests of $\{\lambda\}$, which is just $\det G$ according to the matrix-tree theorem.

For the off-diagonal elements of the matrix product (4.92) the same steps can be performed. To show that in this case the result is zero, it is convenient to investigate those terms that contain p'_j, and afterwards those that do not. The ones that contain p'_j are

$$p'_j L \sum_{\substack{\{\lambda^+\}\cup\{\lambda^-\} \\ \lambda_{j,k}\in\{\lambda^+\}}} \left(\sum_{\mathcal{T}} \prod_{l_{pq}\in\mathcal{T}} \varphi_{pq}\right)\left(\sum_{\mathcal{F}} \prod_{n\in R(\mathcal{F})} p'_n L \prod_{l_{uv}\in\mathcal{F}} \varphi_{uv}\right) - \sum_{\substack{s=1 \\ s\neq j}}^{N} \left(\varphi_{js} \sum_{\substack{\{\lambda^+\}\cup\{\lambda^-\} \\ \lambda_{k,s}\in\{\lambda^+\} \\ \lambda_j\in\{\lambda^-\}}} \left(\sum_{\mathcal{T}} \prod_{l_{pq}\in\mathcal{T}} \varphi_{pq}\right)\left(\sum_{\substack{\mathcal{F} \\ n\in R(\mathcal{F}) \\ j\in R(\mathcal{F})}} \prod p'_n L \prod_{l_{uv}\in\mathcal{F}} \varphi_{uv}\right) \right). \tag{4.95}$$

In the second line $j \in R(\mathcal{F})$ denotes that here we consider only those spanning trees of $\{\lambda^-\}$ in which λ_j is one of the roots. Because of this we can pull out a $p'_j L$ factor from it. Similarly to the previous argument, it can be shown that this whole expression is zero: in the second line, for every partition the spanning tree in $\mathcal{F}$ that originates from λ_j is connected to a spanning tree in $\mathcal{T}$ by φ_{js}, and the result of this connection is

still a spanning tree. Since there is a summation over s, all possible connections are included. This means that the second line contains all such spanning trees that include λ_j and λ_k, beside all the spanning forests of $\{\lambda^-\}$. But the first line is exactly the same, so their difference is zero. The terms that do not contain p'_j are

$$\sum_{\substack{s=1\\ s\neq j}}^{N}\Bigg[\varphi_{js}\sum_{\substack{\{\lambda^+\}\cup\{\lambda^-\}\\ \lambda_{j,k}\in\{\lambda^+\}\\ \lambda_s\in\{\lambda^-\}}}\left(\sum_{\mathcal{T}}\prod_{l_{pq}\in\mathcal{T}}\varphi_{pq}\right)\left(\sum_{\mathcal{F}}\prod_{n\in R(\mathcal{F})}p'_nL\prod_{l_{uv}\in\mathcal{F}}\varphi_{uv}\right)- \\ -\varphi_{js}\sum_{\substack{\{\lambda^+\}\cup\{\lambda^-\}\\ \lambda_{k,s}\in\{\lambda^+\}\\ \lambda_j\in\{\lambda^-\}}}\left(\sum_{\mathcal{T}}\prod_{l_{pq}\in\mathcal{T}}\varphi_{pq}\right)\left(\sum_{\mathcal{F}}\prod_{\substack{n\in R(\mathcal{F})\\ j\notin R(\mathcal{F})}}p'_nL\prod_{l_{uv}\in\mathcal{F}}\varphi_{uv}\right)\Bigg]. \tag{4.96}$$

Here in the first line $\lambda_j\in\{\lambda^+\}$ and $\lambda_s\in\{\lambda^-\}$, and they are connected by φ_{js}, while in the second line they are reversed. Since we sum up for every s and every bi-partition (and since λ_j cannot be a root in the second line) the difference is zero. This completes the summation of the expansion and the entire proof of the mean value formulae (4.4), (4.5) as well.

This completes the proof of the current mean value formulae: by summing up the form factors of the current operators according to the previously proven Theorem 1, we showed that (4.4) and (4.5) indeed correctly give the current mean values. Although in most of our calculations in the last two sections, we focused on the generalized current operators, the expression for the physical currents (4.4) follows from (4.5) as a special case.

4.5 Summary

In this chapter, we presented our results for the mean values of current operators in Bethe Ansatz solvable systems, based on the work [82]. The main result is given by equations (4.4) and (4.5). These formulae can be considered as the finite volume version of (2.9), and as such serve as a rigorous theoretical foundation for one of the underlying assumptions of GHD.

Even though at some points of our proof, we focused on the special case of the XXZ model, our result is rather general and applicable to other Bethe Ansatz solvable models. The key ingredient of the proof is the form factor expansion theorem (4.22), which we proved for the XXZ model, by analyzing the singularity properties of the form factors. However, similar expansion theorems can be established for other integrable models as well (for integrable QFTs see [90], while for the Lieb-Liniger model [91]). Once the expansion theorem is obtained, the remaining steps of the proof are the same: first, to calculate the symmetric form factors of the conserved charge and (by utilizing the continuity equation) the corresponding current operators.

Then, to sum up these form factors, according to the expansion theorem.

The connection between our finite size results and (2.9) were established by a semi-classical picture. Due to integrability and the factorized and completely elastic scatterings, the derivations within the semi-classical picture are valid in the full quantum theory as well.

In this work, we restricted our attention to strictly local charges. However, in the GGE description and therefore in GHD, quasi-local charges have non-negligible effects. For these quasi-local charges our result is expected to hold up to exponential corrections in the system size, caused by the contributions of operators with exponentially decreasing amplitudes in the charge densities.

After the completion and publication of [82], a series of works investigated the current mean values in integrable models: Nested systems, where the fundamental excitations possess internal degrees of freedom were treated in [98], using a connection to long range deformed models. The algebraic construction of current operators were obtained in [99], embedding the currents to the well-known framework of QISM. The results of [82, 98, 99] were also summarized in the review article [83], together with some new results. In [100], the results (4.4) and (4.5) were rederived in an integrable QFT setting. Independently, in [101] the current mean values were studied directly in the thermodynamic limit, using a completely different method compared to ours, and (2.9) was verified. Finally, the extension of the results (4.4) and (4.5) to non $U(1)$ symmetric systems were given in [73], based on the algebraic construction of the current operators [99]. This extension is the topic of the next chapter.

Chapter 5

Current mean values in the XYZ model

In the previous chapter, we obtained a formula for the current mean values of the XXZ model in finite volume, and argued that this result supports the assumptions of Generalized Hydrodynamics. Our derivations used the Algebraic Bethe Ansatz technique, and as such heavily relied on the $U(1)$ symmetry of the investigated model. However, there exist integrable systems without $U(1)$ symmetry, and GHD itself does not depend on the $U(1)$ symmetry either, only on the existence of the extra conserved charges. Despite of this fact, all previously studied cases in the literature were models with particle number conservation. This circumstance naturally raises the question: how can we establish a GHD description in integrable systems that lack $U(1)$ symmetry? In this chapter, we take a first step in answering this question, by calculating the current mean values in the XYZ model.

Similarly to the case of the XXZ model, computing the expectation values of local operators is interesting in its own rights as well, independently from GHD. Due to its mathematically more involved solution, there are fewer results known in the XYZ model, however. The works that treated this system include the calculation of correlation functions at the so-called cyclic points in [102] and the computation of multiple integral formulas in [103] and in [104–106] as well. Also, the scalar products of Bethe states were considered in [107, 108] and more recently even form factors of local operators were calculated in the framework of generalized ABA, in the free fermion limit [109]. Our study of the expectation values of certain local operators, namely the currents, fits into this line of research.

The work presented in this chapter is based on [73] and is organized as follows: first, in Section 5.1, we state our main result for the current mean values. As we shall see, these take functionally the same form as in the $U(1)$ symmetric case. However, the proof of the results is carried out in a completely different way. It builds on the algebraic construction of the current operators, which is summarized in Section 5.2. Using this algebraic construction together with the generalized ABA technique that was introduced in Subsection 3.3.3, our proof is completed in Section 5.3.

5.1 Current mean value formula

In this chapter, we obtain a mean value formula for the currents of the XYZ model. The current operators are still defined as in equations (4.1) and (4.3). Explicit expressions for the first few operators can also be found in Appendix B.

Our main result for the mean values of these current operators in the (normalized) eigenstates of the system take the same functional form just like in the $U(1)$ symmetric case:

$$\langle \lambda_1, \dots, \lambda_n | j_\alpha^\beta(j) | \lambda_1, \dots, \lambda_n \rangle = \mathbf{q}'_\beta \cdot G^{-1} \cdot \mathbf{q}_\alpha, \tag{5.1}$$

where $\mathbf{q}_\alpha$ and $\mathbf{q}'_\beta$ are still n-component vectors ($n = L/2$) with elements now given by the one-particle charge eigenvalues (3.86), while the Gaudin matrix G is the logarithmic derivative of the Bethe equations (3.83). Here only the formula for the generalized currents is written, the special case of the physical currents simply follows from it.

The fact that the same functional form still holds in the model with broken $U(1)$ symmetry, is not trivial. Due to the lack of particle number conservation, CBA breaks down, and even though the Hamiltonian can be diagonalized by a generalization of the ABA, the interpretation of the rapidity variables is not so clear in this framework. Moreover, there are no single particle excitations, all eigenstates of the model contain $n = L/2$ rapidities. As a result, the simple semi-classical picture of Subsection 4.1.1 cannot be applied anymore. Nevertheless, the fact that (5.1) is still valid shows that the rapidity parametrization of the generalized ABA method is useful to describe not just the charge, but the current mean values as well, and that the key ingredient behind all of these considerations is integrability, regardless of $U(1)$ symmetry.

In the rest of this chapter, we prove (5.1), by closely following the steps and presentation of [73].

5.2 Algebraic construction of the current operators

The Quantum Inverse Scattering Method, which we summarized in Section 3.3, has long been used to construct the conserved charge operators in integrable systems. Nevertheless, current operators have only recently been incorporated into this framework [99]. Our proof of (5.1) relies on this algebraic construction, so we briefly review the findings of [99] here.

We examine a general integrable system characterized by an R-matrix $R(u)$ that meets the Yang-Baxter equation (3.35) and the regularity and unitarity conditions (3.40). The model's monodromy and transfer matrices are given by (3.39) and (3.32), respectively. Rather than calculating each conserved charge operator individually as in (3.37), we define a generating function for all the global charges:

$$\hat{Q}(u) = (-i) t^{-1}(u) \frac{d}{du} t(u). \tag{5.2}$$

This definition agrees with (3.51) (up to factors of i) and the canonical charges are given as the coefficients

of the Taylor expansion of $\hat{Q}(u)$, around $u = 0$. A charge density for this generating function can be found: $\hat{Q}(u) = \sum_{j=1}^{L} \hat{q}(u,j)$ with

$$\hat{q}(u,j) = (-i)t^{-1}(u)\mathrm{Tr}_a\left[T_a^{[L,j+1]}(u)\partial_u R_{a,j}(u)T_a^{[j-1,1]}(u)\right]. \tag{5.3}$$

Here $T_a^{[j_2,j_1]}(u)$ is a partial monodromy matrix defined on the segment $[j_1,\ldots,j_2]$:

$$T_a^{[j_2,j_1]}(u) = R_{a,j_2}(u)\ldots R_{a,j_1}(u). \tag{5.4}$$

Similarly to the charge operators, we can define a generating operator for the currents as well:

$$\hat{J}(u,v,j) = \sum_{\alpha=2}^{\infty}\sum_{\beta=2}^{\infty}\frac{u^{\alpha-2}}{(\alpha-2)!}\frac{v^{\beta-2}}{(\beta-2)!}\hat{J}_\alpha^\beta(j), \tag{5.5}$$

where $\hat{J}_\alpha^\beta(j)$ are the generalized currents, defined in (4.3). The generating functions $\hat{Q}(u)$ and $\hat{J}(u,v,j)$ satisfy the generalized continuity equation:

$$i\left[\hat{Q}(u),\hat{q}(v,j)\right] = \hat{J}(u,v,j) - \hat{J}(u,v,j+1). \tag{5.6}$$

Using this continuity equation and the Yang-Baxter equation (3.35), it can be shown [99] that the current generating function is given by the following expression:

$$\hat{J}(u,v,j) = -t(v)\partial_v\hat{\Omega}(u,v,j-1)t^{-1}(v), \tag{5.7}$$

where $\hat{\Omega}(u,v,j)$ is a „double-row" operator defined as

$$\hat{\Omega}(\lambda,\mu,j) = t^{-1}(\mu)t^{-1}(\lambda)\mathrm{Tr}_{ab}[T_a^{[L,j+1]}(\lambda)T_b^{[L,j+1]}(\mu)\Theta_{a,b}(\lambda,\mu)T_a^{[j,1]}(\lambda)T_b^{[j,1]}(\mu)]. \tag{5.8}$$

Here a and b are two different auxiliary spaces, and $\Theta_{a,b}(\lambda,\mu)$ is an operator acting on these auxiliary spaces:

$$\Theta_{a,b}(\lambda,\mu) = (-i)R_{b,a}(\mu,\lambda)\partial_\lambda R_{a,b}(\lambda,\mu). \tag{5.9}$$

From (5.7) it simply follows that the mean values of the current generator in the eigenstates of the model are given by:

$$\langle\Psi|\hat{J}(\lambda,\mu,j)|\Psi\rangle = -\partial_\mu\langle\Psi|\hat{\Omega}(\lambda,\mu,j-1)|\Psi\rangle. \tag{5.10}$$

Expressions (5.7) and (5.10) show, how the current operators and their mean values can be constructed in the QISM framework. Moreover, using a trick first developed in [110], the mean values of the operator $\hat{\Omega}(\lambda,\mu,j)$ can be related to the eigenvalues of a transfer matrix of an enlarged spin chain. Let's consider

the following monodromy matrix:

$$T_a^+(\lambda) = R_{a,L+2}(\lambda, \mu+\varepsilon) R^{t_{L+1}}_{L+1,a}(\mu,\lambda) T_a(\lambda), \tag{5.11}$$

where $T_a(\lambda)$ is the original monodromy matrix of a chain of length L, and $[\dots]^{t_{L+1}}$ denotes partial transposition with respect to the physical space at site $L+1$. Since the R-matrices introduced on the two extra sites also satisfy the Yang-Baxter relation, it implies that the transfer matrix defined as

$$t^+(\lambda) = \mathrm{Tr}_a[T_a^+(\lambda)] \tag{5.12}$$

also forms a one parameter family of commuting operators. At $\varepsilon = 0$ the two extra sites decouple from the rest of the chain, and the eigenstates of the enlarged transfer matrix take the following form:

$$t^+(\lambda)\big(|\delta\rangle \otimes |\Psi\rangle\big) = \Lambda_f(\lambda)\big(|\delta\rangle \otimes |\Psi\rangle\big), \tag{5.13}$$

where the „delta-state" $|\delta\rangle$ is given by the components $\delta_{i,j}$ in the computational basis, while $|\Psi\rangle$ is an eigenstate and $\Lambda_f(\lambda)$ is the corresponding eigenvalue of the original transfer matrix $t(\lambda)$. Switching on a non-zero ε affects the eigenstates and eigenvalues. Let $|\Psi^+\rangle$ be the eigenstate of $t^+(\lambda)$ that in the $\varepsilon \to 0$ limit becomes $|\delta\rangle \otimes |\Psi\rangle$, and $\Lambda^+(\lambda|\mu,\varepsilon)$ the eigenvalue corresponding to $|\Psi^+\rangle$. Then a first order perturbation theory computation gives that

$$\langle\Psi|\hat{\Omega}(\lambda,\mu,j)|\Psi\rangle = i\frac{d}{d\varepsilon}\log\Lambda^+(\mu|\lambda,\varepsilon)\Big|_{\varepsilon=0}. \tag{5.14}$$

Accordingly, the mean values of the current generating function are then given by:

$$\langle\Psi|\hat{f}(\lambda,\mu,j)|\Psi\rangle = -i\partial_\mu\left(\frac{d}{d\varepsilon}\log\Lambda^+(\mu|\lambda,\varepsilon)\Big|_{\varepsilon=0}\right). \tag{5.15}$$

Expression (5.15) shows that the current mean values are closely related to transfer matrix eigenvalues, which can be calculated by standard methods of integrability. For the case of the XXZ model, (5.15) was evaluated in [99]. In the next section, we extend this calculation to the case of the XYZ model, proving (5.1).

5.3 Proof of the mean value formula

As discussed in the previous section, the mean values of the currents are directly linked to an auxiliary eigenvalue problem for an enlarged transfer matrix. This eigenvalue problem can be addressed using standard integrability techniques, which accounts for the existence of simple formulae for the mean values of the current operators. In the rest of this chapter, we solve this auxiliary eigenvalue problem and perform the required differentiation in (5.15) to establish our main result (5.1). Our approach closely follows the

calculation in [99] for the XXZ spin chain. The primary difference here is that, rather than the traditional Algebraic Bethe Ansatz, we employ the generalized method outlined in Subsection 3.3.3.

First, we apply local gauge transformations to the additional two sites in exactly the same manner as in (3.67), with the transformation matrix still defined by (3.69). The resulting enlarged, gauge-transformed monodromy matrix is then given by

$$T_a^{+,l}(\lambda) = M_{L+2+l}^{-1}(\lambda) T_a^+(\lambda) M_l(\lambda) = \begin{pmatrix} A_l^+(\lambda) & B_l^+(\lambda) \\ C_l^+(\lambda) & D_l^+(\lambda) \end{pmatrix}. \tag{5.16}$$

As the next step, we need to define local reference states for the additional two sites. Using the crossing relation (3.47) and the addition theorems for the theta functions (see Appendix D), it is straightforward to verify that the local state at site $L+1$, defined as

$$\left|\omega_{L+1}^l(\mu)\right\rangle = \vartheta_4(s+(L+l)\eta-\mu)\,|\uparrow_{L+1}\rangle - \vartheta_1(s+(L+l)\eta-\mu)\,|\downarrow_{L+1}\rangle \tag{5.17}$$

satisfies the following relations:

$$\begin{aligned} \alpha_{L+1}^l(\lambda)\left|\omega_{L+1}^l(\mu)\right\rangle &= \frac{h(\lambda-\mu)}{h(\lambda-\mu-\eta)}\left|\omega_{L+1}^{l-1}(\mu)\right\rangle, \\ \delta_{L+1}^l(\lambda)\left|\omega_{L+1}^l(\mu)\right\rangle &= \left|\omega_{L+1}^{l+1}(\mu)\right\rangle, \\ \gamma_{L+1}^l(\lambda)\left|\omega_{L+1}^l(\mu)\right\rangle &= 0. \end{aligned} \tag{5.18}$$

Similarly, for site $L+2$ the reference state can be chosen as

$$\left|\omega_{L+2}^l(\mu,\varepsilon)\right\rangle = \vartheta_1(s+(L+2+l)\eta-\mu-\varepsilon)\,|\uparrow_{L+2}\rangle + \vartheta_4(s+(L+2+l)\eta-\mu-\varepsilon)\,|\downarrow_{L+2}\rangle\,. \tag{5.19}$$

The action of the local operators are then given by:

$$\begin{aligned} \alpha_{L+2}^l(\lambda)\left|\omega_{L+2}^l(\mu,\varepsilon)\right\rangle &= \left|\omega_{L+2}^{l-1}(\mu,\varepsilon)\right\rangle, \\ \delta_{L+2}^l(\lambda)\left|\omega_{L+2}^l(\mu,\varepsilon)\right\rangle &= \frac{h(\lambda-\mu-\varepsilon)}{h(\lambda-\mu-\varepsilon+\eta)}\left|\omega_{L+2}^{l+1}(\mu,\varepsilon)\right\rangle, \\ \gamma_{L+2}^l(\lambda)\left|\omega_{L+2}^l(\mu,\varepsilon)\right\rangle &= 0. \end{aligned} \tag{5.20}$$

Based on the local actions (5.18) and (5.20), it is clear that the global state written as

$$\left|\Omega_l^+\right\rangle = \left|\omega_1^l\right\rangle \otimes \left|\omega_2^l\right\rangle \otimes \cdots \otimes \left|\omega_L^l\right\rangle \otimes \left|\omega_{L+1}^l(\mu)\right\rangle \otimes \left|\omega_{L+2}^l(\mu,\varepsilon)\right\rangle \tag{5.21}$$

is a proper reference state, satisfying the following relations:

$$\begin{aligned} A_l^+(\lambda)\left|\Omega_l^+\right\rangle &= \frac{h(\lambda-\mu)}{h(\lambda-\mu-\eta)}\left|\Omega_{l-1}^+\right\rangle, \\ D_l^+(\lambda)\left|\Omega_l^+\right\rangle &= \frac{h(\lambda-\mu-\varepsilon)}{h(\lambda-\mu-\varepsilon+\eta)}\left(\frac{h(\lambda)}{h(\lambda+\eta)}\right)^L\left|\Omega_{l+1}^+\right\rangle, \\ C_l^+(\lambda)\left|\Omega_l^+\right\rangle &= 0. \end{aligned} \tag{5.22}$$

In order to obtain the eigenstates and eigenvalues of the enlarged transfer matrix, we again consider the more general transformations

$$T_a^{+,k,l}(\lambda) = M_k^{-1}(\lambda)T_a^+(\lambda)M_l(\lambda) = \begin{pmatrix} A_{k,l}^+(\lambda) & B_{k,l}^+(\lambda) \\ C_{k,l}^+(\lambda) & D_{k,l}^+(\lambda) \end{pmatrix}. \tag{5.23}$$

The R-matrices introduced at the two additional sites satisfy the Yang-Baxter equation, so the RTT-relation (3.36) continues to hold even for the enlarged monodromy matrix $T_a^+(\lambda)$. As the transformation matrices remain unchanged, the elements of the enlarged, gauge-transformed monodromy matrix $T_a^{+(k,l)}(\lambda)$ obey the same commutation relations (3.76) as the operators $A_{k,l}(\lambda)$, $B_{k,l}(\lambda)$, $C_{k,l}(\lambda)$, and $D_{k,l}(\lambda)$ in Subsection 3.3.3. Consequently, the eigenstates and eigenvalues of the enlarged transfer matrix can be derived in the same manner as for the original chain. The only differences compared to the expressions (3.80), (3.82) and (3.83) are that the eigenvalues of the operators $A_l(\lambda)$ and $D_l(\lambda)$ must be replaced according to (5.22), and the number of rapidities n increases by 1, as the length of the chain is extended by 2. Thus, the state

$$\left|\Psi_\theta^+(\lambda_1,\ldots,\lambda_m)\right\rangle = \sum_{l=-\infty}^{\infty} e^{2\pi i l\theta}\left|\Psi_l^+(\lambda_1,\ldots,\lambda_m)\right\rangle \tag{5.24}$$

with

$$\left|\Psi_l^+(\lambda_1,\ldots,\lambda_m)\right\rangle = B_{l+1,l-1}^+(\lambda_1)\ldots B_{l+m,l-m}^+(\lambda_m)\left|\Omega_{l-m}^+\right\rangle \tag{5.25}$$

and $m = n+1 = L/2+1$, is an eigenstate of the enlarged transfer matrix, with eigenvalue

$$\begin{aligned} \Lambda^+(\lambda|\mu,\varepsilon) = e^{2\pi i\theta}\frac{h(\lambda-\mu)}{h(\lambda-\mu-\eta)}\prod_{k=1}^m \alpha(\lambda,\lambda_k) + e^{-2\pi i\theta}\frac{h(\lambda-\mu-\varepsilon)}{h(\lambda-\mu-\varepsilon+\eta)}\times \\ \times\left(\frac{h(\lambda)}{h(\lambda+\eta)}\right)^L\prod_{k=1}^m \alpha(\lambda_k,\lambda), \end{aligned} \tag{5.26}$$

given that the modified Bethe equations are satisfied:

$$\frac{h(\lambda_j-\mu-\eta)h(\lambda_j-\mu-\varepsilon)}{h(\lambda_j-\mu)h(\lambda_j-\mu-\varepsilon+\eta)}\left(\frac{h(\lambda_j)}{h(\lambda_j+\eta)}\right)^L = e^{4\pi i\theta}\prod_{\substack{k=1\\k\neq j}}^m \frac{\alpha(\lambda_j,\lambda_k)}{\alpha(\lambda_k,\lambda_j)}. \tag{5.27}$$

Once the eigenvalue of the enlarged transfer matrix (5.26) is obtained, the remaining task is to carry out the

differentiation in (5.15). To accomplish this, we need to examine how the Bethe roots behave in the limit $\varepsilon \to 0$. As demonstrated in [99], in the limit $\varepsilon \to 0$, the two additional sites decouple, and (some of) the eigenstates of the enlarged chain take the form

$$t^+(\lambda)\left|\Psi^+\right\rangle = \Lambda_f(\lambda|\lambda_1,\dots,\lambda_n)\Big(|\delta\rangle\otimes|\Psi(\lambda_1,\dots,\lambda_n)\rangle\Big), \tag{5.28}$$

where $|\Psi(\lambda_1,\dots,\lambda_n)\rangle$ is the eigenstate and $\Lambda_f(\lambda|\lambda_1,\dots,\lambda_n)$ is the eigenvalue of the original chain. In this limit, the $m = n+1$ rapidities go to the set $\{\mu,\lambda_1,\dots,\lambda_n\}$, where $\{\lambda_1,\dots,\lambda_n\}$ are the Bethe roots of the original chain. This becomes apparent by examining the transfer matrix eigenvalue (5.26):

$$\begin{aligned} &e^{2\pi i\theta}\frac{h(\lambda-\mu)}{h(\lambda-\mu-\eta)}\alpha(\lambda,\tilde{\mu})\prod_{k=1}^{n}\alpha(\lambda,\tilde{\lambda}_k)+\\ &+e^{-2\pi i\theta}\frac{h(\lambda-\mu-\varepsilon)}{h(\lambda-\mu-\varepsilon+\eta)}\left(\frac{h(\lambda)}{h(\lambda+\eta)}\right)^{L}\alpha(\tilde{\mu},\lambda)\prod_{k=1}^{n}\alpha(\tilde{\lambda}_k,\lambda), \end{aligned} \tag{5.29}$$

which clearly goes to $\Lambda_f(\lambda|\lambda_1,\dots,\lambda_n)$ in the limit $\varepsilon\to 0$, $\tilde{\mu}\to\mu$, and $\tilde{\lambda}_i\to\lambda_i$ (using the fact that $h(\lambda)$ is odd).

Therefore, in the limit $\varepsilon\to 0$, the solutions of the Bethe equations (5.27) become

$$\tilde{\mu} = \mu+\varepsilon\gamma+\mathcal{O}(\varepsilon^2), \qquad \tilde{\lambda}_j = \lambda_j+\varepsilon\Delta\lambda_j+\mathcal{O}(\varepsilon^2). \tag{5.30}$$

The results of [11] and [69] suggest that the parameter θ in the Bethe equations does not change as ε varies, which we also checked numerically. Thus, it is sufficient to focus on the ε-dependence of the Bethe roots, with θ treated as a constant throughout the calculation.

The factor γ can be obtained from the Bethe equation written for the rapidity $\tilde{\mu}$:

$$\frac{h(\tilde{\mu}-\mu-\eta)h(\tilde{\mu}-\mu-\varepsilon)}{h(\tilde{\mu}-\mu)h(\tilde{\mu}-\mu-\varepsilon+\eta)}\left(\frac{h(\tilde{\mu})}{h(\tilde{\mu}+\eta)}\right)^{L}\prod_{k=1}^{n}\frac{\alpha(\tilde{\lambda}_k,\tilde{\mu})}{\alpha(\tilde{\mu},\tilde{\lambda}_k)} = e^{4\pi i\theta}. \tag{5.31}$$

For $|x|\ll 1$, the function $h(x)$ behaves linearly ($h(x)\approx x$), so taking the limit $\varepsilon\to 0$ in (5.31) results in:

$$\frac{1-\gamma}{\gamma}\left(\frac{h(\mu)}{h(\mu+\eta)}\right)^{L}\prod_{k=1}^{n}\frac{\alpha(\lambda_k,\mu)}{\alpha(\mu,\lambda_k)} = e^{4\pi i\theta}. \tag{5.32}$$

Therefore, γ is given by:

$$\gamma = \frac{\mathfrak{a}(\mu)}{1+\mathfrak{a}(\mu)}, \qquad \text{where} \qquad \mathfrak{a}(u) = e^{-4i\pi\theta}\left(\frac{h(u)}{h(u+\eta)}\right)^{L}\prod_{k=1}^{n}\frac{\alpha(\lambda_k,u)}{\alpha(u,\lambda_k)}. \tag{5.33}$$

Similarly, $\Delta\lambda_j$ can be obtained from the logarithmic form of the other Bethe equations:

$$p(\tilde{\lambda}_j-\mu-\varepsilon)+p(\tilde{\lambda}_j-\mu-\eta)+\delta(\tilde{\lambda}_j-\tilde{\mu})+Lp(\tilde{\lambda}_j)+\sum_{k\neq j}\delta(\tilde{\lambda}_j-\tilde{\lambda}_k)=2\pi\big(Z_j+2\theta\big), \tag{5.34}$$

where $Z_j\in\mathbb{Z}$, and the functions $p(\lambda)$ and $\delta(\lambda)$ are defined as:

$$e^{ip(\lambda)}=\frac{h(\lambda)}{h(\lambda+\eta)}, \qquad\qquad e^{i\delta(\lambda)}=\frac{h(\lambda+\eta)}{h(\lambda-\eta)}. \tag{5.35}$$

From (5.34), the vector of rapidity shifts $\Delta\boldsymbol{\lambda}$ can be expressed as:

$$G\cdot\Delta\boldsymbol{\lambda}=\mathbf{H}(\mu), \tag{5.36}$$

where

$$G_{jk}=\left.\frac{\partial(2\pi Z_k)}{\partial\lambda_j}\right|_{\varepsilon=0}=\delta_{jk}\left[Lp'(\lambda_j)+\sum_{l=1}^{n}\varphi(\lambda_j-\lambda_l)\right]-\varphi(\lambda_j-\lambda_k) \tag{5.37}$$

is the Gaudin matrix with $\varphi(\lambda)$ being equal to $\delta'(\lambda)$. It is important to note that the first three terms in (5.34) do not contribute to the Gaudin matrix, since their λ-derivatives vanish when ε is set to zero. The quantity $\mathbf{H}(\mu)$ is a column vector with entries given by:

$$H_k(\mu)=p'(\lambda_k-\mu)+\frac{\mathfrak{a}(\mu)}{1+\mathfrak{a}(\mu)}\varphi(\lambda_k-\mu). \tag{5.38}$$

The derivative of the transfer matrix eigenvalue of the enlarged chain (5.26) then can be calculated by using (5.33) and (5.36). A somewhat lengthy and technical computation yields the result:

$$i\left(\frac{d}{d\varepsilon}\log\Lambda^{+}(\nu|\mu,\varepsilon)\bigg|_{\varepsilon=0}\right)=\mathbf{H}(\nu)\cdot G^{-1}\cdot\mathbf{H}(\mu)+l(\mu,\nu)+l(\nu,\mu), \tag{5.39}$$

where

$$l(\mu,\nu)=\frac{p'(\nu-\mu)}{(1+\mathfrak{a}(\mu))(1+\mathfrak{a}^{-1}(\nu))}. \tag{5.40}$$

To calculate the current mean values, one needs to differentiate (5.39) with respect to ν and perform a Taylor expansion in μ and ν around zero. For $|u|\ll 1$, the function $\mathfrak{a}(u)$ behaves as $\mathfrak{a}(u)\sim u^L$, allowing us to safely substitute it with zero. Consequently, $\mathbf{H}(\mu)$ can be approximated as $H_k(\mu)\approx p'(\lambda_k-u)$. Additionally, $l(\mu,\nu)$ can simply be set to zero. With these substitutions, we arrive at the exact result for the current mean values:

$$\langle\lambda_1,\ldots,\lambda_n|\hat{J}^{\beta}_{\alpha}(j)|\lambda_1,\ldots,\lambda_n\rangle=\mathbf{q}'_{\beta}\cdot G^{-1}\cdot\mathbf{q}_{\alpha}, \tag{5.41}$$

where $\mathbf{q}_\alpha$ and $\mathbf{q}'_\beta$ are column vectors with elements given by

$$\big(\mathbf{q}_\alpha\big)_j = q_\alpha(\lambda_j), \qquad \big(\mathbf{q}'_\beta\big)_j = \frac{dq_\beta(\lambda_j)}{d\lambda}, \tag{5.42}$$

with $q_\alpha(\lambda)$ being the charge eigenfunctions, defined in (3.86). Here, we also used that $p'(u) = (-i)e(u)$ is the energy eigenfunction. This completes the proof of the main result (5.1).

In Appendix C, we also provide numerical validations of the main result (5.1).

5.4 Summary

In this chapter, we extended the results of Chapter 4 to an integrable system without $U(1)$ symmetry by obtaining a current mean value formula (5.1) for the XYZ model in finite volume. The proof of this formula was carried out by using the algebraic construction of the current operators and a generalization of the ABA framework that allows one to diagonalize the XYZ Hamiltonian.

Remarkably, the formula (5.1) takes the same functional form as its $U(1)$ symmetric counterpart (4.5) in Chapter 4. At first glance, this might be surprising considering that the Bethe states have a significantly different structure in the non $U(1)$ symmetric case: there are no single particle excitations and the semi-classical picture of Subsection 4.1.1 breaks down. However, as it was already argued in Chapter 4, the key element behind the derivations is integrability, which still holds for the XYZ model. The eigenstates and the charge eigenvalues still can be characterized by a set of rapidities, and our result shows that these variables also convenient for describing the current mean values.

As for possible directions for further research, here we only considered finite volume situations with a system of even length. It would be interesting to extend the results to odd length by considering the current operators with other techniques, such as SoV.

There are also other integrable models that lack $U(1)$ symmetry, a fascinating example being the so-called „golden chain" [111]. This model is connected to several interesting fields of research (such as non-Abelian anyons, PXP and RSOS models), thus it might be more appealing to treat this system instead of the rather exotic XYZ spin chain. Moreover, the Hamiltonian of the golden chain arises as a representation of the Temperley-Lieb algebra, just like the XXZ model. Utilizing this connection, conjectures for the current mean values in the golden chain were established in [112].

Most importantly, it would be interesting to take the thermodynamic limit of our result and then to establish a GHD description for non $U(1)$ symmetric models. This could lead to predictions for the transport properties of the model that could be compared to earlier results that were obtained numerically [113].

Chapter 6

Folded XXZ model

In the previous two chapters, we derived exact results for the current mean values in various integrable lattice systems. These results provide a theoretical background for some of the assumptions behind Generalized Hydrodynamics. Also, in recent years, GHD has been used in countless works to calculate the transport properties of different integrable models (see the contributions to the special issue [53], especially [114]) and its predictions were also verified in experimental setups [50–52]. Still, GHD is an effective theory of quantum many-body models that builds on the hydrodynamic assumption of dividing the system in question into mesoscopic fluid cells and imposing local entropy maximization. To better understand the theory and its range of applicability, it would be desirable to compare its predictions to results obtained from the microscopic laws governing the systems. However, this is, in general, a very hard problem. Even though Bethe Ansatz techniques provide a way of diagonalizing the Hamiltonian, solving the time-evolution following an (in)homogeneous quantum quench also requires calculating overlaps between the initial state and the eigenstates, and evaluating spectral sums, which are impossible in most cases.

These difficulties then beg the question: what are the simplest, genuinely interacting, integrable models in which we may hope to overcome the aforementioned problems? By genuinely interacting models, we mean systems that cannot be mapped to free fermions, like the XY model. Obviously, „being simple" is not a well-defined physical property, however, there are some examples in the literature that should give an idea of what we mean by it. Here, we mention three such examples with similarities between their particle scattering properties.

One of the oldest and most important models in this category is the one-dimensional hard rod gas. It describes a system of impenetrable particles with a fixed width, moving on a continuous line, and scattering elastically on each other. The finite particle size affects the dynamics by decreasing the available space for the propagation of the particles, or equivalently by introducing a finite displacement following particle collisions, with the size of the displacement given by the hard rod length. The model was studied both in the classical [115–119] and in the quantum [120–122] cases. Moreover, in the classical case, the emergence of a hydrodynamic description was verified, and the Euler equation was derived [117], together with a Navier-Stokes type correction [118], for a wide range of initial states satisfying natural conditions.

Another, maybe less well-known example of a simple integrable system is the so-called phase model, which is obtained from the q-boson model as the $q \to \infty$ limit. It was first introduced and studied in [123–125]. Equilibrium correlation functions of the system were calculated in [126–130], while real-time dynamics was investigated, and the predictions of GGE were verified in [131]. The dynamics of the model is such that the scattering of fundamental bosons results in the displacement of particles by one lattice site.

A third example is the so-called Rule 54 model, which is a classical, deterministic cellular automaton that belongs to the family of dual-unitary quantum gate models [132, 133]. These systems are generally non-integrable (although the Rule 54 is integrable), but they still allow for exact solutions. The Rule 54 model was first introduced in [134], while for a review, see [135]. The model supports two types of particles (the left- and right-movers), which propagate on the lattice with a fixed velocity, while their scattering on each other results in the displacement of the particles by one lattice site. Remarkably, it was the first model in which the predictions of GHD following an inhomogeneous quantum quench were verified by exact computation [136].

In the present chapter, we introduce an integrable lattice spin model, the so-called folded XXZ model that shares similar properties to the systems listed above. It possesses a very simple scattering phase, and as a result, the Bethe equations, the structure of the Bethe roots, and the eigenstates of the model also take a remarkably simple form. Therefore, the model can be considered a possible candidate in which the predictions of GHD might be verified.

The Hamiltonian of the folded XXZ model first appeared in [137]. Later, in [138] and in [139, 140], it was re-derived by considering the large anisotropy limit of the XXZ model. The name folded was coined in [139], because of their method that splits the Hamiltonian of the XXZ model with large anisotropy to a fast oscillatory part, and an effective (folded) Hamiltonian, whose spectrum is identical to the spectrum of the original model modulo some typical energy value proportional to the anisotropy parameter. Remarkably, the eigenstates and eigenvalues of the model were also obtained in [139].

In this chapter, we present our work on the folded XXZ model that was carried out as part of a larger collaboration with numerous other researchers and was published in [141]. The paper [141] provides a complementary view on the folded XXZ model compared to the aforementioned works, alongside with brand new results.

The chapter is organized as follows: first, we introduce the model and show its integrability. This is done in a different way with a more immediate connection to the charges of the XXZ model, compared to the derivation of [139]. Then, we present the Bethe Ansatz solution of the system and discuss its ground state properties. Finally, to illustrate the attainability of exact results for real-time dynamics, arising from the simplicity of the system, we compute the expectation values of special local observables following a homogeneous quantum quench. The folded XXZ model also exhibits Hilbert space fragmentation, which is investigated together with its consequences on equilibration in the next chapter. Except the Bethe Ansatz solution, all the results discussed in this chapter are new and first appeared in [141].

6.1 The model and its integrability

All the examples of simple integrable systems listed above share the common property that in them scattering events result in the displacement of the particles by a fixed value. Alternatively, this means that in these models, the scattering phase is a linear function of the quasi-momenta. Using this observation, we can introduce an integrable spin model with the same property, starting from the XXZ model. From (3.17), we know that the scattering phase of the XXZ model is given by:

$$S^{XXZ}(p_j,p_k) = -\frac{e^{i(p_j+p_k)}+1-2\Delta e^{ip_k}}{e^{i(p_j+p_k)}+1-2\Delta e^{ip_j}}. \tag{6.1}$$

Clearly, in the $\Delta \to \infty$ limit (6.1) depends only on the difference of the quasi-momenta $p = p_j - p_k$ and is given by

$$\lim_{\Delta\to\infty} S^{XXZ}(p_j,p_k) = S(p) = -e^{-ip}, \tag{6.2}$$

that is, the scattering phase becomes linear in the quasi-momenta. This suggests that by (somehow) taking the $\Delta \to \infty$ limit of the XXZ model, we can hope to derive a system with simpler dynamics. This statement is of course not mathematically rigorous, however, we can use this observation as a starting point.

Our procedure is as follows: we start with the conserved charges of the XXZ model, listed in Appendix B. These are obviously polynomials in Δ, with some operator coefficients. We can then obtain a set of new charges (that corresponds to the $\Delta \to \infty$ limit) by taking the operator coefficients of the highest order Δ term from each of the original XXZ charges. For example, the first charge in the XXZ model is the total magnetization $\hat{S}^z$, which doesn't depend on Δ at all. Therefore, the first new charge can be chosen to be $\hat{S}^z$ itself, or alternatively

$$\hat{Q}_1 = \frac{1}{2}\sum_{j=1}^{L}(\mathbb{1}-\sigma_j^z), \tag{6.3}$$

where the constant term and the factor of -1/2 were introduced for later purposes. Similarly, the next XXZ charge is the Hamiltonian (3.8) itself. This has a linear term in Δ, so the second new charge is given by

$$\hat{Q}_2 = \frac{1}{2}\sum_{j=1}^{L}(\mathbb{1}-\sigma_j^z\sigma_{j+1}^z), \tag{6.4}$$

where again a factor of -1/2 was introduced. Obviously, both (6.3) and (6.4) are diagonal in the computational basis and generate trivial dynamics. In order to obtain a non-trivial model, we have to go further. Applying the same technique to the third charge of the XXZ model, which is again linear in Δ, gives

$$\hat{Q}_3 = \frac{i}{4}\sum_{j=1}^{L}\left(\sigma_j^z+\sigma_{j+3}^z\right)\left(\sigma_{j+1}^+\sigma_{j+2}^- - \sigma_{j+1}^-\sigma_{j+2}^+\right). \tag{6.5}$$

This operator has a three-site density, written here in a more convenient four-site form. The factor of $i/4$ was again introduced for later convenience and to ensure hermiticity. Even though $\hat{Q}_3$ is dynamical and

generates non-trivial time evolution, it lacks spin flip symmetry. In order to obtain a model that is invariant under spin flips, we need to go one step further. The fourth charge of the XXZ model is quadratic in Δ and produces the new charge

$$\hat{Q}_4 = -\frac{1}{4}\sum_{j=1}^{L}(\mathbb{1}+\sigma_j^z\sigma_{j+3}^z)\big(\sigma_{j+1}^+\sigma_{j+2}^- + \sigma_{j+1}^-\sigma_{j+2}^+\big). \tag{6.6}$$

This is now a dynamical charge with four-site operator density that has spin flip symmetry. The factor of $-1/4$ is included in (6.6) so that later the one-particle eigenvalues of the model become simpler. Now the Hamiltonian of the folded XXZ model can be defined as

$$H = \hat{Q}_4 + h\hat{Q}_1 + \mu\hat{Q}_2, \tag{6.7}$$

where h and μ are two parameters of the model that can be thought of as a magnetic field and chemical potential, respectively.

The procedure that was used to create the charges $\hat{Q}_\alpha,\ \alpha = 1,\dots,4$ guarantees that they mutually commute with each other: the original charges of the XXZ model, which are polynomials in Δ, commute, therefore their commutators (which are consequently also polynomials in Δ) have to vanish in all orders of Δ. However, the leading orders of the original commutators are nothing else but the commutators of the new charges, which thus have to be zero. The existence of two commuting dynamical charges (in this case, $\hat{Q}_3$ and $\hat{Q}_4$) is enough to claim the integrability of a model [142], therefore, we can state that the folded XXZ model is integrable. Moreover, one can continue with the algorithm explained above, and higher charges can be obtained as well. There is one technicality that one needs to keep in mind to do so. The fifth charge of the XXZ model is quadratic in Δ, and as it turns out, the quadratic term's operator coefficient is proportional to $\hat{Q}_3$ given in (6.5). Thus, to calculate the proper fifth charge of the folded model, one needs to subtract from the original fifth charge $\hat{Q}_3$ multiplied by the proper factor, and then take the leading term from the remainder. The result of this procedure is

$$\begin{aligned}\hat{Q}_5 = \sum_{j=1}^{L}&\big(\sigma_j^z+\sigma_{j+4}^z\big)\big(\sigma_{j+1}^x\sigma_{j+3}^y - \sigma_{j+1}^y\sigma_{j+3}^x\big) + \big(\sigma_j^z+\sigma_{j+5}^z\big)\big(\sigma_{j+1}^x\sigma_{j+2}^x + \sigma_{j+1}^y\sigma_{j+2}^y\big)\times\\ &\times\big(\sigma_{j+3}^y\sigma_{j+4}^x - \sigma_{j+3}^x\sigma_{j+4}^y\big) + \big(\mathbb{1}+\sigma_j^z\sigma_{j+4}^z\big)\sigma_{j+2}^z\big(\sigma_{j+1}^x\sigma_{j+3}^y - \sigma_{j+1}^y\sigma_{j+3}^x\big),\end{aligned} \tag{6.8}$$

which has (after expanding the products) a five-site operator density that is written in a six-site form only for convenience. Higher charges of the model can be obtained recursively in a similar manner. At present, we do not have closed form expressions for these higher charges, however, obtaining such expressions might be possible using the results of [143, 144].

We also note that the new charges of the folded XXZ model cannot be obtained from the QISM construction of the XXZ model in a trivial way. This is transparent from the following reasoning: in models where the transfer matrix is built from the R-matrices, the charges can be computed recursively by using

the boost operator (for more details on this method, see Appendix B). Accordingly, in the XXZ model, the boost operator construction yields the appropriate charges. On the contrary, in the folded model, it is easy to check that the commutator of $\hat{Q}_2$ and the boost operator does not produce $\hat{Q}_3$. This signals that the usual QISM method breaks down in the $\Delta \to \infty$ limit.

Since the publication of [141], however, it has become understood that the folded XXZ model can still be embedded into the QISM framework of the so-called medium-range models. This was worked out in [145]. Here, we do not present this method, just note that a transfer matrix can be found for the folded model (but this construction fundamentally differs from that of the XXZ model), and the charges can be obtained algebraically.

6.2 Bethe Ansatz solution

As a result of the extra conserved charges, the model is integrable and solvable by means of CBA: its eigenstates together with their eigenvalues can be constructed exactly. This was first done in [139], but here we present a slightly different approach based on [141].

6.2.1 Particle states

The model exhibits spin-flip symmetry, therefore either the state with all spins up, or all spins down can be chosen as a reference state above which the eigenstates are created. Here, we choose the state $|0\rangle = |\uparrow\uparrow\uparrow\ldots\rangle$ as our reference, and use the notations that were introduced in Section 3.2. Looking at the dynamical part $\hat{Q}_4$ in the Hamiltonian (6.7), it can be seen that it describes the hopping of particles between neighboring sites, with the hopping amplitude being controlled by the two other neighboring sites. From the special form of this control, it is also easy to see that blocks of two or more consecutive down-spins in a sea of up-spins are frozen: they have zero eigenvalue under $\hat{Q}_4$. Because of this, first we only consider scattering states with particles, i.e. states, in which there are no two or more consecutive down-spins. It is important to note, however, that even though these configurations are immobile on their own, unlike to the case of restricted models [146], they are not excluded from the Hilbert space, and we treat them separately in the next subsection.

Single particle states

The wave function of an eigenstate with a single particle can be written as:

$$|p\rangle = \sum_x e^{ipx} |x\rangle \,, \tag{6.9}$$

where the quasi-momentum p is quantized according to the Bethe equation that arises when the periodic boundary condition is imposed:

$$e^{ipL} = 1. \tag{6.10}$$

Direct computation shows that (6.9) is indeed an eigenstate of $\hat{Q}_4$ (and therefore the full Hamiltonian (6.7)), with eigenenergy $e(p) = -\cos(p)$. (For the time being, we assume $h = \mu = 0$ in (6.7) and only consider the eigenvalues of $\hat{Q}_4$.)

Two-particle states

Following the usual steps of coordinate Bethe Ansatz, we can look for the two-particle states in the form

$$|p_1, p_2\rangle = \sum_{x_1<x_2} \chi(x_1, x_2)\, |x_1, x_2\rangle\,, \tag{6.11}$$

with $\chi(x_1, x_2)$ being the sum of plane waves multiplied by the appropriate phases just like in (3.16). Then it is easy to verify by direct substitution that the wave function $\chi(x_1, x_2)$ is given by

$$\chi(x_1, x_2) = e^{i[p_1 x_1 + p_2(x_2-1)]} - e^{i[p_2 x_1 + p_1(x_2-1)]}. \tag{6.12}$$

The state (6.11) is an eigenstate of $\hat{Q}_4$ with energy $E = e(p_1) + e(p_2) = -\big(\cos(p_1) + \cos(p_2)\big)$.

The form of the wave function resembles free fermions, however, extra phases are present in the two terms in (6.12) that appear due to the model being interacting. From (6.12), we can read off the two-particle scattering phase:

$$S(p_1, p_2) = e^{i\delta(p_1,p_2)} = -e^{-i(p_1-p_2)}, \tag{6.13}$$

which is linear in the quasi-momenta, just as we expected from simply taking the limit of the XXZ model in the previous section. The form of $\chi(x_1, x_2)$ is also consistent with our previous considerations: the wave function vanishes whenever the particles are on neighboring sites. This constraint, however, emerges dynamically and is not imposed externally.

N-particle states

Looking at the two-particle wave function, one can notice that it can be written in a convenient determinant form, which actually generalizes to the N-particle case as well. Namely, the N-particle wave function is given by the determinant

$$\chi(x_1, x_2, \ldots, x_N) = \det C, \tag{6.14}$$

where the elements of the matrix C are defined as

$$C_{jk} = e^{ip_j(x_k - k + 1)}. \tag{6.15}$$

The state (6.14) is an eigenstate of $\hat{Q}_4$, with eigenvalue $E = \sum_{j=1}^{N} e(p_j)$. Moreover, the wave function (6.14) still has the property that it vanishes whenever two particles are on neighboring sites.

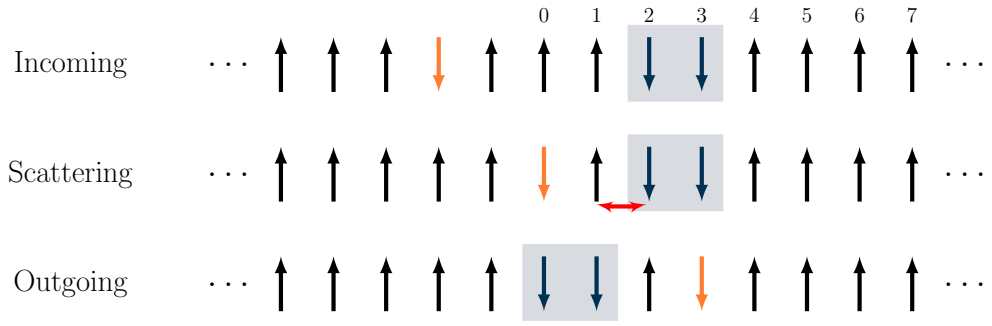

Figure 6.1: Scattering of a particle on a bound state of length two. The particle is incoming from the left, while the bound state occupies sites 2 *and* 3*. Once the particle reaches site* 0*, hopping between sites* 1 *and* 2 *becomes possible. As a result, the bound state gets shifted by two sites to site* 0 *and* 1*, while the particle also suffers a displacement by two sites. Based on a similar figure in Ref. [141].*

Due to the simple scattering phase (6.13), the Bethe equations take a remarkably simple form as well:

$$e^{iPL} = 1, \qquad e^{ip_j(L-N)} = (-1)^{N-1} e^{-iP}, \tag{6.16}$$

where we introduced the total momentum $P = \sum_{j=1}^{N} p_j$. Again, these equations appear almost free: the values of the individual quasi-momenta p_j do not depend explicitly on the values of all other momenta, only on the value of the total momentum P, which shows up in the Bethe equations as a twist. Thus, one can find the Bethe roots by solving the quantization conditions (second equation in (6.16)) individually while keeping in mind that the constraint for the total momentum (first equation in (6.16)) has to be satisfied. Another result of the interaction between particles is the appearance of a modified volume, $L-N$. The particularly simple form of the Bethe equations can be exploited to exactly calculate the time-evolution following certain quench scenarios, which is illustrated in Section 6.4.

6.2.2 Bound states

As we already established, states with sequences of two or more neighboring down-spins have zero eigenvalue. Nevertheless, they are not excluded from the Hilbert space of the system, therefore we have to investigate them separately. To do this, it is useful to introduce the notion of domain walls (DW's), which are just the boundaries between two such regions of the chain that have different spin orientations and are at least two sites long. Domain walls separated by more than one site are frozen, have zero eigenvalue under $\hat{Q}_4$. This fact leads to a huge degeneracy in the reference state, since every configuration with arbitrary many DW's, but without particles will share the same zero eigenvalue. The block of immobile down-spins between DW's can be thought of as the bound states of particles.

Despite the fact that these bound states are not dynamical under the time-evolution dictated by $\hat{Q}_4$, they effect the propagation of particles. This can already be seen from the simplest scenario involving a particle and a bound state of length two, depicted on Fig. 6.1. Initially, the bound state sits at sites 2 and 3, while a

particle is approaching from the left. As the particle reaches site 0, the up- and down-spins on sites 1 and 2 become mobile and swap places. As a result, the bound state gets shifted to sites 0 and 1, while the particle also suffers a displacement by 2 sites.

In order for the configuration described above to be an eigenstate of the system in finite volume with periodic boundary condition, we have to assign a quasi-momentum to the bound state and perform a Fourier-transform, which leads to the state

$$|\Psi\rangle = \sum_{y>x+1} e^{i\left(px+k(y-2)\right)} |x,y,y+1\rangle + \sum_{x>y+2} e^{i\left(p(x-2)+ky\right)} |y,y+1,x\rangle . \tag{6.17}$$

From (6.17), it is then simply read off that the scattering phase of a particle and a bound state of length two is

$$S_{p,2DW}(p,k) = e^{-2i(p-k)}, \tag{6.18}$$

while the Bethe equations arising from the boundary condition read as

$$e^{ip(L-3)} = e^{-iP}, \qquad e^{ik(L-3)} = e^{-iP}, \tag{6.19}$$

with $P = p+k$ being the total momentum. It is also easy to calculate that the energy of the state does not depend on the domain walls, and is still given by $E = e(p)$.

By extending the above computation to the case of longer bound states (DW's further away from each other than two sites), it can be easily shown that the scattering of a particle on two domain walls is independent of the distance between the two DW's. Moreover, it is also possible by this method to calculate the scattering of two bound states on each other. (Even though, these are immobile on their own, through their interactions with particles, they can be displaced, which can eventually lead to them scattering on each other.) It is, however, easier to investigate this scenario by considering the $\Delta \to \infty$ limit of the known string solutions of the XXZ model. Here, we omit the details of this calculation (see [141]) and only present the final results.

The scattering phase describing the interaction between two bound states with $n > 1$ and $m > 1$ down-spins, respectively, is given by:

$$S_{m,n}(p) = \begin{cases} e^{-2mip}, & \text{if } m < n, \\ -e^{-2inp}, & \text{if } m = n, \end{cases} \tag{6.20}$$

with p being the difference between the quasi-momenta of the two bound states. The most general form of the Bethe equations, with both particles and bound states of different length present, is then written as

$$e^{ip_{j,n}} \prod_{\substack{(m,k) \\ (j,n)\neq(m,k)}} S_{n,m}(p_{j,n} - p_{k,m}) = 1, \tag{6.21}$$

where it is understood that

$$S_{1,1}(p) = -e^{-ip}, \qquad S_{1,n}(p) = e^{-2ip}, \tag{6.22}$$

just like in (6.13) and (6.18). Moreover, $p_{j,n}$ denotes the quasi-momentum of the j^{th} bound state (or particle, if $n = 1$) with n consecutive down-spins. In the case of $h = \mu = 0$, the energy of such a state still does not depend on the bound states and is simply given by $E = \sum_j e(p_{j,1})$. Turning on a non-zero magnetic field and chemical potential modifies the energies to

$$E = \sum_j e(p_{j,1}) + h \sum_{m=1} m N_m + 2\mu \sum_{m=1} N_m, \tag{6.23}$$

where N_m is the number of bound states (or particles, if $m = 1$), with m consecutive down-spins.

6.2.3 Hilbert space fragmentation

As it was explained in Chapter 2, Hilbert space fragmentation refers to the property of a model that its Hilbert space splits up to an exponentially large number of sectors between which the Hamiltonian does not have transition matrix elements, while the sectors being easily constructable through some simple rules that does not involve actually solving the model. The phenomenon often arises and was first observed in models with two non-dynamical, local charges that commute with the Hamiltonian, like in the case of simultaneous charge and dipole conservation [26].

In the folded XXZ model, two such charges exist in the form of $\hat{Q}_1$ and $\hat{Q}_2$, which indeed leads to Hilbert space fragmentation, as it was already observed in [138–140]. Accordingly, the eigenstates of the system arrange themselves into sectors corresponding to the different eigenvalue pairs $(m,\ N_{DW})$, where m is the magnetization (the eigenvalue of $\hat{Q}_1$) and N_{DW} is the domain wall number (the eigenvalue of $\hat{Q}_2$). Moreover, within these sectors, there is an additional splitting that corresponds to the distribution of consecutive down-spins among the different frozen configurations with the same overall magnetization and domain wall number.

Closely connected to Hilbert space fragmentation, we can also observe a huge number of degeneracies in the spectrum of the model. This is most transparent from looking at the general Bethe equations (6.21). Domain walls do not contribute to the energy of states (if $h = \mu = 0$), moreover they only enter the Bethe equations through their total number and total momentum, but not their distribution. This leads to a huge degeneracy, which usually scales exponentially with volume. The exact number of degenerate states, however, depends on the actual particle content of the state. For the reference state (state with eigenvalue 0), it was calculated in [138, 139], and was found to grow as α^L with the system size, where $\alpha = (1+\sqrt{5})/2$ is the golden ratio. On the other hand, the ground state is only finitely degenerate even in the thermodynamic limit, as it is shown in the next section.

Hilbert space fragmentation and the huge number of degeneracies present in the spectrum have dramatic effects on the equilibration of the system, which is discussed in the next chapter.

6.3 Ground state

In this section, we describe the ground state of the Hamiltonian (6.7) and calculate its energy density for various parameter regimes of h and μ.

Firstly, we consider the scenario where $h = 0$ and $\mu = 0$. Under these conditions, our findings are consistent with those presented in [147] and [146]. Given that the Hamiltonian (6.7) remains invariant under spin-flip when $h = 0$, the ground state exhibits double degeneracy. Here, we focus on the state with positive magnetization ($N < L/2$). Simple reasoning and numerical verification indicate that the ground state consists solely of particles, with no bound states present. Nevertheless, the particle density is a non-trivial quantity that we compute here. Starting with a finite volume L, the Bethe equations for N particles are given by:

$$e^{ip_jL}\prod_{k=1}^{N}\left(-e^{-i(p_j-p_k)}\right) = -1, \tag{6.24}$$

which is equivalent to (6.16). Taking the logarithm of (6.24), we obtain

$$p_jL = (N-1)\pi + \sum_{k=1}^{N}(p_j - p_k) + 2\pi I_j, \tag{6.25}$$

where $I_j \in \mathbb{Z}$. Given that in the ground state $P = \sum_{k=1}^{N} p_k = 0$, this simplifies to

$$p_j = \frac{2\pi}{L-N}\tilde{I}_j. \tag{6.26}$$

Here, $\tilde{I}_j = I_j + (N-1)/2$ is an integer or half-integer depending on whether N is odd or even. In the ground state, the $\tilde{I}_j$ values are symmetrically distributed around zero, ranging from $-\frac{N-1}{2}$ to $\frac{N-1}{2}$. The energy of the state is given by

$$E = -\sum_{j=1}^{N}\cos\left(\frac{2\pi}{L-N}\tilde{I}_j\right). \tag{6.27}$$

In the thermodynamic limit ($L, N \to \infty$, $N/L = n$ is fixed), the energy density becomes:

$$\varepsilon = \frac{E}{L} = -\int_{-p_F}^{p_F} dp \frac{L(1-n)}{2\pi L}\cos(p) = -\frac{1-n}{\pi}\sin(p_F) = -\frac{1-n}{\pi}\sin\left(\frac{n\pi}{1-n}\right), \tag{6.28}$$

where we used the fact that $p_F = \frac{2\pi}{L-N}\cdot\frac{N-1}{2} \to \frac{n}{1-n}\pi$. The particle density n_0 that minimizes ε is found by solving $\partial\varepsilon/\partial n|_{n=n_0} = 0$, leading to:

$$\frac{1-n_0}{\pi}\tan\left(\frac{n_0\pi}{1-n_0}\right) = 1. \tag{6.29}$$

Solving this equation numerically gives $n_0 \approx 0.3008$.

Including bound states, their effect is to decrease the effective length by $2M$, where M is the number

of bound states of arbitrary length. Consequently, the energy density for a state with particle density n and bound state density $M/L = m$ is:

$$\varepsilon = -\frac{1-n-2m}{\pi}\sin\left(\frac{n}{1-n-2m}\pi\right). \tag{6.30}$$

This expression reaches its minimum at $n = n_0 \approx 0.3008$ and $m = 0$. Since the $\hat{Q}_2$ term gives the same energy to a particle and a bound state, and the $\hat{Q}_1$ term energetically favors particles over bound states, the ground state will not include bound states even when h and μ are non-zero.

Next, we consider the case where $h \neq 0$ while keeping $\mu = 0$. Given that $\hat{Q}_2$ and $\hat{Q}_4$ are invariant and $\hat{Q}_1$ changes sign under a spin flip, it suffices to examine the $h > 0$ case. The energy density of the system in the thermodynamic limit, for a state with particle density n, is

$$\varepsilon = -\frac{1-n}{\pi}\sin\left(\frac{n}{1-n}\pi\right) + hn. \tag{6.31}$$

To determine n_0 that minimizes this energy density, we take the derivative with respect to n, yielding the constraint:

$$h = \frac{1}{1-n}\cos\left(\frac{n\pi}{1-n}\right) - \frac{1}{\pi}\sin\left(\frac{n\pi}{1-n}\right). \tag{6.32}$$

The expression on the r.h.s. has a maximum value of 1 at $n = 0$. Thus, if $h < 1$, the ground state is characterized by a finite particle density n_0 given by (6.32). Conversely, if $h > 1$, the reference state with all spins up becomes the ground state. Expanding (6.32) around 0, we find that n scales as:

$$n \propto (h_c - h)^{1/2}, \tag{6.33}$$

as h approaches the critical value $h_c = 1$.

Finally, we address the case where both h and μ are non-zero. Given the model's symmetries, it is sufficient to consider $h > 0$, while μ can be negative. The energy density for a state with particle density n is:

$$\varepsilon = -\frac{1-n}{\pi}\sin\left(\frac{n\pi}{1-n}\right) + (h+2\mu)n. \tag{6.34}$$

Taking the derivative with respect to n and rearranging the equation, we obtain:

$$h + 2\mu = \frac{1}{1-n}\cos\left(\frac{n\pi}{1-n}\right) - \frac{1}{\pi}\sin\left(\frac{n\pi}{1-n}\right). \tag{6.35}$$

The r.h.s. of this equation has a maximum value of 1 at $n = 0$ and a minimum value of -2 at $n = 1/2$. Hence, if $h + 2\mu > 1$, the reference state with all spins up is the ground state. On the other hand, if $h + 2\mu < -2$, the ground state is characterized by $n = 1/2$, corresponding to the doubly degenerate Néel and anti-Néel states. Between these two extremes, the ground state has a finite n_0 given by the constraint (6.35).

6.4 Solvable quench dynamics

One of the main motivations of studying the folded XXZ model is that because of its simple nature, it may serve as a toy model to test GHD by comparing its predictions to results obtained from the microscopic dynamics of the system. In the present work, we do not attempt to go this far, but to illustrate the simplicity of the system, we calculate the real time-evolution of some specific local observables following a homogeneous quantum quench. This task in general integrable models is usually impossible, however, in the case of the folded XXZ model is manageable.

In this section, we only consider quenches that can be described using only the particle excitations without domain walls. (The presence of domain walls leads to very interesting dynamical phenomenon which is the topic of the next chapter.) To achieve this, we choose an initial state $|\psi_0\rangle$ that has zero overlap with states containing domain walls. It is not hard to see that this property is guaranteed if there are no two or more neighboring down spins in $|\psi_0\rangle$. The simplest such state is the Néel state with down spins at every other site, however, it is actually an eigenstate of the Hamiltonian (6.7), with eigenvalue zero. The next simplest such state is the state $|\tilde{\psi}_0\rangle$ with down spins at every third site:

$$|\tilde{\psi}_0\rangle = |3,6,9,\ldots\rangle\,, \tag{6.36}$$

where now we assume that the system size L is a multiple of 3, so we have N particles in a volume of $L = 3N$. To further simplify the situation, we will only consider the zero momentum sector, so we choose our initial state as

$$|\psi_0\rangle = \frac{\mathbb{1} + U + U^2}{\sqrt{3}}\,|\tilde{\psi}_0\rangle\,, \tag{6.37}$$

where U is the one-site shift operator.

We will also restrict our attention to special local operators, the ones that measure the so-called emptiness formation probabilities (EFP), and are defined as

$$\mathbb{E}_l(x) = \prod_{j=1}^{l} \frac{\mathbb{1} + \sigma^z_{x-1+j}}{2}. \tag{6.38}$$

It is easy to see that when summed over the whole chain, $\sum_{x=1}^{L} \mathbb{E}_l(x)$ for $l = 1,2$ are just linear combinations of the first two conserved charges $\hat{Q}_1$ and $\hat{Q}_2$, therefore their dynamics is trivial. Because of this, we will focus mainly on $\mathbb{E}_3$. The calculations presented below closely follow a similar derivation in [131].

Once the initial state and the local observables of interest are chosen, the time-evolution of the expectation value of operators can be calculated by inserting two full sets of states and evaluating the double sum:

$$\langle \mathcal{O}(t)\rangle = \sum_{\mathbf{p},\mathbf{k}} \frac{\langle\psi_0|\mathbf{p}\rangle\,\langle\mathbf{p}|\mathcal{O}|\mathbf{k}\rangle\,\langle\mathbf{k}|\psi_0\rangle}{\langle\mathbf{p}|\mathbf{p}\rangle\,\langle\mathbf{k}|\mathbf{k}\rangle}\, e^{-i(E_{\mathbf{k}}-E_{\mathbf{p}})t}. \tag{6.39}$$

The necessary ingredients in order to evaluate (6.39) are the overlaps between the eigenstates of the system

and the initial state $|\psi_0\rangle$, and the matrix elements of the operators (6.38) between the eigenstates of the model. First, we calculate the overlaps.

From the Vandermonde-like structure of the eigenstates of the model (6.14), it is easy to see that the overlap between the initial state $|\psi_0\rangle$ and an eigenstate of the system characterized by the quasi-momenta $\{p_i\}$ is given by

$$|\langle\psi_0|\mathbf{p}\rangle|^2 = 3\prod_{j<k}|e^{i2p_j}-e^{i2p_k}|^2. \tag{6.40}$$

To evaluate (6.40), first we need to find the quasi-momenta $\mathbf{p}$ that give non-zero overlap with $|\psi_0\rangle$. In the zero total momentum sector, the Bethe equations (6.16) simplify to

$$e^{i2Np_j} = -1, \tag{6.41}$$

where for simplicity we assumed that N is even. (It does not restrict our derivation, and the final result will be also valid in the case of N odd.) The solutions are trivially given by

$$p_j = \frac{\pi(2I_j-1)}{2N}, \qquad I_j = 1,2,\ldots,2N. \tag{6.42}$$

In order to comply with the zero total momentum constraint, we need to choose an N-element subset

$$\{e^{ip_j}\}_N \subset \{\omega_k\}_{2N} \qquad \text{with} \qquad \omega_k = e^{\frac{i\pi(2k-1)}{2N}}, \quad k = 1,2,\ldots,2N, \tag{6.43}$$

that also satisfies $\prod_j e^{ip_j} = 1$. It is easy to see that the possible solutions ω_k can be arranged into pairs that are each others negatives, $\{\omega_k\}_{2N} = \{(\omega_k,-\omega_k)\}_N$. However, from (6.40), it follows that in order to end up with a non-zero overlap, we have to choose from each such pair exactly one rapidity. Thus, the Bethe states that give a non-vanishing overlap with $|\psi_0\rangle$ are described by the rapidities

$$a_j = s_j\omega_j \qquad \text{with} \qquad s_j = \pm 1, \quad j = 1,2,\ldots,N, \tag{6.44}$$

with the zero total momentum restriction that now takes the form

$$\prod_{j=1}^{N} a_j = \prod_{j=1}^{N} s_j\omega_j = e^{i\pi N/2}\prod_{j=1}^{N} s_j = 1. \tag{6.45}$$

Since N is assumed to be even, in (6.45) we can choose $N-1$ signs arbitrarily. Accordingly, there are 2^{N-1} states that have non-vanishing overlap with $|\psi_0\rangle$. Moreover, since the overlaps (6.40) depend on the squares of the solutions a_j, we can conclude that for all non-vanishing cases (6.40) will assume the same value. To calculate this value, we use the fact that the norm of the eigenstates are known (see [148]) and given by

$$\langle\mathbf{p}|\mathbf{p}\rangle = L(L-N)^{N-1} = 3N(2N)^{N-1}. \tag{6.46}$$

Because the Bethe states form a complete basis, the sum of the normalized overlaps (6.40) has to be one. But since in our case both (6.40) and (6.46) takes the same value for all solutions, we can conclude that

$$\sum_{\mathbf{p}} \frac{|\langle\psi_0|\mathbf{p}\rangle|^2}{\langle\mathbf{p}|\mathbf{p}\rangle} = 1 \quad \rightarrow \quad \frac{|\langle\psi_0|\mathbf{p}\rangle|^2}{\langle\mathbf{p}|\mathbf{p}\rangle} = \frac{1}{2^{N-1}} \quad \rightarrow \quad |\langle\psi_0|\mathbf{p}\rangle|^2 = 3N^N. \tag{6.47}$$

Continuing the calculation, we can use the fact that the matrix elements of the operators $\mathbb{E}_l(x)$ were already computed in the works [149, 150] and are given by

$$\langle\mathbf{p}|\mathbb{E}_l(x)|\mathbf{k}\rangle = \prod_{j\leq k} \frac{\det\mathcal{T}}{\left(e^{ip_j}-e^{ip_k}\right)\left(e^{ik_j}-e^{ik_k}\right)}, \tag{6.48}$$

where the matrix $\mathcal{T}$ is defined as

$$\mathcal{T}_{jk} = \frac{1-e^{i(k_j-p_k)(L-l)}e^{i(p_k-k_j)(N-1)}}{e^{ik_j}-e^{ip_k}}. \tag{6.49}$$

In order to compute the expectation values of the operators (6.38), it is useful to rewrite the matrix $\mathcal{T}$ in the following form

$$\mathcal{T}_{jj} = (N-L+l-1)e^{-ip_j}, \qquad k_j = p_j, \tag{6.50}$$

$$\mathcal{T}_{jk} = e^{i(l-1)(k_j+p_k)}\frac{\sin\left((l-1)(k_j-p_k)\right)}{\sin(k_j-p_k)}, \qquad k_j \neq p_k, \tag{6.51}$$

and consider its rank. From the form of (6.50), it can be seen that the rank of the diagonal part of $\mathcal{T}$ is given by the number of coinciding momenta in $\mathbf{p}$ and $\mathbf{k}$. By using this observation, we can evaluate the expectation value of $\mathbb{E}_l(x)$ for the first few l:

- $l = 1$: In this case, the off-diagonal part of $\mathcal{T}$ is zero, therefore the only non-zero contribution to $\langle\psi(t)|\mathbb{E}_1(x)|\psi(t)\rangle$ comes from the case $\mathbf{p} = \mathbf{k}$, which leads to a constant expectation value without time-dependence.

- $l = 2$: In this case, the off-diagonal part of $\mathcal{T}$ has rank 1, thus in order to obtain non-trivial time dependence, we would need the diagonal part to have rank at least $N-1$. Accordingly, the sets $\mathbf{p}$ and $\mathbf{k}$ should have at least $N-1$ common elements. Because of the zero total momentum constraint, however, it is not possible to have two such sets $\mathbf{p}$ and $\mathbf{k}$ that have non-zero overlap with the initial state and only differ from each other in one element. Therefore, we end up again with a static expectation value. These results are consistent with the previously mentioned fact that $\mathbb{E}_1$ and $\mathbb{E}_2$ are linear combinations of the first two charges, hence are constants in time.

- $l = 3$: In this case, the off-diagonal part of $\mathcal{T}$ has rank 2. This means that there is a non-zero contribution to the expectation value when the sets $\mathbf{p}$ and $\mathbf{k}$ differ in two elements, which introduces non-trivial time dependence in $\langle\psi(t)|\mathbb{E}_3(x)|\psi(t)\rangle$.

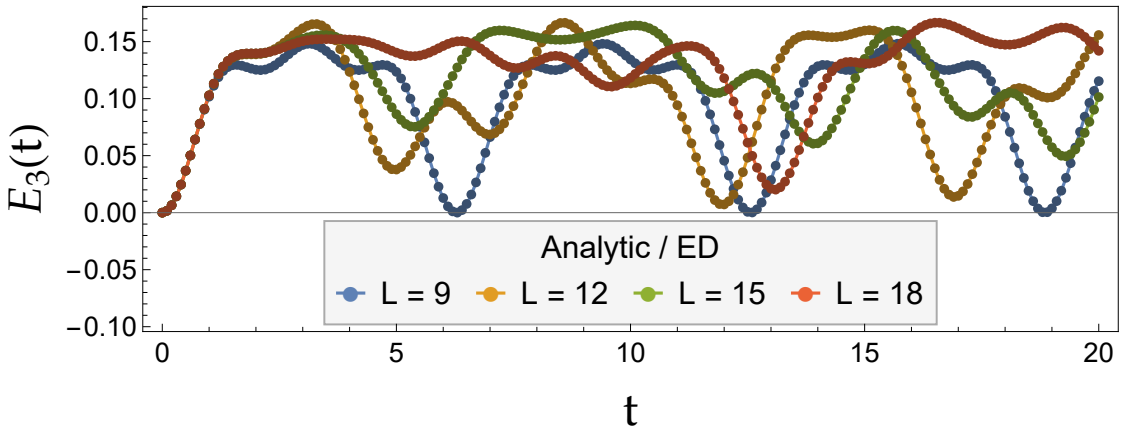

(a)

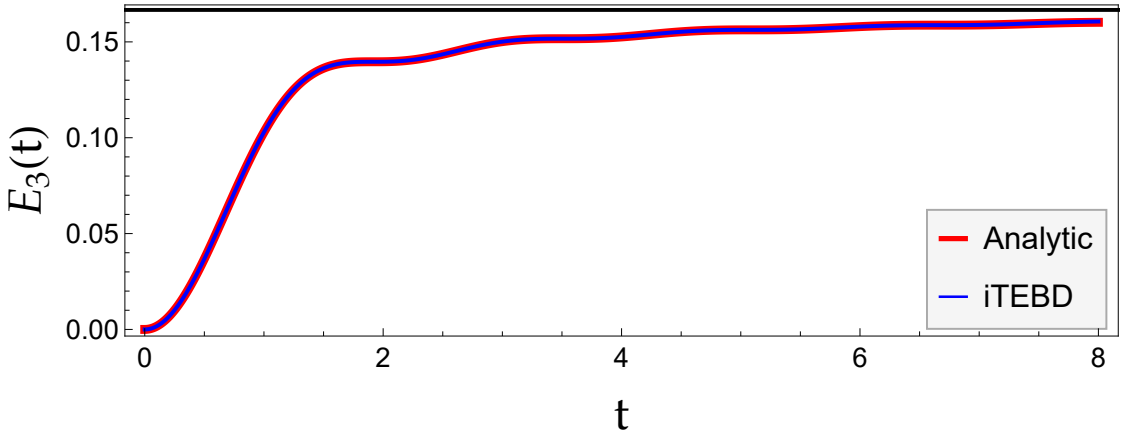

(b)

Figure 6.2: (a) Expectation value of $\mathbb{E}_3$ as a function of time following a quantum quench in the folded XXZ model, starting from the state $|\psi_0\rangle$, for different system sizes. The continuous lines correspond to the analytic result (6.52)*, while the dots are obtained from exact diagonalization. The agreement between the analytic and numeric results is perfect. (b) The same expectation value in the thermodynamic limit. The red line corresponds to the analytic result* (6.53)*, while the blue is obtained from iTEBD simulation. The black line denotes the asymptotic value of 1/6.*

From this point on, the calculation goes exactly the same way as in [131], therefore here we omit the details and only present the final results. The time-evolution of the operator $\mathbb{E}_3(x)$ is given by

$$\langle\psi(t)|\mathbb{E}_3(x)|\psi(t)\rangle = \frac{1}{6} - \frac{1}{6}\left(\frac{1}{N}\sum_a \cos\left(2t\cos(c_a)\right)\right)^2 - \frac{1}{6}\left|\frac{1}{N}\sum_a \sin\left(2t\cos(c_a)\right)e^{ic_a}\right|^2, \tag{6.52}$$

with $c_a = \frac{\pi(2a-1)}{2N}$, $a = 1,2,\ldots,N$. (In the case of odd N, the expression (6.52) is still valid with $c_a = \frac{\pi a}{N}$, $a =$

$1,2,\dots,N$.) In the thermodynamic limit, (6.52) becomes

$$\langle\psi(t)|\mathbb{E}_3(x)|\psi(t)\rangle = \frac{1}{6} - \frac{1}{6}\left(\int_0^\pi \cos\left(2t\cos(z)\right)\frac{dz}{\pi}\right)^2 - \frac{1}{6}\left|\int_0^\pi \sin\left(2t\cos(z)\right)e^{iz}\frac{dz}{\pi}\right|^2 = \\ = \frac{1}{6}\left[1-(J_0(2t))^2-(J_1(2t))^2\right], \tag{6.53}$$

where $J_0(x)$ and $J_1(x)$ are the Bessel functions of the first kind. In the long time limit, (6.53) asymptotically behaves as

$$\langle\psi(t)|\mathbb{E}_3(x)|\psi(t)\rangle = \frac{1}{6}\left[1-\frac{1}{\pi t}+\mathcal{O}(t^{-2})\right]. \tag{6.54}$$

To verify the analytic expressions (6.52) and (6.53), we compared them to numerical results obtained from exact diagonalization and iTEBD simulation, respectively. (The iTEBD algorithm is introduced in the next chapter and in Appendix E.) The agreement is perfect within the numerical precision, as it can be seen in Fig. 6.2.

6.5 Summary

In this chapter, we investigated the so-called folded XXZ model. The system was derived from the $\Delta \to \infty$ limit of the well-known XXZ model, in a way that guarantees its integrability: the conserved charges of the folded model can be recursively obtained from the charges of the XXZ model.

The eigenstates and eigenenergies of the system were calculated using coordinate Bethe Ansatz. The important properties of the dynamics of the system can be summarized in the following statements: (i) the scattering of particles is described by a scattering phase that is linear in the particle momenta, (ii) there are domain walls present in the spectrum, which do not contribute to the energies and are immobile on their own, however, (iii) they cause large degeneracies in the spectrum and are responsible for Hilbert space fragmentation, which is discussed in more detail in the next chapter.

Due to the simple scattering phase, the Bethe equations also simplify. This simplification enables one to evaluate spectral sums and exactly treat real-time dynamics. We illustrated this fact by computing the expectation values of special local operators following a homogeneous quantum quench. We believe that the folded XXZ model is a good candidate to carry out similar calculations for inhomogeneous quantum quenches as well, in order to verify the predictions of GHD.

Besides the topics that were discussed in the present chapter, the original work [141] also contains several other new results, which we list here:

- The CBA was formulated for different boundary conditions.
- The thermodynamics of the model was also described in three different formulations.
- A connection to the Maassarani-Mathieu model and to the $T\bar{T}$-deformations was pointed out.

These aspects of the model were not treated here, because of the authors limited (or non-existent) contribution to them. However, they are essential to paint a more detailed picture of the folded XXZ model.

Additionally, since the publication of [141], it has been established that the folded XXZ model is a special case of the so-called hard-rod deformation of the XXZ spin chain, namely it is the hard-rod deformed XX model [151]. The algebraic origin of the model and its conserved charges was also understood and embedded into the framework of Yang-Baxter integrability through the study of medium-range systems [145].

Chapter 7

Hilbert space fragmentation and persistent oscillations

In the previous chapter, we introduced and studied the folded XXZ model. We found that its spectrum exhibits Hilbert space fragmentation and contains a large number of degeneracies, and foretold that it would have serious consequences for the non-equilibrium dynamics of the system. Here, we discuss the origins of this fragmentation in more detail, together with its implications for thermalization.

As was already mentioned in Chapter 2, models that exhibit Hilbert space fragmentation have an exponentially large (in the system size) number of kinetically disconnected sectors in their spectrum, i.e. sectors with states between which the matrix-elements of the Hamiltonian vanish. Accordingly, in these models exists a symmetry algebra whose elements commute with the Hamiltonian and whose dimension also scales exponentially with the volume [25].

For the case of the folded XXZ model, these symmetry operators were obtained in [152]. More precisely, in [152] a non-integrable extension of the folded XXZ model with two parameters was introduced, based on hard-rod deformations [151]. It was shown that this family of models possesses symmetry operators that form a non-commutative algebra, and can be constructed as Matrix Product Operators (MPOs) with fixed and small bond dimensions.

In this chapter, we present the connected results of the papers [141] and [152] regarding Hilbert space fragmentation and thermalization: in Section 7.1, we introduce the non-integrable extension of the folded XXZ model. Then, in Section 7.2, we summarize how the symmetry operators of the system can be constructed as MPOs. Finally, in Section 7.3, we investigate the effects of fragmentation on non-equilibrium dynamics by numerically simulating quantum quenches. It is important to note that the author's contribution to the paper [152] was limited to the topics discussed in Subsection 7.1.1 and Section 7.3. However, for the sake of completeness, we feel that a short description of the construction of the symmetry operators is required, hence the inclusion of Section 7.2.

7.1 Integrability breaking extension

In this chapter, we study the two-parameter family of models given by the Hamiltonian

$$H = \sum_{j=1}^{L} \left[h_f(j) + \Delta h_{ZZ}(j) + \kappa h_{ni}(j) \right], \tag{7.1}$$

with $\Delta,\ \kappa \in \mathbb{R}$ and the Hamiltonian densities being

$$\begin{aligned} h_f(j) &= \left(\sigma^x_{j+1}\sigma^x_{j+2} + \sigma^y_{j+1}\sigma^y_{j+2}\right)\Pi^+_{j,j+3}, \\ h_{ZZ}(j) &= \Pi^+_{j,j+3}\Pi^-_{j+1,j+2}, \\ h_{ni}(j) &= \Pi^+_{j,j+5}\Pi^-_{j+1,j+2}\Pi^-_{j+2,j+3}\Pi^-_{j+3,j+4}. \end{aligned} \tag{7.2}$$

Here we introduced the notation

$$\Pi^{\pm}_{j,k} = \frac{\mathbb{1} \pm \sigma^z_j \sigma^z_k}{2}. \tag{7.3}$$

In the case of $\Delta = \kappa = 0$, (7.1) reduces to the folded XXZ model (6.6) (here a factor of -1/4 was dropped, just to keep the notation consistent with [152]). As it was discussed in the previous chapter, this is the kinetic term, describing a conditional hopping. Turning on a non-zero Δ introduces an interaction and results in the so-called hard rod deformed XXZ model, which is still integrable and solvable by the Bethe Ansatz [151]. Switching on a non-zero κ as well, however, breaks integrability. Since the only kinetic term is h_f, the fundamental dynamics is the same as in the folded XXZ model.

The terms h_{ZZ} and h_{ni} were chosen in such a way that the first two charges of the folded XXZ model, $\hat{Q}_1$ and $\hat{Q}_2$ given by (6.3) and (6.4) still commute with (7.1) for arbitrary values of Δ and κ. As a result, the statements of Subsection 6.2.3 remain valid and the model exhibits Hilbert space fragmentation.

7.1.1 Level spacing statistics

To illustrate that the term $h_{ni}(j)$ indeed breaks integrability, we numerically calculate the level spacing statistics (LSS) of the model. The behavior of the LSS serves as an indicator of integrability breaking. Since the model (7.2) contains a huge number of degeneracies, even compared to integrable systems, it is actually more practical to compute the LSS in the XXC model (introduced in the next section) after spin-charge separation, given by (7.14).

The LSS of a given Hamiltonian H with eigenvalues ε_i are determined by calculating the differences $S_i = \varepsilon_{i+1} - \varepsilon_i$ of the eigenenergies arranged in ascending order, $\varepsilon_1 \leq \varepsilon_2 \leq \ldots$. The level spacing distribution $P(s)$ is then defined as the distribution of the normalized spacings $s_i = S_i/\overline{S}$, where $\overline{S}$ represents the average level spacing. According to random matrix theory, for a non-integrable Hamiltonian from the Gaussian orthogonal ensemble, in the infinite volume limit, $P(s)$ follows the Wigner-Dyson distribution:

$$P_{ni}(s) = \frac{\pi}{2} s e^{-\frac{\pi}{4}s^2}. \tag{7.4}$$

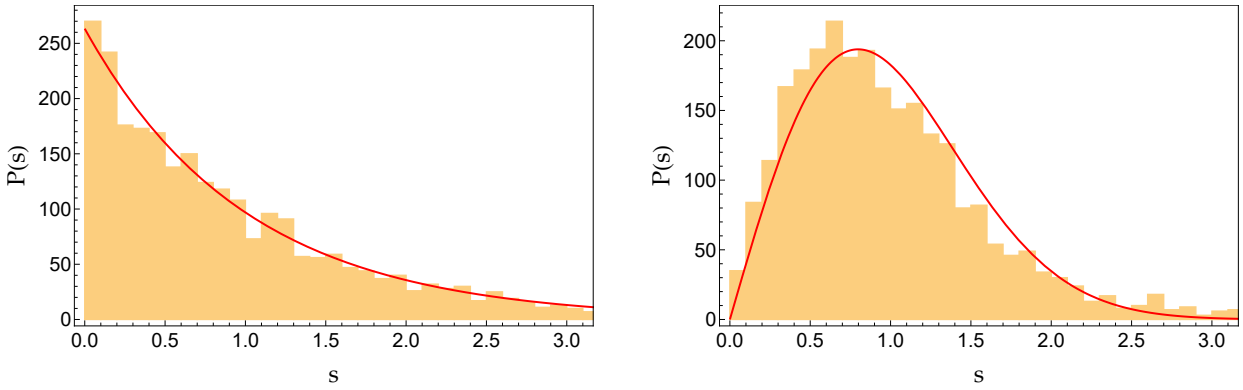

Figure 7.1: Level spacing statistics for $L = 20$, $\Delta = 0.2$ with: (a) $\kappa = 0$ and (b) $\kappa = 0.5$. The red curves represent the fitted exponential and Wigner-Dyson distributions, respectively. The integrability breaking effect of a non-zero κ is clearly visible.

Conversely, for an integrable system, $P(s)$ is given by the exponential distribution:

$$P_i(s) = e^{-s}. \tag{7.5}$$

Given that the model defined by (7.14) exhibits trivial symmetries, we compute the eigenvalues within the invariant subspace characterized by zero total momentum, even spatial parity, and a fixed z-component of the total spin, with $S_z = 2$. (Similar results can be obtained for other values of S_z; however, for $S_z = 0$, an additional spin-flip symmetry must be removed.) Additionally, we consider only the energy levels from the middle third of the spectrum, as the quasi-particle excitations at the spectrum's edges lead to deviations from the random matrix predictions.

The level spacing distributions for $L = 20$ and $\Delta = 0.2$ are illustrated in Fig. 7.1, with $\kappa = 0$ on the left (integrable case, derived from a total of 2620 energy levels) and $\kappa = 0.5$ on the right (non-integrable case, derived from a total of 2629 energy levels). The results align well with the exponential and Wigner-Dyson distributions (depicted by red curves in Fig. 7.1), with the total normalization of the distributions being the sole fitting parameter. The minor deviations from theoretical predictions are attributed to the finite size of the system. Nevertheless, the alteration in $P(s)$ due to a non-zero κ clearly illustrates the integrability breaking effect of the term $h_{ni}(j)$.

7.2 Algebraic origin of the Hilbert space fragmentation

The algebraic origin of the Hilbert space fragmentation in the family of models given by the Hamiltonian (7.2) was understood in [152]. As we already noted, the author's contribution to the paper [152] was limited to the numerical simulations of quantum quenches and the calculation of level spacing statistics. For the sake of completeness, however, here we also summarize the construction of the symmetry operators responsible

for the fragmentation.

The idea behind obtaining these symmetry operators is to transform the original model (7.2) through two consecutive mappings into a form, where these symmetries are more transparent and easier to formulate. First, we apply a bond-site transformation, then a non-local mapping that takes our original system to the so-called XXC model. As we shall see, in this model there is a complete spin-charge separation, and the symmetry operators responsible for the Hilbert space fragmentation can be found as Matrix Product Operators with fixed bond dimensions that act only on the spin degrees of freedom. (For the definition of an MPO, see Appendix E.) As a final step, these MPOs can be transformed back into the original basis.

In this section, we go through these steps in a nutshell. For more details on the construction, we refer to [152].

7.2.1 Bond-site transformation

The bond-site transformation [141, 147] is defined on the level of basis states by introducing new variables with two possible values on the bonds between sites, according to the following rules: if the spins on neighboring sites have the same orientation, the bond between them is empty (or equivalently, spin up), denoted by $|\circ\rangle$, while if the spins have opposite orientations, the bond is occupied (spin down), denoted by $|\bullet\rangle$. Graphically, the transformation is represented as

$$|\uparrow\uparrow\rangle\,,\ |\downarrow\downarrow\rangle \to |\circ\rangle\,, \qquad\qquad |\uparrow\downarrow\rangle\,,\ |\downarrow\uparrow\rangle \to |\bullet\rangle\,. \tag{7.6}$$

Starting from the rules for the basis states, the transformation on the level of local operators can be worked out and is given by

$$\sigma^z_j\sigma^z_{j+1} \to \sigma^z_{j+1/2}, \qquad \sigma^x_j \to \sigma^x_{j-1/2}\sigma^x_{j+1/2}. \tag{7.7}$$

Using (7.7), the Hamiltonian densities (7.2) in the bond picture become

$$\begin{aligned} h^B_f(j) &= (\sigma^x_j\sigma^x_{j+2} + \sigma^y_j\sigma^y_{j+2})P_{j+1}, \\ h^B_{ZZ}(j) &= (N_jP_{j+2} + P_jN_{j+2})P_{j+1}, \\ h^B_{ni}(j) &= (N_jP_{j+4} + P_jN_{j+4})P_{j+1}P_{j+2}P_{j+3}, \end{aligned} \tag{7.8}$$

where we dropped the half-site shifts in the subscripts and the projector operators N_j and P_j are defined as

$$N_j = \frac{\mathbb{1} + \sigma^z_j}{2}, \qquad\qquad P_j = \frac{\mathbb{1} - \sigma^z_j}{2}. \tag{7.9}$$

The kinetic term h^B_f describes the hopping of two neighboring down spins: $|\circ\bullet\bullet\rangle \leftrightarrow |\bullet\bullet\circ\rangle$, while a single down spin in a sea of up spins is immobile. This is where the name of hard rod deformation comes from: the fundamental mobile particles are composites of down spins with a fixed length, in this case $l = 2$.

We note that the bond-site transformation is unambiguous only up to boundary effects. For open bound-

aries, the original model with length L is mapped to a bond model with length $L-1$, while for periodic boundaries, the original model is equivalent to a bond model of the same length, only in the sector, where the number of $|\bullet\rangle$ states is even.

7.2.2 XXC model

As a second step, the bond model is transformed further by a non-local mapping (used for example in [153] and [141]) into a system with a three-dimensional local Hilbert space. For the computational basis states, the transformation rules are the following: starting from the first site of the chain, we consecutively „read-in" the states at each site. If we come across the state $|\circ\rangle$, we replace it by $|1\rangle$, while if we see the state $|\bullet\rangle$, we also look at the next site. If it is a $|\circ\rangle$ or $|\bullet\rangle$, we replace the original two-site sequence by $|2\rangle$ or $|0\rangle$, respectively. Here $|0\rangle$, $|1\rangle$ and $|2\rangle$ are the three local basis states of the new model. Graphically, the transformation rules read as:

$$|\circ\rangle \to |1\rangle\,, \qquad |\bullet\bullet\rangle \to |0\rangle\,, \qquad |\bullet\circ\rangle \to |2\rangle\,. \tag{7.10}$$

Obviously, this mapping is non-local and volume changing: the length of the new state depends on the content of the original state. As a result, one would assume that local operators of the bond model are transformed to non-local ones. While this is true in general, it can be shown that there are special operators that remain local under the mapping, and that our Hamiltonian (7.8) is among these special operators (this is a non-trivial statement, for details see [152]). After the transformation, the Hamiltonian densities become:

$$\begin{aligned} h_f^C(j) &= \boldsymbol{s}_j^+ \cdot \boldsymbol{s}_{j+1}^- + \boldsymbol{s}_j^- \cdot \boldsymbol{s}_{j+1}^+, \\ h_{ZZ}^C(j) &= n_j p_{j+1} + p_j n_{j+1}, \\ h_{ni}^C(j) &= n_j n_{j+1} p_{j+2} + p_j n_{j+1} n_{j+2}, \end{aligned} \tag{7.11}$$

where the two component vectors $\boldsymbol{s}_j^{\pm}$ and the projectors n_j and p_j are defined as:

$$\boldsymbol{s}^- = \left(\boldsymbol{s}^+\right)^\dagger = (s_1^-, s_2^-), \quad \text{with} \quad s_\alpha^- = |\alpha\rangle\langle 0| \quad (\alpha = 1,2), \tag{7.12}$$

$$n = |0\rangle\langle 0|\,, \qquad p = |1\rangle\langle 1| + |2\rangle\langle 2|\,. \tag{7.13}$$

It is important to note that the transformation does not actually map the densities (7.8) individually to (7.11), but the equivalence is true for the total (summed-up) Hamiltonians.

The model (7.11) with only h_f^C first appeared in [154], while with the extra term h_{ZZ}^C in [155], where it was named the XXC model. The deformation introduced by h_{ni}^C was first studied in [152].

7.2.3 Spin-charge separation and MPO symmetries

The kinetic term h_f^C describes the transitions $|01\rangle \leftrightarrow |10\rangle$ and $|02\rangle \leftrightarrow |20\rangle$, while the transition $|12\rangle \leftrightarrow |21\rangle$ is forbidden. As a result, the ordering of the states $|1\rangle$ and $|2\rangle$ is a constant of motion, it does not change during time-evolution. Moreover, the actions of the diagonal interaction terms h_{ZZ}^C and h_{ni}^C are insensitive to the distinction between the states $|1\rangle$ and $|2\rangle$. Thus, if one interprets $|0\rangle$ as the vacuum, while $|1\rangle$ and $|2\rangle$ as the two possible states of a particle with an internal degree of freedom (with a spin-1/2), a complete spin-charge separation takes place. The wave-function of the system can be separated into a charge and a spin part, where the latter is constant and does not effect the former, the motion of the particles. The effective Hamiltonian describing the time-evolution of the charge part becomes

$$\begin{aligned} h_{XX}(j) &= \sigma_j^x \sigma_{j+1}^x + \sigma_j^y \sigma_{j+1}^y, \\ h_{ZZ}^{ch}(j) &= N_j P_{j+1} + P_j N_{j+1}, \\ h_{ni}^{ch}(j) &= N_j P_{j+1} P_{j+2} + P_j P_{j+1} N_{j+2}, \end{aligned} \tag{7.14}$$

where the σ-s and the projectors N and P are acting again on the usual two-dimensional local Hilbert space $\mathbb{C}^2$. For the technical details of the spin-charge separation and the derivation of (7.14), see [152].

The spin-charge separation is deeply connected to Hilbert space fragmentation: the different configurations of the spin degrees of freedom correspond to the different disconnected sectors in the spectrum. It also enables one to construct the extra symmetry operators of the model as MPOs with fixed bond dimension D. For this, we can set $D = 2$ and choose the local tensor $\mathcal{L}$ (for its definition, see Appendix E) as:

$$\mathcal{L} = \mathbb{1} \otimes |0\rangle\langle 0| + \sum_{\alpha,\beta=1,2} F^{(\alpha,\beta)} |\alpha\rangle\langle\beta|, \tag{7.15}$$

where $\mathbb{1}$ is the 2×2 identity acting on the auxiliary space, while $F^{(\alpha,\beta)}$ are four other matrices also acting on the auxiliary space. The form (7.15) ensures that the MPO acts as the identity on the local state $|0\rangle$, while it might change the states $|1\rangle$ and $|2\rangle$ between each other. As a result, the MPO built from (7.15) does not change the positions of the particles, it only acts non-trivially on the spin-degrees of freedom. Thus, it must commute with the Hamiltonian (7.11).

One can introduce two classes of MPOs with the form (7.15): diagonal and off-diagonal ones. In the case of the diagonal MPOs, the matrices $F^{(1,2)}$ and $F^{(2,1)}$ are chosen to be identically zero. Consequently, these operators do not change the spin pattern, however, their eigenvalues depend on the values of the spin degrees of freedom. It can be shown that these diagonal symmetry operators can be parameterized by five independent parameters in the following way:

$$F^{(1,1)} = \begin{pmatrix} x & y \\ y & z \end{pmatrix}, \qquad F^{(2,2)} = \begin{pmatrix} u & 0 \\ 0 & v \end{pmatrix}. \tag{7.16}$$

The off-diagonal MPOs are the ones that change the spin pattern. By focusing only on those that conserve

both the number of $|1\rangle$ and $|2\rangle$ states, we can describe them also by five independent parameters:

$$F^{(1,2)} = \left(F^{(2,1)}\right)^{\dagger} = \gamma\sigma^{-}, \qquad F^{(1,1)} = \begin{pmatrix} \alpha & 0 \\ 0 & \delta \end{pmatrix}, \qquad F^{(2,2)} = \begin{pmatrix} \beta & 0 \\ 0 & \varepsilon \end{pmatrix}. \tag{7.17}$$

Once the symmetry operators are constructed in the XXC model, the last step is to invert the non-local mapping and the bond-site transformation to obtain the symmetry operators in the basis of our original family of models. This is, however, quite a difficult task. In [152], it was achieved by using the techniques of [156], where an MPO is viewed as an automaton with a finite number of internal states. The transitions between these internal states can incorporate the rules of the non-local mapping (7.10) and the bond-site transformation (7.6), eventually yielding the MPO symmetries in our original basis. Here we omit the technical details of this computation and only present the final results.

To account for the non-local nature of the mapping (7.10), the bond dimension D of the MPOs in the original basis has to be increased. The local tensors can be written in the form

$$\mathcal{L} = \mathcal{A} \otimes |\uparrow\rangle\langle\uparrow| + \mathcal{B} \otimes |\uparrow\rangle\langle\downarrow| + \mathcal{C} \otimes |\downarrow\rangle\langle\uparrow| + \mathcal{D} \otimes |\downarrow\rangle\langle\downarrow|, \tag{7.18}$$

where $\mathcal{A}$, $\mathcal{B}$, $\mathcal{C}$ and $\mathcal{D}$ are $D \times D$ matrices acting on the auxiliary space. For the diagonal symmetries $\mathcal{B} = \mathcal{C} = 0$, the bond dimension is $D = 8$ and the number of independent parameters is five. In the case of the off-diagonal ones, the bond dimension is $D = 10$, and the number of independent parameters is still five. The actual form of the matrices can be found in [152].

The MPOs do not depend on the parameters of the Hamiltonian, they commute with (7.1) for arbitrary values of Δ and κ. Moreover, the diagonal symmetries commute among each other, and also commute with the individual Hamiltonian densities $h(j)$, thus they belong to the commutant algebra [25]. On the other hand, the off-diagonal ones do not commute with each other, only with the full Hamiltonian.

The property that the MPOs in the XXC model conserve spin (the number of $|1\rangle$ and $|2\rangle$ states) translates to the conservation of domain walls in the original basis. As a result, all the symmetry operators commute with the charge $\hat{Q}_2$. The diagonal ones also do not change the spin pattern, which means that they commute with $\hat{Q}_1$ as well. The off-diagonal ones, however, can interchange between the states $|1\rangle$ and $|2\rangle$, which in the original basis corresponds to the displacement of domain walls. Therefore, the off-diagonal MPOs do not commute with $\hat{Q}_1$.

The diagonal MPOs already appeared in [25], while the off-diagonal ones were first observed in [152] and they constitute the first off-diagonal MPO symmetries in any non-integrable system.

7.3 Persistent oscillations

To illustrate the ergodicity breaking effect of Hilbert space fragmentation, we consider quantum quenches in the family of models given by (7.1). We prepare our system in an initial state $|\Psi_0\rangle$, let it evolve according

to the Hamiltonian (7.1) and study the expectation value of some local operator $\langle \hat{\mathcal{O}}(t) \rangle$. By inserting two complete sets of states (the eigenstates of the system), we can write this time-dependent expectation value in finite volume as:

$$\langle \hat{\mathcal{O}}(t) \rangle = \sum_{a,b} \langle \Psi_0 | a \rangle \, \langle a | \hat{\mathcal{O}} | b \rangle \, \langle b | \Psi_0 \rangle \, e^{-i(E_b - E_a)t}. \tag{7.19}$$

In accordance of what we already discussed in Chapter 2, in the long time limit (7.19) usually reduces to the diagonal ensemble, since in systems without too many degeneracies, the phases of the off-diagonal terms are sufficiently independent and cancel out. Therefore we get:

$$\lim_{T\to\infty} \frac{1}{T} \int_0^T \langle \hat{\mathcal{O}}(t) \rangle \, dt = \sum_a |\langle a | \Psi_0 \rangle|^2 \langle a | \hat{\mathcal{O}} | a \rangle . \tag{7.20}$$

It is then argued, based on the (Generalized) Eigenstate Thermalization Hypothesis, that the predictions of the diagonal ensemble (7.20) are reproduced by the (Generalized) Gibbs Ensemble for (integrable) non-integrable models. Systems in which these hypotheses hold are assumed to equilibrate and not support any oscillations in the expectation values of local observables.

The situation is different, however, if there are an exponentially large number of degeneracies present in the spectrum of the model. In this case, the double sum of (7.19) can be reduced to the following, different double sum:

$$\lim_{t\to\infty} \langle \hat{\mathcal{O}}(t) \rangle = \sum_a \sum_{j,k} \langle \Psi_0 | a, j \rangle \, \langle a, j | \hat{\mathcal{O}} | a, k \rangle \, \langle a, k | \Psi_0 \rangle , \tag{7.21}$$

where now a runs over the energy levels in the spectrum, while j and k label the different degenerate eigenstates within an energy level, so that $|a, j\rangle$ and $|a, k\rangle$ are two independent eigenstates with the same eigenvalue E_a. From (7.21), it is clear that in this case the long-time limits of local expectation values are not simply given by the diagonal ensemble, but they also involve off-diagonal terms. Moreover, if the degeneracies in the spectrum can be lifted in such a way that their differences remain commensurable, one can expect to observe persistent oscillations.

To demonstrate this phenomenon, we consider a particular example in our family of models. We choose our initial state to be the state with all spins polarized in the x-direction:

$$|\Psi_0\rangle = |X\rangle = \bigotimes_{j\in\mathbb{Z}} \left(\frac{|\uparrow_j\rangle + |\downarrow_j\rangle}{\sqrt{2}} \right). \tag{7.22}$$

This is a useful choice, because it breaks the $U(1)$ symmetry of the models and excites states with all possible values of the total magnetization, or equivalently, all sorts of combinations of particles and domain walls. Starting from this state, we study the time-evolution of the local operator σ^x. (Since both the system and the initial state are translationally invariant, the placement of the operator is irrelevant, and we omit the site index j.) More precisely, we investigate the expectation value $X(t) = \langle \Psi(t) | \sigma^x | \Psi(t) \rangle$. Obviously, (7.20) gives zero for the case of this operator, since it breaks the $U(1)$ symmetry: it changes the total magnetization,

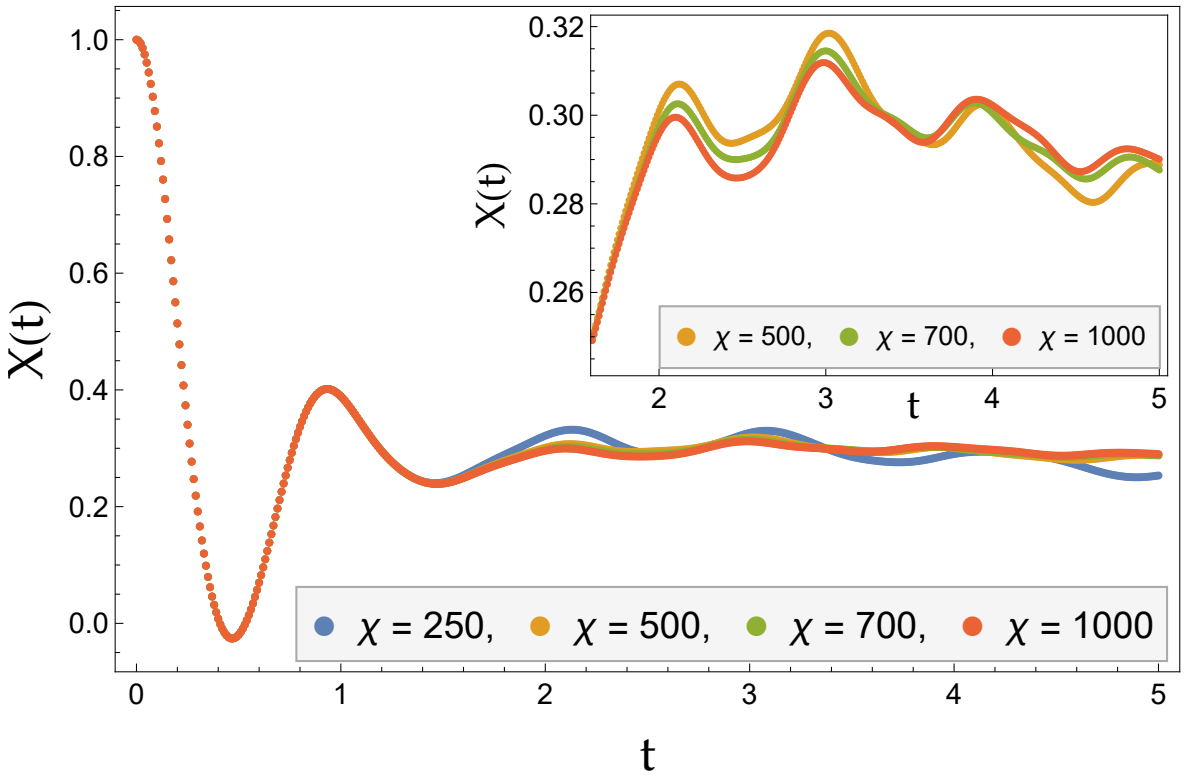

Figure 7.2: Expectation value of σ^x as a function of time following a quantum quench in the folded XXZ model ($\Delta = \kappa = 0$) without a magnetic field ($h = 0$), starting from the state $|X\rangle$. The different curves correspond to increasing maximal bond dimensions, while the Trotter time step is invariably $\delta t = 0.01$. The inset shows the same curves magnified for times $t > 1.6$. The data confirms the non-vanishing asymptotic value of $X(t)$ in the numerically reachable time-window.

while the eigenstates of the Hamiltonian are also eigenstates of the z-component of the total spin. Therefore a non-zero long-time limit of the expectation value of the σ^x operator clearly signals the break-down of the equilibration process to the diagonal ensemble. Furthermore, since the degenerate states correspond to the different placements of the domain walls, we can split up these degeneracies by introducing a magnetic field h and adding the term $h\hat{Q}_1$ to the Hamiltonian (7.1). As a result, we expect to observe oscillations in the expectation value of σ^x, with a frequency directly given by h.

7.3.1 Numerical simulations

We support our claims regarding persistent oscillations with numerical data, obtained from iTEBD [157, 158] simulations. A detailed description of this numerical technique can be found in Appendix E. Here, we only list the specifications of the performed simulations.

Depending on whether we investigate the folded XXZ model or its non-integrable extension (i.e. whether κ is zero/non-zero), we represent the state of the system by an infinite Matrix Product State (MPS) with four or six site unit-cells, respectively. The time-evolution operator is approximated by its first order Suzuki-

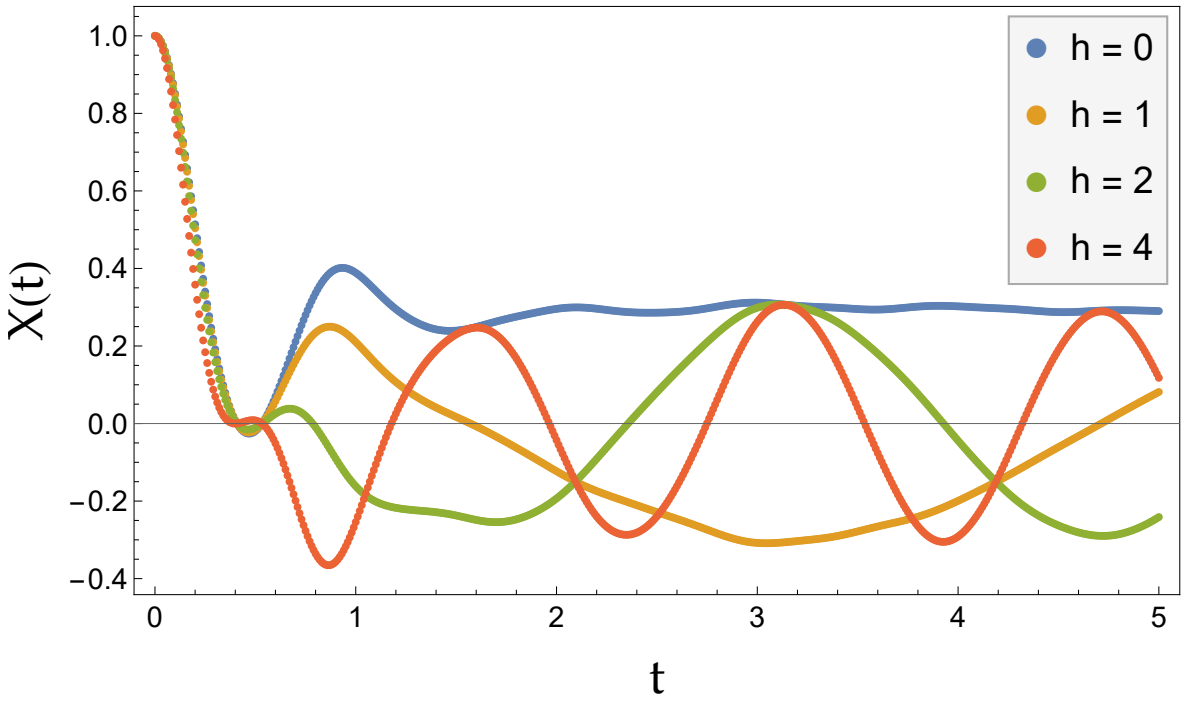

Figure 7.3: Expectation value of σ^x as a function of time following a quantum quench in the folded XXZ model ($\Delta = \kappa = 0$) starting from the state $|X\rangle$. The different curves correspond to different values of the magnetic field h. The maximal bond dimension is $\chi_{max} = 1000$, while the Trotter time step is $\delta t = 0.01$. The numerical data confirms the theoretical expectations in the simulated time frame: the introduction of a non-zero magnetic field results in the appearance of persistent oscillations with a frequency directly given by h.

Trotter decomposition. The Trotter time step δt and the maximal bond dimension $\chi_{\max}$ vary throughout different simulations, and are indicated in the caption of each figure. The computer code implementing the algorithm was developed by the author, based on the example of [159].

First, we consider the folded XXZ model without its non-integrable extension, i.e. the case $\Delta = \kappa = 0$ in the Hamiltonian (7.1). The numerical results corresponding to this case are presented in Fig. 7.2 and Fig. 7.3. Fig. 7.2 shows $X(t)$ as a function of time, in the absence of a magnetic field, approaching a non-zero asymptotic value. Unfortunately, the iTEBD algorithm used to obtain the numerical data is limited to short times by the rapidly growing entanglement entropy in the system (as it is explained in more detail in Appendix E). Nevertheless, in the observed time-window, the numerics agree with our expectations. To check the validity of our results, we also used several different maximal bond dimensions.

The result of switching on a non-zero magnetic field is shown in Fig. 7.3, and it also supports our theoretical considerations: instead of approaching a constant value, the expectation value $X(t)$ now shows non-decaying oscillations with a frequency given by h.

The situation is very similar even in the non-integrable extension of the folded XXZ model, as it can be seen in Fig. 7.4, where $\Delta = 0.2$ and $\kappa = 0.5$: in the absence of a magnetic field, the expectation value of σ^x tends to a non-zero stationary value in the simulated time-window. Switching on a magnetic field again

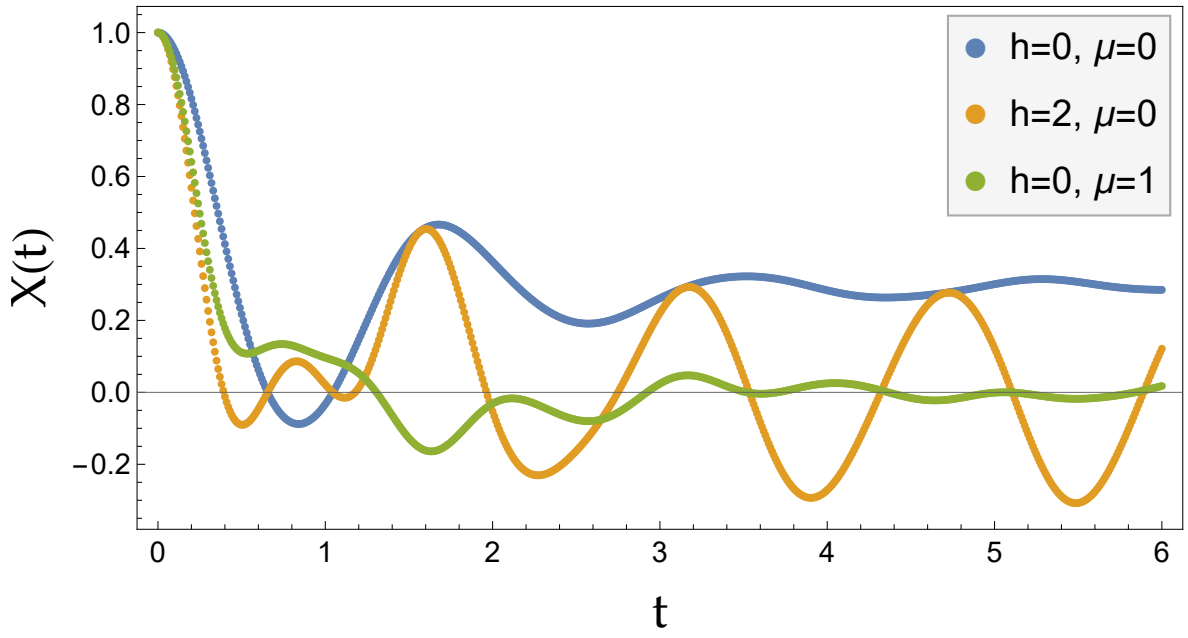

Figure 7.4: Expectation value of σ^x as a function of time following a quantum quench starting from the state $|X\rangle$. The parameters of the Hamiltonian (7.1) are $\Delta = 0.2$, $\kappa = 0.5$. The Trotter time step of the iTEBD simulation is $\delta t = 0.01$, while the maximal bond dimension is $\chi_{max} = 500$. For $h = \mu = 0$, the expectation value has a non-zero stationary value, while for $h \neq 0$, it exhibits oscillations, both being a sign of the break-down of thermalization. Turning on a non-zero μ breaks all MPO symmetries leading to the vanishing of $X(t)$.

leads to non-decaying oscillations in $X(t)$, with a frequency given by h.

To illustrate that the lack of relaxation is indeed the result of the Hilbert space fragmentation, one can add the following perturbation to the Hamiltonian (7.1):

$$H_{pert} = \mu \sum_j \sigma_j^z \sigma_{j+1}^z \sigma_{j+2}^z. \tag{7.23}$$

The term (7.23) breaks the MPO symmetries of the model, and consequently the Hilbert space fragmentation. This symmetry breaking results in relaxation to the diagonal ensemble that predicts $X(t)$ to vanish. Our numerical results confirm this expectation.

It is important to note that while the presented numerical results completely agree with our expectations derived from the Hilbert space fragmentation scenario, they cannot be considered as complete evidence, since the attainable time-window is limited by the applied numerical technique.

7.4 Summary

In this chapter, we investigated the origins of Hilbert space fragmentation together with its effects on equilibration in the previously introduced folded XXZ model and its non-integrable extension. The non-integrability of the extended model was verified numerically by calculating the level spacing statistics. We

also outlined the algebraic origins of Hilbert space fragmentation by summarizing the construction of matrix product operators that are responsible for it. However, we stress again that the author did not contribute to this derivation.

The main result of the chapter is the numerical simulations of quantum quenches by means of the iTEBD algorithm. These simulations support the theoretical considerations regarding the breaking of equilibration due to Hilbert space fragmentation and clearly show the signs of persistent oscillations in the numerically reachable time-window.

Chapter 8

Integrable spin ladder model

Even though one-dimensional integrable systems are exactly solvable in the sense that their eigenstates together with their eigenvalues can be constructed analytically, more complicated quantities, such as correlation functions and entanglement entropy are generally hard to compute. This is why finding simple integrable systems is useful: they can serve as toy models to gain insights into physical phenomena, otherwise difficult or impossible to study. In Chapter 6, we already introduced such a simple model, and also listed a few other examples. The systems mentioned there all share the common property of having a simple scattering phase that depends linearly on the quasi-particle momenta. In this chapter, we go a little further and ask the natural question: what is the simplest possible scattering phase (or S-matrix) for an interacting, Hermitian quantum spin chain?

Obviously, the simplest choice would be a constant, meaning that S does not depend on the momenta. However, with just one particle type, there are only two possibilities, $S = \pm 1$, corresponding to free bosons/fermions. On the other hand, with more than one particle species, a non-trivial scattering phase can be introduced between particles of different types. In this chapter, we derive such an integrable spin ladder model with two types of particles that has this property, i.e. has a constant, but non-trivial scattering phase. This feature resembles anyonic [160–162] and parafermionic [163–165] systems, however our model is different in that the anyonic scattering phase is the result of a local interaction between usual spin degrees of freedom.

The work presented here is based on [166], and is organized as follows: in Section 8.1, we introduce the model and point out its connection to quantum circuits. Section 8.2 contains the solution of the model by means of Jordan-Wigner transformation and the coordinate Bethe Ansatz. Finally, in Section 8.3, we investigate the entanglement properties of the system both analytically and numerically.

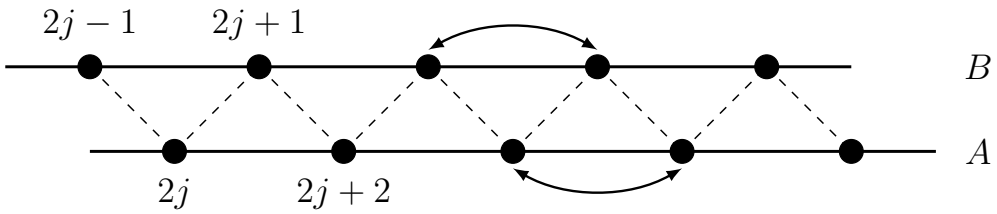

Figure 8.1: The geometry of the spin zig-zag ladder. Particles can hop separately either on sub-lattice A or B. Their hopping amplitude, however, depends on the occupation number of the other sub-lattice as well.

8.1 The model

We introduce and investigate a one-dimensional spin-chain defined by the Hamiltonian

$$H(\gamma) = \sum_{j=1}^{L/2} \left[h_{2j,2j+1,2j+2}(\gamma) + h_{2j+1,2j+2,2j+3}(-\gamma) \right], \tag{8.1}$$

where the Hamiltonian density is given by

$$h_{j,j+1,j+2}(\gamma) = -\left[\sigma_j^- e^{i\gamma\sigma_{j+1}^z} \sigma_{j+2}^+ + \sigma_j^+ e^{-i\gamma\sigma_{j+1}^z} \sigma_{j+2}^- \right] = -\left[\sigma_j^- D_{j+1} \sigma_{j+2}^+ + \sigma_j^+ D_{j+1}^\dagger \sigma_{j+2}^- \right]. \tag{8.2}$$

Here the σ_j-s are the usual Pauli matrices acting on site j, γ is a real parameter of the model and we assume that the length of the chain L is even. Moreover, we introduced the notation $D_j = e^{i\gamma\sigma_j^z} = \cos(\gamma)\mathbb{1} + i\sin(\gamma)\sigma_j^z$, and consider (if otherwise not stated) periodic boundary condition.

The Hamiltonian (8.1) is invariant with respect to spin-flips. Also, it is easy to verify that it conserves the z-component of the total spin separately on the sub-lattices composed of the even and odd sites:

$$\left[H, \sum_{j=1}^{L/2} \sigma_{2j}^z \right] = \left[H, \sum_{j=1}^{L/2} \sigma_{2j+1}^z \right] = 0. \tag{8.3}$$

Thus, by interpreting the state with all spins up as the vacuum, and down-spins as particles, the Hamiltonian (8.1) can be seen as a spin ladder in a zig-zag geometry (see Fig. 8.1): it describes the hopping of particles separately on the even (denoted by A) and odd (denoted by B) sub-lattices. The hopping amplitude of the particles on one sub-lattice, however, also depends on the occupation number of the other sub-lattice. This fact introduces an interaction between particles that can be tuned by the value of the parameter γ. At $\gamma = 0$, this interaction vanishes and the model reduces to two independent XX chains.

The Hamiltonian (8.1) was originally introduced in [166]. Similar models in the literature include the extended XX model [167, 168], the Bariev model [169] and a super-symmetric hopping model [170]. We also note that in [171] a very similar model was considered and some of their findings regarding the entanglement entropy overlap with our results presented in Section 8.3.

The model is integrable for arbitrary values of γ, meaning that it has infinitely many conserved charges

that are in involution. These charges can be obtained as diagonal dressings of the known charges of the XX model [172], and they are organized into four families corresponding to the sub-lattices A and B and two „chiralities". Due to their locality, the charges are written as sums of local densities:

$$\hat{Q}_\alpha^{A,+} = \sum_{j=1}^{L/2} \hat{q}_\alpha^{A,+}(2j), \qquad \hat{Q}_\alpha^{B,+} = \sum_{j=1}^{L/2} \hat{q}_\alpha^{B,+}(2j+1), \tag{8.4}$$

together with their adjoints $\hat{Q}_\alpha^{A/B,-} = (\hat{Q}_\alpha^{A/B,+})^\dagger$. The label α gives the span of the charge density and can assume any odd integer value. The first charges correspond to $\alpha = 3$, and are actually terms from the Hamiltonian:

$$\hat{q}_3^{A,+}(2j) = \sigma_{2j}^+ D_{2j+1}^\dagger \sigma_{2j+2}^-, \qquad \hat{q}_3^{B,+}(2j+1) = \sigma_{2j+1}^+ D_{2j+2} \sigma_{2j+3}^-. \tag{8.5}$$

Higher charges are obtained by dressing the hopping terms $\sigma_k^+ \sigma_{k+\alpha-1}^-$ according to the following rule: we insert an operator σ_j^z for every site $k < j < k+\alpha-1$, if j belongs to the same sub-lattice as k, while an operator D_j, if we j belongs to the other sub-lattice. For $\alpha = 5$, this algorithm yields:

$$\hat{q}_5^{A,+}(2j) = \sigma_{2j}^+ D_{2j+1}^\dagger \sigma_{2j+2}^z D_{2j+3}^\dagger \sigma_{2j+4}^-, \qquad \hat{q}_5^{B,+}(2j+1) = \sigma_{2j+1}^+ D_{2j+2} \sigma_{2j+3}^z D_{2j+4} \sigma_{2j+5}^-. \tag{8.6}$$

The commutation of the charges constructed this way can be verified by direct computations.

We note that the model can also be embedded into the QISM framework of medium-range systems, developed in [145]. A local Lax-operator together with an R-matrix can be found and the charges can be generated from a transfer matrix. Here, however, we do not discuss this construction.

8.1.1 Connection to an integrable quantum circuit model

Above we claimed that the model possesses an infinite tower of conserved charges and therefore is integrable. This claim can be made even more rigorous by relating the Hamiltonian (8.1) to an integrable quantum circuit, which we do in this section. To establish this connection, we use the integrable Trotterization scheme developed in [173]. First, we sketch the method in general and then show, how it can be used to recover the Hamiltonian (8.1).

We start with a continuous time, integrable model corresponding to some (unitary) R-matrix in finite volume and even length. For our purposes, the XXZ model is needed, however, the method is actually applicable more generally. In the case of the continuous time model, the time-evolution is generated by the Hamiltonian via

$$|\psi(t)\rangle = e^{-iHt} |\psi(0)\rangle, \tag{8.7}$$

while the aim of the Trotterization scheme is to obtain an integrable discrete time-evolution operator $\mathcal{V}$, such that the equation

$$|\psi_{n+1}\rangle = \mathcal{V} |\psi_n\rangle \tag{8.8}$$

recovers (8.7) in the appropriate limit. This can be achieved by choosing the operator

$$U_{j,j+1} = \check{R}_{j,j+1}(\delta) \tag{8.9}$$

as the building block of time-evolution, i.e. the local unitary quantum gate that acts on two neighboring sites. Here $\check{R}(u) = \mathcal{P}R(u)$, with $\mathcal{P}$ being the permutation operator, while the value of the parameter δ will be important to recover the continuous dynamics. One can then construct a brick-work type time-evolution operator $\mathcal{V}$ (see Fig. 8.2) as

$$\mathcal{V} = \mathcal{V}_2\mathcal{V}_1, \tag{8.10}$$

where $\mathcal{V}_1$ and $\mathcal{V}_2$ are given by

$$\mathcal{V}_1 = U_{1,2}U_{3,4}\dots U_{L-1,L}, \qquad \mathcal{V}_2 = U_{2,3}U_{4,5}\dots U_{L,1}. \tag{8.11}$$

The continuous dynamics is recovered from the discrete time-evolution by setting the rapidity parameter δ to be infinitesimal: $\delta = -it/n$, with n being large. Using the regularity property of the R-matrix, and the construction of the Hamiltonian from the R-matrix, we then arrive at $U_{j,j+1} \simeq \mathbb{1} - ith_{j,j+1}/n$. Accordingly, taking the $n \to \infty$ limit leads to

$$\lim_{n\to\infty} \mathcal{V}^n = e^{-itH}. \tag{8.12}$$

The important feature of this construction is that $\mathcal{V}$ is a member of a set of commuting, conserved charges. More precisely, a staggered, inhomogeneous transfer matrix can be defined as

$$t(u) = \mathrm{Tr}_a \left[R_{aL}(u-\delta/2)R_{aL-1}(u+\delta/2)\dots R_{a1}(u+\delta/2)\right], \tag{8.13}$$

which commutes for different values of the rapidities: $[t(u),t(v)] = 0$. It can be shown [173], that the discrete time-evolution operator $\mathcal{V}$ stems from $t(u)$ through the expression

$$\mathcal{V} = \left[t(-\delta/2)\right]^{-1} t(\delta/2). \tag{8.14}$$

Moreover, $t(u)$ can be used to generate two sets of local, commuting conserved charges:

$$\hat{Q}_n^{\pm} = \frac{d^n}{du^n} \log t(u)\Big|_{u=\pm\delta/2}, \tag{8.15}$$

which are invariant under translations by two lattice sites, and have charge densities that span $2n+1$ sites. The existence of these charges means that $\mathcal{V}$ is indeed integrable.

So far, we described the Trotterization scheme in general. Now, we choose an explicit example for the quantum gate U and show that it originates from the XXZ spin chain as a special limit and that it is also related to our spin ladder model.

Since we are interested in simple systems, we try to choose the simplest possible U as well. The most

trivial cases are $U = \mathbb{1}$ and $U = \mathcal{P}$. However, the former does not generate any dynamics at all, while the latter results in the free propagation of particles. To see some non-trivial dynamics, one can modify the permutation operator $\mathcal{P}$ with some constant phase factors and choose U in the following way:

$$U = \begin{pmatrix} 1 & 0 & 0 & 0 \\ 0 & 0 & e^{i\gamma} & 0 \\ 0 & e^{i\gamma} & 0 & 0 \\ 0 & 0 & 0 & 1 \end{pmatrix}. \tag{8.16}$$

As it turns out, this slight modification is enough to introduce interaction between particles. (This can be checked for example by numerically simulating the time-evolution generated by U after a quantum quench, using the iTEBD algorithm and calculating the bipartite entanglement entropy. It increases linearly in time, signaling that indeed there is interaction between the two halves of the system.)

The quantum circuit model corresponding to (8.16) was investigated in [174]. For us, it is however more important that U can be obtained from the R-matrix of the XXZ model (3.42) with (3.44) as the limit

$$U = \lim_{u \to -i\infty} \check{R}^{XXZ}(u)\big|_{\eta = i\gamma}. \tag{8.17}$$

This means that the considerations presented above are valid for the discrete time-evolution operator built from (8.16). To illustrate its connection to our original spin ladder Hamiltonian (8.1), we calculate the first conserved charges according to (8.15). This gives local operators

$$\hat{Q}_1^+ = \sum_{j=1}^{L/2} \hat{q}_1^+(2j), \qquad \hat{Q}_1^- = \sum_{j=1}^{L/2} \hat{q}_1^-(2j+1). \tag{8.18}$$

where the charge densities can be expressed in terms of a general R-matrix as:

$$\begin{aligned} \hat{q}_1^+(1) &= R_{12}(-\delta)\check{R}'_{13}(0)R_{12}(\delta) + R_{12}(-\delta)R'_{12}(\delta), \\ \hat{q}_1^-(1) &= R_{12}(\delta)\check{R}'_{13}(0)R_{12}(-\delta) + R_{12}(\delta)R'_{12}(-\delta), \end{aligned} \tag{8.19}$$

where $(\dots)'$ denotes differentiation w.r.t. the rapidity. Substituting in here the R-matrix of the XXZ model with $\eta = i\gamma$ and taking the $\delta \to -i\infty$ limit gives the charges that commute with the time-evolution operator built from (8.16). In terms of Pauli matrices, these charge densities are given by

$$\begin{aligned} \hat{q}_1^+(1) &= \frac{1}{2}\big[\sin(\gamma)(\sigma_1^x\sigma_2^z\sigma_3^y - \sigma_1^y\sigma_2^z\sigma_3^x) + \cos(\gamma)(\sigma_1^x\sigma_3^x + \sigma_1^y\sigma_3^y + \sigma_1^z\sigma_3^z - \mathbb{1})\big], \\ \hat{q}_1^-(1) &= \frac{1}{2}\big[\sin(-\gamma)(\sigma_1^x\sigma_2^z\sigma_3^y - \sigma_1^y\sigma_2^z\sigma_3^x) + \cos(-\gamma)(\sigma_1^x\sigma_3^x + \sigma_1^y\sigma_3^y + \sigma_1^z\sigma_3^z - \mathbb{1})\big], \end{aligned} \tag{8.20}$$

which are just (up to a similarity transformation) the terms in the Hamiltonian (8.1). Thus, our model fits into the family of charges generated by (8.15), which guarantees its integrability.

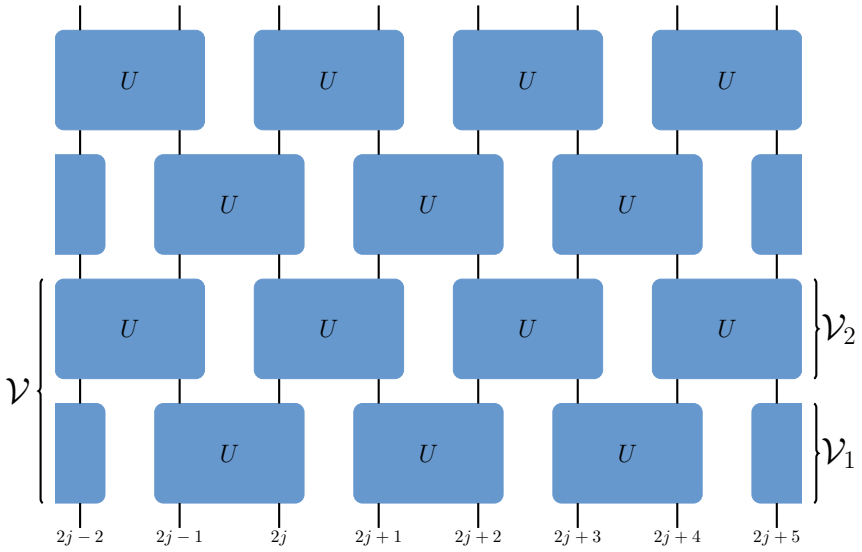

Figure 8.2: Brick-work type time-evolution implemented by $\mathcal{V}$. At each time step, first $\mathcal{V}_1$, then $\mathcal{V}_2$ acts on the appropriate sites. Based on a similar illustration in Ref. [173].

8.2 Solving the model

Due to its integrability, the model allows for an exact solution that we construct in this section.

8.2.1 Jordan-Wigner transformation

As it was already mentioned, in the case of $\gamma = 0$, the two sub-lattices decouple to two independent XX spin chains. It is well known that the XX model is free and solvable through Jordan-Wigner transformation [175]. As it turns out, a similar transformation is possible even for non-zero γ. To show this, let's introduce creation/annihilation operators for the two sub-lattices in the following way:

$$\begin{aligned} c^A(2j) &= D_1\sigma_2^z D_3\sigma_4^z \dots \sigma_{2j-2}^z D_{2j-1}\sigma_{2j}^+, \\ c^B(2j+1) &= \sigma_1^z D_2\sigma_3^z D_4 \dots \sigma_{2j-1}^z D_{2j}\sigma_{2j+1}^+, \end{aligned} \tag{8.21}$$

and also their adjoints $c^{A\dagger}(2j)$ and $c^{B\dagger}(2j+1)$. It is then not hard to directly compute the anti-commutation relations of these operators. Within the same sub-lattice, we get:

$$\{c^A(2j), c^A(2k)\} = 0, \qquad \{c^A(2j), c^{A\dagger}(2k)\} = \delta_{jk}, \tag{8.22}$$

$$\{c^B(2j+1), c^B(2k+1)\} = 0, \qquad \{c^B(2j+1), c^{B\dagger}(2k+1)\} = \delta_{jk}, \tag{8.23}$$

which are just the well-known anti-commutation relations of free fermions. In the relation between operators of different types, however, a non-trivial phase factor is present:

$$c^A(2j)c^B(2k+1) = e^{2i\gamma}c^B(2k+1)c^A(2k), \qquad j<k. \tag{8.24}$$

The appearance of the factor $\exp(2i\gamma)$ signals a partially anyonic behavior. In terms of the creation/annihilation operators, the Hamiltonian (8.1) is written as

$$H = -\sum_{j=1}^{L/2-1}\left[c^{A\dagger}(2j+2)c^A(2j) + c^{B\dagger}(2j+3)c^B(2j+1)\right] + h.c. \tag{8.25}$$

This Hamiltonian is quadratic i.e. all effects of the interactions are contained within the definitions of the creation/annihilation operators.

From the anti-commutation relations, it is also clear that the model interpolates between two free systems. Not surprisingly, for $\gamma = 0$ operators belonging to different sub-lattices commute with each other. Therefore the sub-lattices decouple, and we are left with two usual Jordan-Wigner transformations for two independent XX spin chains of length $L/2$. The other free point corresponds to $\gamma = \pi/2$. In this case, (8.22)-(8.24) reduce to a single usual Jordan-Wigner transformation for a chain of length L. The Hamiltonian, however, does not become the XX Hamiltonian, but one of its higher charges.

8.2.2 Bethe Ansatz solution

At the free points, the Hamiltonian (8.25) is diagonalizable through Fourier-transformation (see for example [176]). For generic values of γ, this is not possible, however, the eigenstates can still be obtained using CBA. We choose the state with all spins up as the vacuum, and interpret down spins as particles. Since particles can only hop within the same sub-lattice and the particle number is separately conserved on each of the sub-lattices, we can introduce two particle types A and B. We denote their coordinates by $\mathbf{a} = \{a_j\}_{j=1,\dots,N_A}$ and $\mathbf{b} = \{b_j\}_{j=1,\dots,N_B}$ (with N_A and N_B being the number of type A and type B particles) which can assume values from the even and odd numbers, respectively.

One-particle states

Direct computation shows that the states with one A or B particle, defined as

$$\left|p^A\right\rangle = \sum_a e^{i(p^A-\gamma)a/2}\left|a\right\rangle, \qquad \left|p^B\right\rangle = \sum_b e^{i(p^B+\gamma)b/2}\left|b\right\rangle \tag{8.26}$$

are eigenstates of the Hamiltonian (8.1), with one-particle eigenvalue $e(p) = -2\cos(p)$. The parameter γ appears in the wave functions due to the hopping amplitude depending on it, while the factor of $1/2$ in the exponents is the result of the fact that the particles effectively live on a chain of length $L/2$, while their coordinates a and b are „measured" with respect to the whole chain. The periodic boundary condition

provides the following quantization conditions for the momenta:

$$e^{i(p^A-\gamma)L/2}=1, \qquad e^{i(p^B+\gamma)L/2}=1. \tag{8.27}$$

Two-particle states

Eigenstates containing two particles belonging to the same sub-lattice can be constructed as

$$|p_1^\alpha, p_2^\alpha\rangle = \sum_{\alpha_1<\alpha_2}\left[e^{i(\tilde{p}_1^\alpha\alpha_1+\tilde{p}_2^\alpha\alpha_2)/2}-e^{i(\tilde{p}_1^\alpha\alpha_2+\tilde{p}_2^\alpha\alpha_1)/2}\right]|\alpha_1,\alpha_2\rangle\,, \quad (\alpha=A,B), \tag{8.28}$$

where for $\alpha=A$, we have $\tilde{p}^A=p^A-\gamma$, while for $\alpha=B$, $\tilde{p}^B=p^B+\gamma$. From (8.28), it can be read off that the scattering phase between particles of the same type is given by

$$S_{AA}=S_{BB}=-1, \tag{8.29}$$

which corresponds to free fermions. In contrast, states containing one A and one B particle are written as

$$\left|p^A,p^B\right\rangle = \sum_{a,b}e^{i(p^A-\gamma)a/2}e^{i(p^B+\gamma)b/2}\prod_{a<b}e^{-i\gamma}\prod_{b<a}e^{i\gamma}|a,b\rangle\,. \tag{8.30}$$

From (8.30), it then follows that the scattering phase between particles of different types is

$$S_{AB}=(S_{BA})^{-1}=e^{2i\gamma}. \tag{8.31}$$

The scattering phases (8.29) and (8.31) are consistent with the anti-commutation relations, (8.22)-(8.24). The eigenenergies of the states (8.28) and (8.30) are given by the sum of the one-particle energies, $E=-2(\cos(p_1^\alpha)+\cos(p_2^\alpha))$.

***N*-particle states**

Thanks to integrability, the two-particle scattering phases completely determine the dynamics, and are enough to construct all eigenstates of the model. The wave function of an eigenstate with particle numbers N_A and N_B is given by

$$\chi(\boldsymbol{a},\boldsymbol{b})=\det\mathcal{A}\det\mathcal{B}\prod_{a<b}e^{-i\gamma}\prod_{b<a}e^{i\gamma}|a,b\rangle\,, \tag{8.32}$$

where the matrices $\mathcal{A}$ and $\mathcal{B}$ have components

$$\mathcal{A}_{jk}=e^{i(p_j^A-\gamma)a_k/2}, \qquad \mathcal{B}_{jk}=e^{i(p_j^B+\gamma)b_k/2}. \tag{8.33}$$

The energy eigenvalue is still the sum of the one-particle energies:

$$E = \sum_{j=1}^{N_A} e(p_j^A) + \sum_{j=1}^{N_B} e(p_j^B), \tag{8.34}$$

while the momenta are quantized due to the periodic boundary condition and satisfy the Bethe equations:

$$\begin{aligned} e^{ip_j^A L/2} &= (-1)^{N_A-1} e^{i\gamma(L/2-2N_B)}, \\ e^{ip_j^B L/2} &= (-1)^{N_B-1} e^{-i\gamma(L/2-2N_A)}. \end{aligned} \tag{8.35}$$

These equations are almost free, expect for a twist factor that depends only on the overall particle number and couples the different momenta.

Open boundary condition

We note that with open boundary condition, the situation is even simpler. It can be shown that in this case the Hamiltonian (8.1) for arbitrary value of γ is related to $H(0)$ by a simple diagonal similarity transformation. More precisely, if we introduce the operator

$$\mathcal{D} = \prod_{2j<2k+1} e^{i\gamma\sigma_{2j}^z\sigma_{2k+1}^z/4} \prod_{2j>2k+1} e^{-i\gamma\sigma_{2k+1}^z\sigma_{2j}^z/4}, \tag{8.36}$$

then the following equation holds:

$$\mathcal{D}H(\gamma)\mathcal{D}^{-1} = H(0). \tag{8.37}$$

This means that $\mathcal{D}$ decouples the two sub-lattices and that the spin-ladder model has the same spectrum as two XX spin chains of length $L/2$. Thus, the model is effectively free, and belongs to the class investigated in [177, 178]. The two sub-lattices, however, are still entangled for $\gamma \neq 0$: even though the XX model is free, and is solvable in terms of independent Fourier modes, due to the highly non-local nature of the operator $\mathcal{D}$, there is entanglement between the two legs of the ladder, in the original spin basis.

Thermodynamic limit

It is easy to consider the ground state in the thermodynamic limit by introducing the root densities $\rho^A(p)$ and $\rho^B(p)$. The energy density of the system becomes

$$\lim_{TDL} \frac{E}{L} = \int_{-\pi}^{\pi} \frac{dp}{4\pi} e(p)\big(\rho^A(p) + \rho^B(p)\big). \tag{8.38}$$

In the ground state, the root densities are constants, given by

$$\rho^{A/B}(p) = \begin{cases} 1, & \text{if } |p| < \frac{\pi}{2}, \\ 0, & \text{if } |p| > \frac{\pi}{2}. \end{cases} \tag{8.39}$$

This gives $-2/\pi$ for the energy density, which is the same as in the XX model.

8.3 Entanglement properties

Due to its relative simplicity, the system can serve as a toy model to study different physical phenomena. The most interesting one is most probably the entanglement entropy between the even/odd sub-lattices that can be tuned by varying the coupling constant γ. Here we study this quantity, both analytically and numerically.

8.3.1 Correlations between sub-lattices

To demonstrate that the interaction indeed entangles the two sub-lattices, we calculate the following connected correlation function:

$$C_\psi = \langle\psi|\sigma_0^-\sigma_1^z\sigma_2^+|\psi\rangle - \langle\psi|\sigma_0^-\sigma_2^+|\psi\rangle\,\langle\psi|\sigma_1^z|\psi\rangle\,, \tag{8.40}$$

where $|\psi\rangle$ is an arbitrary eigenstate of the system, with particle numbers N_A and N_B. We choose the operator in (8.40), because of two reasons: one, it contains a hopping term, which is needed to see non-trivial effects, and two, it is a certain combination of the conserved charges of the model, which makes it easy to evaluate (8.40). Accordingly, we can start by computing the expectation value of the conserved charge $\hat{Q}_3^{A-}$:

$$\langle\psi|\cos(\gamma)\sigma_0^-\sigma_2^+ + i\sin(\gamma)\sigma_0^-\sigma_1^z\sigma_2^+|\psi\rangle = \frac{2\langle\hat{Q}_3^{A-}\rangle}{L} = 2W, \tag{8.41}$$

where we introduced

$$W = \frac{1}{L}\sum_{j=1}^{N_A} e^{ip_j^A}. \tag{8.42}$$

By applying the Hellmann-Feynman theorem, we can take the derivative of (8.41) with respect to γ, to obtain:

$$\langle\psi|-\sin(\gamma)\sigma_0^-\sigma_2^+ + i\cos(\gamma)\sigma_0^-\sigma_1^z\sigma_2^+|\psi\rangle = \frac{2}{L}\partial_\gamma W = \frac{2}{L}\sum_{j=1}^{N_A} e^{ip_j^A} i\partial_\gamma(p_j^A) = 2im_B W. \tag{8.43}$$

Here we used the Bethe equations (8.35), to calculate the derivative $\partial_\gamma(p_j^A)$ and introduced the notation $m_B = (L-4N_B)/L$ for the magnetization on sub-lattice B. Equations (8.41) and (8.43) form a system of linear equations for the expectation values $\langle\psi|\sigma_0^-\sigma_1^z\sigma_2^+|\psi\rangle$ and $\langle\psi|\sigma_0^-\sigma_2^+|\psi\rangle$, from which the correlation function C_ψ is easily obtained:

$$C_\psi = 2Wi\sin(\gamma)(m_B^2-1). \tag{8.44}$$

In the thermodynamic limit, W becomes

$$\lim_{TDL} W = \int_{-\pi}^{\pi}\frac{dp}{4\pi}\rho^A(p)e^{ip}, \tag{8.45}$$

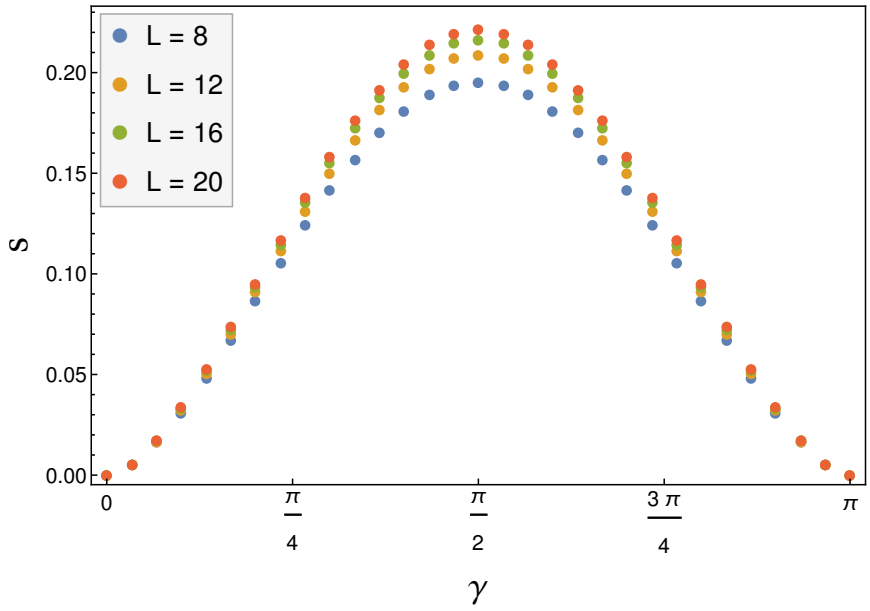

Figure 8.3: Sub-lattice entanglement entropy density in the ground state, as a function of the coupling constant γ, for different system sizes.

which, in general has a finite value, therefore C_ψ is indeed non-zero.

The correlation function vanishes, however, if $\gamma = 0$, which is trivial, since in this case the two sub-lattices decouple, or in the case when either sub-lattice is fully polarized. If sub-lattice B is fully polarized, i.e. has magnetization $m_B = \pm 1$, the factor $m_B^2 - 1$ gives zero, while if sub-lattice A is fully polarized, its root density becomes constant, and W vanishes.

8.3.2 Numerical results

We also investigate the sub-lattice entanglement entropy by numerical means, both in equilibrium and non-equilibrium situations. To this end, we use exact diagonalization in finite volumes and calculate the von Neumann entropy

$$S = -\mathrm{Tr}(\rho_A \log \rho_A), \tag{8.46}$$

with $\rho_A = \mathrm{Tr}_B \rho$ being the reduced density matrix corresponding to sub-lattice A, while ρ is the density matrix of the whole system. Since S is extensive, we consider its density $s = S/L$. Besides some finite size effects, s is expected to be independent of the length L.

Ground state

We calculated the sub-lattice entanglement entropy in the ground state of the system in different volumes L and different coupling constants γ. The results are presented in Fig. 8.3.

As it can be seen, the entanglement entropy is maximal at $\gamma = \pi/2$, which might be surprising in the

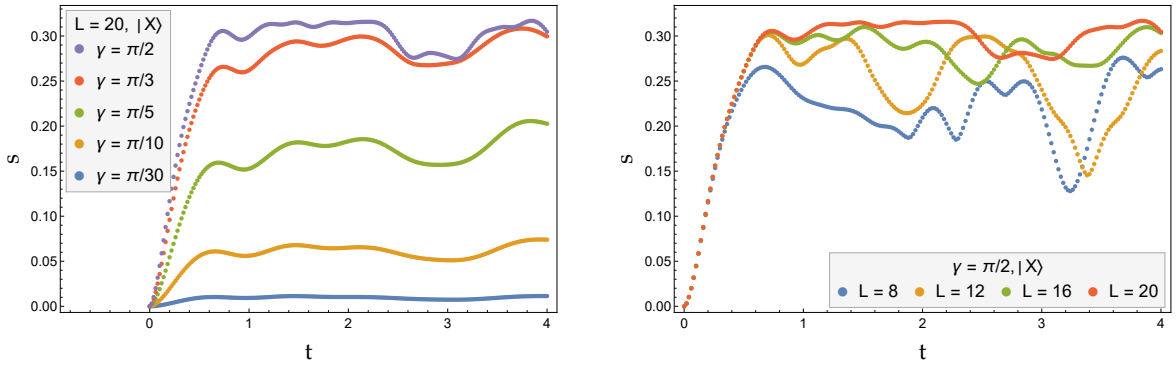

(a) (b)

Figure 8.4: (a) Sub-lattice entanglement following a quantum quench, with $L = 20$ and various coupling constants. (b) Sub-lattice entanglement following a quantum quench, with $\gamma = \pi/2$ and various system sizes.

light of the fact that at this point the model reduces to free fermions, suggesting zero entanglement. This is the a manifestation of a more general phenomenon: entanglement entropy computed in terms of the original spin basis and the fermionic degrees of freedom only agree for connected sub-systems [179]. For non-connected subsystems (such as the even/odd sub-lattices A and B), the Jordan-Wigner transformation causes differences between the two definitions of entanglement.

Quantum quench

We also studied the time-evolution of the entanglement entropy, following a quantum quench that starts from the the state $|X\rangle$, polarized completely along the x-axis:

$$|X\rangle = \bigotimes_{j=1}^{L} \left(\frac{|\uparrow_j\rangle + |\downarrow_j\rangle}{\sqrt{2}} \right). \tag{8.47}$$

We both considered quenches with a fixed length and different coupling constants (see Fig. 8.4 (a)), and different lengths with a fixed coupling constant (see Fig. 8.4 (b)).

It can be seen that the entropy increases quite rapidly and reaches a plateau. The height of the plateau depends on the coupling constant, and similarly to the equilibrium case, it is maximal at $\gamma = \pi/2$. Moreover, it is also apparent that the entanglement entropy is indeed extensive, however there are more significant finite size effects now, compared to the equilibrium situation.

Other initial states lead to qualitatively similar results.

8.4 Summary

In this chapter, we introduced an integrable spin-ladder model that supports two particle types, living on the even/odd sub-lattices of the system. The particles exhibit partially anyonic behavior, and have really simple

scattering phases, which makes this model one of the simplest interacting integrable systems. As a result, it could potentially serve as a toy model to analytically treat such problems that are otherwise out of reach for usual integrable systems. A possible application might be the construction of interacting Bethe states on a quantum computer [180–183].

We constructed the eigenstates of the model by means of CBA and showed that by tuning the coupling constant γ, the system interpolates between two free fermionic points.

We also studied the behavior of the entanglement entropy between the even/odd sub-lattices, both analytically and numerically, in and out-of-equilibrium.

Chapter 9

Thesis statements

1. I worked out a rigorous proof for a formula that describes the mean values of the (generalized) current operators of the XXZ spin-$1/2$ chain in finite volume. (The formula was originally conjectured by my supervisor.) The proof is based on a form-factor expansion that I established for the XXZ model by using its ABA solution and the solution of the quantum inverse scattering problem. Using this expansion theorem, I first calculated the form factors of the charge operators, and then, by utilizing the continuity equation, I computed the form factors of the currents. By the repeated application of the form-factor expansion theorem and with the help of the newly obtained current form factors, I calculated the expectation values of the (generalized) current operators in arbitrary eigenstates of the XXZ model in finite volume. This result provides a rigorous theoretical foundation for one of the underlying assumptions of GHD and was published in [82].

2. I extended the results described in the previous point to the non $U(1)$ symmetric XYZ spin-$1/2$ model. To this end, I used the known generalized ABA solution of the XYZ model and the algebraic construction of the current operators that was first found by my supervisor. Using these tools, I calculated the mean values of the (generalized) current operators in arbitrary eigenstates of the XYZ model in finite volume and proved a similar formula to that of the previous point. The results were published in [73].

3. As part of a larger collaboration, I re-derived and studied the so-called folded XXZ model, which is an integrable system with a particularly simple two-particle scattering phase. Our results were published in [141]. My main contributions to [141] were the calculation of the charges of the folded model starting from the known charges of the XXZ spin-$1/2$ chain, the calculation of the ground state properties of the folded model and the numerical simulation of the time-evolution, following a quantum quench. Additionally, I also contributed to obtaining the Bethe Ansatz solution of the folded model and to the calculation of the exact time evolution of the so-called emptiness formation probability, following a specific quantum quench scenario.

   The folded XXZ model exhibits Hilbert space fragmentation, leading to the breakdown of thermal-

ization in this system. I studied this phenomenon by numerically simulating the real time-evolution following a global quantum quench using the iTEBD algorithm. My implementation of the numerical method is based on previously existing code that I modified to the needs of the medium-range folded XXZ model. My numerical results support the theoretical considerations and show persistent oscillations that signal the breakdown of equilibration. I also performed the same analysis in the case of a non-integrable extension of the folded XXZ model, whose non-integrability I demonstrated by numerically calculating its level spacing statistics. The results related to this non-integrable extension were published in [152].

4. As part of a collaboration, I introduced and studied a one-dimensional anyon-like spin chain, which constitutes one of the simplest interacting integrable systems. My main contribution to this research was the derivation of the charges of the model through its connection to a particular limit of the integrable Trotterization of the XXZ spin chain. Moreover, I also contributed to solving the model via CBA and to the analytical and numerical calculations of the entanglement entropy in the system, in both in- and out-of-equilibrium situations. Our results were published in [166].

Bibliography

[1] W. Heisenberg, "Zur Theorie des Ferromagnetismus," *Zeitschrift für Physik* **49** no. 9, (Sep, 1928) 619–636, https://doi.org/10.1007/BF01328601.

[2] H. Bethe, "Zur Theorie der Metalle," *Zeitschrift für Physik* **A71** (1931) 205–226, https://doi.org/10.1007/BF01341708.

[3] E. H. Lieb and W. Liniger, "Exact Analysis of an Interacting Bose Gas. I. The General Solution and the Ground State," *Phys. Rev.* **130** (1963) 1605, https://doi.org/10.1103/PhysRev.130.1605.

[4] C. N. Yang and C. P. Yang, "One-Dimensional Chain of Anisotropic Spin-Spin Interactions. I. Proof of Bethe's Hypothesis for Ground State in a Finite System," *Phys. Rev.* **150** (Oct, 1966) 321–327, https://doi.org/10.1103/PhysRev.150.321.

[5] C. N. Yang and C. P. Yang, "Thermodynamics of a One-Dimensional System of Bosons with Repulsive Delta-Function Interaction," *Journal of Mathematical Physics* **10** no. 7, (07, 1969) 1115–1122, https://doi.org/10.1063/1.1664947.

[6] E. H. Lieb, "Exact solution of the f model of an antiferroelectric," *Phys. Rev. Lett.* **18** (Jun, 1967) 1046–1048, https://doi.org/10.1103/PhysRevLett.18.1046.

[7] E. H. Lieb, "Residual entropy of square ice," *Phys. Rev.* **162** (Oct, 1967) 162–172, https://doi.org/10.1103/PhysRev.162.162.

[8] E. H. Lieb, "Exact Solution of the Two-Dimensional Slater KDP Model of a Ferroelectric," *Phys. Rev. Lett.* **19** (Jul, 1967) 108–110, https://doi.org/10.1103/PhysRevLett.19.108.

[9] B. Sutherland, "Exact solution of a two-dimensional model for hydrogen-bonded crystals," *Phys. Rev. Lett.* **19** (Jul, 1967) 103–104, https://doi.org/10.1103/PhysRevLett.19.103.

[10] L. Onsager, "Crystal Statistics. I. A Two-Dimensional Model with an Order-Disorder Transition," *Phys. Rev.* **65** (1944) 117–149, https://doi.org/10.1103/PhysRev.65.117.

[11] *Exactly Solved Models in Statistical Mechanics*, R. J. Baxter. London: Academic Press Inc, 1982.

[12] *Quantum Inverse Scattering Method and Correlation Functions*, V. Korepin, N. Bogoliubov, and A. Izergin. Cambridge University Press, 1993.

[13] I. Bloch, J. Dalibard, and W. Zwerger, "Many-body physics with ultracold gases," *Rev. Mod. Phys.* **80** (Jul, 2008) 885–964, https://doi.org/10.1103/RevModPhys.80.885.

[14] T. Langen, R. Geiger, and J. Schmiedmayer, "Ultracold atoms out of equilibrium," *Annual Review of Condensed Matter Physics* **6** no. 1, (Mar., 2015) 201–217, https://doi.org/10.1146/annurev-conmatphys-031214-014548.

[15] J. M. Deutsch, "Quantum statistical mechanics in a closed system," *Phys. Rev. A* **43** (Feb, 1991) 2046–2049, https://doi.org/10.1103/PhysRevA.43.2046.

[16] M. Srednicki, "Chaos and quantum thermalization," *Phys. Rev. E* **50** (Aug, 1994) 888–901, https://doi.org/10.1103/PhysRevE.50.888.

[17] L. D'Alessio, Y. Kafri, A. Polkovnikov, and M. Rigol, "From quantum chaos and eigenstate thermalization to statistical mechanics and thermodynamics," *Advances in Physics* **65** no. 3, (May, 2016) 239–362, https://doi.org/10.1080/00018732.2016.1198134.

[18] M. Rigol, V. Dunjko, and M. Olshanii, "Thermalization and its mechanism for generic isolated quantum systems," *Nature* **452** no. 7189, (Apr., 2008) 854–858, https://doi.org/10.1038/nature06838.

[19] W. Beugeling, R. Moessner, and M. Haque, "Finite-size scaling of eigenstate thermalization," *Physical Review E* **89** no. 4, (Apr., 2014) , https://doi.org/10.1103/physreve.89.042112.

[20] R. Steinigeweg, J. Herbrych, and P. Prelovšek, "Eigenstate thermalization within isolated spin-chain systems," *Phys. Rev. E* **87** (Jan, 2013) 012118, https://doi.org/10.1103/PhysRevE.87.012118.

[21] C. Neuenhahn and F. Marquardt, "Thermalization of interacting fermions and delocalization in Fock space," *Phys. Rev. E* **85** (Jun, 2012) 060101, https://doi.org/10.1103/PhysRevE.85.060101.

[22] M. Rigol, "Quantum quenches and thermalization in one-dimensional fermionic systems," *Physical Review A* **80** no. 5, (Nov., 2009) , https://doi.org/10.1103/physreva.80.053607.

[23] R. Mondaini, K. R. Fratus, M. Srednicki, and M. Rigol, "Eigenstate thermalization in the two-dimensional transverse field Ising model," *Physical Review E* **93** no. 3, (Mar., 2016) , https://doi.org/10.1103/physreve.93.032104.

[24] *Beautiful Models*, B. Sutherland. World Scientific Publishing Company, 2004.

[25] S. Moudgalya and O. I. Motrunich, "Hilbert Space Fragmentation and Commutant Algebras," *Physical Review X* **12** no. 1, (Mar, 2022) , https://doi.org/10.1103/physrevx.12.011050.

[26] P. Sala, T. Rakovszky, R. Verresen, M. Knap, and F. Pollmann, "Ergodicity Breaking Arising from Hilbert Space Fragmentation in Dipole-Conserving Hamiltonians," *Physical Review X* **10** no. 1, (Feb, 2020) , https://doi.org/10.1103/physrevx.10.011047.

[27] H. Bernien, S. Schwartz, A. Keesling, H. Levine, A. Omran, H. Pichler, S. Choi, A. S. Zibrov, M. Endres, M. Greiner, V. Vuletić, and M. D. Lukin, "Probing many-body dynamics on a 51-atom quantum simulator," *Nature* **551** no. 7682, (Nov, 2017) 579–584, https://doi.org/10.1038/nature24622.

[28] S. Moudgalya, S. Rachel, B. A. Bernevig, and N. Regnault, "Exact excited states of nonintegrable models," *Phys. Rev. B* **98** (Dec, 2018) 235155, https://doi.org/10.1103/PhysRevB.98.235155.

[29] M. Serbyn, D. A. Abanin, and Z. Papić, "Quantum many-body scars and weak breaking of ergodicity," *Nature Physics* **17** no. 6, (May, 2021) 675–685, https://doi.org/10.1038/s41567-021-01230-2.

[30] S. Moudgalya, B. A. Bernevig, and N. Regnault, "Quantum many-body scars and Hilbert space fragmentation: a review of exact results," *Reports on Progress in Physics* **85** no. 8, (Jul, 2022) 086501, https://doi.org/10.1088/1361-6633/ac73a0.

[31] P. W. Anderson, "Absence of diffusion in certain random lattices," *Phys. Rev.* **109** (Mar, 1958) 1492–1505, https://doi.org/10.1103/PhysRev.109.1492.

[32] R. Nandkishore and D. A. Huse, "Many-body localization and thermalization in quantum statistical mechanics," *Annual Review of Condensed Matter Physics* **6** no. 1, (2015) 15–38, https://doi.org/10.1146/annurev-conmatphys-031214-014726.

[33] D. A. Abanin, E. Altman, I. Bloch, and M. Serbyn, "Colloquium: Many-body localization, thermalization, and entanglement," *Rev. Mod. Phys.* **91** (May, 2019) 021001, https://doi.org/10.1103/RevModPhys.91.021001.

[34] T. Kinoshita, T. Wenger, and D. S. Weiss, "A quantum Newton's cradle," *Nature* **440** (2006) 900, https://doi.org/10.1038/nature04693.

[35] M. Rigol, V. Dunjko, V. Yurovsky, and M. Olshanii, "Relaxation in a completely integrable many-body quantum system: An ab initio study of the dynamics of the highly excited states of 1d lattice hard-core bosons," *Phys. Rev. Lett.* **98** no. 5, (2007) 050405, https://doi.org/10.1103/PhysRevLett.98.050405.

[36] L. Vidmar and M. Rigol, "Generalized Gibbs ensemble in integrable lattice models," *J. Stat. Mech.* **6** (2016) 064007, https://doi.org/10.1088/1742-5468/2016/06/064007.

[37] B. Wouters, J. De Nardis, M. Brockmann, D. Fioretto, M. Rigol, and J.-S. Caux, "Quenching the Anisotropic Heisenberg Chain: Exact Solution and Generalized Gibbs Ensemble Predictions," *Physical Review Letters* **113** no. 11, (Sept., 2014) , https://doi.org/10.1103/physrevlett.113.117202.

[38] B. Pozsgay, M. Mestyán, M. Werner, M. Kormos, G. Zaránd, and G. Takács, "Correlations after Quantum Quenches in the XXZ Spin Chain: Failure of the Generalized Gibbs Ensemble," *Physical Review Letters* **113** no. 11, (Sept., 2014) , https://doi.org/10.1103/physrevlett.113.117203.

[39] E. Ilievski, M. Medenjak, and T. Prosen, "Quasilocal conserved operators in the isotropic Heisenberg spin 1/2 chain," *Physical Review Letters* **115** no. 12, (Sept., 2015) , https://doi.org/10.1103/physrevlett.115.120601.

[40] E. Ilievski, M. Medenjak, T. Prosen, and L. Zadnik, "Quasilocal charges in integrable lattice systems," *Journal of Statistical Mechanics: Theory and Experiment* **2016** no. 6, (June, 2016) 064008, https://doi.org/10.1088/1742-5468/2016/06/064008.

[41] E. Ilievski, J. De Nardis, B. Wouters, J.-S. Caux, F. Essler, and T. Prosen, "Complete Generalized Gibbs Ensembles in an Interacting Theory," *Physical Review Letters* **115** no. 15, (Oct., 2015) , https://doi.org/10.1103/physrevlett.115.157201.

[42] A. C. Cassidy, C. W. Clark, and M. Rigol, "Generalized thermalization in an integrable lattice system," *Physical Review Letters* **106** no. 14, (Apr., 2011) , https://doi.org/10.1103/physrevlett.106.140405.

[43] M. Kollar, F. A. Wolf, and M. Eckstein, "Generalized Gibbs ensemble prediction of prethermalization plateaus and their relation to nonthermal steady states in integrable systems," *Physical Review B* **84** no. 5, (Aug., 2011) , https://doi.org/10.1103/physrevb.84.054304.

[44] B. Bertini, F. H. Essler, S. Groha, and N. J. Robinson, "Prethermalization and thermalization in models with weak integrability breaking," *Physical Review Letters* **115** no. 18, (Oct., 2015) , https://doi.org/10.1103/physrevlett.115.180601.

[45] *Large Scale Dynamics of Interacting Particles*, H. Spohn. Texts and monographs in physics. Springer-Verlag, 1991.

[46] O. A. Castro-Alvaredo, B. Doyon, and T. Yoshimura, "Emergent Hydrodynamics in Integrable Quantum Systems Out of Equilibrium," *Phys. Rev. X* **6** no. 4, (2016) 041065, https://doi.org/10.1103/PhysRevX.6.041065.

[47] B. Bertini, M. Collura, J. De Nardis, and M. Fagotti, "Transport in Out-of-Equilibrium XXZ Chains: Exact Profiles of Charges and Currents," *Phys. Rev. Lett.* **117** no. 20, (2016) 207201, https://doi.org/10.1103/PhysRevLett.117.207201.

[48] E. Ilievski, J. De Nardis, B. Wouters, J.-S. Caux, F. Essler, and T. Prosen, "Complete Generalized Gibbs Ensembles in an Interacting Theory," *Physical Review Letters* **115** no. 15, (Oct., 2015) , https://doi.org/10.1103/physrevlett.115.157201.

[49] E. Ilievski, E. Quinn, and J.-S. Caux, "From interacting particles to equilibrium statistical ensembles," *Physical Review B* **95** no. 11, (Mar., 2017) , https://doi.org/10.1103/physrevb.95.115128.

[50] M. Schemmer, I. Bouchoule, B. Doyon, and J. Dubail, "Generalized HydroDynamics on an Atom Chip," *Phys. Rev. Lett.* **122** no. 9, (2019) 090601, https://doi.org/10.1103/PhysRevLett.122.090601.

[51] J.-S. Caux, B. Doyon, J. Dubail, R. Konik, and T. Yoshimura, "Hydrodynamics of the interacting Bose gas in the Quantum Newton Cradle setup," *SciPost Physics* **6** no. 6, (Jun, 2019) , https://doi.org/10.21468/scipostphys.6.6.070.

[52] N. Malvania, Y. Zhang, Y. Le, J. Dubail, M. Rigol, and D. S. Weiss, "Generalized hydrodynamics in strongly interacting 1d bose gases," *Science* **373** no. 6559, (Sep, 2021) 1129–1133, https://doi.org/10.1126/science.abf0147.

[53] A. Bastianello, B. Bertini, B. Doyon, and R. Vasseur, "Introduction to the Special Issue on Emergent Hydrodynamics in Integrable Many-Body Systems," *Journal of Statistical Mechanics: Theory and Experiment* **2022** no. 1, (Jan, 2022) 014001, https://doi.org/10.1088/1742-5468/ac3e6a.

[54] B. Doyon, "Lecture notes on Generalised Hydrodynamics," *SciPost Phys. Lect. Notes* (2020) 18, https://doi.org/10.21468/SciPostPhysLectNotes.18.

[55] Q.-Q. Shi, S.-H. Li, and H.-Q. Zhou, "Duality and ground-state phase diagram for the quantum XYZ model with arbitrary spin s in one spatial dimension," *Journal of Physics A: Mathematical and Theoretical* **53** no. 15, (Mar, 2020) 155301, https://doi.org/10.1088/1751-8121/ab78cd.

[56] S. A. Jafari, "Exact phase boundaries and topological phase transitions of the XYZ spin chain," *Physical Review E* **96** no. 1, (July, 2017) , https://doi.org/10.1103/physreve.96.012159.

[57] M. Karabach, G. Müller, H. Gould, and J. Tobochnik, "Introduction to the Bethe Ansatz I," *Computer in Physics* **11** no. 1, (01, 1997) 36–43, https://doi.org/10.1063/1.4822511.

[58] *An Introduction to Integrable Techniques for One-Dimensional Quantum Systems*, F. Franchini. Springer Cham, 2017.

[59] *Introduction to the Statistical Physics of Integrable Many-body Systems*, L. Šamaj and Z. Bajnok. Cambridge University Press, 2013.

[60] E. H. Lieb, "Exact Analysis of an Interacting Bose Gas. II. The Excitation Spectrum," *Phys. Rev.* **130** no. 4, (1963) 1616–1624, https://doi.org/10.1103/PhysRev.130.1616.

[61] M. Gaudin, B. M. McCoy, and T. T. Wu, "Normalization Sum for the Bethe's Hypothesis Wave Functions of the Heisenberg-Ising Chain," *Phys. Rev. D* **23** (1981) 417–419, https://doi.org/10.1103/PhysRevD.23.417.

[62] V. E. Korepin, "Calculation of Norms of Bethe Wave Functions," *Comm. Math. Phys.* **86** (1982) 391, https://doi.org/10.1007/BF01212176.

[63] *The Bethe Wavefunction*, M. Gaudin. Cambridge University Press, 2014.

[64] *Hamiltonian Methods in the Theory of Solitons*, L. D. Faddeev and L. A. Takhtajan. Springer-Verlag Berlin Heidelberg, 2007.

[65] *Introduction to Classical Integrable Systems*, O. Babelon, D. Bernard, and M. Talon. Cambridge Monographs on Mathematical Physics. Cambridge University Press, 2003.

[66] A. Doikou, S. Evangelisti, G. Feverati, and N. Karaiskos, "Introduction to Quantum Integrability," *Int. J. Mod. Phys.* **A25** (2010) 3307–3351, https://doi.org/10.1142/S0217751X10049803.

[67] J. D. Nardis, D. Bernard, and B. Doyon, "Diffusion in generalized hydrodynamics and quasiparticle scattering," *SciPost Physics* **6** no. 4, (Apr, 2019) , https://doi.org/10.21468/scipostphys.6.4.049.

[68] *The One-Dimensional Hubbard Model*, F. H. L. Essler, H. Frahm, F. Göhmann, A. Klümper, and V. E. Korepin. Cambridge University Press, Cambridge, 2005.

[69] L. A. Takhtajan and L. D. Faddeev, "The Quantum Method of the Inverse Problem and the Heisenberg XYZ Model," *Russ. Math. Surv.* **34** no. 5, (1979) 11–68, https://doi.org/10.1070/RM1979v034n05ABEH003909.

[70] G. Niccoli and V. Terras, "The eight-vertex model with quasi-periodic boundary conditions," *Journal of Physics A: Mathematical and Theoretical* **49** no. 4, (Dec, 2015) 044001, https://doi.org/10.1088/1751-8113/49/4/044001.

[71] J. Cao, S. Cui, W.-L. Yang, K. Shi, and Y. Wang, "Spin-1/2 XYZ model revisit: General solutions via off-diagonal Bethe ansatz," *Nucl. Phys. B* **886** (2014) 185–201, https://doi.org/10.1016/j.nuclphysb.2014.06.026.

[72] *Off-Diagonal Bethe Ansatz for Exactly Solvable Models*, Y. Wang, W.-L. Yang, J. Cao, and K. Shi. Springer-Verlag Berlin Heidelberg, 2015.

[73] L. Pristyák and B. Pozsgay, "Current mean values in the XYZ model," *SciPost Physics* **14** no. 6, (Jun, 2023) , https://doi.org/10.21468/scipostphys.14.6.158.

[74] A. Urichuk, Y. Oez, A. Klümper, and J. Sirker, "The Spin Drude Weight of the XXZ Chain and Generalized Hydrodynamics," *SciPost Phys.* **6** (2019) 5, https://doi.org/10.21468/SciPostPhys.6.1.005.

[75] N. Kitanine, J. Maillet, and V. Terras, "Correlation functions of the XXZ Heisenberg spin-1/2 chain in a magnetic field," *Nuclear Physics B* **567** no. 3, (Feb., 2000) 554–582, https://doi.org/10.1016/s0550-3213(99)00619-7.

[76] F. Göhmann, A. Klümper, and A. Seel, "Integral representations for correlation functions of the XXZ chain at finite temperature," *Journal of Physics A: Mathematical and General* **37** no. 31, (July, 2004) 7625–7651, https://doi.org/10.1088/0305-4470/37/31/001.

[77] N. Kitanine, J. Maillet, N. Slavnov, and V. Terras, "Dynamical correlation functions of the XXZ spin-1/2 chain," *Nuclear Physics B* **729** no. 3, (Nov., 2005) 558–580, https://doi.org/10.1016/j.nuclphysb.2005.08.046.

[78] H. Boos, M. Jimbo, T. Miwa, F. Smirnov, and Y. Takeyama, "Algebraic representation of correlation functions in integrable spin chains," *Annales Henri Poincaré* **7** no. 7–8, (Nov., 2006) 1395–1428, https://doi.org/10.1007/s00023-006-0285-5.

[79] N. Kitanine, K. K. Kozlowski, J. M. Maillet, N. A. Slavnov, and V. Terras, "Algebraic Bethe ansatz approach to the asymptotic behavior of correlation functions," *Journal of Statistical Mechanics: Theory and Experiment* **2009** no. 04, (Apr., 2009) P04003, https://doi.org/10.1088/1742-5468/2009/04/p04003.

[80] K. K. Kozlowski, "Asymptotic Analysis and Quantum Integrable Models," *ArXiv e-prints* (2015) , arXiv:1508.06085 [math-ph].

[81] J. Sato, B. Aufgebauer, H. Boos, F. Göhmann, A. Klümper, M. Takahashi, and C. Trippe, "Computation of Static Heisenberg-Chain Correlators: Control over Length and Temperature Dependence," *Phys. Rev. Lett.* **106** no. 25, (2011) 257201, https://doi.org/10.1103/PhysRevLett.106.257201.

[82] M. Borsi, B. Pozsgay, and L. Pristyák, "Current Operators in Bethe Ansatz and Generalized Hydrodynamics: An Exact Quantum/Classical Correspondence," *Phys. Rev. X* **10** (2020) 011054, https://doi.org/10.1103/PhysRevX.10.011054.

[83] M. Borsi, B. Pozsgay, and L. Pristyák, "Current operators in integrable models: a review," *Journal of Statistical Mechanics: Theory and Experiment* **2021** no. 9, (Sep, 2021) 094001, https://doi.org/10.1088/1742-5468/ac0f6b.

[84] *The Formal Properties of Nuclear Collisions.*, L. Eisenbud. PhD thesis, Princeton University, New Jersey, Jan., 1948.

[85] E. P. Wigner, "Lower limit for the energy derivative of the scattering phase shift," *Phys. Rev.* **98** (Apr, 1955) 145–147, https://doi.org/10.1103/PhysRev.98.145.

[86] R. Vlijm, M. Ganahl, D. Fioretto, M. Brockmann, M. Haque, H. G. Evertz, and J.-S. Caux, "Quasi-soliton scattering in quantum spin chains," *Physical Review B* **92** no. 21, (Dec, 2015) , https://doi.org/10.1103/physrevb.92.214427.

[87] B. Pozsgay and G. Takács, "Form factors in finite volume I: Form factor bootstrap and truncated conformal space," *Nuclear Physics B* **788** no. 3, (Jan, 2008) 167–208, https://doi.org/10.1016/j.nuclphysb.2007.06.027.

[88] F. A. Smirnov, "Form Factors in Completely Integrable Models of Quantum Field Theory," *Adv. Ser. Math. Phys.* **14** (1992) 1–208.

[89] B. Pozsgay, W.-V. van Gerven Oei, and M. Kormos, "On form factors in nested Bethe Ansatz systems," *J. Phys. A* **45** (2012) 465007, https://doi.org/10.1088/1751-8113/45/46/465007.

[90] B. Pozsgay and G. Takács, "Form factors in finite volume II: Disconnected terms and finite temperature correlators," *Nuclear Physics B* **788** no. 3, (Jan, 2008) 209–251, https://doi.org/10.1016/j.nuclphysb.2007.07.008.

[91] B. Pozsgay, "Mean values of local operators in highly excited Bethe states," *J. Stat. Mech.* **2011** (2011) P01011, https://doi.org/10.1088/1742-5468/2011/01/P01011.

[92] A. LeClair and G. Mussardo, "Finite temperature correlation functions in integrable QFT," *Nuclear Physics B* **552** no. 3, (Jul, 1999) 624–642, https://doi.org/10.1016/s0550-3213(99)00280-1.

[93] B. Pozsgay, "Local correlations in the 1D Bose gas from a scaling limit of the XXZ chain," *Journal of Statistical Mechanics: Theory and Experiment* **2011** no. 11, (Nov., 2011) P11017, https://doi.org/10.1088/1742-5468/2011/11/p11017.

[94] N. Kitanine, J. Maillet, and V. Terras, "Form factors of the XXZ Heisenberg finite chain," *Nuclear Physics B* **554** no. 3, (Aug, 1999) 647–678, https://doi.org/10.1016/s0550-3213(99)00295-3.

[95] F. Göhmann and V. E. Korepin, "Solution of the quantum inverse problem," *Journal of Physics A: Mathematical and General* **33** no. 6, (Feb, 2000) 1199–1220, https://doi.org/10.1088/0305-4470/33/6/308.

[96] J. Maillet and V. Terras, "On the quantum inverse scattering problem," *Nuclear Physics B* **575** no. 3, (2000) 627–644, https://doi.org/https://doi.org/10.1016/S0550-3213(00)00097-3.

[97] S. Chaiken and D. J. Kleitman, "Matrix Tree Theorems," *Journal of Combinatorial Theory, Series A* **24** no. 3, (1978) 377–381, https://doi.org/https://doi.org/10.1016/0097-3165(78)90067-5.

[98] B. Pozsgay, "Current operators in integrable spin chains: lessons from long range deformations," *SciPost Phys.* **8** (2020) 016, https://doi.org/10.21468/SciPostPhys.8.2.016.

[99] B. Pozsgay, "Algebraic Construction of Current Operators in Integrable Spin Chains," *Phys. Rev. Lett.* **125** no. 7, (2020) 070602, https://doi.org/10.1103/physrevlett.125.070602.

[100] Z. Bajnok and I. Vona, "Exact finite volume expectation values of conserved currents," *Phys. Lett. B* **805** (2020) 135446, https://doi.org/10.1016/j.physletb.2020.135446.

[101] T. Yoshimura and H. Spohn, "Collision rate ansatz for quantum integrable systems," *SciPost Phys.* **9** (2020) 40, https://doi.org/10.21468/SciPostPhys.9.3.040.

[102] D. Levy-Bencheton and V. Terras, "An algebraic Bethe ansatz approach to form factors and correlation functions of the cyclic eight-vertex solid-on-solid model," *Journal of Statistical Mechanics: Theory and Experiment* **2013** no. 04, (Apr, 2013) P04015, https://doi.org/10.1088/1742-5468/2013/04/p04015.

[103] H. Boos, M. Jimbo, T. Miwa, F. Smirnov, and Y. Takeyama, "Traces on the Sklyanin algebra and correlation functions of the eight-vertex model," *Journal of Physics A: Mathematical and General* **38** no. 35, (Aug, 2005) 7629, https://doi.org/10.1088/0305-4470/38/35/003.

[104] M. Lashkevich and Y. Pugai, "Free field construction for correlation functions of the eight-vertex model," *Nuclear Physics B* **516** no. 3, (1998) 623–651, https://doi.org/https://doi.org/10.1016/S0550-3213(98)00086-8.

[105] J. Shiraishi, "Free Field Constructions for the Elliptic Algebra $A_{q,p}(\{sl\}_{2)}$ and Baxter's Eight-Vertex Model," *Int. J. Mod. Phys. A* **19** (2004) 363–380, https://doi.org/10.1142/S0217751X0402052X.

[106] Y.-H. Quano, "Form factors, correlation functions and vertex operators in the eight-vertex model at reflectionless points," arXiv:hep-th/0410084 [hep-th].

[107] N. Slavnov, A. Zabrodin, and A. Zotov, "Scalar products of Bethe vectors in the 8-vertex model," *Journal of High Energy Physics* **2020** no. 6, (Jun, 2020) , https://doi.org/10.1007/jhep06(2020)123.

[108] G. Kulkarni and N. A. Slavnov, "Scalar products of Bethe vectors in the generalized algebraic Bethe ansatz," *Theoretical and Mathematical Physics* **217** no. 1, (Oct, 2023) 1574–1594, https://doi.org/10.1134/S0040577923100100.

[109] G. Kulkarni and N. A. Slavnov, "Form factor of local operators in the generalized algebraic Bethe ansatz," arXiv:2308.15748 [math-ph].

[110] H. E. Boos, F. Göhmann, A. Klümper, and J. Suzuki, "Factorization of the finite temperature correlation functions of the XXZ chain in a magnetic field," *J. Phys. A* **40** (2007) 10699, https://doi.org/10.1088/1751-8113/40/35/001.

[111] A. Feiguin, S. Trebst, A. W. W. Ludwig, M. Troyer, A. Kitaev, Z. Wang, and M. H. Freedman, "Interacting anyons in topological quantum liquids: The golden chain," *Physical Review Letters* **98** no. 16, (Apr, 2007) , https://doi.org/10.1103/physrevlett.98.160409.

[112] K. Fukai, R. Kleinemühl, B. Pozsgay, and E. Vernier, "On correlation functions in models related to the Temperley-Lieb algebra," *SciPost Physics* **16** no. 1, (Jan., 2024) , https://doi.org/10.21468/scipostphys.16.1.003.

[113] M. Schulz, S. R. Taylor, C. A. Hooley, and A. Scardicchio, "Energy transport in a disordered spin chain with broken U(1) symmetry: Diffusion, subdiffusion, and many-body localization," *Phys. Rev. B* **98** (Nov, 2018) 180201, https://doi.org/10.1103/PhysRevB.98.180201.

[114] J. D. Nardis, B. Doyon, M. Medenjak, and M. Panfil, "Correlation functions and transport coefficients in generalised hydrodynamics," *Journal of Statistical Mechanics: Theory and Experiment* **2022** no. 1, (Jan, 2022) 014002, https://doi.org/10.1088/1742-5468/ac3658.

[115] L. Tonks, "The complete equation of state of one, two and three-dimensional gases of hard elastic spheres," *Phys. Rev.* **50** (Nov, 1936) 955–963, https://doi.org/10.1103/PhysRev.50.955.

[116] T. Nagamiya, "Statistical mechanics of one-dimensional substances I," *Proceedings of the Physico-Mathematical Society of Japan. 3rd Series* **22** no. 8-9, (1940) 705–720, https://doi.org/10.11429/ppmsj1919.22.8-9_705.

[117] C. Boldrighini, R. L. Dobrushin, and Y. M. Sukhov, "One-dimensional hard rod caricature of hydrodynamics," *J. Stat. Phys.* **31** no. 3, (1983) 577–616, https://doi.org/10.1007/BF01019499.

[118] C. Boldrighini and Y. M. Suhov, "One-Dimensional Hard-Rod Caricature of Hydrodynamics: "Navier-Stokes Correction" for Local Equilibrium Initial States," *Comm. Math. Phys.* **189** no. 2, (1997) 577–590, https://doi.org/10.1007/s002200050218.

[119] B. Doyon and H. Spohn, "Dynamics of hard rods with initial domain wall state," *Journal of Statistical Mechanics: Theory and Experiment* **2017** no. 7, (Jul, 2017) 073210, https://doi.org/10.1088/1742-5468/aa7abf.

[120] R. J. Rubin, "Quantum-mechanical properties of a one-dimensional system composed of hard spheres," *J. Chem. Phys.* **23** no. 7, (1955) 1183–1186, https://doi.org/10.1063/1.1742236.

[121] J. Cardy and B. Doyon, "$T\overline{T}$ deformations and the width of fundamental particles," *Journal of High Energy Physics* **2022** no. 4, (Apr, 2022) , https://doi.org/10.1007/jhep04(2022)136.

[122] Y. Jiang, "$T\overline{T}$-deformed 1d Bose gas," *SciPost Physics* **12** no. 6, (Jun, 2022) , https://doi.org/10.21468/scipostphys.12.6.191.

[123] N. M. Bogoliubov and R. K. Bullough, "A q-deformed completely integrable Bose gas model," *J. Phys. A* **25** no. 14, (1992) 4057, https://doi.org/10.1088/0305-4470/25/14/020.

[124] N. M. Bogoliubov and R. K. Bullough, "Completely integrable model of interacting q-bosons," *Phys. Lett. A* **168** (1992) 264–269, https://doi.org/10.1016/0375-9601(92)91129-F.

[125] N. M. Bogoliubov, R. K. Bullough, and G. D. Pang, "Exact solution of a q-boson hopping model," *Phys. Rev. B* **47** (1993) 11495–11498, https://doi.org/10.1103/PhysRevB.47.11495.

[126] N. Bogoliubov, A. Izergin, and N. Kitanine, "Correlation functions for a strongly correlated boson system," *Nucl. Phys. B* **516** no. 3, (1998) 501 – 528, https://doi.org/http://dx.doi.org/10.1016/S0550-3213(98)00038-8.

[127] K. Shigechi and M. Uchiyama, "Boxed skew plane partition and integrable phase model," *J. Phys. A* **38** (2005) 10287–10306, https://doi.org/10.1088/0305-4470/38/48/003.

[128] N. M. Bogoliubov, "Boxed plane partitions as an exactly solvable boson model," *J. Phys. A* **38** no. 43, (2005) 9415, https://doi.org/10.1088/0305-4470/38/43/002.

[129] N. Bogoliubov, "Enumeration of plane partitions and the algebraic bethe anzatz," *Theoretical and Mathematical Physics* **150** no. 2, (2007) 165–174, https://doi.org/10.1007/s11232-007-0012-5.

[130] N. Bogoliubov and J. Timonen, "Correlation functions for a strongly coupled boson system and plane partitions," *Royal Society of London Philosophical Transactions Series A* **369** (2011) 1319–1333, https://doi.org/10.1098/rsta.2010.0322.

[131] B. Pozsgay, "Quantum quenches and generalized Gibbs ensemble in a Bethe Ansatz solvable lattice model of interacting bosons," *J. Stat. Mech.* **10** (2014) 45, https://doi.org/10.1088/1742-5468/2014/10/P10045.

[132] B. Bertini, P. Kos, and T. Prosen, "Exact correlation functions for dual-unitary lattice models in $1+1$ dimensions," *Phys. Rev. Lett.* **123** (Nov, 2019) 210601, https://doi.org/10.1103/PhysRevLett.123.210601.

[133] L. Piroli, B. Bertini, J. I. Cirac, and T. Prosen, "Exact dynamics in dual-unitary quantum circuits," *Phys. Rev. B* **101** (Mar, 2020) 094304, https://doi.org/10.1103/PhysRevB.101.094304.

[134] A. Bobenko, M. Bordemann, C. Gunn, and U. Pinkall, "On two integrable cellular automata," *Comm. Math. Phys.* **158** no. 1, (1993) 127 – 134, https://doi.org/10.1007/BF02097234.

[135] B. Buča, K. Klobas, and T. Prosen, "Rule 54: exactly solvable model of nonequilibrium statistical mechanics," *Journal of Statistical Mechanics: Theory and Experiment* **2021** no. 7, (Jul, 2021) 074001, https://doi.org/10.1088/1742-5468/ac096b.

[136] K. Klobas and B. Bertini, "Exact relaxation to Gibbs and non-equilibrium steady states in the quantum cellular automaton Rule 54," *SciPost Physics* **11** no. 6, (Dec, 2021) , https://doi.org/10.21468/scipostphys.11.6.106.

[137] M. Fagotti, "On conservation laws, relaxation and pre-relaxation after a quantum quench," *Journal of Statistical Mechanics: Theory and Experiment* **2014** no. 3, (Mar, 2014) P03016, https://doi.org/10.1088/1742-5468/2014/03/p03016.

[138] Z.-C. Yang, F. Liu, A. V. Gorshkov, and T. Iadecola, "Hilbert-Space Fragmentation from Strict Confinement," *Physical Review Letters* **124** no. 20, (May, 2020) , https://doi.org/10.1103/physrevlett.124.207602.

[139] L. Zadnik and M. Fagotti, "The folded spin-1/2 XXZ model: I. diagonalisation, jamming, and ground state properties," *SciPost Physics Core* **4** no. 2, (Apr, 2021) , https://doi.org/10.21468/scipostphyscore.4.2.010.

[140] L. Zadnik, K. Bidzhiev, and M. Fagotti, "The folded spin-1/2 XXZ model: II. thermodynamics and hydrodynamics with a minimal set of charges," *SciPost Physics* **10** no. 5, (May, 2021) , https://doi.org/10.21468/scipostphys.10.5.099.

[141] B. Pozsgay, T. Gombor, A. Hutsalyuk, Y. Jiang, L. Pristyák, and E. Vernier, "Integrable spin chain with Hilbert space fragmentation and solvable real-time dynamics," *Physical Review E* **104** no. 4, (Oct, 2021) , https://doi.org/10.1103/physreve.104.044106.

[142] P. P. Kulish, "Factorization of the classical and the quantum S matrix and conservation laws," *Theor Math Phys* **26** (1976) 132, https://doi.org/10.1007/BF01079418.

[143] Y. Nozawa and K. Fukai, "Explicit construction of local conserved quantities in the XYZ Spin-1/2 chain," *Physical Review Letters* **125** no. 9, (Aug, 2020) , https://doi.org/10.1103/physrevlett.125.090602.

[144] B. Nienhuis and O. Huijgen, "The local conserved quantities of the closed XXZ chain," *Journal of Physics A: Mathematical and Theoretical* (Jun, 2021) , https://doi.org/10.1088/1751-8121/ac0961.

[145] T. Gombor and B. Pozsgay, "Integrable spin chains and cellular automata with medium-range interaction," *Physical Review E* **104** no. 5, (Nov, 2021) , https://doi.org/10.1103/physreve.104.054123.

[146] F. C. Alcaraz and R. Z. Bariev, "An Exactly Solvable Constrained XXZ Chain," *arXiv e-prints* (1999) , arXiv:cond-mat/9904042 [cond-mat.stat-mech].

[147] L. Zadnik and M. Fagotti, "The Folded Spin-1/2 XXZ Model: I. Diagonalisation, Jamming, and Ground State Properties," *SciPost Phys. Core* **4** (2021) 10, https://doi.org/10.21468/SciPostPhysCore.4.2.010.

[148] N. Abarenkova and A. Pronko, "Temperature correlation function in the absolutely anisotropic XXZ Heisenberg magnet," *Theor. Math. Phys.* **131** (2002) 690–703, https://doi.org/10.1023/A:1015480916713.

[149] N. M. Bogoliubov and C. L. Malyshev, "Ising limit of a Heisenberg XXZ magnet and some temperature correlation functions," *Theoretical and Mathematical Physics* **169** no. 2, (Nov., 2011) 1517–1529, https://doi.org/10.1007/s11232-011-0129-4.

[150] N. M. Bogolyubov and C. L. Malyshev, "Integrable models and combinatorics," *Russ. Math. Surv.* **70** no. 5, (2015) 789–856, https://doi.org/10.1070/RM2015v070n05ABEH004964.

[151] B. Pozsgay, T. Gombor, and A. Hutsalyuk, "Integrable hard rod deformation of the Heisenberg spin chains," *Phys. Rev. E* **104** no. 6, (2021) , https://doi.org/10.1103/physreve.104.064124.

[152] M. Borsi, L. Pristyák, and B. Pozsgay, "Matrix product symmetries and breakdown of thermalization from hard rod deformations," *Physical Review Letters* **131** no. 3, (Jul, 2023) , https://doi.org/10.1103/physrevlett.131.037101.

[153] G. I. Menon, M. Barma, and D. Dhar, "Conservation laws and integrability of a one-dimensional model of diffusing dimers," *Journal of Statistical Physics* **86** no. 5-6, (Mar, 1997) 1237–1263, https://doi.org/10.1007/bf02183622.

[154] Z. Maassarani and P. Mathieu, "The su(n) XX model," *Nuclear Physics B* **517** no. 1-3, (Apr, 1998) 395–408, https://doi.org/10.1016/s0550-3213(98)80004-7.

[155] Z. Maassarani, "The XXC models," *Physics Letters A* **244** no. 1-3, (Jul, 1998) 160–164, https://doi.org/10.1016/s0375-9601(98)00322-3.

[156] G. M. Crosswhite and D. Bacon, "Finite automata for caching in matrix product algorithms," *Physical Review A* **78** no. 1, (Jul, 2008) , https://doi.org/10.1103/physreva.78.012356.

[157] G. Vidal, "Efficient classical simulation of slightly entangled quantum computations," *Phys. Rev. Lett.* **91** (Oct, 2003) 147902, https://doi.org/10.1103/PhysRevLett.91.147902.

[158] G. Vidal, "Classical simulation of infinite-size quantum lattice systems in one spatial dimension," *Phys. Rev. Lett.* **98** (Feb, 2007) 070201, https://doi.org/10.1103/PhysRevLett.98.070201.

[159] F. Pollmann, "Efficient numerical simulations using matrix-product states," https://www.ggi.infn.it/sft/SFT_2016/LectureNotes/Pollmann.pdf.

[160] O. I. Pâţu, V. E. Korepin, and D. V. Averin, "Correlation functions of one-dimensional Lieb–Liniger anyons," *Journal of Physics A: Mathematical and Theoretical* **40** no. 50, (Nov., 2007) 14963–14984, https://doi.org/10.1088/1751-8113/40/50/004.

[161] Y. Hao, Y. Zhang, and S. Chen, "Ground-state properties of hard-core anyons in one-dimensional optical lattices," *Physical Review A* **79** no. 4, (Apr., 2009) , https://doi.org/10.1103/physreva.79.043633.

[162] T. M. Wright, M. Rigol, M. J. Davis, and K. V. Kheruntsyan, "Nonequilibrium dynamics of one-dimensional hard-core anyons following a quench: Complete relaxation of one-body observables," *Physical Review Letters* **113** no. 5, (July, 2014) , https://doi.org/10.1103/physrevlett.113.050601.

[163] P. Fendley, "Free parafermions," *Journal of Physics A: Mathematical and Theoretical* **47** no. 7, (Jan., 2014) 075001, https://doi.org/10.1088/1751-8113/47/7/075001.

[164] D. Rossini, M. Carrega, M. Calvanese Strinati, and L. Mazza, "Anyonic tight-binding models of parafermions and of fractionalized fermions," *Physical Review B* **99** no. 8, (Feb., 2019) , https://doi.org/10.1103/physrevb.99.085113.

[165] A. S. Mastiukova, D. V. Kurlov, V. Gritsev, and A. K. Fedorov, "Free Fock parafermions in the tight-binding model with dissipation," 2022. https://arxiv.org/abs/2203.03554.

[166] B. Pozsgay, A. Hutsalyuk, L. Pristyák, and G. Takács, "Sublattice entanglement in an exactly solvable anyonlike spin ladder," *Phys. Rev. E* **106** (Oct, 2022) 044120, https://doi.org/10.1103/PhysRevE.106.044120.

[167] M. Suzuki, "Relationship among Exactly Soluble Models of Critical Phenomena. I*): 2D Ising Model, Dimer Problem and the Generalized XY-Model," *Progr. Theor. Phys.* **46** no. 5, (1971) 1337–1359, https://doi.org/10.1143/PTP.46.1337.

[168] I. Titvinidze and G. I. Japaridze, "Phase diagram of the spin-1/2 extended XY model," *Eu. Phys. J. B* **32** no. 3, (2003) 383–393, https://doi.org/10.1140/epjb/e2003-00113-8.

[169] R. Z. Bariev, "Integrable spin chain with two- and three-particle interactions," *J. Phys. A* **24** no. 10, (1991) L549–L553, https://doi.org/10.1088/0305-4470/24/10/010.

[170] P. Fendley and K. Schoutens, "Cooper pairs and exclusion statistics from coupled free-fermion chains," *Journal of Statistical Mechanics: Theory and Experiment* **2007** no. 02, (Feb, 2007) P02017–P02017, https://doi.org/10.1088/1742-5468/2007/02/p02017.

[171] S. Santra, A. Agarwala, and S. Bhattacharjee, "Statistics-tuned entanglement of the boundary modes in coupled Su-Schrieffer-Heeger chains," *Physical Review B* **103** no. 19, (May, 2021) , https://doi.org/10.1103/physrevb.103.195134.

[172] M. Grabowski and P. Mathieu, "Structure of the conservation laws in quantum integrable spin chains with short range interactions," *Annals of Physics* **243** no. 2, (Nov, 1995) 299–371, https://doi.org/10.1006/aphy.1995.1101.

[173] M. Vanicat, L. Zadnik, and T. Prosen, "Integrable Trotterization: Local Conservation Laws and Boundary Driving," *Physical Review Letters* **121** no. 3, (Jul, 2018) , https://doi.org/10.1103/physrevlett.121.030606.

[174] G. Giudice, G. Giudici, M. Sonner, J. Thoenniss, A. Lerose, D. A. Abanin, and L. Piroli, "Temporal entanglement, quasiparticles, and the role of interactions," *Physical Review Letters* **128** no. 22, (Jun, 2022) , https://doi.org/10.1103/physrevlett.128.220401.

[175] E. Lieb, T. Schultz, and D. Mattis, "Two soluble models of an antiferromagnetic chain," *Annals of Physics* **16** no. 3, (1961) 407–466, https://doi.org/https://doi.org/10.1016/0003-4916(61)90115-4.

[176] V. Ohanyan, "Introduction to quantum spin chains," *Lecture Notes* , http://training.hepi.tsu.ge/rtn/activities/sources/Ohanyan.pdf.

[177] P. Fendley, "Free fermions in disguise," *Journal of Physics A: Mathematical and Theoretical* **52** no. 33, (Jul, 2019) 335002, https://doi.org/10.1088/1751-8121/ab305d.

[178] S. J. Elman, A. Chapman, and S. T. Flammia, "Free fermions behind the disguise," *Communications in Mathematical Physics* **388** no. 2, (Oct, 2021) 969–1003, https://doi.org/10.1007/s00220-021-04220-w.

[179] F. Iglói and I. Peschel, "On reduced density matrices for disjoint subsystems," *EPL (Europhysics Letters)* **89** no. 4, (Feb, 2010) 40001, https://doi.org/10.1209/0295-5075/89/40001.

[180] R. I. Nepomechie, "Bethe ansatz on a quantum computer?," *Quantum Information and Computation* **21** no. 3-4, (Mar, 2021) , https://doi.org/https://doi.org/10.26421/QIC21.3-4-4.

[181] J. S. V. Dyke, G. S. Barron, N. J. Mayhall, E. Barnes, and S. E. Economou, "Preparing Bethe Ansatz Eigenstates on a Quantum Computer," *PRX Quantum* **2** no. 4, (Nov, 2021) , https://doi.org/10.1103/prxquantum.2.040329.

[182] W. Li, M. Okyay, and R. I. Nepomechie, "Bethe states on a quantum computer: success probability and correlation functions," *Journal of Physics A: Mathematical and Theoretical* **55** no. 35, (Aug, 2022) 355305, https://doi.org/10.1088/1751-8121/ac8255.

[183] A. Sopena, M. H. Gordon, D. García-Martín, G. Sierra, and E. López, "Algebraic Bethe Circuits," *Quantum* **6** (Sep, 2022) 796, https://doi.org/10.22331/q-2022-09-08-796.

[184] M. G. Tetelman, "Lorentz group for two-dimensional integrable lattice systems," *Sov. Phys. JETP* **1981** (55) 306–310.

[185] K. Sogo and M. Wadati, "Boost Operator and Its Application to Quantum Gelfand-Levitan Equation for Heisenberg-Ising Chain with Spin One-Half," *Progress of Theoretical Physics* **69** no. 2, (1983) 431–450, https://doi.org/10.1143/PTP.69.431.

[186] K. Fabricius and B. McCoy, "Bethe's Equation is Incomplete for the XXZ Model at Roots of Unity," *Journal of Statistical Physics* **103** no. 5-6, (2001) 647–678, https://doi.org/10.1023/A:1010380116927.

[187] W. Hao, R. I. Nepomechie, and A. J. Sommese, "Completeness of solutions of Bethe's equations," *Physical Review E* **88** no. 5, (Nov, 2013) , https://doi.org/10.1103/physreve.88.052113.

[188] *Table of integrals, series, and products*, I. S. Gradshteyn and I. M. Ryzhik. Elsevier/Academic Press, Amsterdam, seventh ed., 2007. Translated from the Russian, Translation edited and with a preface by Alan Jeffrey and Daniel Zwillinger.

[189] R. Orús, "A practical introduction to tensor networks: Matrix product states and projected entangled pair states," *Annals of Physics* **349** (Oct, 2014) 117–158, https://doi.org/10.1016/j.aop.2014.06.013.

[190] D. N. Page, "Average entropy of a subsystem," *Physical Review Letters* **71** no. 9, (Aug, 1993) 1291–1294, https://doi.org/10.1103/physrevlett.71.1291.

[191] J. Eisert, M. Cramer, and M. B. Plenio, "Colloquium: Area laws for the entanglement entropy," *Rev. Mod. Phys.* **82** (Feb, 2010) 277–306, https://doi.org/10.1103/RevModPhys.82.277.

[192] M. B. Hastings, "An area law for one-dimensional quantum systems," *Journal of Statistical Mechanics: Theory and Experiment* **2007** no. 08, (Aug, 2007) P08024, https://doi.org/10.1088/1742-5468/2007/08/P08024.

[193] J. Hauschild and F. Pollmann, "Efficient numerical simulations with tensor networks: Tensor network python (TeNPy)," *SciPost Physics Lecture Notes* (Oct, 2018) , https://doi.org/10.21468/scipostphyslectnotes.5.

[194] U. Schollwöck, "The density-matrix renormalization group in the age of matrix product states," *Annals of Physics* **326** no. 1, (Jan, 2011) 96–192, https://doi.org/10.1016/j.aop.2010.09.012.

[195] S. Singh, R. N. C. Pfeifer, and G. Vidal, "Tensor network decompositions in the presence of a global symmetry," *Phys. Rev. A* **82** (Nov, 2010) 050301, https://doi.org/10.1103/PhysRevA.82.050301.

[196] S. Singh, R. N. C. Pfeifer, and G. Vidal, "Tensor network states and algorithms in the presence of a global U(1) symmetry," *Phys. Rev. B* **83** (Mar, 2011) 115125, https://doi.org/10.1103/PhysRevB.83.115125.

Appendix A

Commutation relations of the monodromy matrix elements

For the sake of completeness, here we present the commutation relations between the elements of the monodromy matrix for the XXZ model. The commutation relations are contained within the expression (3.36) and the R-matrix has the form (3.42). Their explicit forms read as:

$$
\begin{aligned}
A(u)B(v) &= f(v,u)B(v)A(u) + g(u,v)B(u)A(v),\\
B(u)A(v) &= f(v,u)A(v)B(u) + g(u,v)A(u)B(v),\\
D(v)B(u) &= f(v,u)B(u)D(v) + g(u,v)B(v)D(u),\\
B(v)D(u) &= f(v,u)D(u)B(v) + g(u,v)D(v)B(u),\\
A(v)C(u) &= f(v,u)C(u)A(v) + g(u,v)C(v)A(u),\\
C(v)A(u) &= f(v,u)A(u)C(v) + g(u,v)C(u)A(v),\\
D(u)C(v) &= f(v,u)C(v)D(u) + g(u,v)C(u)D(v),\\
C(u)D(v) &= f(v,u)D(v)C(u) + g(u,v)D(u)C(v),\\
[A(v),D(u)] &= g(v,u)\{C(u)B(v) - C(v)B(u)\},\\
[D(v),A(u)] &= g(v,u)\{B(u)C(v) - B(v)C(u)\},\\
[B(v),C(u)] &= g(v,u)\{D(u)A(v) - D(v)A(u)\},\\
[C(v),B(u)] &= g(v,u)\{A(u)D(v) - A(v)D(u)\},\\
[A(v),A(u)] &= [B(v),B(u)] = [C(v),C(u)] = [D(v),D(u)] = 0,
\end{aligned}
\tag{A.1}
$$

where the functions $f(u,v)$ and $g(u,v)$ are defined in (3.54).

Appendix B

Explicit form of the charge and current operators

Here we present the explicit form of the first few charge and current operators in the XXZ and XYZ models. The set of local conserved charges is encoded by the transfer matrix. However, a practically more convenient way of explicitly calculating these charge operators is provided by the boost operator $\mathcal{B}$, which is defined on an infinite chain by the formal expression [184, 185]

$$\mathcal{B} = \sum_{j=-\infty}^{\infty} j h_{j,j+1}, \tag{B.1}$$

where $h_{j,j+1}$ is the Hamiltonian density. With the help of $\mathcal{B}$, the charge operators can be obtained recursively:

$$\hat{Q}_{\alpha+1} = i\big[\mathcal{B}, \hat{Q}_{\alpha}\big] + \text{const.} \tag{B.2}$$

The constant term on the r.h.s. of (B.2) is not fixed by the boost operator. In the expressions below, we chose them to match the construction coming from the transfer matrix according to (3.48) or (3.51). First, we consider the more general case of the XYZ model.

B.1 XYZ model

It is convenient to introduce the vectors $\underline{\sigma}_j$, $\underline{\hat{\sigma}}_j$ and $\underline{\tilde{\sigma}}_j$ with elements given by

$$\big(\underline{\sigma}_j\big)_a = \sigma_j^a, \qquad \big(\underline{\hat{\sigma}}_j\big)_a = \sqrt{J_a}\,\sigma_j^a, \qquad \big(\underline{\tilde{\sigma}}_j\big)_a = \sqrt{\frac{J_x J_y J_z}{J_a}}\,\sigma_j^a, \tag{B.3}$$

where σ_j^a $(a = x,y,z)$ is the appropriate Pauli matrix at site j and the J_a's are the coefficients in the Hamiltonian (3.10). Using this notation, the first three higher charge densities can be written as [143]:

$$\begin{aligned}
\hat{q}_3(j) &= -\frac{1}{2}\Big(\underline{\hat{\sigma}}_j \times \underline{\tilde{\sigma}}_{j+1}\Big)\cdot\underline{\hat{\sigma}}_{j+2},\\
\hat{q}_4(j) &= \big(\big(\underline{\hat{\sigma}}_j \times \underline{\tilde{\sigma}}_{j+1}\big)\times\underline{\tilde{\sigma}}_{j+2}\big)\cdot\underline{\hat{\sigma}}_{j+3} + J_xJ_yJ_z\underline{\sigma}_j\cdot\underline{\sigma}_{j+2} + \sum_{a=x,y,z} J_a^2\hat{\sigma}_j^a\hat{\sigma}_{j+1}^a -\\
&\quad -2\big(J_x^2+J_y^2+J_z^2\big)h_{j,j+1} + C_4,\\
\hat{q}_5(j) &= -3\Bigg\{\Big[\Big(\big(\underline{\hat{\sigma}}_j\times\underline{\tilde{\sigma}}_{j+1}\big)\times\underline{\tilde{\sigma}}_{j+2}\Big)\times\underline{\tilde{\sigma}}_{j+3}\Big]\cdot\underline{\hat{\sigma}}_{j+4} + \sum_{a,b,c}\frac{J_xJ_yJ_z}{J_a}\varepsilon_{abc}\big(\hat{\sigma}_j^a\tilde{\sigma}_{j+2}^b\hat{\sigma}_{j+3}^c +\\
&\quad +\hat{\sigma}_j^b\tilde{\sigma}_{j+1}^c\hat{\sigma}_{j+3}^a\big) - \sum_{a,b,c}\varepsilon_{abc}J_b^2\hat{\sigma}_j^a\tilde{\sigma}_{j+1}^b\hat{\sigma}_{j+2}^c\Bigg\} - 4\big(J_x^2+J_y^2+J_z^2\big)\hat{q}_3(j).
\end{aligned} \tag{B.4}$$

Here $\cdot$ and $\times$ denote the usual scalar and vector products, respectively, while ε_{abc} is the Levi-Civita symbol. The constant C_4 is defined as:

$$C_4 = \frac{1}{2}\,\frac{d^3}{du^3}\Big(\log h(u+\eta)\Big)\Big|_{u=0}. \tag{B.5}$$

The current and generalized current operators describing the flows of the charges are defined through the continuity equations (4.1) and (4.3), respectively. The first few of these current operators are given by:

$$\begin{aligned}
\hat{J}_2(j) &= \frac{1}{2}\Big(\underline{\hat{\sigma}}_{j-1}\times\underline{\tilde{\sigma}}_j\Big)\cdot\underline{\hat{\sigma}}_{j+1},\\
\hat{J}_3(j) &= -\frac{1}{2}\big(\big(\underline{\hat{\sigma}}_{j-1}\times\underline{\tilde{\sigma}}_j\big)\times\underline{\tilde{\sigma}}_{j+1}\big)\cdot\underline{\hat{\sigma}}_{j+2} + \frac{1}{2}\left(\sum_{a=x,y,z}J_a^2\hat{\sigma}_j^a\hat{\sigma}_{j+1}^a - 2\big(J_x^2+J_y^2+J_z^2\big)h_{j,j+1}\right),\\
\hat{J}_2^3(j) &= -\frac{1}{2}\Bigg\{\big(\big(\underline{\hat{\sigma}}_{j-2}\times\underline{\tilde{\sigma}}_{j-1}\big)\times\underline{\tilde{\sigma}}_j\big)\cdot\underline{\hat{\sigma}}_{j+1} + \big(\big(\underline{\hat{\sigma}}_{j-1}\times\underline{\tilde{\sigma}}_j\big)\times\underline{\tilde{\sigma}}_{j+1}\big)\cdot\underline{\hat{\sigma}}_{j+2} +\\
&\quad + \sum_{a=x,y,z}J_a^2\big(\hat{\sigma}_{j-1}^a\hat{\sigma}_j^a + \hat{\sigma}_j^a\hat{\sigma}_{j+1}^a\big) - 2\big(J_x^2+J_y^2+J_z^2\big)\big(h_{j-1,j}+h_{j,j+1}\big) + 2J_xJ_yJ_z\underline{\sigma}_{j-1}\cdot\underline{\sigma}_{j+1}\Bigg\}.
\end{aligned} \tag{B.6}$$

From (B.4) and (B.6) it can be seen that $\hat{J}_2(j) = -\hat{q}_3(j-1)$.

B.2 XXZ model

Obviously, the charges and currents of the XXZ model can be recovered from (B.4) and (B.6) by substituting in $J_x = J_y = 1$ and $J_z = \Delta$. However, for the sake of completeness, and because our conventions for the XXZ

and XYZ models slightly differ, here we also list them separately:

$$
\begin{aligned}
\hat{q}_3(j) &= \frac{1}{2(\Delta^2-1)}\Big(\underline{\hat{\sigma}}_j \times \underline{\tilde{\sigma}}_{j+1}\Big)\cdot \underline{\hat{\sigma}}_{j+2},\\
\hat{q}_4(j) &= \frac{1}{(\Delta^2-1)^{3/2}}\Big[\Delta\left(\underline{\sigma}_j\cdot\underline{\sigma}_{j+2}-\underline{\tilde{\sigma}}_j\cdot\underline{\tilde{\sigma}}_{j+1}\right)+\left(\left(\underline{\hat{\sigma}}_j\times\underline{\tilde{\sigma}}_{j+1}\right)\times\underline{\tilde{\sigma}}_{j+2}\right)\cdot\underline{\hat{\sigma}}_{j+3}-h_{j,j+1}\Big],\\
\hat{q}_5(j) &= \frac{1}{(\Delta^2-1)^2}\Bigg\{3\left[\left(\left(\underline{\hat{\sigma}}_j\times\underline{\tilde{\sigma}}_{j+1}\right)\times\underline{\tilde{\sigma}}_{j+2}\right)\times\underline{\tilde{\sigma}}_{j+3}\right]\cdot\underline{\hat{\sigma}}_{j+4}+3\sum_{a,b,c}\left(\delta_{az}(1-\Delta)+\Delta\right)\varepsilon_{abc}\\
&\quad\left(\hat{\sigma}^a_j\tilde{\sigma}^b_{j+2}\hat{\sigma}^c_{j+3}+\hat{\sigma}^b_j\tilde{\sigma}^c_{j+1}\hat{\sigma}^a_{j+3}\right)-3\sum_{a,b,c}\left(1+\delta_{bz}(\Delta-1)\right)^2\varepsilon_{abc}\hat{\sigma}^a_j\tilde{\sigma}^b_{j+1}\hat{\sigma}^c_{j+2}+\\
&\quad+2\Delta\left(7-5\Delta^2+2\Delta^4\right)\hat{q}_3(j)\Bigg\},
\end{aligned}
\tag{B.7}
$$

where the vectors $\underline{\hat{\sigma}}_j$, $\underline{\tilde{\sigma}}_j$ and $\underline{\sigma}_j$ are still defined as in (B.3), but with the special choice $J_x = J_y = 1$ and $J_z = \Delta$. The current operators are given by:

$$
\begin{aligned}
\hat{J}_2(j) &= \frac{1}{\sqrt{\Delta^2-1}}\Big(\underline{\hat{\sigma}}_{j-1}\times\underline{\tilde{\sigma}}_j\Big)\cdot\underline{\hat{\sigma}}_{j+1},\\
\hat{J}_3(j) &= -\frac{1}{\Delta^2-1}\left\{\left(\left(\underline{\hat{\sigma}}_{j-1}\times\underline{\tilde{\sigma}}_j\right)\times\underline{\tilde{\sigma}}_{j+1}\right)\cdot\underline{\hat{\sigma}}_{j+2}+\left(\sum_{a=x,y,z}J_a^2\hat{\sigma}^a_j\hat{\sigma}^a_{j+1}-2\left(2+\Delta^2\right)h_{j,j+1}\right)+2\Delta\cdot\mathbb{1}\right\},\\
\hat{J}^3_2(j) &= -\frac{1}{2(\Delta^2-1)^{3/2}}\Bigg\{\left(\left(\underline{\hat{\sigma}}_{j-2}\times\underline{\tilde{\sigma}}_{j-1}\right)\times\underline{\tilde{\sigma}}_j\right)\cdot\underline{\hat{\sigma}}_{j+1}+\left(\left(\underline{\hat{\sigma}}_{j-1}\times\underline{\tilde{\sigma}}_j\right)\times\underline{\tilde{\sigma}}_{j+1}\right)\cdot\underline{\hat{\sigma}}_{j+2}+\\
&+\sum_{a=x,y,z}J_a^2\left(\hat{\sigma}^a_{j-1}\hat{\sigma}^a_j+\hat{\sigma}^a_j\hat{\sigma}^a_{j+1}\right)-2\left(2+\Delta^2\right)\left(h_{j-1,j}+h_{j,j+1}\right)+2\Delta\underline{\sigma}_{j-1}\cdot\underline{\sigma}_{j+1}+2\Delta\cdot\mathbb{1}\Bigg\}.
\end{aligned}
\tag{B.8}
$$

Appendix C

Numerical validation of the current mean value formulae

In order to numerically verify our mean value formulae, we compared expectation values obtained from exact diagonalization to the predictions of (4.4), (4.5) and (5.1). Here, we present these numerical results both for the XXZ and XYZ spin chains, for several different volumes and parameters of the models.

C.1 XXZ model

The first few charge and (generalized) current operators of the XXZ model are presented in Appendix B. To obtain their mean values by exact diagonalization, one needs to calculate numerically the exact eigenstates of the XXZ Hamiltonian (3.5). However, the direct diagonlization of H alone is not the most convenient, because of the large number of degeneracies present in the energy spectrum. Therefore, we numerically constructed in a finite volume L the first 5 charges of the XXZ model, and diagonalized their sum. (Equivalently, one can lift the degeneracies by constructing the transfer matrix of the model at a few random values of the spectral parameter, and diagonalizing the sum of these operators, instead of the Hamiltonian.)

To evaluate the formulae (4.4) and (4.5), one needs to find the Bethe roots describing the eigenstates of the model. The Bethe equations (3.28) can be solved by using some standard iterative numerical method, for example Newton's method. (To do this, it is actually more convenient to consider the logarithmic form of the Bethe equations (3.29).)

Here, we use a more elegant way of finding the Bethe roots that does not require the selection of some appropriate initial values, like the aforementioned iterative techniques, and that can yield all eigenstates of the model. This method was originally developed in [186] and is based on Baxter's famous $T-Q$ relation, which he used to diagonalize the transfer matrix of the six-vertex model [11]. Without details, we present here the relevant statements of Baxter's construction in order to lay the foundation for the numerical method. (Detailed derivations can be found in [11], while [58] contains a shorter, but more pedagogical discussion.)

Starting from the existence of commuting transfer matrices, it can be shown that there exists a matrix

$Q(u)$[1] that commutes with the transfer matrix and with itself for different values of the spectral parameter. Moreover, the matrix $Q(u)$ satisfies a functional matrix equation together with the transfer matrix $t(u)$, called the $T-Q$ relation. This equation holds on the level of the eigenvalues $q(u)$ and $\Lambda(u)$ as well, and reads as:

$$\phi(u+i\eta)\Lambda(u)q(u+i\eta/2) = \phi(u+i\eta)q(u-i\eta/2)+\phi(u)q(u+3i\eta/2), \tag{C.1}$$

with $\phi(u)=\sin^L(u)$, and where the eigenvalues of $Q(u)$ can be written as $q(u)=\prod_{j=1}^{N}\sin(u-\lambda_j)$, with the λ_j's being the Bethe roots and N is the particle number. (Since $Q(u)$ commutes with the transfer matrix, they share the same eigenvectors, therefore for each eigenvalue of $Q(u)$ corresponds a well-defined particle number N.) We note that the $T-Q$ relation is usually written in a slightly different form

$$\tilde{\Lambda}(\tilde{u})\tilde{q}(\tilde{u}) = \tilde{\phi}(\tilde{u}+\tilde{\eta})\tilde{q}(\tilde{u}-2\tilde{\eta})+\tilde{\phi}(\tilde{u}-\tilde{\eta})\tilde{q}(\tilde{u}+2\tilde{\eta}), \tag{C.2}$$

where the tildes over the symbols are meant to clarify that these are not the same quantities as in (C.1). The differences of (C.1) compared to (C.2) amount to a shift in the rapidities, a redefinition of the parameter η and a change in the overall normalization of the transfer matrix, and were put forward just to stay consistent with our conventions introduced in the main text.

The $T-Q$ relation is basically equivalent to the Bethe equations: after dividing both sides of (C.1) by $q(u+i\eta/2)$, it appears that the r.h.s. is singular at the points $u=\lambda_j-i\eta/2$. However, it is known that $\Lambda(u)$ is an entire function of the spectral parameter, therefore the l.h.s is regular. To resolve this contradiction, the following consistency relations have to hold:

$$\frac{\phi(\lambda_j+i\eta/2)}{\phi(\lambda_j-i\eta/2)} = -\frac{q(\lambda_j+i\eta)}{q(\lambda_j-i\eta)}, \qquad \text{for} \qquad j=1,\dots,N, \tag{C.3}$$

which are nothing else, but the Bethe equations (3.28).

After this brief theoretical introduction, we can now describe the numerical method used to calculate the Bethe roots:

1. First, we construct the transfer matrix $t(u)$ in a finite volume L, and at a random point u, and calculate its eigenvalues and eigenvectors. Because of the commutativity of the transfer matrices, the eigenvectors do not depend on u.

2. Then, we calculate the transfer matrix eigenvalues at additional points u_k, by constructing $t(u_k)$ and acting on its eigenstates obtained earlier. The number of points u_k in which $\Lambda(u_k)$ has to be known is $N+1$ for an eigenstate with N particles.

[1] This matrix is denoted by Q for historical reasons, however it is important to note that it is different from the charge operators or the charge generating function, defined in the main text.

	λ_1	λ_2	λ_3
1.	0.508 i	0	- 0.508 i
2.	0.2034 i	- 0.2034 i	
3.	1.571	0.1533 i	- 0.1533 i
4.	-0.597	0.597	0
5.	1.571 + 0.5911 i	- 0.04908 i	- 0.5421 i
6.	- 0.1525 i	- 0.9518 i	
7.	0.9879 i	- 0.2253 i	
8.	0		
9.	-1.571 + 0.3284 i	0.2451 i	- 0.5735 i
10.	-0.5973 + 0.2708 i	0.5973 + 0.2708 i	- 0.5415 i
11.	- 0.4147 i		
12.	-1.571	0	
13.	1.571 - 0.642 i	-1.571 + 0.642 i	0
14.	-1.571	0.6199 i	- 0.6199 i
15.	-1.571 + 0.215 i	- 0.2791 i	
16.	1.015 i	- 1.015 i	
17.	0.597	-0.597	
18.	-1.571 - 0.4162 i	1.571 + 0.7059 i	- 0.2898 i
19.	1.571 + 0.6998 i	-0.5976 - 0.3499 i	0.5976 - 0.3499 i
20.	1.571 + 1.254 i		
21.	1.571 + 0.6456 i	1.234 i	
22.	-1.184	1.184	0
23.	1.571	-0.597	0.597
24.	1.571 + 0.2924 i	- 1.055 i	
25.	1.571 - 0.09704 i	-1.571 + 0.7548 i	- 0.6577 i
26.	1.571		
27.	-1.571 - 0.3468 i	1.571 + 0.3468 i	
28.	1.571 - 0.7959 i	1.571	1.571 + 0.7959 i

Table C.1: Bethe roots in the XXZ model for $\Delta = 1/e$ and $L = 6$. For brevity, whenever two degenerate states are connected by space or spin reflection, we only kept one of them.

3. By introducing the variable $x = e^{iu}$, the function $q(u)$ can be written as a polynomial in x:

$$q(x) = \sum_{k=0}^{N} c_k x^{2k-N}, \tag{C.4}$$

where the c_k's are $N+1$ unknown coefficients. However, the $T-Q$ relation (C.1) together with the transfer matrix eigenvalues calculated in the previous point provide $N+1$ algebraic equations which can fix the c_k's and therefore determine the function $q(u)$.

4. From the form of the function $q(u)$, it is obvious that $q(u = \lambda_j) = 0$, therefore finding the zeros of $q(u)$ yields the Bethe roots.

Tables C.1 and C.3 contain the Bethe roots for systems with $L = 6$, $\Delta = 1/e$ and $L = 7$, $\Delta = 2$, respectively, while Tables C.2 and C.4 contain the corresponding charge and current expectation values. We find that the numerical results coming from exact diagonalization and the mean value formulae (4.4), (4.5) agree with high precision (therefore we only display them once, just for the sake of reproducibility). Here we only present numerical data for the XXZ model. The solutions of the Bethe equations for the XXX spin chain, obtained by the method explained above, are presented in [187], and can be used to confirm the predictions of the mean value formulae in that model as well.

	E	$\langle\hat{Q}_3\rangle$	$\langle\hat{Q}_4\rangle$	$\langle\hat{Q}_5\rangle$	$\langle\hat{J}_2\rangle$	$\langle\hat{J}_3\rangle$	$\langle\hat{J}_2^3\rangle$
1.	-11.264	0	9.752	0	0	26.814	9.752
2.	-9.661	0	17.279	0	0	14.396	17.279
3.	-7.652	0	20.575	0	0	7.278	20.575
4.	-6.943	0	20.447	0	0	0	20.447
5.	-6.526	-5.062	13.574	-40.724	9.415	6.674	13.574
6.	-6.223	-3.800	9.476	-63.910	7.068	9.652	9.476
7.	-5.749	-2.003	4.405	-77.430	3.725	13.168	4.405
8.	-5.472	0	18.617	0	0	0	18.617
9.	-4.943	-0.529	-0.899	57.104	0.984	17.150	-0.899
10.	-4.048	-2.581	-2.949	5.591	4.799	12.663	-2.949
11.	-3.472	-3.477	-2.729	-27.971	6.466	12.045	-2.729
12.	-2.943	0	14.641	0	0	0	14.641
13.	-2.479	0	19.898	0	0	-7.370	19.898
14.	-2.070	0	-13.564	0	0	18.400	-13.564
15.	-2.001	-4.256	0.545	-71.577	7.915	6.162	0.545
16.	-1.972	0	-4.979	0	0	9.255	-4.979
17.	-1.472	0	1.830	0	0	0	1.830
18.	-0.943	-3.477	2.729	-53.830	6.466	3.272	2.729
19.	0.111	-1.585	2.282	-12.753	2.948	-3.402	2.282
20.	0.528	-0.529	0.899	1.147	0.984	-1.834	0.899
21.	0.867	-0.456	-0.870	-7.666	0.848	-0.498	-0.870
22.	0.914	0	-1.882	0	0	0.978	-1.882
23.	1.057	0	-2.146	0	0	0	-2.146
24.	1.334	-2.003	-4.405	-4.994	3.725	2.148	-4.405
25.	1.633	-3.110	-7.416	6.737	5.784	4.487	-7.416
26.	2.528	0	-3.976	0	0	0	-3.976
27.	4.275	0	-3.149	0	0	-3.229	-3.149
28.	4.893	0	-1.836	0	0	-5.256	-1.836

Table C.2: Charge and current mean values in the XXZ model for $\Delta = 1/e$ and $L = 6$, corresponding to the eigenstates listed in Table C.1.

	λ_1	λ_2	λ_3
1.	0.6165	-0.2515	0.1193
2.	1.446	0.3559	-0.02927
3.	-0.7611	0.6998	0.1649
4.	1.571	0.3907	-0.3907
5.	0.3085	-0.03205	
6.	0.2474 + 0.6585 i	0.09582	0.2474 - 0.6585 i
7.	0.3457	-0.3457	
8.	-0.9404 - 0.6281 i	-0.9404 + 0.6281 i	0.05295
9.	0.7628	-0.07524	
10.	-0.4062 + 0.6588 i	0.2798	-0.4062 - 0.6588 i
11.	0.7062	0.2207	
12.	0.795 - 0.6407 i	0.795 + 0.6407 i	0.3019
13.	1.514 - 0.7277 i	1.514 + 0.7277 i	0.1589
14.	-1.062 - 0.6138 i	-1.062 + 0.6138 i	0.4153
15.	1.531	0.1447	
16.	0.007529 + 0.6585 i	0.6182	0.007529 - 0.6585 i
17.	-0.8217	0.3979	
18.	1.336 - 0.7323 i	1.336 + 0.7323 i	0.5941
19.	0.8267	-0.5637 + 0.6605 i	-0.5637 - 0.6605 i
20.	1.43	0.4975	
21.	1.389	0.2887 + 0.6584 i	0.2887 - 0.6584 i
22.	0.131		
23.	1.571 - 0.4703 i	1.571	1.571 + 0.4703 i
24.	0.9179	-0.9179	
25.	0.4315		
26.	0.1952 + 0.6585 i	0.1952 - 0.6585 i	
27.	0.6032 + 0.6595 i	0.6032 - 0.6595 i	
28.	0.2181 + 1.318 i	0.2166	0.2181 - 1.318 i
29.	0.6637 + 1.315 i	0.6553	0.6637 - 1.315 i
30.	1.122 - 1.33 i	1.094	1.122 + 1.33 i
31.	-1.571 - 1.361 i	1.571	1.571 + 1.361 i
32.	1.07 - 0.6443 i	1.07 + 0.6443 i	
33.	1.571 - 0.683 i	1.571 + 0.683 i	
34.	-0.8756		
35.	-1.571		

Table C.3: Bethe roots in the XXZ model for $\Delta = 2$ and $L = 7$. For brevity, whenever two degenerate states are connected by space or spin reflection, we only kept one of them.

	E	$\langle\hat{Q}_3\rangle$	$\langle\hat{Q}_4\rangle$	$\langle\hat{Q}_5\rangle$	$\langle\hat{J}_2\rangle$	$\langle\hat{J}_3\rangle$	$\langle\hat{J}_2^3\rangle$
1.	-29.539	-1.252	12.725	-6.465	-4.338	-28.782	12.725
2.	-25.677	-2.721	12.737	23.120	-9.425	-14.317	12.737
3.	-24.094	-2.242	2.089	48.616	-7.768	-29.595	2.089
4.	-22.604	0	-2.520	0	0	-31.977	-2.520
5.	-22.108	-2.416	16.133	30.010	-8.368	-11.549	16.133
6.	-19.625	-1.619	13.416	36.958	-5.609	-1.883	13.416
7.	-19.518	0	1.999	0	0	-26.448	1.999
8.	-18.800	-0.067	12.217	20.539	-0.232	-4.351	12.217
9.	-18.004	-0.796	9.255	-30.458	-2.756	-9.658	9.255
10.	-18.000	-2.285	4.619	41.134	-7.916	-13.333	4.619
11.	-17.464	-4.480	2.912	47.979	-15.520	-14.265	2.912
12.	-17.271	-3.559	1.845	42.484	-12.330	-15.653	1.845
13.	-17.064	-1.992	9.098	46.495	-6.901	-3.165	9.098
14.	-15.783	-2.333	-2.392	26.220	-8.081	-18.688	-2.392
15.	-15.525	-1.884	8.698	44.012	-6.525	-3.770	8.698
16.	-15.178	-2.353	-2.126	2.539	-8.146	-14.752	-2.120
17.	-15.018	-1.319	-4.031	32.163	-4.569	-21.499	-4.031
18.	-13.031	-2.535	-3.969	5.049	-8.780	-12.770	-3.969
19.	-13.017	-1.060	-2.839	-8.543	-3.671	-9.469	-2.839
20.	-12.298	-2.963	-4.362	12.866	-10.263	-12.434	-4.362
21.	-11.882	-0.690	-0.617	0.889	-2.392	-0.743	-0.617
22.	-11.604	-1.678	10.833	41.804	-5.814	-2.913	10.833
23.	-10.904	0	-3.370	0	0	-5.985	-3.370
24.	-10.611	0	-5.880	0	0	-11.512	-5.880
25.	-8.890	-2.889	-1.560	22.987	-10.008	-11.267	-1.560
26.	-7.901	-0.286	1.311	2.036	-0.991	-0.149	1.311
27.	-7.204	-0.568	0.207	3.403	-1.967	-0.168	0.207
28.	-7.195	-0.069	0.383	0.647	-0.240	0.230	0.383
29.	-7.056	-0.178	0.082	1.130	-0.615	-0.237	0.082
30.	-6.787	-0.178	-0.304	0.042	-0.616	-0.494	-0.304
31.	-6.491	0	-0.269	0	0	0.628	-0.269
32.	-6.478	-0.461	-0.871	0.341	-1.596	-1.173	-0.871
33.	-5.872	0	-0.738	0	0	0.626	-0.738
34.	-5.506	1.435	-3.114	4.112	4.971	-4.488	-3.114
35.	-4.000	0	-1.540	0	0	0	-1.540

Table C.4: Charge and current mean values in the XXZ model for $\Delta = 2$ and $L = 7$, corresponding to the eigenstates listed in Table C.3.

C.2 XYZ model

The exact diagonalization works in the same way for the XYZ model as for the XXZ. However, the method used to obtain the Bethe roots breaks down: since in the case of the XYZ model, the Q function is built up from elliptic and not trigonometric/hyperbolic functions, there is no such variable for which a polynomial equation could be written. Because of this, we used Newton's method to obtain the Bethe roots.

Numerical solutions to the Bethe equations for the XYZ model were considered previously in [71], in the framework of the so called Off-Diagonal Bethe Ansatz. However, to the best of our knowledge, in that paper the explicit values of the Bethe roots were only given for a special choice of η, which satisfies the constraint (3.87). Our result works for that special choice as well, but here we consider the general case. Therefore, we solved the Bethe equations (3.83) numerically (with $\theta = 0$), for randomly chosen parameters of the model, and calculated the charge and current mean values according to the generalized Bethe Ansatz solution and our main result. These results agreed with the ones obtained from the exact diagonalization with high numerical precision. It is important to note that the current operators (B.6) are defined by the continuity equation only up to a free constant term. However, the current generating function (5.7) (and consequently our main result) is well-defined. As a result, the current mean values obtained from exact diagonalization may differ by a constant from the ones calculated by (5.1). We disregarded these constant terms, and in the tables below, displayed the results calculated according to (5.1). Unfortunately, solving the Bethe equations numerically for the whole spectrum proved to be a difficult task, and we were only able to obtain the Bethe roots for a subset of the eigenstates of the Hamiltonian. Nevertheless, in the cases found, the current mean values agreed with our main result.

In Tables C.5-C.8, we present the numerical results for chain lengths $L = 4$ and $L = 6$ with different parameters of the Hamiltonian.

	λ_1	λ_2
1.	-0.461 + 2.693 i	-0.461 - 2.693 i
2.	-0.461	1.11
3.	1.11 - 2.597 i	-0.461 + 2.597 i
4.	-0.461 - 2.597 i	1.11 + 2.597 i
5.	0.2075 - 1.479 i	-1.129 + 1.479 i
6.	1.11 + 1.479 i	-0.461 - 1.479 i
7.	1.11 - 2.406 i	1.11 + 2.406 i

Table C.5: Bethe roots in the XYZ model for $\eta = 0.922$, $q = 2.70 \times 10^{-3}$ *and* $L = 4$.

	E	$\langle \hat{Q}_3 \rangle$	$\langle \hat{Q}_4 \rangle$	$\langle \hat{J}_2 \rangle$	$\langle \hat{J}_3 \rangle$	$\langle \hat{J}_2^3 \rangle$
1.	-5.952	0	0	0	7.499	0
2.	-3.034	0	38.224	0	0	-9.556
3.	-1.538	6.277	-9.391	-1.569	2.348	2.348
4.	-1.538	-6.277	-9.391	1.569	2.348	2.348
5.	-0.116	0	0	0	-0.144	0
6.	-0.041	0	-0.661	0	0	0.165
7.	1.456	0	0	0	-0.312	0

Table C.6: Charge and current mean values in the XYZ mdoel for $\eta = 0.922,\ q = 2.70 \times 10^{-3}$ *and* $L = 4$.

	λ_1	λ_2	λ_3
1.	-0.3102 + 0.1242 i	1.261 + 0.2323 i	-0.3102 - 0.3565 i
2.	-0.3102	-1.027 - 1.969 i	0.4069 + 1.969 i
3.	-0.3102 - 1.969 i	-0.3102	1.261 + 1.969 i
4.	1.261 + 0.6368 i	1.261 - 0.6368 i	-0.3102
5.	0.4093 - 2.063 i	-1.03 + 1.875 i	-0.3102 + 0.1875 i
6.	-1.03 - 1.875 i	-0.3102 + 3.75 i	0.4093 - 1.875 i
7.	-3.452 + 4.125 i	-3.452 - 2.06 i	1.261 - 2.065 i
8.	-0.3102 + 2.06 i	1.261 - 1.873 i	-0.3102 - 0.1872 i
9.	-0.3102 - 0.1711 i	1.261 - 0.5394 i	1.261 + 0.7105 i
10.	1.261 + 3.227 i	-0.3102 - 3.767 i	1.261 + 0.5394 i
11.	1.261 - 0.5463 i	-0.6228 + 0.2731 i	0.002408 + 0.2731 i
12.	-0.6228 - 0.2731 i	0.002408 - 0.2731 i	1.261 + 0.5463 i
13.	-0.3102 + 0.6256 i	0.4476 + 1.656 i	-1.068 - 2.282 i
14.	-1.068 - 1.656 i	0.4476 + 2.282 i	-0.3102 - 0.6256 i
15.	-0.3102 - 0.6307 i	-0.3102 - 1.634 i	1.261 + 2.265 i
16.	1.261 + 1.673 i	-0.3102 - 2.304 i	-0.3102 + 0.6307 i
17.	-0.3102 + 0.4694 i	1.261 + 3.133 i	1.261 - 3.603 i
18.	1.261 + 0.8047 i	-0.3102 - 0.4694 i	1.261 - 0.3353 i
19.	0.3602 + 1.969 i	1.261	-0.9806 - 1.969 i
20.	-0.3102 - 1.969 i	1.261	1.261 + 1.969 i
21.	1.261 - 0.939 i	1.261 - 2.999 i	1.261 + 3.938 i

Table C.7: Bethe roots in the XYZ model for $\eta = 0.620,\ q = 3.80 \times 10^{-4}$ *and* $L = 6$.

	E	$\langle\hat{Q}_3\rangle$	$\langle\hat{Q}_4\rangle$	$\langle\hat{Q}_5\rangle$	$\langle\hat{J}_2\rangle$	$\langle\hat{J}_3\rangle$	$\langle\hat{J}_2^3\rangle$
1.	-7.323	-3.208	11.558	1024.882	0.535	10.821	-1.926
2.	-6.260	0	133.886	0	0	-0.022	-22.314
3.	-6.246	0	133.802	0	0	0	-22.300
4.	-5.385	0	133.987	0	0	-0.214	-22.331
5.	-4.535	-13.460	-5.165	571.976	2.243	6.685	0.861
6.	-4.535	13.460	-5.165	-571.976	-2.243	6.685	0.861
7.	-4.528	-13.468	-5.054	574.289	2.245	6.678	0.842
8.	-4.528	13.468	-5.054	-574.289	-2.245	6.678	0.842
9.	-3.870	13.460	5.165	-686.283	-2.243	5.727	-0.861
10.	-3.870	-13.460	5.165	686.283	2.243	5.727	-0.861
11.	-1.741	-3.154	8.965	134.472	0.526	-0.400	-1.494
12.	-1.741	3.154	8.965	-134.472	-0.526	-0.400	-1.494
13.	-1.085	-3.189	-11.482	-48.155	0.531	1.584	1.914
14.	-1.085	3.189	-11.482	48.155	-0.531	1.584	1.914
15.	-1.083	3.208	-11.558	48.281	-0.535	1.591	1.926
16.	-1.083	-3.208	-11.558	-48.281	0.535	1.591	1.926
17.	-0.848	-5.843	-22.634	-88.228	0.974	2.491	3.772
18.	-0.848	5.843	-22.634	88.228	-0.974	2.491	3.772
19.	0.607	0	-1.487	0	0	-0.020	0.248
20.	0.637	0	-1.499	0	0	0	0.250
21.	1.214	0	-0.524	0	0	-0.132	0.087

Table C.8: Charge and current mean values in the XYZ model for $\eta = 0.620,\ q = 3.80 \times 10^{-4}$ and $L = 6$.

Appendix D

Elliptic functions

Here we present the definitions of the elliptic theta functions and a list of their properties, which are used in the main text. For more details on them, see [188]. The theta functions can be defined as infinite sums:

$$\begin{aligned}
\vartheta_1(u,q) &= -i\sum_{n=-\infty}^{\infty}(-1)^n q^{(n+1/2)^2}e^{i(2n+1)u} = 2\sum_{n=1}^{\infty}(-1)^{n+1}q^{(n-1/2)^2}\sin\big((2n-1)u\big),\\
\vartheta_2(u,q) &= \sum_{n=-\infty}^{\infty} q^{(n+1/2)^2}e^{i(2n+1)u} = 2\sum_{n=1}^{\infty} q^{(n-1/2)^2}\cos\big((2n-1)u\big),\\
\vartheta_3(u,q) &= \sum_{n=-\infty}^{\infty} q^{n^2}e^{i2nu} = 1+2\sum_{n=1}^{\infty} q^{n^2}\cos\big(2nu\big),\\
\vartheta_4(u,q) &= \sum_{n=-\infty}^{\infty}(-1)^n q^{n^2}e^{i2nu} = 1+2\sum_{n=1}^{\infty}(-1)^n q^{n^2}\cos\big(2nu\big).
\end{aligned} \tag{D.1}$$

Here q is the nome of the functions ($|q|<1$). The notation $\vartheta_j(u|\tau)$, $(j\in\{1,2,3,4\})$ is also used, where τ ($\mathrm{Im}\,\tau>0$) is called the parameter of the function, and is related to q as $q=e^{i\pi\tau}$. For brevity, we do not denote either q or τ, and simply use the notation $\vartheta_j(u)$. From (D.1) it is obvious that $\vartheta_1(u)$ is odd, while $\vartheta_2(u)$, $\vartheta_3(u)$ and $\vartheta_4(u)$ are even functions of u. The theta functions are quasiperiodic functions with periods π and $\pi\tau$:

$$\begin{aligned}
\vartheta_1(u+\pi) &= -\vartheta_1(u), & \vartheta_1(u+\pi\tau) &= -\frac{1}{q}e^{-2iu}\vartheta_1(u),\\
\vartheta_2(u+\pi) &= -\vartheta_2(u), & \vartheta_2(u+\pi\tau) &= \frac{1}{q}e^{-2iu}\vartheta_2(u),\\
\vartheta_3(u+\pi) &= \vartheta_3(u), & \vartheta_3(u+\pi\tau) &= \frac{1}{q}e^{-2iu}\vartheta_3(u),\\
\vartheta_4(u+\pi) &= \vartheta_4(u), & \vartheta_4(u+\pi\tau) &= -\frac{1}{q}e^{-2iu}\vartheta_4(u).
\end{aligned} \tag{D.2}$$

The theta functions also satisfy addition theorems, which are used throughout the main text:

$$\begin{aligned}
&\vartheta_1(u)\vartheta_1(v)\vartheta_1(w)\vartheta_1(u+v+w)+\vartheta_4(u)\vartheta_4(v)\vartheta_4(w)\vartheta_4(u+v+w)= \\
&\qquad\qquad =\vartheta_4(0)\vartheta_4(u+v)\vartheta_4(u+w)\vartheta_4(v+w), \\
&\vartheta_1(u)\vartheta_1(v)\vartheta_4(w)\vartheta_4(u+v+w)+\vartheta_4(u)\vartheta_4(v)\vartheta_1(w)\vartheta_1(u+v+w)= \\
&\qquad\qquad =\vartheta_4(0)\vartheta_4(u+v)\vartheta_1(u+w)\vartheta_1(v+w), \\
&\vartheta_4(u-v)\vartheta_1(u+v)-\vartheta_4(u+v)\vartheta_1(u-v)=\frac{2\vartheta_1(v)\vartheta_2(u)\vartheta_3(u)\vartheta_4(v)}{\vartheta_2(0)\vartheta_3(0)}.
\end{aligned} \tag{D.3}$$

Appendix E

Matrix Product States and the iTEBD algorithm

Numerically simulating interacting quantum many-body systems in and out-of-equilibrium on a classical computer is a difficult problem. The dimension of the Hilbert space scales exponentially with the system size. As a result, the exact diagonalization of the Hamiltonian becomes basically impossible above a couple dozens of sites. However, there are some powerful tools that allow one to efficiently approximate quantum states and time-evolution in order to treat systems with larger sizes, or in some cases even in the thermodynamic limit. Here, we review one such method applicable to one-dimensional models, the so-called infinite Time Evolving Block Decimation (iTEBD) algorithm, which is based on the Matrix Product State (MPS) representation of quantum states. The iTEBD algorithm was used to obtain the numerical results in Chapter 7. Our overview presented in this appendix follows closely that of [159]. For another detailed treatise on the topic, we refer to [189].

E.1 Area law

As it was mentioned above, the dimension of the Hilbert space of a quantum many-body system scales exponentially with the size of the system. Consequently, it requires exponentially many coefficients to exactly describe states in some complete basis. In a system consisting of N sites (for the time being, we do not specify the spatial dimension), with some local Hilbert space of dimension d at each site, a generic quantum state can be written as

$$|\psi\rangle = \sum_{i_1=1}^{d} \sum_{i_2=1}^{d} \cdots \sum_{i_N=1}^{d} c_{i_1,i_2,\ldots,i_N} |i_1, i_2, \ldots, i_N\rangle \,, \tag{E.1}$$

where the sums run over the local basis states $i_j = 1, \ldots, d$. The collection of coefficients, $c_{i_1,i_2,\ldots,i_N}$ consists of d^N numerical values. One can think of $c_{i_1,i_2,\ldots,i_N}$ as a rank-N tensor, and can graphically represent it

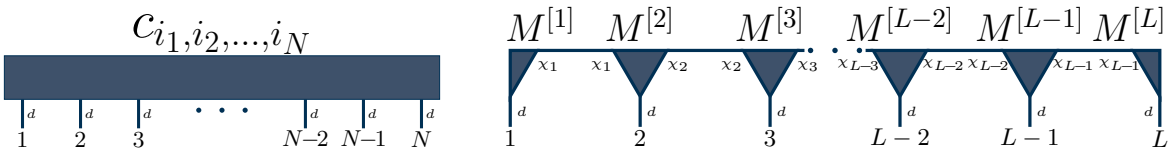

(a) (b)

Figure E.1: (a) Graphical representation of the state (E.1) *as a rank-N tensor. (b) Graphical representation of the generic MPS* (E.6)*: The M-s are three-legged objects, with one physical and two virtual legs. The number of different values each leg can assume are denoted. Connected legs represent tensor contractions, i.e. summations over the appropriate indices. Based on a similar illustration in Ref. [159].*

as in Fig. E.1 (this kind of graphical notation will be very useful in what follows). Unfortunately, the representation of a quantum state as in (E.1) is usually not efficient and technically unattainable for larger sizes.

The problem arising from the exponential growth of the Hilbert space dimension, however, can be dealt with. As it turns out, in a lot of physically relevant situations, only a small fraction of the whole Hilbert space plays a significant role, while the rest can be neglected. The corner of the Hilbert space that contains the important states, can be characterized by investigating the behavior of entanglement entropy. To define this quantity, we divide the system into to parts labeled by A and B. Given that the whole system is in a pure state $|\psi\rangle$, a reduced density matrix describing part A can be introduced, by tracing over the degrees of freedom in part B:

$$\rho_A = \mathrm{Tr}_B\big(|\psi\rangle\langle\psi|\big). \tag{E.2}$$

The bipartite entanglement entropy is then defined as the von Neumann entropy of ρ_A:

$$S = -\mathrm{Tr}\big(\rho_A \log \rho_A\big). \tag{E.3}$$

Another way of defining the same entanglement entropy is to perform a Schmidt decomposition. In this method, the pure state $|\psi\rangle$ of the whole system is written as a sum of product states

$$|\psi\rangle = \sum_\alpha \Lambda_\alpha |\alpha_A\rangle \otimes |\alpha_B\rangle, \tag{E.4}$$

where $|\alpha_{A/B}\rangle$ form an orthonormal basis in subsystem A/B, and $\Lambda_\alpha \geq 0$ are the so-called Schmidt values. For normalized states, we have $\sum_\alpha \Lambda_\alpha^2 = 1$. In terms of this decomposition, the entanglement entropy is given by

$$S = -\sum_\alpha \Lambda_\alpha^2 \log \Lambda_\alpha^2, \tag{E.5}$$

which is equivalent to (E.3).

It can be shown that for a „typical" (or randomly chosen) state in the Hilbert space, the entanglement entropy (E.3) scales with the volume of the subsystems [190]. In particular, for a system of size N with local

Hilbert space dimension d, the entanglement entropy behaves like $S(N) \sim N/2 \log d$, when divided to equal halves. States satisfying this type of scaling are said to follow the so-called volume law.

In contrast, the ground states and low-energy states of local, gapped Hamiltonians follow instead an area law [191, 192]. This means that in these states, the entanglement entropy is proportional to the boundary between the subsystems. In one dimension, this implies that $S(N) \sim$ const. for sufficiently large N ($\xi \lesssim N$, where ξ is the correlation length). This behavior is quite intuitive from a physical point of view: since the interaction in the system is local, only degrees of freedom close to each other along the boundary (within the correlation length ξ) can get entangled. Therefore, when simulating many-body systems with local Hamiltonians, it is often sufficient to consider area law states, which comprise only an exponentially small corner of the whole Hilbert space. Fortunately, these states can be described much more efficiently than in (E.1) with the help of Tensor Network States (TNS), or in the special case of one spatial dimension, with Matrix Product States.

E.2 Matrix Product States

Tensor Network States are a special way of representing quantum states. Since in the present thesis, we are interested in one-dimensional systems, we will focus only on the 1d example of TNS, the so-called Matrix Product States. For generalizations to higher spatial dimensions, we refer to [189].

For a one-dimensional chain of length L, with local Hilbert space dimension d and open boundary condition, an MPS is written in the following form:

$$|\psi\rangle = \sum_{i_1=1}^{d} \sum_{i_2=1}^{d} \cdots \sum_{i_L=1}^{d} M^{[1]i_1} M^{[2]i_2} \ldots M^{[L]i_L} |i_1, i_2, \ldots, i_L\rangle \,, \tag{E.6}$$

where the sums still run over the local basis states, and the $M^{[n]i_n}$-s are $\chi_{n-1} \times \chi_n$ matrices, with the χ_n-s being the so-called bond dimensions. One can think of the M-s as rank-3 tensors, graphically represented as three-legged objects (see Fig. E.1), with one physical leg (in (E.6) denoted by i_n) that can assume d different values, and two virtual legs with values ranging from 1 to χ_{n-1} or χ_n. The matrices at the boundary ($n = 1$ and $n = L$) are actually vectors, meaning $\chi_0 = \chi_L = 1$, so that the final result of the matrix product in (E.6) is a scalar. The superscript $[n]$ is included, because in a general state, different sets of matrices are required for the different sites of the chain. We note that MPS with periodic boundary condition can also be defined, by taking the trace of the matrix product in (E.6), instead of requiring the matrices at the end of the chain to be vectors. Since we are ultimately interested in the thermodynamic limit, the boundary condition does not really matter, and for simplicity we stick to the open case.

The MPS are dense in the Hilbert space, meaning that every quantum state can be represented as in (E.6), by choosing sufficiently large bond dimensions. To illustrate this, one can actually start from a generic state (E.1) and transform it to the form (E.6) by successively applying Schmidt decompositions between the sites of the chain. For the details of this procedure, see [159]. The problem for generic states is that the bond

dimensions grow exponentially with the system size. However, for low entangled area law states, we can make a good approximation by restricting the maximal bond dimension at some fixed value χ. It can be shown that in this case the entanglement entropy behaves like $S \sim \mathcal{O}(\log(\chi))$, which is just the area law, if χ is fixed. In other words, MPS with fixed bond dimensions represent exactly that part of the whole Hilbert space that is most relevant for the simulation of many-body systems with local Hamiltonians.

E.2.1 Canonical form

The MPS state (E.6) is not unique: given a set of invertable, $\chi_n \times \chi_n$ matrices X_n ($n = 1, \ldots, L$), the transformed matrices

$$\tilde{M}^{[n]i_n} = X_{n-1} M^{[n]i_n} X_n^{-1} \tag{E.7}$$

reproduce the same state as the original $M^{[n]}$-s. This freedom gives the opportunity to introduce the so-called canonical form of an MPS, which possesses useful properties.

Without loss of generality, we can rewrite the state (E.6) as

$$|\psi\rangle = \sum_{i_1=1}^{d} \sum_{i_2=1}^{d} \cdots \sum_{i_L=1}^{d} \Gamma^{[1]i_1} \Lambda^{[1]} \Gamma^{[2]i_2} \Lambda^{[2]} \ldots \Lambda^{[L-1]} \Gamma^{[L]i_L} |i_1, i_2, \ldots, i_L\rangle \,, \tag{E.8}$$

where the $\Lambda^{[n]}$-s are positive real valued, diagonal square matrices and the $\Gamma^{[n]i_n}$-s are matrices of sizes $\chi_{n-1} \times \chi_n$. The original $M^{[n]}$-s are then given by $M^{[n]i_n} = \Lambda^{[n-1]} \Gamma^{[n]i_n}$. (To keep the notation general, one can introduce the matrix $\Lambda^{[0]} = 1$ at the boundary.)

The representation (E.8) can be used to define the canonical form. Any bond between any two sites splits the system into two halves and gives a bipartition. One can then obtain left and right states $|\alpha_L\rangle_{[1,2,\ldots,n]}$ and $|\alpha_R\rangle_{[n+1,n+2,\ldots,L]}$ by multiplying together the appropriate matrices on the left and on the right of the chosen bond, respectively, so that the whole state takes the form:

$$|\psi\rangle = \sum_{\alpha=1}^{\chi_n} \Lambda_\alpha^{[n]} |\alpha_L\rangle_{[1,2,\ldots,n]} \otimes |\alpha_R\rangle_{[n+1,n+2,\ldots,L]} \,. \tag{E.9}$$

We say that the MPS (E.8) is in canonical form, if for every bond n, the decomposition (E.9) obtained from (E.8) is the Schmidt decomposition corresponding to that bond. This means that for every bond $\langle \alpha_L | \alpha'_L \rangle_{[1,2,\ldots,n]} = \delta_{\alpha_L, \alpha'_L}$, $\langle \alpha_R | \alpha'_R \rangle_{[n+1,n+2,\ldots,L]} = \delta_{\alpha_R, \alpha'_R}$ and $\sum_{\alpha=1}^{\chi_n} \left(\Lambda_\alpha^{[n]} \right)^2 = 1$.

Every MPS can be transformed into canonical form, which has the advantage that the expectation values of local operators are evaluated by contracting tensors only locally. This is best seen from Fig. E.2.

E.2.2 Infinite MPS

Generally, the matrices $M^{[n]i_n}$ (or equivalently $\Lambda^{[n]}$ and $\Gamma^{[n]i_n}$) can differ from each other for the different sites n of the chain. This fact limits the maximal system size for which a MPS representation is technically

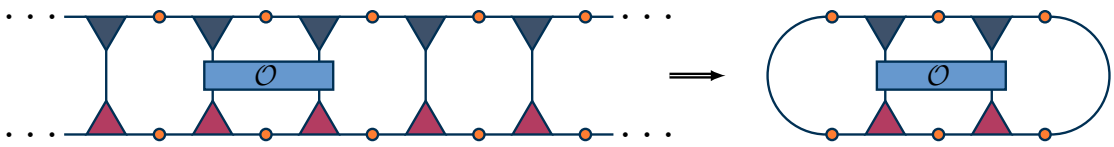

Figure E.2: Calculating the expectation value of a local operator $\mathcal{O}$. The orange circles represent the Λ matrices, while the triangles pointing downwards/upwards the Γ tensors and their adjoints, respectively. The local operator $\mathcal{O}$ acting on two neighboring sites is denoted by the blue rectangle. Due to the MPS being in canonical form, states on the left and right of the operator are orthogonal, simplifying the computation. As a result, only local tensor contractions have to be evaluated. Based on a similar illustration in Ref. [193].

applicable, since for every site a separate set of matrices has to be stored. However, by assuming translational invariance, one can consider states even in the thermodynamic limit and obtain results free of any finite size effect. To describe states that are invariant under translations by l sites ($l \in \mathbb{N}^+$), only l different sets of matrices are needed. For example, in the case of $l = 2$ (illustrated in Fig. E.3), only two sets of Γ and two Λ matrices are necessary. Denoting these by Γ^A, Γ^B, Λ^A and Λ^B, we can write:

$$\Gamma^{[2n]i} = \Gamma^{A,i}, \qquad \Gamma^{[2n+1]i} = \Gamma^{B,i}, \tag{E.10}$$

$$\Lambda^{[2n]} = \Lambda^A, \qquad \Lambda^{[2n+1]} = \Lambda^B, \tag{E.11}$$

for every $n \in \mathbb{Z}$. As an explicit example, we give here the matrices corresponding to the state of spin-1/2-s polarized in the x-direction:

$$|X\rangle = \bigotimes_{j\in\mathbb{Z}} \left(\frac{|\uparrow_j\rangle + |\downarrow_j\rangle}{\sqrt{2}} \right), \tag{E.12}$$

which is used in Chapter 7 as an initial state for quantum quenches. This is a trivial example, since it is a product state and has a one-site unit cell, therefore only requires one set of matrices both for Γ and Λ. Moreover, these matrices are actually scalars:

$$\Gamma^{\uparrow} = \frac{1}{\sqrt{2}}, \qquad \Gamma^{\downarrow} = \frac{1}{\sqrt{2}}, \qquad \Lambda = 1. \tag{E.13}$$

Other, more complicated explicit examples with bigger unit cells can be found in [159, 189].

To define the canonical form for infinite MPS, one needs to introduce the left and right transfer matrices as

$$T^L_{\alpha\alpha';\beta\beta'} = \sum_{i=1}^{d} \Lambda_\alpha \Lambda_{\alpha'} \Gamma^i_{\alpha\beta} \overline{\Gamma^i_{\alpha'\beta'}} \tag{E.14}$$

and

$$T^R_{\alpha\alpha';\beta\beta'} = \sum_{i=1}^{d} \Gamma^i_{\alpha\beta} \overline{\Gamma^i_{\alpha'\beta'}} \Lambda_\beta \Lambda_{\beta'}, \tag{E.15}$$

where $\overline{(\dots)}$ denotes complex conjugation, and for simplicity we assumed a state with a one-site unit cell. In terms of the transfer matrices, the constraint of canonical form becomes the following: an infinite MPS is

in canonical form, if its left (right) transfer matrix has a dominant left (right) eigenvector $\delta_{\alpha,\alpha'}$ ($\delta_{\beta,\beta'}$) with eigenvalue 1. Again, the advantage of the canonical form is that it allows the calculation of local expectation values by contracting tensors only locally.

E.3 Matrix Product Operators

The formalism of Matrix Product States can be extended to the space of operators as well. An operator acting on a one-dimensional chain of length L, with local Hilbert space dimension d and open boundary condition is written in Matrix Product Operator (MPO) form as

$$\mathcal{O} = \sum_{\substack{i_1,i_2,\ldots,i_L=1 \\ i'_1,i'_2,\ldots,i'_L=1}}^{d} \mathbf{v}_L \, M^{[1]i_1 i'_1} M^{[2]i_2 i'_2} \ldots M^{[L]i_L i'_L} \, \mathbf{v}_R \, |i_1, i_2, \ldots, i_L\rangle \langle i'_1, i'_2, \ldots, i'_L| \,, \tag{E.16}$$

where the sums run over the local basis states, the $M^{[n]}$-s are rank-4 tensors with two physical and two virtual legs and $\mathbf{v}_{L/R}$ are vectors, so the result of the matrix multiplication in (E.16) is a scalar.

In the case of periodic boundary condition, one can rewrite (E.16) in a form familiar from the definition of the transfer matrix (3.32) of an integrable system:

$$\mathcal{O} = \mathrm{Tr}_a[\mathcal{L}_{a,L}\mathcal{L}_{a,L-1}, \ldots, \mathcal{L}_{a,1}]. \tag{E.17}$$

Here $\mathcal{L}_{a,n}$ is a local tensor that acts on the tensor product space of the local Hilbert space $\mathbb{C}^d$ (corresponding to the physical legs of $M^{[n]}$) and an auxiliary space (corresponding to the virtual legs of $M^{[n]}$), whose dimension is given by the bond dimension. The trace implements the periodic boundary condition.

Similarly to MPS, MPOs also satisfy an area law: their operator space entanglement entropy is bounded from above by a constant, $2\log\chi$, with χ being the bond dimension.

MPOs provide a useful representation of operators for several reasons. First, their action on a MPS can be evaluated easily. Together with the fact that local, short range Hamiltonians can be expressed as MPOs with fixed, small bond dimensions (for explicit examples, see [159]) this provides the foundation behind the widely used Density Matrix Renormalization Group (DMRG) method. An introduction to this technique can be found in [159], while for more details, see [194].

From our point of view, it is also important that the symmetry operators responsible for the Hilbert space fragmentation in the family of models studied in Chapter 7 can be obtained as MPOs with some small and fixed bond dimension.

E.4 The iTEBD algorithm

The infinite Time Evolving Block Decimation algorithm, originally introduced in [157, 158] provides an efficient numerical technique to simulate the time-evolution of one-dimensional, translationally invariant

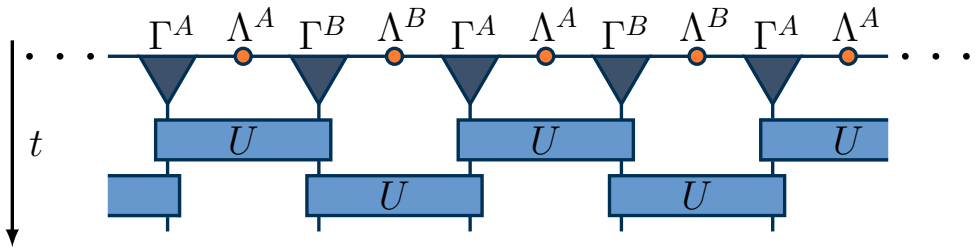

Figure E.3: Graphical depiction of the brick-work type time-evolution implemented by (E.21)*. Based on a similar illustration in Ref. [159].*

quantum systems in the thermodynamic limit. The method is based on the infinite MPS representation of quantum states and uses the Suzuki-Trotter decomposition of the time-evolution operator. It can be used both in real and imaginary time to evaluate the time-evolution of a quantum state:

$$|\psi(t)\rangle = U(t)\,|\psi(0)\rangle\,, \tag{E.18}$$

where $U(t)$ is the time-evolution operator, in real time given by $U(t) = \exp(-itH)$, while in imaginary time by $U(\tau) = \exp(-\tau H)$, with H being the Hamiltonian. The latter can be used to obtain the ground state of the system in question. The fact that in this case U is not unitary has some implications, but here we will focus only on the case of real time.

To numerically calculate (E.18), the algorithm utilizes the Suzuki-Trotter decomposition, which approximates the exponent of a sum of (non-commuting) operators by the product of the exponents of the individual operators. In first order, this decomposition reads as:

$$e^{(\hat{F}+\hat{G})\delta} = e^{\hat{F}\delta}e^{\hat{G}\delta} + \mathcal{O}(\delta^2). \tag{E.19}$$

Higher order expansions are possible, however our numerical results presented in Chapter 7 were obtained by using (E.19). To make use of the Suzuki-Trotter decomposition, we assume that the Hamiltonian in question describes nearest neighbor interaction and write it as a sum of two terms, containing only the contributions of odd/even sites:

$$H = H_{\text{even}} + H_{\text{odd}} = \sum_{n\in\mathbb{Z}} h_{2n,2n+1} + \sum_{n\in\mathbb{Z}} h_{2n-1,2n}. \tag{E.20}$$

The operator generating real time-evolution by δt is then approximated by

$$U(\delta t) \approx \left[\prod_{n\in\mathbb{Z}} U_{2n,2n+1}(\delta t)\right]\left[\prod_{n\in\mathbb{Z}} U_{2n-1,2n}(\delta t)\right], \tag{E.21}$$

with

$$U_{n,n+1}(\delta t) = e^{-i\delta t h_{n,n+1}}. \tag{E.22}$$

As a result of the decomposition of the time-evolution operator in (E.21), one needs to represent the quantum state of the system as an MPS with a 2-site unit cell, even if the initial state has full translational invariance. The operator $U(\delta t)$ then implements a brick-work type time-evolution on this MPS, graphically represented in Fig. E.3.

The main part of the algorithm is the update of the local tensors Γ^A, Γ^B and Λ^A, Λ^B by the local time-evolution operator (E.22). This can be achieved in four steps, depicted in Fig. E.4.

We focus on an AB bond, since the inequivalent BA bonds are updated similarly, by exchanging the roles of the A and B tensors. As a first step, we obtain the wave function in the basis given by the left and right states $|\alpha_L\rangle_{[1,2,\ldots,n-1]}$ and $|\gamma_R\rangle_{[n+2,n+3,\ldots,L]}$, corresponding to the segments $[1,2,\ldots,n-1]$ and $[n+2,n+3,\ldots,L]$, and the one-site basis states $|j_n\rangle$ and $|k_{n+1}\rangle$:

$$|\psi\rangle = \sum_{\alpha_L,j,k,\gamma_R} \Theta^{jk}_{\alpha\gamma} |\alpha_L\rangle_{[1,2,\ldots,n-1]} |j_n\rangle |k_{n+1}\rangle |\gamma_R\rangle_{[n+2,n+3,\ldots,L]}, \tag{E.23}$$

where the coefficient $\Theta^{jk}_{\alpha\gamma}$ is given by

$$\Theta^{jk}_{\alpha\gamma} = \sum_{\beta=1}^{\chi_A} \Lambda^B_\alpha \Gamma^{A,j}_{\alpha\beta} \Lambda^A_\beta \Gamma^{B,k}_{\beta\gamma} \Lambda^B_\gamma. \tag{E.24}$$

As a second step, we apply the local time-evolution operator on (E.24):

$$\tilde{\Theta}^{jk}_{\alpha\gamma} = \sum_{j',k'=1}^{d} U^{jk}_{j'k'} \Theta^{j'k'}_{\alpha\gamma}. \tag{E.25}$$

Once this is done, we want to extract the updated local tensors. So as a third step, we rearrange the tensor $\tilde{\Theta}^{jk}_{\alpha\gamma}$ to become a $d\chi_A \times d\chi_A$ matrix and then apply on this matrix a Single Value Decomposition (SVD):

$$\tilde{\Theta}_{j\alpha;k\gamma} = \sum_\beta X_{j\alpha;\beta} D_\beta Y_{\beta;k\gamma}. \tag{E.26}$$

Here D is a diagonal matrix containing the Schmidt values corresponding to the AB bonds, meaning that $\tilde{\Lambda}^A = D$, while X and Y are isometries. In step four, the updated tensors $\tilde{\Gamma}^A$ and $\tilde{\Gamma}^B$ are recovered from X and Y:

$$\begin{aligned} \tilde{\Gamma}^{A,j}_{\alpha\beta} &= \left(\Lambda^B\right)^{-1}_\alpha X_{j\alpha;\beta}, \\ \tilde{\Gamma}^{B,k}_{\beta\gamma} &= Y_{\beta;k\gamma} \left(\Lambda^B\right)^{-1}_\gamma. \end{aligned} \tag{E.27}$$

The procedure described above simultaneously implements the update of all AB bonds. Moreover, the updated tensors are still in canonical form. The downside is that due to the time-evolution, entanglement entropy increases and the bond dimension at the updated bond becomes $d\chi_A$. Repeated application of the update rules therefore leads to an exponential growth in the bond dimension. To prevent this, we can

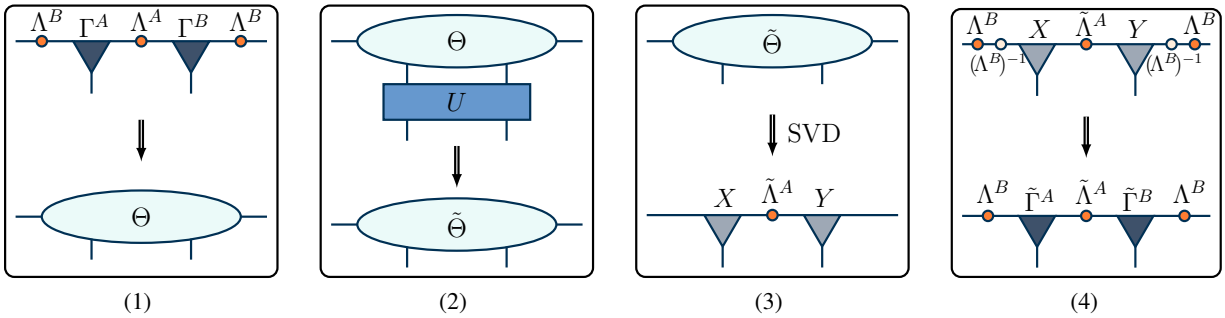

Figure E.4: Graphical representation of the iTEBD algorithm for nearest neighbor interaction: (1) The wave function Θ is obtained by multiplying together the appropriate matrices. (2) The wave function is updated by the time-evolution operator U. (3) Single Value Decomposition is applied on the state to obtain the updated Schmidt values at the middle bond. (4) The updated tensors $\tilde{\Gamma}^A$ and $\tilde{\Gamma}^B$ are recovered after multiplication by $\left(\Lambda^B\right)^{-1}$. Based on a similar illustration in Ref. [159].

approximate the state of the system by keeping only a fixed number of Schmidt states after performing the SVD. This means that at each time step, we order the Schmidt values decreasingly, and truncate the sum in (E.26) after a fixed number (χ) of terms. To keep the whole state normalized, we also need to renormalize $\tilde{\Lambda}$, so that the constraint $\sum_{\alpha=1}^{\chi}(\tilde{\Lambda}_\alpha)^2 = 1$ is fulfilled. The computational memory and time costs of the algorithm are of order $\mathcal{O}(d\chi^2)$ and $\mathcal{O}(d^3\chi^3)$, respectively.

So far, we only discussed the case of a Hamiltonian with nearest neighbor interaction. However, the models treated in Chapter 7 have longer range interactions. The extension of the iTEBD method to these systems is rather trivial. For a system with interaction range l, one only needs to use an infinite MPS with an l-site unit cell and write the time-evolution operator as a product of l terms, with the sites not being grouped together modulo 2, but modulo l. The steps depicted in Fig. E.4 then get modified accordingly. The biggest change is that in this case, in Step 3 not one, but $l-1$ consecutive SVDs have to be performed, which leads to a substantial slow-down.

It is worth mentioning that the algorithm presented above is the simplest version of iTEBD. The method can be significantly sped up by taking into account the symmetries of the investigated model. For details on how global (Abelian) symmetries can be incorporated, see [195, 196].

We also note that there is a Python library called TenPy [193] available to implement simulations based on TNS. We, however, did not work with this library, instead used the example code presented in [159] and modified it to our purposes.